University of Southampton

Faculty of Medicine

Clinical and Experimental Sciences

An *In Vitro* Model of Intramural Periarterial Drainage. Significance for Alzheimer's Disease

by

Abby Charlotte Keable

Thesis for the degree of Doctor of Philosophy

July 2020

University of Southampton

Abstract

Faculty of Medicine

Clinical and Experimental Sciences

Thesis for the degree of Doctor of Philosophy

An *In Vitro* Model of Intramural Periarterial Drainage. Significance for Alzheimer's disease

by

Abby Charlotte Keable

Alzheimer's disease is the commonest form of dementia and one of the key features is the deposition of amyloid-beta peptides in the walls of capillaries and arteries as cerebral amyloid angiopathy (CAA). This is due to a failure of clearance of amyloid-beta (Aβ) from the ageing brain. The basement membranes of capillaries and arteries represent the intramural periarterial drainage (IPAD) pathways of the brain and IPAD fails with increasing age and possession of Apolipoprotein E4 genotype. The motive force for IPAD is provided by the contraction of vascular smooth muscle cells (VSMC) that receive adrenergic innervation from locus coeruleus, a structure that degenerates very early in Alzheimer's disease. As IPAD pathways are both small (100nm thickness) and inaccessible, there is an urgent need to employ new methods to investigate their targeting for treatment. The aim of this thesis is to firstly study the pattern of synthesis of basement membrane proteins by cells of the vascular wall, secondly to assess how these proteins change in response to ApoE genotype and hypoxia and thirdly to characterise the distribution of adrenergic receptors on the vascular smooth muscle cells as a look to their future therapeutic targeting of IPAD.

Materials and Methods: Human vascular smooth muscle cells, pericytes, endothelial cells and astrocytes were cultured and their expression of collagen IV, laminin, fibronectin and perlecan was examined after immunofluorescence and confocal microscopy. Astrocytes expressing ApoE2/3/4 were also examined by correlated light and electron microscopy. A novel millifluidics system called Quasi-Vivo was employed to pilot flow of Aβ peptides over vascular smooth muscle cells. Adrenergic receptors on VSMCs were studied by immunofluorescence and confocal microscopy.

Results: All cells synthesised proteins of the basement membranes in varying amounts. APOE4 astrocytes express high amounts of fibronectin. Vascular smooth muscle cells produce the highest amount of basement membrane proteins compared to pericytes, endothelial cells and astrocytes, with collagen IV and laminin expressed at their highest amount in VSMC compared to the other

cells. Flow of Aβ 1-40 or Aβ1-42 did not alter the composition of the basement membranes under normoxic conditions. Hypoxia alone resulted in an upregulation of laminin with no effect of the addition of Aβ 1-40, but a decrease in laminin and collagen IV when Aβ1-42 was added. Adrenergic receptors are expressed on VSMCs, with the highest concentration of α1B receptors.

Discussion: This study demonstrates that cells contributing to the IPAD pathways express basement membrane proteins in different concentrations, with VSMCs synthesising the highest amounts of collagen IV and laminin, responding to hypoxia and to flow of Aβ 1-42 and expressing a high concentration of α1B adrenergic receptors.

Conclusion: The unique basement membrane characteristics of the VSMCs and their response to hypoxia and flow of Aβ supports the working hypothesis that Aβ may be a signalling molecule for IPAD pathways that are sensitive to hypoxic changes and may be targeted therapeutically by adrenergic interventions.

Table of Contents

Detailed Table of Contents

Table of Tables

Table of Figures

Table of Figures

Research Thesis: Declaration of Authorship

Print name: Abby Charlotte Keable

Title of thesis: An *In Vitro* Model of Intramural Periarterial Drainage. Significance for Alzheimer's Disease

I declare that this thesis and the work presented in it are my own and has been generated by me as the result of my own original research.

I confirm that:

1. This work was done wholly or mainly while in candidature for a research degree at this University;
2. Where any part of this thesis has previously been submitted for a degree or any other qualification at this University or any other institution, this has been clearly stated;
3. Where I have consulted the published work of others, this is always clearly attributed;
4. Where I have quoted from the work of others, the source is always given. With the exception of such quotations, this thesis is entirely my own work;
5. I have acknowledged all main sources of help;
6. Where the thesis is based on work done by myself jointly with others, I have made clear exactly what was done by others and what I have contributed myself;
7. Parts of this work have been published as:

ApoE4 Astrocytes Secrete Basement Membranes Rich in Fibronectin and Poor in Laminin Compared to ApoE3 Astrocytes. Keable A, O'Neill R, MacGregor Sharp M, Gatherer M, Yuen HM, Johnston DA, Weller RO, Carare RO.Int J Mol Sci. 2020 Jun 19;21(12):E4371. doi: 10.3390/ijms21124371. PMID: 32575521

Signature: Date:

Acknowledgements

Firstly and most importantly I would like to thank my supervisors Prof Roxana Carare and Dr Neil Smyth for without their support and guidance this work would not have been possible.

There have been many people that have offered guidance and support throughout this project. I would like to extend my thanks to Malcolm Wilkinson and his team at Kirkstall Ltd who demonstrated the usefulness of the Quasi Vivo system to me hosted me for 3 months whilst on placement. I would also like to thank my colleagues for their knowledge and support throughout this project.

I would like to thank David Holtzman and his team in Washington for allowing me to use the transgenic mouse astrocytes that he developed for part of this study. I would also like to acknowledge medical student Ronan O'Neill for performing the quantification of astrocytic processes obtained from the CLEM data and Daniel Baseley from Cardiff School of Biosciences who performed the immunocytochemical staining and imaging for adrenergic receptors. I would also like to acknowledge my colleague Matthew Sharp who captured the electron micrographs of cerebral vessels and gave his permission for me to use them.

Phenom World and Charlotte Worthy must be thanked for the agreement of the loan of the Delphi and the training on how to use it.

Thank you to my friends and family who have been a great support through the tough times, and especially my sister Hollie who has given me love and support throughout the most trying times.

Finally a big thank you to BBSRC who have provided the funding for this research.

Definitions and Abbreviations

ACE	angiotensin-converting enzyme
AD	Alzheimer's disease
ADRDA	Alzheimer's Disease and Related Disorders Association
ANOVA	analysis of variance
ApoE	apoliprotein E protein
APOE	apoliprotein E gene
APP	amyloid precursor protein
AQP4	aquaporin IV
ARIA	Amyloid-related imaging abnormalities
Aβ	amyloid beta
Aβ 1-40	40 amino acid long amyloid beta peptide
Aβ 1-42	42 amino acid long amyloid beta peptide
BACE	beta-site APP cleaving enzyme/beta secretase
BBB	blood-brain barrier
bFGF	basic fibroblast growth factor
CAA	cerebral amyloid angiopathy
CArG box	repeating nuecleotide sequence forming a transcription signal
CLEM	correlative light and electron microscopy
CNS	central nervous system
COX-2	cyclooxygenase 2
CSF	cerebrospinal fluid
CTE	chronic traumatic encephalopathy
DAG	diaglycerol

Definitions and Abbreviations

DAPI	4’,6-diamidino-2-phenylindole
DMEM	Dulbecco’s modified eagle’s medium
DMSO	dimethyl sulphoxide
DPC	dystrophin-associated protein complex
ECE	Endothelin-converting enzyme
EM	electron microscopy
EMMPRIN	extracellular matrix-metalloproteinase inducer
FAD	familial Alzheimer’s disease
FAK	focal adhesion kinase
FBS	foetal bovine serum
GA	glutaraldehyde
GFAP	glial fibrillary acidic protein
HA	human astrocytes
HBVSMC	human brain vascular smooth muscle cells
hCMEC/D3	human cerebral microvascular endothelial cell line
hMMEL	human membrane metallopeptidase-like protein
HP	human pericytes
IDE	insulin degrading enzyme
IP_3	inositol triphosphate
IPAD	intramural periarterial drainage
ISF	interstitial fluid
ITO	indium tin oxide
JAM	junctional adhesion molecule
LOAD	late onset Alzheimer’s disease

LDL-R	low density lipoprotein receptor
LED	light emitting diode
LRP-1	low density lipoprotein receptor-related protein 1
MMP	matrix metalloproteinase
MRI	magnetic resonance imaging
MSC	microbiological safety cabinet
MTS	(4,5-dimethylthiazol-2-yl)-5-(3-carboxymethoxyphenyl)-2-(4-sulfophenyl)-2H-tetrazolium
NEP	neprilysin
NEP 2	neprilysin 2
NGS	normal goat serum
NINCDS	National Institute of Neurological and Communicative Disorders and Stroke
NMDA	N-methyl-D-aspartate
PBS	phosphate buffered saline
PDMS	polydimethylsiloxane
PECAM	platelet endothelial cell adhesion molecule
PET	positron emission tomography
PFA	paraformaldehyde
PIP_2	phosphatidylinositol bisphosphorate
QDs	Quantum dot nanocrystals
SEM	scanning electron microscopy
SMC	smooth muscle cell
SRF	serum response factor
TEER	trans-endothelial electrical resistance
TGF-β1	transforming growth factor β1

TIMP	tissue inhibitor of metalloproteinase
VEGF	vascular endothelial growth factor
VSMCs	vascular smooth muscle cells
ZO-1	zonula occludens-1

Chapter 1 Introduction

1.1 Dementia and Alzheimer's disease

The word dementia, from the Latin demens meaning out of one's mind (Oxford English dictionary) is a broad term used to describe the cognitive and behavioural changes due to progressive neurological disorders caused by brain disease or injury. Dementia is characterised by a loss of memory, personality disorders and impaired reasoning. According to the 2015 World Alzheimer Report there were approximately 46.8 million people living with dementia costing the global economy an estimated $818 billion US dollars and these figures are set to double every 20 years (Martin Prince, 2015). This exponential increase will place a massive strain on the global economy. The impact of dementia can be felt on a much more personal level with many families struggling to meet the financial and emotional demands of caring for a relative with dementia (Schneider *et al.*, 1999).

Dementia is not a normal part of the aging process. Dementia is primarily caused by disease and the most common cause is Alzheimer's disease (AD), accounting for approximately two thirds of all cases of dementia.

It is estimated there is a new case of AD every 7 seconds (Ferri *et al.*, 2005) and the disease itself is becoming a pandemic as the global population ages (Anand, Gill and Mahdi, 2014). Such is the prevalence of AD and dementia in the UK that for the first time dementia is now the leading cause of death (office of national statistics), overtaking heart disease.

AD may be classified broadly into two categories based on age of onset. Early onset AD (also known as familial AD) accounts for between 1% and 6% of cases and age of onset is typically between 30 and 60 years (Anand, Gill and Mahdi, 2014). Early onset AD has a strong genetic component and is a result of mutation. Most reported cases are caused by a mutation in chromosomes 21, 14 or 1 resulting in early onset familial Alzheimer's disease (FAD). Mutations on chromosome 21 alter the amyloid precursor protein (APP) and lead to an increased production of amyloid beta (Aβ). Mutations on chromosomes 14 and 1 lead to abnormal presenilin 1 and presenilin 2 respectively (Bird, 1999), affecting the catalytic activity of γ secretase, though how this affects Aβ production and onset of AD is unclear and a topic of hot debate (Kelleher and Shen, 2017). These mutations alter the processing of APP and lead to Aβ accumulation, one of the hallmarks of disease discussed later.

Late onset Alzheimer's disease (LOAD) makes up more than 90% of all cases and age of onset is typically over 60 (Anand, Gill and Mahdi, 2014). LOAD is sporadic and the causes are unknown, but it is thought that genetic, environmental and lifestyle factors play a role in its development.

1.2 Risk factors for Alzheimer's disease

There are many factors that increase the risk of development of LOAD and the most common are discussed below.

1.2.1 Age

From grey hair to wrinkles, the outward changes to the human body are very apparent with age. Although it is much less obvious the brain also changes significantly with age. After reaching maximum size in early adult life the human brain progressively decreases in size (Dekaban, 1978) (see **Figure 1-1**). The changes in brain mass may also be visualised with non-invasive imaging such as magnetic resonance imaging (MRI) and positron emission tomography (PET). Such techniques can demonstrate the shrinkage of the aged brain. Synapses naturally decrease with age (Dale Purves *et al.*, 2012) so the neural circuits of the aged brain and therefore cognitive ability are diminished to some extent.

The natural changes that occur in the brain with age make it more vulnerable to injury and disease. AD is a disease of aging so with increasing age the likelihood of developing the disease also increases. 15% of those with AD are ages 65-74 and this increases to 44% for those ages 75-84 (AlzheimersAssociation, 2016). A person's risk of developing AD doubles roughly every 5 years beyond age 65 (NIH, 2017) and with an increasingly aging population the diseases of age are set to become more and more prominent.

Even though age is the biggest risk factor for developing AD, it is not currently thought to be a normal part of aging and advancing age is not sufficient to cause the disease by itself.

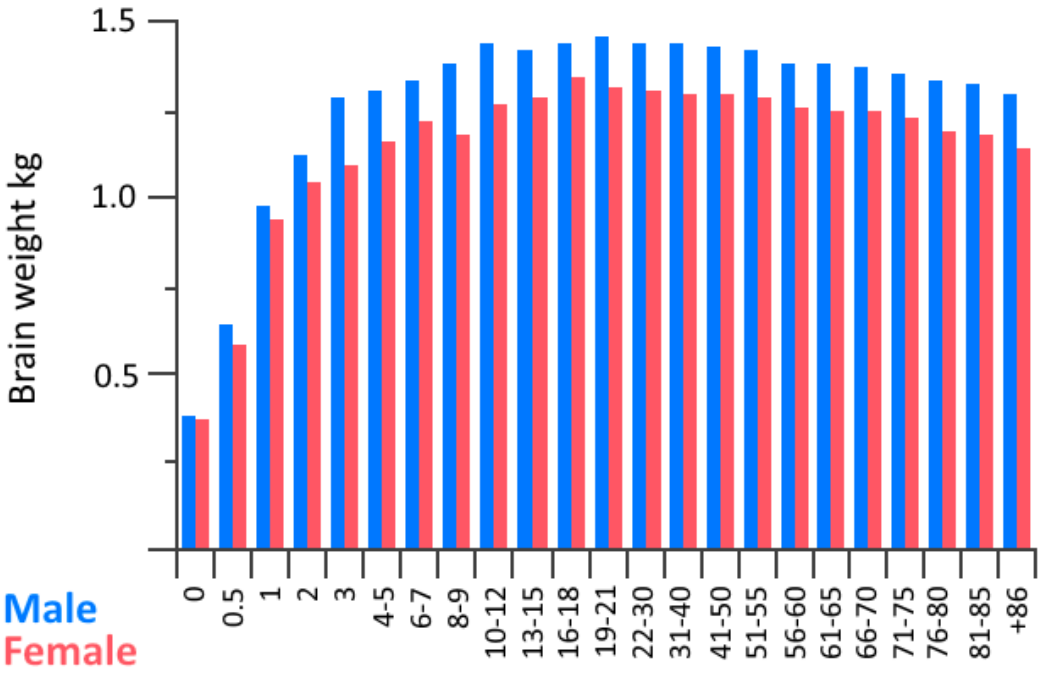

Figure 1-1 A graph to show the relationship between age and brain weight, adapted from (Dekaban, 1978)

Between the ages of 16-21 the brain reaches its maximum weight. From this point there is a progressive linear decline in brain weight which is thought to represent the natural shrinkage of the brain and loss of synapses that occurs with aging.

1.2.2 Apolipoprotein E genotype

The APOE gene encodes a protein called apolipoprotein E (ApoE). This protein combines with lipids in the body to form molecules called lipoproteins. ApoE is the main cholesterol chaperone in the brain and is responsible for transporting cholesterol into neurons via ApoE receptors. APOE is polymorphic and has 3 major isoforms: ε2 - the rarest type with an allele frequency of 7%, ε3 – the most common with an allele frequency of 79% and ε4 with an allele frequency of 14% (Suarez and Schonfeld, 1981; Alzforum, 2010; Jun *et al.*, 2017). The biggest genetic risk factor for development of late onset sporadic AD is possession of one or more copies of the APOE ε4 allele. It is estimated that 40%-65% of individuals with AD have at least one copy of APOE ε4 (AlzheimersAssociation, 2016).

The primary structure of these homologous lipoproteins is shown in **Figure 1-2**. It has been suggested that the single amino acid substitutions that determine the three ApoE isoforms cause significant alterations to the tertiary structure and function of ApoE (Mahley, Weisgraber and Huang, 2009), however as ApoE is lipidated its 3D structure has not been fully determined and therefore the structure of biologically active ApoE is still not well understood (Henry *et al.*, 2018).

Figure 1-2 the difference between ApoE genotypes

There are two important amino acids that determine the isoform of ApoE that is expressed. At positions 112 and 158 the presence of a cysteine (Cys) or an arginine (Arg) residue will determine the ApoE genotype. The most common type, ApoE ε3, has Cys at position 112 and Arg at position 158. ApoE ε2, which is thought to have a protective function against AD, replaces the Arg at position 158 with a Cys and ApoE ε4, the major genetic risk factor for AD, replaces Cys at position 112 with Arg. There are no other differences in the primary structure of these lipoproteins.

APOE ε4 is not a determinant of AD, at least a third of AD patients do not possess an APOE ε4 allele and there are some APOE ε4 homozygotes will never develop AD. Nevertheless, the link between APOE genotype and AD is very strong. The APOE genotype alters the risk for AD in a dose-dependent manner (ε2<ε3<ε4). Individuals that are heterozygous (ε3/ ε4) have around 5 times increased risk when compared with ε3/ε3 and this increases to approximately 20 times increased risk for homozygous (ε4/ ε4) individuals (Hauser and Ryan, 2013). It is thought that possession of an APOE ε2 allele may offer some protection, reducing the risk of developing AD by approximately half (Conejero-Goldberg *et al.*, 2014), however the mechanisms underlying this have not been explored in great depth (Wu and Zhao, 2016).

1.2.3 Traumatic brain injury

There is strong evidence to suggest a causal link between traumatic brain injury and AD (McKee *et al.*, 2014; McKee and Robinson, 2014; Sundman, Hall and Chen, 2014; Li *et al.*, 2017). The more severe the brain injury is and the greater the number of injuries, the greater the risk of developing AD. A study carried out on war veterans in North Carolina showed that moderate head injury resulted in a 2.3 fold increase in risk and severe head injury more than quadrupled the risk (Gottlieb, 2000). The 'punch drunk syndrome' now more formally known as chronic traumatic encephalopathy (CTE) has been reported in a wide range of contact sports and it is a potential neurodegenerative cause of dementia (Ling *et al.*, 2017). Increased neurodegenerative disease

mortality has also been observed in former professional football players – most likely due to the trauma suffered when repeatedly heading the ball (Mackay *et al.*, 2019). This growing body of evidence is particularly concerning for professional sportspersons, such as boxers, who take repeated blows to the head as part of their daily life.

1.2.4 Cystatin C

Cystatin C is an endogenous cysteine proteinase inhibitor (Mussap and Plebani, 2004) It is produced by nearly all human cells and is present in all body fluids. Studies have shown that cystatin C inhibits the aggregation of Aβ (Levy *et al.*, 2001; Sastre *et al.*, 2004), a pathological hallmark of Alzheimer's disease and lower serum levels of cystatin C are associated with a higher incidence of Alzheimer's disease (Sundelöf *et al.*, 2008). Interestingly a mutation in cystatin C leads to a rare hereditary autosomal dominant disorder known as Icelandic cerebral amyloid angiopathy, named after the region where it was first diagnosed (Jensson *et al.*, 1989). This disorder results in stroke followed by dementia, with individuals typically suffering their first stroke in their twenties (NIH, 2020), however this cystatin C amyloid angiopathy is distinct from the Aβ cerebral amyloid angiopathy seen in Alzheimer's disease (Coria and Rubio, 1996). Low levels of cystatin C may therefore be considered a risk factor for Alzheimer's disease, whereas mutated cystatin C is a cause of cystatin C amyloid angiopathy.

1.2.5 Lifestyle

Although it is impossible to completely negate the risk of developing Alzheimer's disease certain lifestyle changes can help to reduce the risk. There is a growing body of evidence to suggest the health of the brain is linked to the health of the heart and blood vessels (Sabayan *et al.*, 2016; Hooghiemstra *et al.*, 2017; Moroni *et al.*, 2018). According to Dementia UK 'what is good for the heart is good for the brain'. Leading a healthy lifestyle by stopping smoking, reducing alcohol intake, eating healthily and exercising regularly can help to decrease the likelihood of AD and other types of dementia (Valenzuela *et al.*, 2012; Iwamoto, 2014; Orrell *et al.*, 2015). Controlling cholesterol and lowering blood pressure will also have a positive effect as it has been shown that midlife hypertension and high cholesterol lead to a significantly higher risk of Alzheimer's disease in later life (Kivipelto et al., 2001). There is also evidence that making effort to continue to use the fullest range of human memory abilities may somewhat offset the clinical symptoms of AD (Cabeza et al., 2002), however mild cognitive decline is a natural process of aging.

1.3 The pathological hallmarks of Alzheimer's disease

A diagnosis of AD may be tentatively given based on the clinical symptoms a patient presents with according to the National Institute of Neurological and Communicative Disorders and Stroke and the Alzheimer's Disease and Related Disorders Association (NINCDS-ADRDA) criteria as described in (McKhann *et al.*, 1984), however it is impossible to differentiate AD from other types of dementia based solely on this and as a result there is a misdiagnosis rate of about 30% (Knopman *et al.*, 2001). More recently clinical presentation combined with MRI and CSF biomarkers has increased the accuracy of AD diagnosis (Frisoni *et al.*, 2010) but it is still not 100% accurate. AD has a very distinctive cellular neuropathology that results in a specific profile of histopathological changes in the brain that are only evident post mortem, hence a definitive diagnosis can only be given upon death.

The histopathological changes consist of: accumulation of intraneuronal neurofibrillary tangles, a diffuse loss of neurons and a build-up of amyloid beta (Aβ) as insoluble senile plaques (Markesbery, 1997) and in the walls of cerebral blood vessels as cerebral amyloid angiopathy (CAA) (see **Figure 1-3**). The neurofibrillary tangles are the result of a hyperphosphorylation of the microtubule-associated protein tau; this hyperphosphorylation prevents tau from binding to microtubules and is thought to result in microtubule destabilization and axonal loss (Trojanowski and Lee, 1995). Aβ is a peptide of 37-49 amino acids that is derived from the proteolytic processing of the amyloid precursor protein by β and γ secretases (Chen *et al.*, 2017). There are two forms implicated in Alzheimer's disease, a 42 amino acid peptide called Aβ 1-42 that is the principal component of the insoluble plaques (Van Dorpe *et al.*, 2000) and a smaller more soluble 40 amino acid peptide known as Aβ 1-40. Aβ 1-40 is associated mainly with CAA, though it can be found in plaques just as Aβ 1-42 may be found in the walls of blood vessels (Van Dorpe *et al.*, 2000). Aβ is usually fibrillary, forming a cross-β structure where β-sheets run parallel and β-strands run perpendicular to the fibril axis (Luhrs *et al.*, 2005) , though smaller soluble peptides exist in the form of monomers, dimers and other oligomers. Typically, when left to accumulate, oligomers readily form insoluble fibrils which accumulate as plaques.

It has long been theorised, by the amyloid cascade hypothesis, that the build-up of Aβ is central in the cause and progression of AD (Karran, Mercken and De Strooper, 2011). The production of Aβ remains relatively unchanged throughout life and is normally counterbalanced by various elimination pathways, regulating its function and preventing accumulation (Ramanathan *et al.*, 2015). The build-up of Aβ in AD is due to either an overproduction of Aβ, as is the case with genetic mutations seen in FAD, or a failure of the clearance mechanisms designed to remove excess solutes, including Aβ, from the brain parenchyma (Mawuenyega *et al.*, 2010).

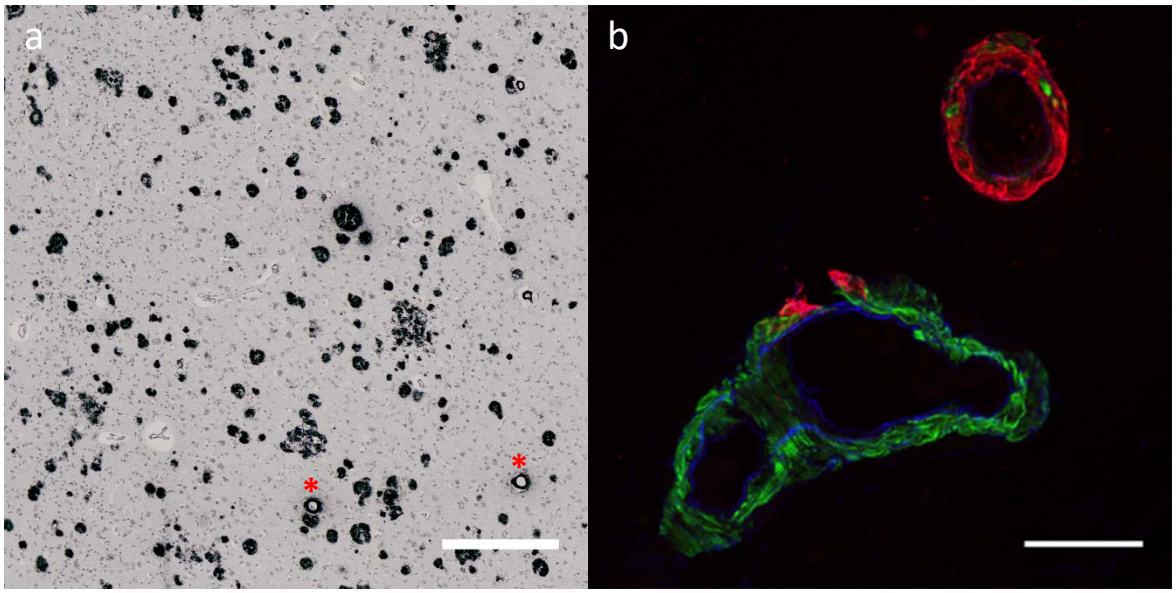

Figure 1-3 - Immunohistochemical staining demonstrating Aβ plaques and CAA in an AD brain

Human occipital cortex sections diagnosed with AD were obtained from the Newcastle Brain Tissue Resource and immunostained for Aβ using a 4G8 antibody (SIG39220, Covance) (a). Plaques can vary greatly in size and density and the distribution appears random throughout the grey matter. Some examples of CAA are marked by asterisk, scale bar 200µm. The brain sections were also stained by triple immunofluorescence using anti-collagen IV (ab6586, AbCam), shown in blue; anti-smooth muscle actin (F3777, Sigma) and anti-Aβ (SIG39220, Covance), shown in red (b). The Aβ builds up in the vessel walls and slowly replaces the smooth muscle cells compromising the integrity of the vessel wall and its contractile capabilities. Both images are from my own studies Scale bar 50µm.

1.4 Mechanisms of clearance

Unlike other major organs of the body, the brain lacks a traditional lymphatic system of large vessels designed to remove waste solutes (Weller *et al.*, 2009). This is because the brain is kept in an immune privileged state by a specialised endothelial layer of tight junctions, known as the blood brain barrier (BBB), which serves to restrict the passage of molecules between the blood and the brain tissue to protect the brain from harmful pathogens transported in the blood (Ballabh, Braun and Nedergaard, 2004; Engelhardt and Sorokin, 2009). Instead the brain deals with the elimination of Aβ and other solutes in many ways discussed below and summarised in **Figure 1-4**.

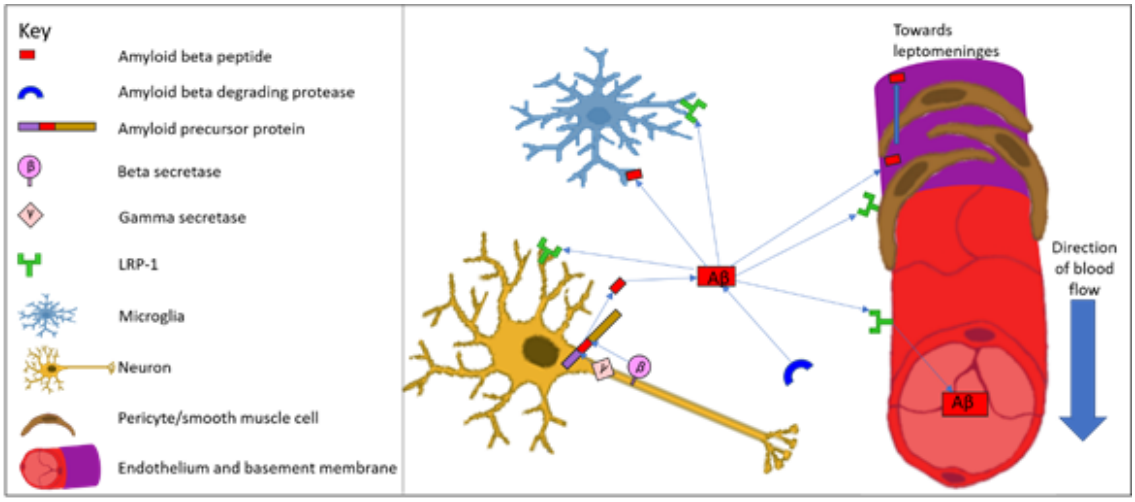

Figure 1-4 Aβ clearance mechanisms in the brain

Aβ is produced by the actions of β and γ secretase on the amyloid precursor protein. The Aβ peptide may be removed by LRP-1 mediated endocytosis that may cause the Aβ to pass into the blood or be taken up into cells for lysosomal degradation. Proteolytic enzymes may also act directly on Aβ in the extracellular space causing its degradation. Aβ can also enter the basement membranes of cerebral capillaries and drain towards the leptomeningeal arteries via the intramural periarterial drainage pathway.

1.4.1 LRP-1 mediated transport

Low density lipoprotein receptor-related protein 1 (LRP-1) is a member of the LDL-R family that is expressed in the majority of cells in the brain, most notably vascular smooth muscle cells, neurons and endothelial cells (Zlokovic *et al.*, 2010). LRP-1 has over 40 known ligands including Aβ and ApoE (Shibata *et al.*, 2000). The major route of clearance of unbound monomeric Aβ is transcytosis across the BBB via LRP-1 localised on the abluminal side of the endothelium (Shibata *et al.*, 2000) with the rate of clearance estimated to be 0.21pmol/min/g ISF for Aβ 1-40 and 1.9 fold slower for Aβ 1-42 (Bell *et al.*, 2007). LRP-1 also mediates uptake of Aβ into cells to be degraded in lysosomes (Kanekiyo and Bu, 2014). Neuronal LRP-1 acts via ApoE and α2M to regulate cellular uptake of Aβ, though this may not facilitate Aβ clearance (Qiu *et al.*, 1999; DeMattos *et al.*, 2004). The levels of LRP-1 decrease with age and in AD (Weller and Nicoll, 2003), reducing the clearance of Aβ and disrupting Aβ homeostasis in the brain.

1.4.2 Microglia

The CNS is host to a population of resident myeloid cells known as microglia (Lai and McLaurin, 2012). Microglia are the resident macrophages of the brain and part of the innate immune system. Upon stress or insult microglia adapt an activated state that is similar to that of peripheral

macrophages and this allows them to exhibit macrophage-like immune functions such as phagocytosis and release of cytokines (Hanisch and Kettenmann, 2007). In addition to LRP-1 mediated clearance, microglia are also capable of clearing Aβ from the brain by phagocytosis. There is much debate on how efficiently microglia phagocytose Aβ and upon uptake and attempted digestion of Aβ microglia may adopt a pro-inflammatory phenotype, producing reactive oxygen species and cytokines that induce neurotoxicity (McGeer and McGeer, 2007). Microglial phagocytosis of fibrillar Aβ can be disturbed by oligomeric Aβ by inducing a potent inflammatory response and downregulating the cell surface receptors CD36 and CD47 that microglia use to interact with the fibrillar Aβ (Pan *et al.*, 2011). This inflammatory response may also be damaging to neurons.

1.4.3 Proteolytic degradation

There are many known proteases that act on Aβ. The proteolytic degradation of Aβ is catalytic and irreversible. **Table 1-1** contains a list of proteases that are known to degrade Aβ either *in vivo* or *in vitro*.

Table 1-1 Proteases implicated in the degradation of Aβ

Protease name	Type	Subcellular localisation
Neprilysin (NEP)	Zinc-Metalloproteinase	Extracellular space, endoplasmic reticulum, golgi
Neprilysin 2 (NEP2)	Zinc-Metalloproteinase	Extracellular space, endoplasmic reticulum, golgi
Human membrane metalloendopeptidase-like protein (hMMEL)	Zinc-Metalloproteinase	Extracellular space, endoplasmic reticulum, golgi
Endothelin-converting enzyme 1 (ECE1)	Zinc-Metalloproteinase	Extracellular space, endoplasmic reticulum, golgi, endosomes
Endothelin-converting enzyme 2 (ECE2)	Zinc-Metalloproteinase	Extracellular space, endoplasmic reticulum, golgi, endosomes
Angiotensin-converting enzyme (ACE)	Zinc-Metalloproteinase	Extracellular space, endoplasmic reticulum, golgi
Matrix-metalloproteinase 2 (MMP2)	Matrix-Metalloproteinase	Extracellular space, endoplasmic reticulum, golgi

Protease name	Type	Subcellular localisation
Matrix-metalloproteinase 9 (MMP9)	Matrix-Metalloproteinase	Extracellular space, endoplasmic reticulum, golgi
Matrix-metalloproteinase 14 (MMP14/MTI-MMP)	Matrix-Metalloproteinase	Extracellular space, endoplasmic reticulum, golgi
Extracellular matrix-metalloproteinase inducer (CD147/EMMPRIN)	Matrix-Metalloproteinase	Extracellular space, endoplasmic reticulum, golgi, endosomes
Insulin-degrading enzyme (IDE)	Metalloproteinase	Extracellular space, endoplasmic reticulum, endosomes, lysosomes, mitochondria
Plasmin	Serine	Extracellular space, endoplasmic reticulum, golgi
Acylpeptide hydrolase	Serine	Extracellular space, cytosol
Myelin basic protein	Serine	Extracellular space, endoplasmic reticulum, golgi
Cathepsin D	Aspartyl	Endosomes, lysosomes
BACE1	Aspartyl	Endosomes, lysosomes
BACE2	Aspartyl	Endosomes, lysosomes
Cathepsin B	Cysteine	Extracellular space, endosomes, lysosomes

*adapted from (Saido and Leissring, 2012)

These proteases may become less efficient with age and NEP and IDE are thought to be impaired by oxidative stress (Wang *et al.*, 2003; Caccamo *et al.*, 2005), which occurs during aging and in AD.

1.4.4 Intramural periarterial drainage

Intramural periarterial drainage (IPAD) best represents the lymphatic drainage of the brain. Although the brain is devoid of traditional large lymphatic vessels, the IPAD pathway of elimination hypothesises that cerebrovascular basement membranes act as the lymphatics of the brain. Carare et al have demonstrated that interstitial fluid (ISF) and solutes diffuse into the

narrow extracellular spaces of the brain and drain along the 100-150nm wide basement membranes in the walls of cerebral arteries and capillaries (Carare *et al.*, 2008). These basement membranes are a highly specialised extracellular matrix composed of a meshwork of glycoproteins and proteoglycans.

IPAD occurs in the opposite direction to blood flow and ceases immediately upon cardiac arrest, indicating a role for the arterial wall in driving the drainage. Theoretical models suggested the driving force for IPAD was contrary waves from arterial pulsations (Schley *et al.*, 2006) however more recent work has demonstrated arterial pulsations are not strong enough to produce the correct drainage velocities observed in experimental models (Diem *et al.*, 2017). Mathematical modelling has proposed that vasomotion, driven by the cycles of contraction and relaxation in smooth muscle cells, is the only mechanism postulated to date that provides a sufficient drainage force for IPAD (Aldea *et al.*, 2019).The contraction of smooth muscle cells is therefore likely to play a major role in the efficiency of the clearance of Aβ from the brain.

The IPAD pathway is slower than other methods of elimination, some six fold slower than LRP mediated absorption into the blood (Bell *et al.*, 2007). A study in 2000 used an anti-LRP-1 antibody to block LRP-1 mediated clearance and reported a 55% reduction in the clearance of Aβ and also an age-related inhibition of Aβ clearance (Shibata *et al.*, 2000), suggesting that IPAD may become much more important as other routes begin to fail with age or are blocked. This highlights the importance of IPAD to the on-going health and functionality of the brain. APOE ε4 is associated with impaired IPAD (Hawkes *et al.*, 2012), so may increase the risk of AD by impeding removal of soluble Aβ.

Methods used to study IPAD involve intracerebral injection of fluorescent tracers such as dextran or ovalbumin into the striatum of animal models, typically mice, which are then sacrificed at various time points and perfusion fixed before the brains are prepared for imaging (Carare et al., 2008). Using this method it has been demonstrated that tracers injected into the caudate putamen initially spread diffusely within the extracellular spaces of gray matter and enter the basement membranes of capillaries and smooth muscle cells within 5 minutes and are totally removed from the parenchyma within 3 hours (Carare *et al.*, 2008; Weller *et al.*, 2008).

Although the IPAD pathway was identified using this method it cannot provide real-time information as it is limited to showing a snapshot of where the tracer is at a given time point. More current methodologies include the use of two photon microscopy (Arbel-Ornath *et al.*, 2013; Iliff *et al.*, 2013) to allow drainage to be visualised in a live mouse. There are however many problems and complications that make this method very difficult to reliably reproduce. The craniotomy and

injection surgeries required for this methodology are difficult to perform and often result in haemorrhage, obscuring the path of the injection dye. Further to this there is limited application of these animal models to humans. Despite the limitations of animal models, there are currently no *in vitro* models dedicated to the study of IPAD in human cerebral cells.

1.5 Therapeutics for Alzheimer's disease

There have been many attempts at developing therapeutics for the treatment of AD. Most of the drugs aim to reduce the amount of Aβ present in the brain. Some of the main targets for therapeutics are discussed below.

1.5.1 Licenced therapeutics

There are a small number of drugs that are licensed for use in the treatment of AD. Acetylcholine is a key neurotransmitter in the CNS and cholinergic neurons, located in the basal forebrain, are severely lost in AD thus reducing the levels of acetylcholine available for signalling. Cholinesterase inhibitors such as rivastigmine work by preventing the hydrolysis of acetylcholine into acetate and choline by inhibiting the action of acetylcholinesterase (Colović *et al.*, 2013; Khoury, Rajamanickam and Grossberg, 2018). This increases the availability of acetylcholine for neurons to utilise and can reduce the symptoms of AD for a limited time. Cholinesterase inhibitors are recommended for use in the early stages of AD where cognitive impairment is mild or moderate.

Memantine is also licenced for the treatment of AD. It is thought that neuronal excitotoxicity, caused by a dysfunction in glutamatergic neurotransmission, is involved in the etiology of Alzheimer's disease. Memantine is a low-affinity voltage-dependent antagonist at glutamatergic N-methyl-D-aspartate (NMDA) receptors (Zhou *et al.*, 2019). It acts by binding to the NMDA receptor and preventing prolonged Ca2+ influx, protecting against NMDA receptor-mediated excitotoxicity (Johnson and Kotermanski, 2006). Memantine is often only recommended in cases of severe AD or where cholinesterase inhibitors are ineffective or inappropriate. Like cholinesterase inhibitors, memantine is not a cure and is only used to relieve the symptoms of AD.

1.5.2 γ secretase inhibitors

γ secretase is a multi-subunit protease complex comprised of 4 key proteins: presenilin 1 or 2, nicastrin, presenilin enhancer 2 and anterior pharynx defective 1 (Wolfe, 2008). This protease complex sits within the plasma membrane and cleaves single-pass transmembrane proteins (Krishnaswamy *et al.*, 2009). The most well-known substrate of γ secretase is APP and when APP is

processed by both β and γ secretase Aβ is produced (see **Figure 1-5**). γ secretase inhibitors block the action of γ secretase, preventing the cleavage of APP and therefore the production of Aβ.

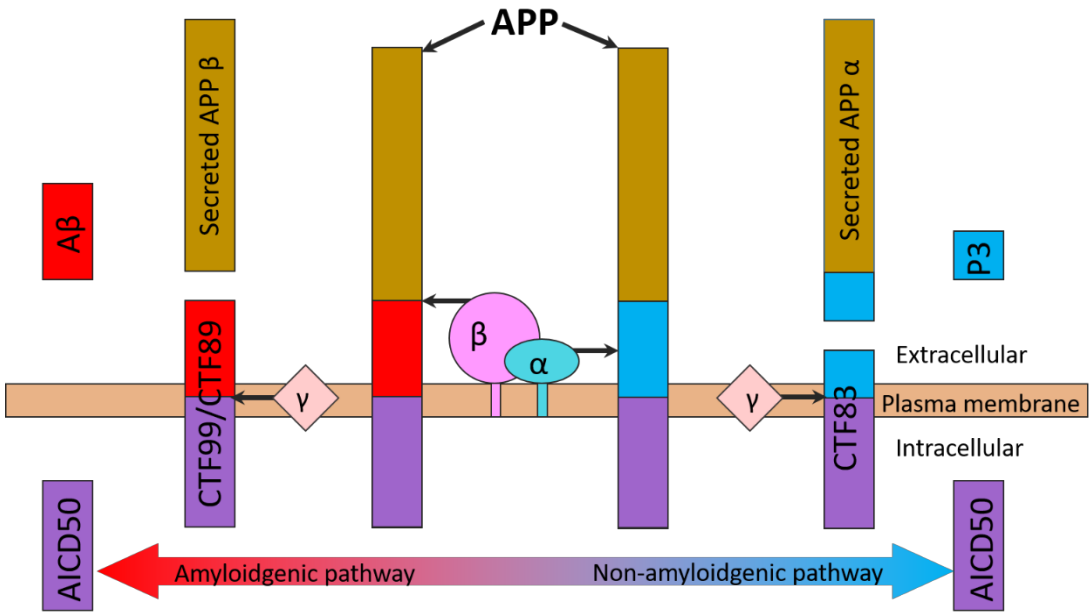

Figure 1-5 APP processing and cleavage products, adapted from (Chow et al., 2010)

The non-amyloidgenic processing of APP involves cleavage with α secretase and γ secretase. This leads to the generation of secreted APP α and CTF83, P3 and AIC50. The amyloidgenic pathway utilizes β and γ secretase cleavage of APP resulting in secreted APP β, C-terminal fragments 89 and 99 and Aβ. The Aβ fragments form oligomers and eventually fibrillise, resulting in AD pathology.

1.5.2.1 Avagacestat

Avagacestat is a γ secretase inhibitor developed by Bristol Myers Squibb. The clinical trials showed no significant differences between the avagacestat and placebo groups. Further to this avagacestat was found to have adverse dose limiting effects including increases in nonmelanoma skin cancer, reversible renal tubule effects and undesirable gastrointestinal tract events (Coric *et al.*, 2015).

γ secretase has multiple targets so it is possible that blocking its action with γ secretase inhibitors can have numerous consequences and potentially dangerous side effects. Most notably interfering with the processing of the Notch receptor by blocking γ secretase can lead to gastrointestinal toxicity and diarrhoea (Garber, 2007).

1.5.2.2 Semagacestat

After semagacestat had been shown to successfully inhibit γ secretase *in vitro* and reduce Aβ levels in the brains, CSF and plasma of transgenic mice carrying human APP with a V717F mutation (May *et al.*, 2004), Eli Lilly launched phase 3 double blind clinical trials. In August 2010, 9 months before the trial was due to finish, it was announced that semagacestat had failed the phase 3 trials. Semagacestat did not improve cognitive status and in higher doses was shown to significantly worsen functional ability, compared to the placebo (Doody *et al.*, 2013). Semagacestat was also associated with adverse side effects including a much higher incidence of skin cancer and infections in the treated group compared to the placebo (Doody *et al.*, 2013).

1.5.3 BACE1 inhibitors

Beta-site APP cleaving enzyme 1 (BACE1), also known as β secretase 1, is an aspartic acid transmembrane protease (Cole and Vassar, 2008). Its active site resides in the extracellular domain and it is has a key role in the production of myelin sheaths in nerve cells (Willem *et al.*, 2006) as well as cleavage of APP to generate Aβ (see **Figure 1-5**).

As the rate limiting step in Aβ production, BACE1 is a very promising target for therapeutic intervention. The combined efforts of academia and industry have led to the development of several BACE1 inhibitors discussed below.

1.5.3.1 Verubecestat

Verubecestat, also known as MK-8931, was developed by Merck Research Laboratories. It is a potent and selective BACE1 inhibitor and has been shown to reduce the concentration of Aβ in the brains of rats, monkeys and human subjects (Kennedy *et al.*, 2016). In February 2017, a press release from Merck announced the phase 2/3 study evaluating verubecestat as a small molecule inhibitor of BACE1 in people with mild to moderate AD was to be stopped following the recommendation of the external Data Monitoring Committee (Merck, 2017). During a safety analysis the committee determined there was 'virtually no chance of finding a positive clinical effect' (Merck, 2017).

1.5.3.2 Lanabecestat

In 2014 AstraZeneca and Eli Lilly announced the joint development of a BACE1 inhibitor known as lanabecestat, after successful phase 1 trials showed a prolonged reduction of Aβ levels in the CSF and plasma in healthy human volunteers (Cebers et al., 2017). FDA fast track designation was

assigned to lanabecestat in August 2016 but the two ongoing phase 3 clinical trials were prematurely stopped due to futility on June 12 2018 (AstraZeneca, 2018).

Despite the recent documented failures, BACE1 inhibitors continue to be a promising target for AD therapy with many more candidates still in development and clinical trials. Only time will tell if the trials reach the primary endpoints and the drugs are safe to administer.

1.5.4 Tau aggregation inhibitors

Pathological tau protein undergoes different post-translational modifications such as glycosylation, ubiquitination or hyperphosphorylation. When tau protein is abnormally phosphorylated it aggregates in filaments (Jouanne, Rault and Voisin-Chiret, 2017). The presence of these neurofibrillary tangles and tau aggregates correlate well with symptom severity and neuron loss in AD (Congdon and Sigurdsson, 2018). Preventing tau aggregation could therefore reduce neuron loss in AD.

1.5.4.1 Methylene blue

Methylene blue was the first identified tau aggregation inhibitor. It works on tau monomers, keeping them in an aggregation-incompetent formation thereby preventing the polymerization of tau (Congdon and Sigurdsson, 2018). After methylene blue was shown to successfully reduce tau pathology and improve cognition in a transgenic mouse, a reduced form with improved tolerability and absorption (LMTX) was developed for clinical trials (Wischik, Harrington and Storey, 2014). Almost 900 participants took part in the first clinical trial, taking LMTX or a placebo twice daily for 15 months. Largely the trial was a failure with no improvement in memory or brain shrinkage compared to the placebo, but interestingly in a small subset of patients on no other Alzheimer's medicine researchers reported a 30-40% reduction in brain shrinkage (Gauthier *et al.*, 2016). TauRx pharmaceuticals latest clinical trial for LMTX, LUCIDITY, is still underway (TauRX, 2020).

1.5.4.2 Curcumin

Curcumin is a polyphenol and a product of the *Curmuma longa* plant (Hewlings and Kalman, 2017) that binds to proteins in β-sheet conformation (Hu *et al.*, 2015), preventing aggregation and reducing tau pathology (Hamaguchi, Ono and Yamada, 2010). Since curcumin has been used in herbal medicine and has a long established history of safety in humans (Hewlings and Kalman, 2017) it passed quickly to phase II trials, however it was shown to have no effect on cognition or biomarkers in the CSF of patients with AD (Congdon and Sigurdsson, 2018).

1.5.5 Immunotherapy targeting amyloid beta

Immunotherapy as a potential treatment for AD was first demonstrated in 1999 after Schenk et al demonstrated that treating APP transgenic mice with a vaccine against Aβ blocked Aβ accumulation with aging (Schenk *et al.*, 1999). The success of the immunotherapy approach was a surprise to the scientific community, given the immune privileged state of the brain and its limited immune surveillance. Nevertheless, this lead to the development of a vaccine. The vaccine consisted of B and T cell epitopes. The presence of T cells in the CNS led to meningeal inflammation in some cases and this, combined with relatively low responsiveness to vaccination, led to the development of passive immunotherapy using monoclonal antibodies, some of which are discussed below.

1.5.5.1 Bapineuzimab

One of the first monoclonal antibodies to be developed for passive immunotherapy of AD was bapineuzimab. The IgG1 antibody binds fibrillar and soluble Aβ and activates microglial phagocytosis and cytokine production (ALZFORUM, 2017). Phase 1 trials demonstrated good levels of tolerance but resulted in a few MRI imaging abnormalities (Black *et al.*, 2010) which became known as amyloid-related imaging abnormalities (ARIA). Despite negative phase 2 trials (Salloway *et al.*, 2009), phase 3 trials were initiated based in a prespecified exploratory analyses. All phase 3 trials were terminated in August 2012 due to studies showing no clinical benefit (ClinicalTrials.gov, 2017). Patients in the initial phase 1 trials were followed up and many came to autopsy. The Southampton group led by James Nicoll issued multiple reports on analyses from these specimens (Nicoll *et al.*, 2003; Nicoll *et al.*, 2006; Holmes *et al.*, 2008). Despite a time-dependent removal of amyloid plaques, there were no cognitive benefits associated with this Aβ clearance (Holmes *et al.*, 2008).

1.5.5.2 Solanezumab

The monoclonal antibody solanezumab, developed by Eli Lilly, made headlines in 2016 by failing to meet the primary endpoint in its phase 3 clinical trials (McCartney, 2015). Patients treated with solanezumab showed no significant slowing of cognitive decline compared to patients treated with a placebo (Lilly, 2016). As a result, Eli Lilly chose to not pursue regulatory submissions and solanezumab will not be used to treat cognitive decline in AD.

1.5.5.3 Aducanumab

Aducanumab, developed by Biogen, came about after screening libraries of human memory B cells for reactivity against aggregated Aβ (Sevigny et al., 2016).The human monoclonal antibody

selectively reacts with Aβ aggregates, including soluble oligomers and insoluble fibrils (Sevigny et al., 2016). Animal studies involving transgenic mice have shown that aducanumab is capable of crossing the blood–brain barrier, engaging its target, and clearing Aβ (Sevigny et al., 2016). Phase 1b clinical trials also showed success in shrinking the Aβ plaques, prompting the launch of 2 large phase 3 trials. There were however a series of adverse side-effects reported including infections of the urinary and upper respiratory tract and amyloid related imaging abnormalities (ARIA), suggesting a deficiency in clearing excess fluid (Sevigny et al., 2016). In March 2019 A futility analysis concluded that the phase 3 trials would not reach their primary endpoint and Biogen halted the trials on 21st March 2019 (Fagan, 2019). Despite the premature end to the phase 3 trials, Biogen announced a new set of statistical analyses that led to submitting aducanumab to the FDA for approval on 22nd October 2019 (Bigica, 2019).

1.5.5.4 Summary of immunotherapy targeting amyloid beta

The immunotherapy strategies for treating AD with antibodies currently focuses on targeting and breaking down the amyloid plaques, however it has been shown that there is no clinical benefit to removal of these plaques and it is likely the disturbance of Aβ plaques increases the amyloid load on an already compromised drainage system, worsening the effects of CAA and accelerating cognitive decline. Nicoll et al have hypothesised a sequence of events that occur after immunotherapy: (1) Anti-Aβ antibodies enter the brain and bind to plaques solubilising the Aβ. (2) The solubilised Aβ diffuses through the brain parenchyma and enters IPAD pathways leading to increased CAA. (3) Affected blood vessels are dysfunctional and, either through ischaemia or impaired drainage of extracellular fluid, result in alteration of the white matter (Weller, Boche and Nicoll, 2009). Nonetheless, the treatment of AD with immunotherapy is a promising one and there have been cases reported where patients had virtually complete absence of Aβ plaques and CAA indicating that given time Aβ can eventually be cleared from the vasculature of the brain (Boche *et al.*, 2008).

1.5.6 Immunotherapy targeting tau

More recently immunotherapy strategies have also been applied to target tau pathology. Currently there are eight tau immunotherapy trials in clinical testing, two are active and six are passive (Sigurdsson, 2018). The most well documented example is the active vaccine AADvac1 developed by Axon neuroscience.

1.5.6.1 AADvac1

AADvac1 is a synthetic peptide made up of amino acids 294-305 of the tau protein couple to a keyhole limpet hemocyanin. It was designed to elicit an immune response against pathologically altered tau. The phase I trials showed AADvac1 had a favourable safety profile, with the exception of injection site reactions, and good immunogenicity(Novak *et al.*, 2017) further trials have shown the vaccine was highly immunogenic in humans and resulted in the production of IgG antibodies against the tau peptide in almost all patients with mild-to-moderate Alzheimer's in the trial (Novak et al., 2019). The results of the first phase II safety trial seemed to indicate no cognitive benefit however there was a trend toward a slower decline in a small subset of the treatment group and a slowing of cortical atrophy (NIH, 2019). Phase II trials for Alzheimer's patients are ongoing.

1.5.7 Alternative approaches

Instead of focusing on the removal of Aβ by directly targeting it, alternative therapies are being developed that aim to rescue the clearance mechanisms of the brain. It has been shown that the contraction of smooth muscle cells is the most likely driving force for IPAD (Aldea *et al.*, 2019) and that this is one of that last clearance systems to fail (Shibata *et al.*, 2000). Smooth muscle cell contraction decreases with age (Tumer *et al.*, 2014; Seawright *et al.*, 2018) which may contribute to its failure. The contraction of smooth muscle cells is driven by adrenergic innervation (Purkayastha and Raven, 2011) so targeting the adrenergic receptors on the surface of smooth muscle cells may help to restore the contractility of the smooth muscle cells and rescue IPAD. There are a few candidates for this approach and they are discussed below.

1.5.7.1 Prazosin

Prazosin is an α1 adrenergic receptor antagonist that is licensed in the treatment of hypertension (2012). Prazosin has also been used to treat post-traumatic stress disorder (De Berardis *et al.*, 2015). A small randomised trial in 2009 showed that prazosin significantly reduced agitation and aggression in Alzheimer's disease patients (Wang *et al.*, 2009) and experimental studies have shown that prazosin was able to reduce the generation of Aβ in mouse neuroblastoma cells and improve memory deficits in APP23 transgenic mice over time (Katsouri *et al.*, 2013). Further clinical trials are needed to see if memory deficits can be improved in Alzheimer's patients.

1.5.7.2 Mesedin

Mesedin is an α2 adrenergic receptor antagonist that has been shown to have neuroprotective, neurogenic and anti-amyloidgenic properties in primary astrocyte cultures (Melkonyan *et al.*,

2017). Mesedin also increased choline acetyltranferase and neprilysin in wild type primary astrocyte cultures (Melkonyan *et al.*, 2017). Further *in vivo* experimental studies are required to assess the full therapeutic significance of these findings.

It is currently unclear if targeting adrenergic receptor activity will have the desired effect on IPAD and further trials need to be carried out to ascertain the exact mechanism of action of these adrenergic receptor drugs but initial findings are promising. Targeting cholinergic and glutamatergic signalling has led to some success in the treatment of the symptom of AD so perhaps investigating adrenergic signalling will yield better results for the treatment of AD.

1.5.8 Summary of therapeutic strategies

Although there are constantly new and evolving strategies for the development of therapeutics for the treatment of AD, there is still currently no effective treatment or cure. Currently licenced treatments only focus on treating the symptoms of the disease and offer short term relief only. Despite the efforts of numerous pharmaceutical companies and countless hours of research

Every minute of every day seven animals are used in research in the UK, totalling 3.5 million animals in 2018 (Office, 2018). Animal testing is an obligatory stage in the process of obtaining regulatory approval for new drugs (EU Directive 2001/83/EC relating to Medicinal Products for Human Use). The exact portion of animals dedicated to Alzheimer's disease therapeutics is unknown however it is clear that a very large number of animals have been used in the development of therapeutics for AD that have ultimately failed in clinical trials.

Computational models and *in vitro* models could be used in place of animal experiments in initial pre-clinical testing to highlight drugs with a favourable outcome and rule out those with detrimental effects. Utilising these approaches would greatly reduce the number of animals used in the early stages of drug discovery. AD has a strong vascular component and most AD cases show significant Aβ deposition in the vessel wall (Brenowitz *et al.*, 2015). Therapeutics to treat AD must target not only plaques, as is the case with immunotherapy, but also improve the CAA in the vessel walls. Development of an *in vitro* model of the cerebrovasculature could therefore prove useful in the pre-clinical testing of potential drug candidates, helping to reduce the number of animals used in pursuit of a drug to cure AD. The development of a novel *in vitro* model of IPAD aligns strongly with the mission statement of NC3Rs to replace, refine and reduce the number of animals used in research.

1.6 Structure of cerebral blood vessel

When developing an *in vitro* model it is important to take into account the correct cellular arrangement to accurately reproduce the *in vivo* environment. The morphology of cerebral blood vessels is summarised below (see **Figure 1-6**)

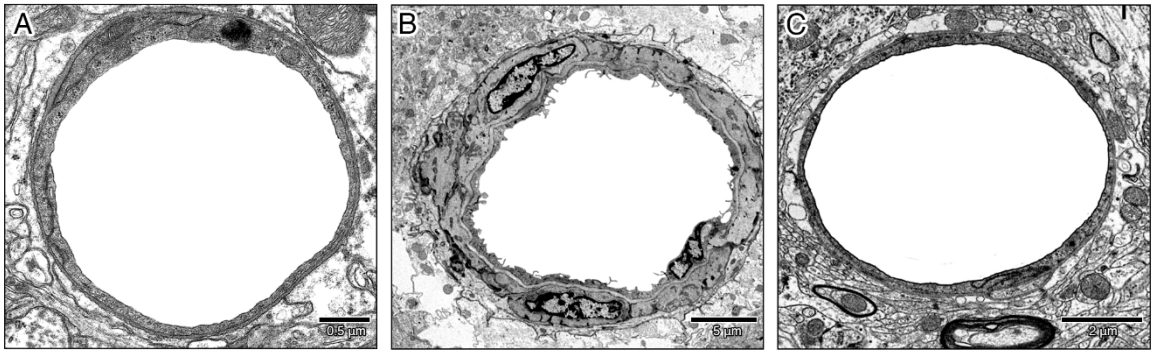

Figure 1-6 electron micrographs of cerebral blood vessels (images obtained from Matthew Sharp)

Capillaries are the smallest blood vessels (a) and are composed of a single endothelial layer and basement membrane. Mural cells such as pericytes may be associated with the endothelial basement membrane. Arteries (b) are larger and have much thicker walls that include an internal elastic lamina and at least one layer of smooth muscle cells. Veins (c) appear very similar in anatomy to capillaries though they tend to be much larger.

1.6.1 The neurovascular unit

The neurovascular unit is a concept first described by Harder (Harder, Zhang and Gebremedhin, 2002). It is defined as a structure composed of cerebral endothelial cells, neurons, astrocytes, basal lamina covered with smooth muscle cells or pericytes and extracellular matrix. A simple diagram depicting part of the neurovascular unit is shown below in **Figure 1-7**. Each component in the neurovascular unit is linked leading to a highly organised and efficient system for the regulation of cerebral blood flow (Abbott and Friedman, 2012). A simple diagram showing a cross-section of a capillary and arteriole highlights the arrangement of cells in the cerebrovasculature (**Figure 1-8**).

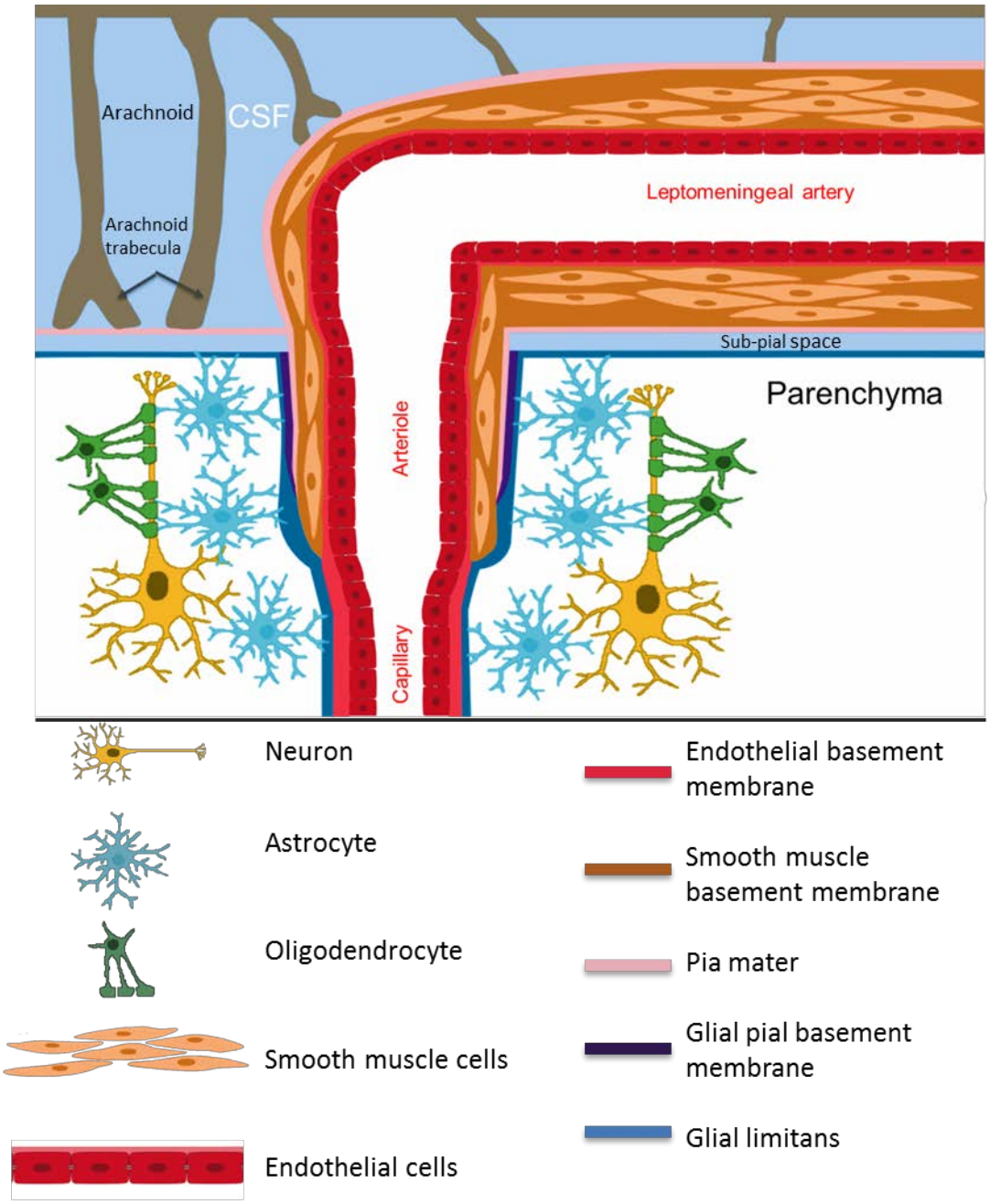

Figure 1-7 – The neurovascular unit

As the leptomeningeal artery at the surface of the brain penetrates the parenchyma it takes with it a layer of pia mater. The multiple layers of smooth muscle cells become one layer in arterioles and eventually diminish in capillaries. Astrocytes line the vessel wall and are connected to neurons which are in turn insulated by oligodendrocytes. Pericytes (not shown) sit within the endothelial basement membrane (shown in red) and make contact with the endothelial cells.

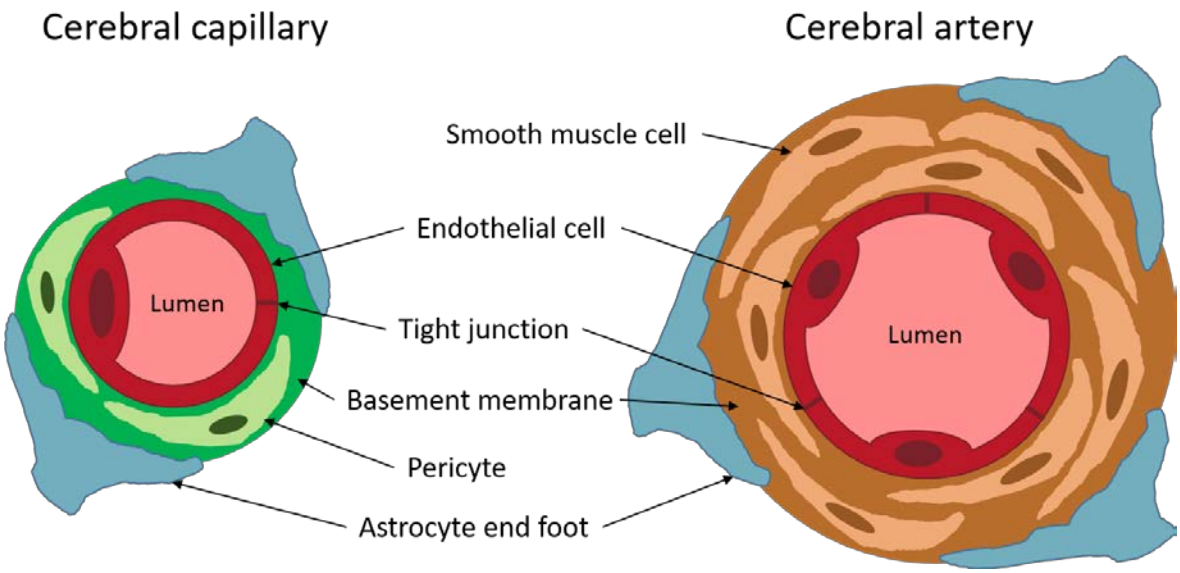

Figure 1-8 schematic diagram of the cross section of a cerebral capillary and arteriole

From the centre a cerebral capillary contains: a lumen (pink), endothelial cells (shown in red) joined by tight junctions, pericytes (light green) embedded in the cerebrovascular basement membrane (dark green) and astrocyte end feet (blue). From the centre a cerebral artery contains: a lumen (pink), endothelial cells (red) joined by tight junctions, several layers of smooth muscle cells (light brown) surrounded by cerebrovascular basement membrane (brown) and astrocyte end feet (blue).

1.6.2 Structure of cerebral artery

Cerebral arteries are comprised of an intact layer of endothelial cells, joined by tight junctions, forming the luminal aspect of the vessel. The wall of cerebral arteries is composed of three layers: a single layer of endothelial cells and the internal elastic lamina, the tunica media which contains layers of smooth muscle cells and their associated basement membrane and the tunica adventitia made up of associated cells such as perivascular nerves and astrocytic end feet (Cipolla, 2009).

1.6.3 Structure of cerebral capillary

Capillaries are the smallest of the cerebral vessels and the walls of cerebral capillaries are formed of an endothelium, joined by tight junctions, and a basement membrane. Astrocytic end feet surround the abluminal capillary surface and are separated from the endothelium by the endothelial basement membrane and their own glial basement membrane. The endothelial and glial basement membranes are mostly fused and inly separate to accommodate mural cells named pericytes.

1.6.4 Structure of cerebral vein

Cerebral veins consist of a layer of endothelial cells and astrocytic end feet, separated by a basement membrane. Some cerebral venules have been shown to contain pericytes and smooth muscle cells. Veins of the brain are also valveless (Cipolla, 2009).

1.6.5 The difference between cerebral vessels

It can be very difficult to differentiate between the small cerebral vessels. Cerebral capillaries, arterioles and venules are all composed of a single layer of endothelial cells ensheathed by astrocytic end feet. Pericytes are embedded in the endothelial basement membrane of capillaries whereas arterioles contain at least a single layer of smooth muscle cells however there is significant crossover in the markers used to identify these cells making them difficult to distinguish. In addition venule walls may also contain smooth muscle actin-expressing cells. Cerebral vessels may accurately distinguished from one another by measuring the ratio of the lumen and the vessel wall area (MacGregor Sharp *et al.*, 2019).

1.6.6 Basement membranes

Each layer of cells in the cerebral vessel walls is separated by basement membrane. This basement membrane is a highly specialised molecular composite of collagen, non-collagenous glycoproteins and proteoglycans (Paulsson, 1992; Jayadev and Sherwood, 2017). They are formed from self-assembly of a variety of intracellularly produced proteins, which are secreted into the surrounding extracellular matrix, and form highly organised regular structures. They serve to compartmentalise various types of tissue and tissue structures, provide a scaffold for structural support of tissues and are important in modulating cellular signalling pathways (Timpl and Aumailley, 1989). Basement membranes are composed many different components with as many as fifty different basement membrane proteins identified (2008). They do however consist of a core set of proteins and are composed mainly of collagen IV, laminin, fibronectin and heparan sulphate proteoglycans, the most common of which is perlecan (Thomsen, Routhe and Moos, 2017b). The structure of a basement membrane is summarised in **Figure 1-9**. Many of the proteins that contribute to the basement membrane exist in more than one state; a good example of this is laminin. Laminins are composed of an α,β and γ chain and there are currently 5 α chains, 3 β chains and 3 γ chains that have been identified, combining into 18 currently known isoforms (Yousif, Di Russo and Sorokin, 2013b). It is becoming increasingly clear that basement membranes in different locations differ in their structural and biological properties (Paulsson,

1992; Song *et al.*, 2013; Di Russo *et al.*, 2017) so basement membranes produced by different cells of the neurovascular unit may also differ in their structure.

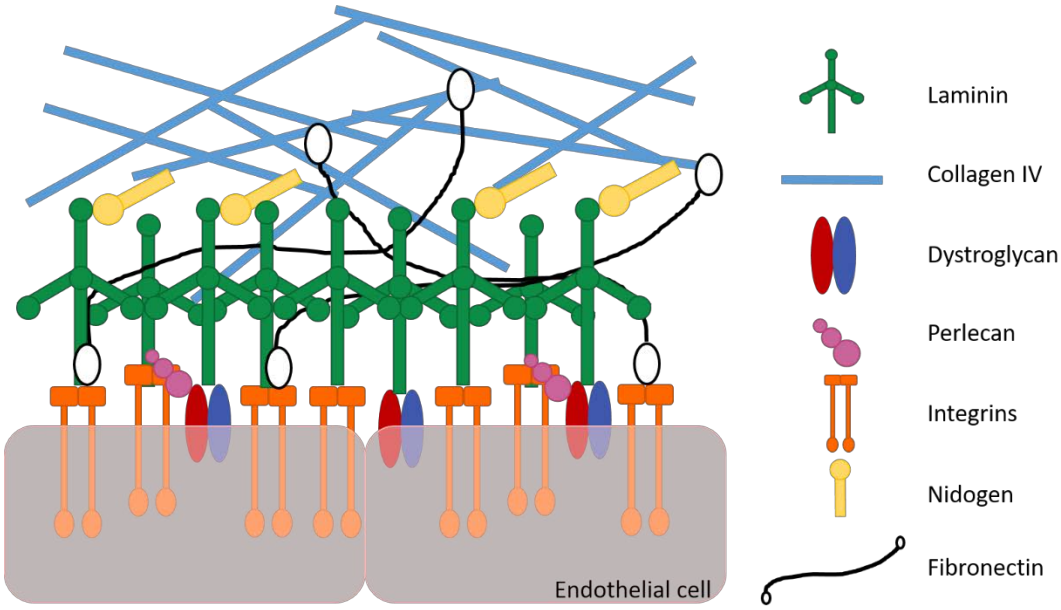

Figure 1-9 the composition and organisation of basement membranes

Assembly of the basement membrane begins when laminin binds to dystrophin-associated protein complex via α-dystroglycan and integrins (Henry and Campbell, 1998). This anchorage allows laminin to polymerise and bind nidogen. Nidogen also binds polymerised collagen IV creating a covalently stabalised network. Proteoglycans such as perlecan and agrin bind various extracellular proteins and form additional links to the cell surface via dystroglycan binding. After fibronectin binds to integrins the clustering effect allows fibronectin to form large insoluble fibrils of extracellular matrix.

1.7 *In vitro* modelling

1.7.1 *In vitro* vs *in vivo* modelling

One of the major pitfalls of *in vitro* models is oversimplification. The basic design of a monolayer monocultures is often not a true representation of the *in vivo* environment and this leads to problems with translational medicine. Results *in vitro* may not correspond to the circumstances in a living organism and therefore *in vitro* to *in vivo* extrapolation is difficult.

In vivo experiments are conducted in living organisms, most commonly small mammals such as mice and rats are used. There are several advantages and disadvantages to this approach summarised in **Table 1-2**.

Table 1-2 – advantages and disadvantages of *in vivo* experiments

Advantages of *in vivo* experiments	**Disadvantages of *in vivo* experiments**
Meet regulatory requirements for testing drugs	Expensive (breeding, nurture, experiments, disposal etc)
Model is systematic and physiologically relevant as whole organ is being used	Animals are different from humans (metabolism,
Experiments may be carried out long term	License is needed for animal experimentation
Multiple age groups can be compared to study the effect of increasing age (important for diseases of age such as dementia and cancer)	Ethical objections
More than one tissue is available for sampling as whole organism is available for testing	Personnel must be trained to handle the animals
Disease models are available*	Complications can arise during surgery and anaesthesia
Behavioural studies can be carried out	There may be problems with inherent genetic mutations in wild type animals

*Although disease models are available no amount of genetic manipulation can make a transgenic mouse human.

In contrast to *in vivo* models, the *in vitro* models are conducted on components of an organism in lab ware such as petri dishes and culture flasks. The *in vitro* approach isolates cellular components from their biological surroundings to allow for more detailed and convenient analysis on a less complex system. *In vitro* models have many advantages over *in vivo* models: they are less expensive, they do not require a licence, they do not require the sacrifice of animals and human cells can be used for human models. However one of the major pitfalls of *in vitro* models, compared to *in vivo,* is oversimplification. Their simplistic design is often not a true representation of what happens *in vivo* which leads to little relatability and problems with translational medicine. Results *in vitro* may not correspond to the circumstances in a living organism as cells in culture do not perfectly mimic cells in a living organism.

1.7.2 *In vitro* to *in vivo* extrapolation

Usually it is not possible to transpose results from *in vitro* experiments to accurately predict what happens *in vivo*; this is especially true in toxicology and pharmacology where the input of other organs can alter pharmacokinetics significantly. There are two commonly accepted solutions to allow the reliable extrapolation of *in vitro* results to *in vivo* translation.

1) Increasing the complexity of the *in vitro* models to more accurately reflect the organisation of cells and their interactions (often referred to as organ on a chip systems).
2) Using mathematical and computer modelling to simulate the system

The neurovascular unit has many cellular components that are connected and support each other therefore single cell culture will not provide a model that can be compared to a living organism. For this reason, a multi-cell model must be considered to provide a more accurate representation of the *in vivo* system.

1.7.3 Co-culture models

Individual cell cultures have limited usefulness, so models that combine multiple cell types can be used to more accurately reflect the *in vivo* environment. Cells do not grow in isolation *in vivo* and it is likely that the cells depend on secreted products from other cell types to function optimally. A good example of this is the matrix metalloproteinases (MMPs). Most MMPs are secreted in an inactive pro form and their activation is mediated by other already active MMPs. Astrocytes secrete proMMP-9 which is activated by MMP-3 however MMP-3 is not produced by astrocytes so it relies on its secretion from pericytes (Cunningham, Wetzel and Rosenberg, 2005). Tight junction formation in endothelial cells is also heavily dependent on the laminin alpha 2 secreted by astrocytes (Yousif, Di Russo and Sorokin, 2013b). Growing cells in co-culture presents many challenges because each cell type needs specialised media and coated surfaces as well as different times to reach confluence. There has been success in using co-cultures to model the brain, specifically the BBB (Lagrange *et al.*, 1999; Kido *et al.*, 2002; Garberg *et al.*, 2005; Hatherell *et al.*, 2011; Adriani *et al.*, 2015). Many of these multi-cell models use Transwell inserts or hydrogels as a scaffold to support the multiple cell layers.

The cerebral vessels have multiple cellular components. At capillary level, where IPAD commences, the cells involved are cerebrovascular endothelial cells and astrocytes. Post capillary arterioles also include layers of smooth muscle cells. Figure 8 shows the basic arrangement of cells in a cerebral capillary and post-capillary arteriole.

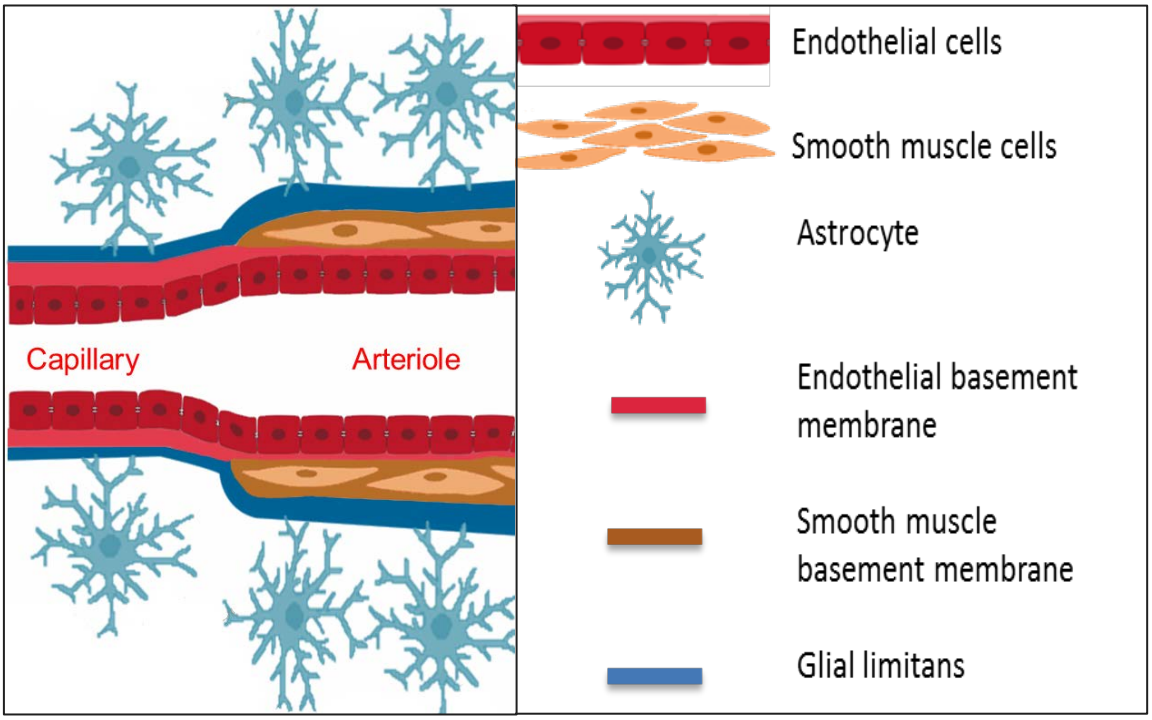

Figure 1-10 – Basic arrangement of cells in cerebral capillary and post-capillary arteriole

Astrocytes and endothelial cells along with their associated basement membranes are the basic components of cerebral capillaries. In addition to this, arterioles also have a layer of smooth muscle cells between the astrocytes and endothelial cells. This arrangement of cells will be taken into account when modelling IPAD.

Multi-cell models allow much better *in vitro* to *in vivo* extrapolation than basic single cell models as they represent the *in vivo* cellular arrangement more closely. IPAD is a dynamic process and the movement of fluid is an important factor when trying to recreate IPAD *in vitro*.

1.7.4 Microfluidics vs millifluidics

There is a lack of models of cerebral vessels that incorporate fluid flow. Such an *in vitro* model could be utilised and easily manipulated to demonstrate the situations in which IPAD fails or can be improved. Traditional cell culture makes use of laboratory ware such as multiwell plates and petri dishes that are static and do not allow the movement of fluid and so would not be suitable for a drainage study that requires a dynamic environment. One potential solution is to introduce flow using specialised systems. Depending on the size of the system and the volume of fluid it delivers these are termed either millifluidics or microfluidics.

1.7.4.1 Microfluidics

Microfluidics refers to systems that process or manipulate small amounts of fluids (typically picolitres to microlitres), using channels with dimensions of tens to hundreds of micrometres (Whitesides, 2006). For a system to fit the category of microfluidic at least one of the dimensions must be in the micrometre range. A microfluidic chip is comprised of a set of micro-channels etched or molded into a material, typically silicon or medical grade polymers such as polydimethylsiloxane (PDMS).

There are several advantages to microfluidics over traditional static cell culture. The most obvious is the ability to apply laminar flow, allowing a more accurate representation of the *in vivo* environment. The small volume of microfluidics systems makes them very cost efficient as whole experiments can take place on a single chip that measures only a few centimetres. Microfluidics systems are also very adaptable and highly customisable. They can be made of a range of materials and can be connected in various configurations to a variety of inputs and outputs, such as syringes, peristaltic pumps or pressure controllers, to achieve the desired characteristics that are optimal for experiments.

Several microfluidics systems have been developed to allow the study of flow (Adriani *et al.*, 2015; Wang *et al.*, 2016) but they are very small scale, sometimes down to single cell level. The flow rates of microfluidic systems are dependent on the overall dimensions of the channel but they are slow and probably do not accurately represent fluid movement in the brain. For example Cheri et al detected speeds between 1.3µL and 4µLmin^{-1} (Cheri *et al.*, 2014) In addition the cells are particularly vulnerable to turbulence and shear stress, even at very low flow rates, due to the relatively high pressure caused by the small internal volume of the micro-channels.

1.7.4.2 Millifluidics

A millifluidics system allows the flow of millilitres of solution through systems that have dimensions in the tens to hundreds of millimetres. Millifluidics systems are typically made up of chambers similar in size to a single well of a 24 well plate and may be composed of a variety of materials similar to microfluidics.

Millifluidics are equally as customisable as microfluidics systems and can be made of a variety of materials. Millifluidics are not as cost efficient as microfluidics as much more cells are used and larger volumes are required to run the systems. Millifluidics are able to achieve higher flow rates with much lower shear stress and turbulence than microfluidics, improving the chances of cell survival.

There are very few millifluidics systems commercially available, possibly because in-house design and construction is preferential (Cheung *et al.*, 2016). Millifluidic flow systems that could potentially be used to model IPAD are discussed below.

Reprocell, a North American biotechnology company, developed the reinnervate perfusion plate to provide a low-cost perfusion system that can combine cell culture with dynamic circulation of cell culture media. The plate is based on the dimensions of a 6 well plate and is compatible with Transwell and hydrogel cultures. Flow is driven by a peristaltic pump. The major drawback of this system is the limited flexibility of the plate. There is a maximum of six wells for each experiment and there is no way to exclude wells as the media must flow through all the wells to complete the circuit. This could be very wasteful if less than six wells are needed.

Kirkstall Ltd, a British biotechnology company, has developed a millifluidics system that has been extensively tested and validated (Mazzei *et al.*, 2010; Vinci *et al.*, 2011; Vinci *et al.*, 2012) and has been shown to provide *in vivo* like conditions for cell growth. The millifluidics system contains a reservoir bottle with air filter for gas exchange, a peristaltic pump to drive the flow system and a chamber where the cells are situated. Everything is connected with tubing and luer locks, creating a closed and recirculating system. The system is highly adaptable with support for up to 10 interconnected chambers and 3 different chambers available. This millifluidics system, known as Quasi Vivo, has also been shown to improve vitality in human midbrain organoids (Berger *et al.*, 2018) and has already been tested on human cerebral cells (Miranda-Azpiazu *et al.*, 2018), It therefore represents the best choice for introducing flow to cerebral cultures to create a model of IPAD.

1.8 Aims

The overall aim of this project is to create an *in vitro* model of IPAD that may be used to study the interaction of solutes with the cerebrovasculature. IPAD is an important mechanism of clearance of Aβ from the brain and the basement membrane has a crucial role in this pathway, providing the conduit along which solutes are eliminated from the brain. There is strong evidence to suggest that the composition of the basement membrane is a key factor in cerebral vessel integrity and the development of CAA therefore the production of basement membrane proteins will be assessed throughout.

In chapter 3 the relationship between ApoE and AD will be explored by assessing the basement membrane production in ApoE2, E3 and E4 expressing astrocytes and I test the hypothesis that protein production in astrocytes is dependent on APOE genotype.

Chapter 4 focuses on examining the basement membrane profile of the individual cells of the cerebral blood vessels: endothelial cells, pericytes, smooth muscle cells and astrocytes. The smooth muscle basement membrane is morphologically distinguishable (Yousif, Di Russo and Sorokin, 2013b) and I hypothesise that it has a distinct protein composition that favours Aβ aggregation, leading to CAA.

Chapter 5 focuses on smooth muscle cells. It is evident that amyloid beta accumulation occurs between the layers of smooth muscle cells in cerebral vessels (Frackowiak, Zoltowska and Wisniewski, 1994; Keable *et al.*, 2016). Here I investigate if Aβ has an effect on the smooth muscle basement membrane by applying a flow of Aβ to smooth muscle cells in culture. I will also use hypoxia as a method of artificially aging the cells and observe if there are any age-related changes to the smooth muscle basement membrane.

In chapter 6 I investigate adrenergic receptors as a potential therapeutic target for improving IPAD and facilitating increased amyloid clearance. IPAD is thought to be driven by contraction and relaxation of the vessel wall and I suggest that a high concentration of adrenergic receptors in contractile cells provides the innervation to drive IPAD.

In the final chapter I discuss ways to improve the IPAD model to increase its physiological relevance by introducing multiple cell types in co-cultures. I also present a modified millifluidics system that may be capable of dual flow, allowing the integration of blood flow into the model as well as the flow of interstitial fluid.

Chapter 2 Materials and methods

2.1 Basic cell culture

All cell culture techniques were carried out in a class II microbiological safety cabinet (MSC) using aseptic technique. All surfaces of the MSC were sprayed with 2% chemgene and 70% ethanol before commencing any work and all external surfaces of materials were sanitised with 70% ethanol before being placed in the MSC.

Basic cell culture protocols include initiating a culture, day to day maintenance, plating cells for experiments and freezing cells for stock. More advanced cell culture techniques include different co-culture set ups.

2.1.1 Basic cell culture protocols – Mouse astrocytes

2.1.1.1 Cell source

Professor David Holtzman of Washington University School of Medicine generously donated cryovials of transgenic ApoE mouse astrocytes for use in this study. The immortalised astrocyte cultures were produced from ApoE knock-in mice expressing homozygous human APOE ε2, APOE ε3 or APOE ε4 under the control of endogenous mouse ApoE promoter according to (Sun *et al.*, 1998; Morikawa *et al.*, 2005). Human ApoE2, ApoE3 and ApoE4 cDNAs were subcloned behind a human glial fibrillary acidic protein promoter and the-apoE transgenic mice were generated in Washington by microinjection of this cDNA into fertilized mouse eggs. The founder mice, identified as transgenic by PCR and southern blot, were bred back to ApoE knock-out mice (10 backcrosses onto C57B16 background) to produce mice that expressed human ApoE in the absence of mouse ApoE (Sun *et al.*, 1998). Primary cultures of forebrain astrocytes were prepared from neonatal mice (1-2 days old) and after 7 days in culture the cells were sub-cultured and transfected with 10µg of the plasmid pSV3-neo containing the SV40 T antigen early regions and neomycin resistance gene. Geneticin was added to select successfully transfected cells. Single colonies of cells were isolated with cloning discs dipped in trypsin/EDTA and were expanded in 6-well plates before cryopreservation. The cells were supplied in cryovials for these experiments.

2.1.1.2 Media composition

The culture media for the three ApoE mouse astrocyte cell lines was composed of advanced Dulbecco's Modified Eagle's Medium (DMEM) supplemented with 10% FBS and 1% geneticin. It

was also enhanced with 1mM sodium pyruvate (Morris, 2015). Table 2-1 contains details of the composition of one bottle of culture medium (approximately 500mL).

Table 2-1 - Culture media recipe for ApoE mouse astrocytes

Media component	Supplier	Catalog number
1 bottle advanced DMEM	Gibco- Thermo Fisher Scientific	#12491-015
50mL FBS	Gibco- Thermo Fisher Scientific	# 10270-106
5mL sodium pyruvate (100mM)	Gibco- Thermo Fisher Scientific	#11360-070
2mL geneticin (50mg/mL)	Gibco- Thermo Fisher Scientific	#10131-035

2.1.1.3 Resurrecting cells

Once the cryovial was removed from liquid nitrogen storage it was rapidly thawed in a 37^{o}C water bath. 1mL of pre-warmed media was slowly added to the cryovial to prevent osmotic shock and the content was then transferred to a labelled T-75 flask containing 10mL pre-warmed media. Flasks were transferred to a 37^{o}C incubator with 5% CO_2. After 24 hours the media was replaced to remove residual dimethyl sulphoxide (DMSO). Cells were monitored and the media changed every 3 days until cells were near confluence, at which point they were either passaged into new flasks or plated onto coverslips for experiments.

2.1.1.4 Passaging/subculturing cells

Passaging of cells was performed when they approached confluence (typically > 80% of culture surface covered). To passage cells, depleted medium was removed from the flask and sterile PBS was used to remove any cell debris and any remaining media. 1mL 0.25% trypsin/EDTA solution (ThermoFisher #25200-072) was added for approximately 2 minutes to digest the anchorage proteins such as integrins. Digestion was monitored with a phase contrast microscope and once cells were detached from substratum the trypsin/EDTA solution was neutralised by adding 5mL media. The solution of cell suspension was split evenly between 3 labelled T-75 flasks containing 10mL fresh pre-warmed media to achieve a 1:3 split ratio. Flasks were labelled with the date and passage number and returned to a 37^{o}C incubator with 5% CO_2.

2.1.1.5 Plating/seeding cells

Plating of cells was also performed at >80% confluence and often in conjunction with passaging. The protocol for plating cells was the same as passaging the cells whereby depleted medium was

removed and cell debris washed away with sterile PBS before the cells were dissociated with 0.25% trypsin/EDTA solution. Once the trypsin/EDTA solution was neutralised, the entire contents of the flask were transferred to a 15mL centrifuge tube and the cell suspension was centrifuged at 1000g for 5 minutes. The centrifugation produced a cell pellet and supernatant. The supernatant was discarded and the cell pellet was resuspended in 1mL culture media. 10µL of the cell suspension was combined with an equal volume of trypan blue and the combined solution was loaded into a haemocytometer for counting cells. This produced an approximate number of cells contained in the cell suspension and using the equation below the volume of cell suspension for a given cell density was calculated. Seeding densities ranged from $0.1x10^5$ to $2x10^5$ cells per 12mm glass coverslip (in a 24 well plate).

The calculated volume of cell suspension was then added to a 24 well plate that contained 1mL pre-warmed media and a 12mm round glass coverslips in each of the wells.

$$\frac{\text{Desired cell number}}{\text{Current cell number (as calculated from cell count)}} \times 1000 = \text{volume of cell suspension needed (µl) to achieve desired cell number}$$

Equation 1 - Equation to calculate the volume required for seeding density

2.1.1.6 Freezing cells

To ensure maintenance of a stock of cryopreserved cells, after initial expansion of the cells, some were frozen for long term storage in liquid nitrogen. The protocol for freezing cells was the same as for plating but with the addition of 10% DMSO (Sigma Aldrich, C6164) into the culture media. A cell density of $5x10^5$ cells per 1mL cryovial was chosen and the cryovials were placed in a freezing container (Sigma Aldrich, C1562) overnight at -80°C to promote a slow controlled decrease in temperature of 1°C per minute; this reduced the possibility of ice crystal formation. The cryovials were then transferred to liquid nitrogen for long term storage.

2.1.2 Basic cell culture protocols - Human primary cells

2.1.2.1 Cell source

Human astrocytes (HA), human brain vascular smooth muscle cells (HBVSMC) and human pericytes (HP) were purchased from Sciencell (#1800, #1100 and #1200 respectively). These cells were isolated from human brain (cerebral cortex) and were cryopreserved at passage one. They were delivered frozen in a cryovial containing a specified number of cells in 1 mL volume

(Sciencell, 2017). The HA and HBVSMC are guaranteed to retain properties for 10 population doublings and the HP up to 15 so the cells were used within these parameters for all experiments.

2.1.2.2 Media composition

The manufacturer recommended medium was used for each of the cells. The medium consisted of a bottle of specific basal medium and additional growth supplement as well as FBS and penicillin/streptomycin to be added as required.

Table 2-2 - Culture media recipe for human primary cells

	Media component	**Supplier**	**Catalog number**
Culture media for human astrocytes	Astrocyte basal medium	Sciencell	#1801-b
	10 mL FBS	Sciencell	#0010
	5mL astrocyte growth supplement	Sciencell	#1852
	5mL penicillin/streptomycin	Sciencell	#0503
Culture media for human brain vascular smooth muscle cells	Smooth muscle cell basal medium	Sciencell	#1101-b
	10 mL FBS	Sciencell	#0010
	5mL smooth muscle cell growth supplement	Sciencell	#1152
	5mL penicillin/streptomycin	Sciencell	#0503
Culture media for human pericytes	pericyte basal medium	Sciencell	#1201-b
	10 mL FBS	Sciencell	#0010
	5mL pericyte growth supplement	Sciencell	#1252
	5mL penicillin/streptomycin	Sciencell	#0503

2.1.2.3 Coating for culture surfaces

Sciencell recommends the use of 2µg/cm^2 poly-L-lysine to coat all surfaces that the cells are grown on (flask, coverslips etc) to promote cell attachment. For a T-75 culture flask poly-L-lysine coating was achieved by adding 10mL of sterile water and 15µl of poly-L-lysine stock solution (Sciencell, #0413) and incubating at 37^{o}C for a minimum of 1 hour. Coverslips were coated by submerging in a solution of 10mL of sterile water and 15µL of poly-L-lysine stock solution made up in a petri dish and incubating at 37^{o}C for 1 hour.

2.1.2.4 Resurrecting cells

A T-75 flask was coated with poly-L-lysine as directed in section 2.1.2.3. The flask was rinsed twice with sterile water and 15mL pre-warmed culture media was added. A frozen cryovial of cells was retrieved from liquid nitrogen and immersed in a 37^{o}C waterbath. Whilst keeping hold of the cryovial, it was gently rotated until the contents completely thawed. The contents of the cryovials were then gently re-suspended and dispensed into the poly-L-lysine coated T-75 flask. After 24 hours the media was replaced to remove any residual DMSO. Cells were monitored and the media changed every other day until cells were approximately 90% confluent, at which point they were either passaged into new flasks or plated onto coverslips for experiments.

2.1.2.5 Passaging/subculturing cells

Coated flasks are prepared prior to subculturing. Reagents such as media, DPBS and trypsin/EDTA solution were warmed to room temperature. Cells were rinsed twice with DPBS. 2mL 0.25% trypsin/EDTA solution (Thermo Fisher, #25200-072) and 8mL DPBS (Sciencell, #0303) was added and the flask was rocked to ensure even coverage before being placed in a 37^{o}C incubator for 2 minutes. After 2 minutes cell detachment was checked using a phase contrast microscope and if necessary the flask was gently tapped to aid with detachment. Once the cells were detached 5mL FBS was added to the flask to neutralise the trypsin and the contents of the flask was transferred to a centrifuge tube and centrifuged for 5 minutes at 1000g. The supernatant was discarded and the cell pellet was resuspended in 1mL media. The cell suspension was split evenly between three new coated T-75 flasks containing 15mL pre-warmed media. Flasks were labelled with the date and passage number and returned to the 37^{o}C incubator with 5% CO_2.

2.1.2.6 Plating/seeding cells

Prior to plating cells, 12mm round glass coverslips were coated with poly-L-lysine as directed in section 2.1.2.3. The coverslips were transferred to a 24 well plate and 1mL media was added to each well that contained a coverslip. Plating of cells was often done alongside passaging as the protocols were the same up until the centrifugation. After the cell pellet was re-suspended in 1mL media, 10µL cell suspension was combined with 10µL trypan blue and the solution was loaded into a haemocytometer and a cell count was performed. Using Equation 1 the volume of cell suspension for a required density was calculated and this was added to the coverslips in the 24 well plate prepared earlier. The plate was gently agitated to spread the cells evenly then it was returned to the 37°C incubator with 5% CO_2. Seeding densities ranged from $1x10^4$ to $2x10^5$ cells per coverslip.

2.1.2.7 Freezing cells

Only one cryovial of cells was purchased so to produce a stock of cells in cryostorage, after initial expansion of the cells, some were frozen for long term storage in liquid nitrogen. The protocol for freezing cells was the same as for plating but with the addition of 10% DMSO (Sigma Aldrich, C6164) into the culture media. A cell density of $1x10^6$ cells per 1mL cryovial was chosen. The required volume of cell suspension was added to a cryovial and topped up to 1mL with freezing media (culture media supplemented with 10% DMSO). The cryovials were placed in a freezing container (Sigma Aldrich, C1562) overnight at -80°C to promote a slow controlled decrease in temperature of 1°C per minute; this reduced the possibility of ice crystal formation. The cryovials were then transferred to liquid nitrogen for long term storage.

2.1.3 Basic cell culture protocols – Human cell line

Probably the most important part of any blood vessel is the interior lining. Known as the endothelium, it serves as the interface between the circulating blood and the rest of the vessel wall. Endothelial cells are a specialised squamous cell that forms the interior of blood vessels, creating the endothelium. Vascular endothelial cells line the entire circulatory system but the endothelial cells that line the cerebral blood vessels are unique. At the interface between the blood and the brain, endothelial cells join together and form tight junctions. Through zonula occludens-1 (ZO-1) anchorage into the endothelial cells, transmembrane proteins such as occludin, claudin and junctional adhesion protein (JAM) form these tight junctions (Anderson and

Van Itallie, 2009), creating a selective barrier that isolates the brain from the blood. This BBB is responsible for the immune privileged state of the brain.

Because of their unique ability to regulate the passage of molecules and cells, cerebral endothelial cells must be used for this study. Endothelial cells isolated from other more readily accessible organs will not form tight junctions and will lack the phenotypic properties of brain endothelium. Although it is possible to isolate primary cerebrovascular endothelial cells from temporal tissue removed during epilepsy surgery (Bernas *et al.*, 2010) it is difficult to obtain a pure uncontaminated culture. Furthermore, the cells cannot be passaged and very rapidly lose their phenotype. As a result a genetically modified cell line that can retain the phenotypic properties of cerebrovascular endothelial cells, most notably the ability to form tight junctions, throughout several generations, was selected for this study.

2.1.3.1 Cell source

The human cerebral microvascular endothelial cell line (hCMEC/D3) was purchased from Sigma Millipore, formerly Merck Millipore (#SCC006). They were received frozen in a cryovial that contained ≥1X10^6 viable cells at passage 25. The hCMEC/D3 was isolated from human temporal lobe microvessels and was immortalised with human telomerase reverse transcriptase and SV40 large T antigen. These cells were extensively characterised for brain endothelial phenotype and these properties were guaranteed for 10 population doublings so were used up to p35.

2.1.3.2 Media composition

The recommended media for hCMEC/D3 is comprised of EndoGRO basal medium and supplement kit enhanced with 1ng/mL basic fibroblast growth factor (bFGF) and 1% penicillin-streptomycin. Table 8 contains the necessary details to make 1 bottle of culture medium.

Table 2-3 - Culture media recipe for hCMEC/D3

Media component	Supplier	Catalog number
1 bottle EndoGRO basal medium	Millipore Sigma	#SCME-BM
1mL EndoGRO-LS supplement	Millipore Sigma	#SCME004-S
0.5mL rhEGF	Millipore Sigma	#SCME004-S
25mL L-glutamine	Millipore Sigma	#SCME004-S
0.5mL hydrocortisone hemisuccinate	Millipore Sigma	#SCME004-S
0.5mL heparin sulphate	Millipore Sigma	#SCME004-S
0.5mL ascorbic acid	Millipore Sigma	#SCME004-S
25mL FBS	Millipore Sigma	#SCME004-S
2.5mL bFGF solution (50µg/mL)	Sigma	#F0291
5mL penicillin-streptomycin (10000 µg/mL)	Gibco- Thermo Fisher Scientific	#15140-122

* note all components in bold are available to purchase as a kit (Millipore, #SCME-004)

2.1.3.3 Coating for culture surfaces

hCMEC/D3 exhibit contact inhibition when cultured on collagen type I or type IV, allowing confluent monolayers to form. Collagen IV is a principal component of the basement membrane and will be included in the immunocytochemical staining, therefore collagen I will be used for coating to prevent interference with the staining.

For collagen I coating, rat tail collagen I (Santa Cruz, sc-136157) was added to a solution of 0.02N acetic acid to a working concentration of 50µg/mL. This diluted collagen I solution was added to culture surfaces such as a T-75 flask for 1 hour at room temperature. Surfaces were thoroughly rinsed with sterile water before use to remove residual acid traces that would be harmful to cells.

2.1.3.4 Resurrecting cells

Prior to removing cells from liquid nitrogen a T-75 flask was coated with collagen I as in section2.1.2.3 and the media was made up (shown in section 2.1.3.2 and ***Table 2-3***) and warmed to 37^{o}C. The cryovial of HCMEC/D3 cells was removed from liquid nitrogen and incubated in a 37^{o}C water bath until thawed. Viability of cells was dependant on rapid and complete thawing so this process was carried out in a timely manner. The contents of the cryovial was transferred to a

15mL centrifuge tube and 9mL pre-warmed media was slowly added dropwise using a 10mL pipette. The cell suspension was slowly pipetted up and down to promote mixing before being centrifuged at 500g for 3 minute to pellet the cells. The cell pellet was resuspended in 10mL media and then added to a coated T-75 flask. The flask was labelled and stored at 37°C in a 5% CO_2 humidified incubator. Cells were monitored with medium replaced the next day and changed every 3 days thereafter until cells reached desired confluence. Once cells are 80% confluent they may be passaged or frozen and stored for later use.

2.1.3.5 Passaging/subculturing cells

After reaching the desired confluence cells could be passaged. Collagen I coated T-75 flasks were prepared beforehand and reagents were warmed to 37°C. Media was removed from the T-75 flask containing the confluent layer of hCMEC/D3 cells. The cells were rinsed gently with DPBS and 2mL 0.25% trypsin/EDTA solution (ThermoFisher #25200-072) was added to dissociate the cells. The flask was inspected with a phase contrast microscope to ensure complete detachment. 8mL pre-warmed media was added to neutralise the trypsin and the flask was gently swirled to mix the cell suspension. The cell suspension was transferred to a 15mL centrifuge tube and centrifuged for 5 minutes at 500g. The supernatant was discarded and the pellet was resuspended in 1mL media. The cell suspension was split evenly between T-75 flasks containing 10mL pre-warmed media. Split ratios ranged from 1:3 to 1:6.

2.1.3.6 Plating/seeding cells

Prior to plating cells, 12mm round glass coverslips were coated with collagen I as directed in section 2.1.3.3.plating was carried out as described in section 2.1.2.6.

2.1.3.7 Freezing cells

Only one cryovial of cells was purchased so to produce a stock of cells in cryostorage, after initial expansion of the cells, some were frozen for long term storage in liquid nitrogen. Freezing was carried out as per the protocol described in section 2.1.3.7.

2.2 Advanced cell culture

These techniques involved the use of more than one cell type to create multi-cell models. For the purposes of this project a direct co-culture refers to two different cell types plated onto the same surface and in direct contact with each other. Examples include a glass coverslip or the same side of a Transwell membrane. Indirect co-culture refers to cultures of multiple cells where the different cell types are plated on opposite sides of a Transwell membrane and are therefore not in

direct contact with each other. See **Figure 2-1** for a representation of direct and indirect co-cultures. To track the different cell populations, fluorescent nanocrystals were loaded into the cells prior to experiments commencing.

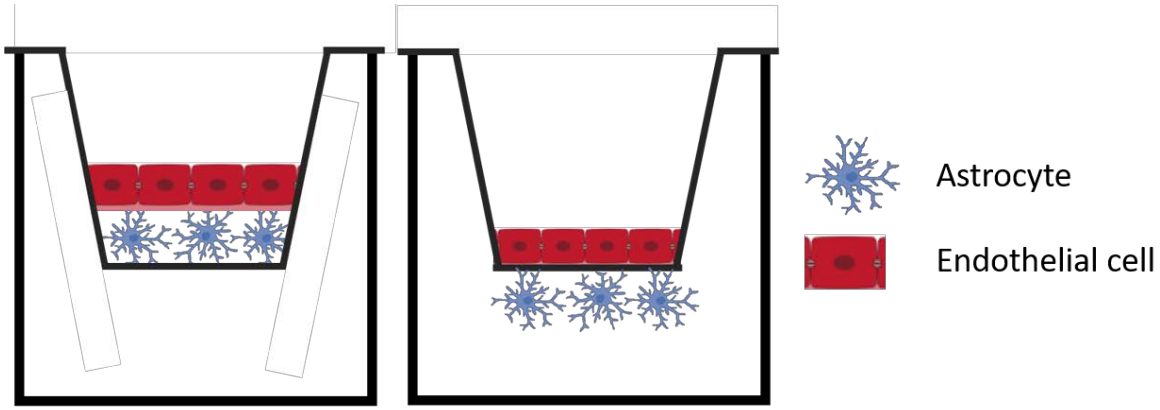

Figure 2-1 a schematic representation of a direct co-culture compared to an indirect co-culture

In a direct co-culture the cells are plated into the same compartment and cells of one type may communicate with another cell type by direct contact. In contrast, indirect co-cultures compartmentalize different cell types and a membrane keeps the cells separated. The membrane is porous and cells are still able to communicate through signalling.

2.2.1 Quantum dot nanocrystal preparation and loading

Quantum dot nanocrystals (QDs) were purchased from ThermoFisher Scientific for the purpose of labelling and tracking cell populations. The Qtracker 585 labelling kit (Q25011MP) and the Qtracker 705 labelling kit (Q25061MP) were selected for these experiment as their emission wavelengths (585nm and 705nm respectively) did not interfere with other cell stains being used.

QD solutions were prepared immediately prior to loading. Equal volumes of component A and component B were combined and thoroughly mixed then left to stand for 5 minutes at room temperature. The solution was then added to an appropriate volume of pre-warmed culture media to achieve the desired concentration (5, 10 or 20nM) and vortexed for 30 seconds. The QD solution was added to the cells and incubated at 37^{o}C for 2 hours, during this time the QDs were delivered into the cytoplasm of the cells. The QD solution was then removed and cells washed twice with complete growth medium before being replaced with fresh culture media. Depending on the experimental set-up, QDs could be loaded into cells before trypsinization in the T75 flask, or immediately after plating in a Transwell or 24-well plate. Once loaded into the live cells, QDs provided intense, stable fluorescence that is not transferrable to adjacent cells but can be passed to daughter cells through several generations, making them an ideal tool for studying co-cultures.

2.2.2 Direct co-cultures

2.2.2.1 Astrocytes and pericytes

Initial co-culture experiments were carried out on glass coverslips before moving on to Transwell inserts. Glass coverslips were sterilised and coated with poly-L-lysine as directed in section 2.1.2.3. Three different combinations of cells and media were tested: 1)Human astrocytes (HA) plated 24 hours prior to human pericytes (HP), 2) HP plated 24 hours before HA and 3) both cells plated at the same time.

1) 705-labelled QDs were loaded into HA and the cells were plated onto glass coverslips in a 24-well plate at a density of $0.5x10^5$ cells/coverslip and incubated at 37°C for 24 hours with astrocyte media. 585-labelled QDs were loaded into HP and the labelled HP were then seeded at a density of $0.5x10^5$ cells/coverslip on top of the HA. The co-culture was incubated for a further 48 hours in pericyte media.
2) 585-labelled QDs were loaded into HP and the cells were seeded at a density of $0.5x10^5$ cells/coverslip. The cells were incubated at 37°C for 24 hours with pericyte media. HA were loaded with the 705-labelled QDs and then seeded at a density of $0.5x10^5$ cells/coverslip on top of the HP. The co-culture was incubated for a further 48 hours in astrocyte media.
3) HP were loaded with the 585-labelled QDs and HA were loaded with the 705-labelled QDs. Both the HA and HP were plated onto glass coverslips in a 24-well plate at a density of $0.5x10^5$ cells/culture/coverslip. The culture was maintained with an equal ratio of astrocyte and pericyte media for 72 hours.

Transwell membranes were coated with poly-L-lysine before HP were plated onto the apical membrane at a density of $0.5x10^5$ cells/Transwell with 100µL pericyte media containing 20nM 585-labelled QDs. After 2 hours the QD solution was removed and the membrane rinsed with fresh culture media. Prior to plating, HA were loaded with 705-labelled QDs. HA were plated on top of the HP on the apical side of the Transwell membrane at a density of $0.5x10^5$ cells/Transwell. Astrocyte media was added to the apical side of the membrane and pericyte media was added to the basolateral side. The co-culture was incubated at 37°C for 72 hours before being fixed and immunostained.

2.2.2.2 Endothelial cells and astrocytes or endothelial cells and pericytes

0.4µm pore size floating Transwell inserts (Merck Millipore, MCHT24H48) were coated with poly-L-lysine as in section 2.1.2.3. 585-labelled QDs were loaded into HA or HP before plating the cells at a density of $1.2x10^4$ cells/Transwell. 200µL and 600µL of the appropriate media was added to

the apical and basolateral compartments respectively. The culture was incubated at 37°C for 48 hours. 705-labelled QDs were loaded into D3 cells prior to plating on top of the HA or HP cell layer at a density of $3x10^4$ cells/Transwell. Media was replaced with EndoGRO media and the co-culture was incubated for a further 72 hours before being fixed with 4% PFA for 10 minutes at room temperature and immunostained.

2.2.3 Indirect co-cultures

2.2.3.1 Astrocytes and pericytes

Both sides of the Transwell membranes were coated with poly-L-lysine as previously described (section 2.1.2.3). Transwells were inverted in a 12-well plate and HP were plated at a density of $0.5x10^5$ cells/Transwell onto the basolateral side with 100µL pericyte media containing 20nM QDs. The culture was incubated for 2 hours at 37°C. Transwells were then reverted to the correct orientation in a 24-well plate and astrocytes were plated into the apical compartment at a density of $0.5x10^5$ cells/Transwell. The basolateral compartment was filled with pericyte media and astrocyte media was added to the apical compartment. The culture was incubated for a further 72 hours at 37°C before being fixed and immunostained.

2.2.3.2 Endothelial cells and astrocytes or endothelial cell and pericytes

The apical side of the Transwell membrane was coated with collagen I solution (as detailed in section 2.1.3.3) for one hour at room temperature. After rinsing with sterile water, the Transwells were inverted in a 12-well plate and the basolateral side of the Transwell membrane was coated with poly-L-lysine solution (see 2.1.2.3). HA or HP were plated onto the basolateral side at a density of $1.2x10^4$ cells/Transwell with 100µL culture media containing 585-labelled QDs and left to adhere for 4 hours at 37°C. The Transwell was then returned to its correct orientation in a 24-well plate and culture media added to both compartments before incubating for a further 48 hours. 705-labelled QDs were loaded into D3 cells which were then plated into the apical compartment at a density of $3x10^4$ cells/Transwell and the apical media was replaced with EndoGRO media. The co-culture was incubated for a further 72 hours before being fixed and immunostained.

2.3 Immunocytochemistry

Cells were fixed with 4% paraformaldehyde (PFA) for 10 minutes at room temperature. The cells were rinsed 3 times with PBS and then blocked with 15% normal goat serum (NGS) for 1 hour at room temperature. Cells were then incubated with a primary antibody overnight at 4°C (see **Table**

2-4 for full antibody details). For intracellular markers, the NGS and primary antibody were diluted with PBS and 0.1% triton to permeabilise the cells. For extracellular markers permeabilisation was not necessary so PBS alone was used for dilutions. After primary antibody incubation, the cells were washed 3 times with PBS incubated with an appropriate Alexa Fluor conjugated secondary antibody for 1 hour at room temperature. The cells were then washed 3 times before 2µg/mL DAPI (Thermo Fisher, D1306) was applied for 10 minutes. Cells were rinsed 3 times with PBS and the coverslips were carefully removed from the wells with curved tweezers, inverted and mounted cell side down onto slides with Mowiol and Citifluor. In the case of Transwells, after the staining was completed the Transwell inserts were removed from the 24-well plate and inverted. The membrane was then carefully cut from the Transwell using a scalpel and mounted between two glass coverslips with Mowiol and Citifluor. This method of mounting allowed both sides of the membrane to be imaged.

Table 2-4 Details of antibodies used for immunofluorescence staining

Antibody type	**Antigen**	**Name provided by supplier**	**Supplier details**	**Optimal dilution**
Primary	Collagen IV	Rabbit anti-collagen IV (ab6586)	Anti-collagen IV antibody polyclonal produced in rabbit, AbCam, Cambridge, UK	1:400
Primary	Laminin	Anti-laminin antibody produced in rabbit (L9393)	Anti-laminin antibody polyclonal produced in rabbit, Sigma Aldrich, St Louis, USA	1:200
Primary	Fibronectin	Anti-fibronectin antibody produced in rabbit (F3648)	Anti-fibronectin antibody polyclonal produced in rabbit, Sigma Aldrich, St Louis, USA	1:400
Primary	Perlecan	Perlecan antibody (H-300) sc-25848	Perlecan (H-300) rabbit polyclonal antibody 200 µg/ml, Santa Cruz Biotechnology, Heidelberg, Germany	1:400

Antibody type	Antigen	Name provided by supplier	Supplier details	Optimal dilution
Primary	Adrenergic receptor alpha 1A	ADRA1A rabbit polyclonal antibody (#19777-1-AP)	ADRA1A-specific polyclonal antibody produced in rabbit, Proteintech, Illinois, USA	1:200
Primary	Adrenergic receptor alpha 1B	ADRA1B rabbit polyclonal antibody (#19776-1-AP)	ADRA1B-specific polyclonal antibody produced in rabbit, Proteintech, Illinois, USA	1:200
Primary	Adrenergic receptor alpha 2A	ADRA2A rabbit polyclonal antibody (#14266-1-AP)	ADRA2A-specific polyclonal antibody produced in rabbit, Proteintech, Illinois, USA	1:200
Primary	Adrenergic receptor alpha 2B	ADRA2B rabbit polyclonal antibody (#19778-1-AP)	ADRA2B-specific polyclonal antibody produced in rabbit, Proteintech, Illinois, USA	1:100
Primary	Aquaporin IV	AQP4 (H80) sc-20812	AQP4 Antibody (H-80) rabbit polyclonal antibody 200 µg/ml, Santa Cruz Biotechnology, Heidelberg, Germany	1:200
Primary	Dystrobrevin	α-Dystrobrevin (H300) sc-33161	Dystrobrevin (H-300) rabbit polyclonal antibody 200µg/ml, Santa Cruz Biotechnology, Heidelberg, Germany	1:50
Primary	TIMP 3	Anti-TIMP3 antibody (ab93637)	Anti-TIMP3 antibody polyclonal produced in rabbit, AbCam, Cambridge, UK	1:100
Primary	GFAP	Anti-GFAP antibody (Z0334)	Polyclonal rabbit anti-GFAP antibody, Dako, Glostrup, Denmark	1:250
Primary	Dystroglycan	Anti-beta dystroglycan antibody (NCL-b-DG)	Novocastra lyophilized mouse monoclonal antibody beta-dystroglycan, Leica Biosystems, Newcastle, UK	1:50

Antibody type	Antigen	Name provided by supplier	Supplier details	Optimal dilution
Primary	ApoJ (clusterin)	Rabbit anti-Apolipoprotein J antibody (ab42673)	Anti-Apolipoprotein J primary antibody polyclonal produced in rabbit, AbCam, Cambridge, UK	1:500
Secondary	Rabbit IgG	Alexa Fluor 488 goat anti-rabbit (A-21071)	Alexa Fluor 488 goat anti-rabbit IgG polyclonal, Invitrogen , Life Technologies, Paisley, UK	1:200
Secondary	Mouse IgG	Alexa Fluor 488 goat anti-mouse (R37120)	Alexa Fluor 488 goat anti-mouse IgG polyclonal, Invitrogen , Life Technologies, Paisley, UK	1:200
Primary	CD31	CD31 polyclonal antibody (ab28364)	Anti CD31 antibody polyclonal produced in rabbit, AbCam, Cambridge, UK	1 in 50
Primary	ZO-1	ZO-1 polyclonal antibody (40-2200)	Anti ZO-1rabbit polyclonal antibody 0.25mg/mL, Invitrogen , Life Technologies, Paisley, UK	1 in 100
Isotype control	Rabbit IgG	Rabbit IgG, polyclonal - Isotype Control (ab37415)	Rabbit IgG polyclonal isotype control 5mg/mL, AbCam, Cambridge, UK	1 in 2000

2.3.1 Controls for immunocytochemistry

To assess the specificity of antibody, binding controls were carried out. An IgG isotype control (AbCam, ab37415) was applied to a control well at the same protein concentration as the antibody being used. The isotype control was used to estimate the non-specific binding of target primary antibodies due to Fc binding. A negative control was also carried out which involved omitting the primary antibody on a control well to assess the non-specific binding of a secondary antibody. These controls were used to set the detector sensitivity on the confocal microscope so only genuine staining was recorded. Example images of the controls are shown in **Figure 2-2**.

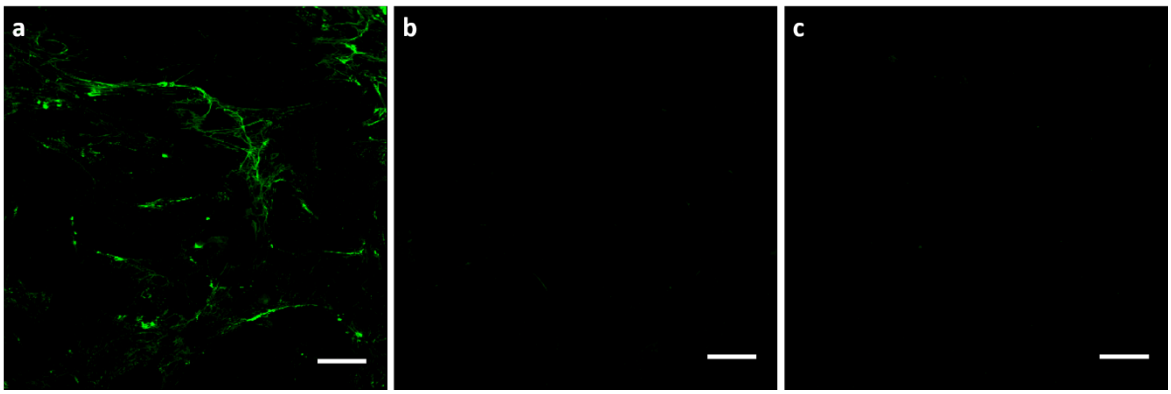

Figure 2-2 representative images of isotype and negative control compared to antibody staining

When control slides were imaged on the confocal microscope using the optimum settings the isotype control (b) and the negative control (c) appeared blank with no staining detected. Whereas the fibronectin staining (a), shown in green, is easily detected and very clear. All of these images were captured using identical settings and were from the same experimental run. Scale bar 50µm.

2.4 Processing and immunostaining for correlative light and electron microscopy

2.4.1 Optimisation

The protocol for fixing and staining the astrocytes for CLEM was adapted from (Peddie *et al.*, 2014).To optimise the protocol, various modifications were made. The fixative was composed of paraformaldehyde (PFA) and glutaraldehyde (GA). Three different ratios made up in different buffers were tested to determine which fixative gave the best result in terms of preservation and staining intensity. The fixatives used were as follows: 4% PFA and 3% GA, 2.5% PFA and 1.25% GA and 2.5% PFA and 0.5% GA. All fixatives were made up in PIPES buffer or phosphate buffer. Permeabilisation steps were removed as the protein of interest was extracellular. Antigen retrieval with TRIS-HCL buffer was also removed as it was an unnecessary step when the 2.5%PFA 0.25% GA fixative was used. Antibody incubation times were extended to strengthen the signal. A quenching step was added to combat the autofluorescence brought on by the electron beam. Sudan black and cupric sulphate were both tested as candidates for quenching. 20 indium tin oxide (ITO) coated coverslips and carrier rings were provided by Phenom World during the loan period for use with the Delphi. The carrier rings were reusable but the coverslips were not, so during optimisation normal 12mm round glass coverslips were used and coated with 7nm platinum on the sputter coater preventing electron charging. Once the protocol was optimised ITO coated coverslips were used, no other coating was required on these coverslips.

2.4.2 Finalised protocol for CLEM

Cells were plated on glass coverslips or ITO coated coverslips. After a designated time, cells were fixed with 2.5% PFA and 0.25% GA in phosphate buffer for 10 minutes at room temperature. The cells were rinsed to remove residual fixative and blocking was done with 15% NGS for 30 minutes at room temperature. The cells were incubated overnight with either laminin (Sigma, L9393) or GFAP (Dako, Z0334) antibody at 4°C. The cells were washed 3 times with PBS and goat anti-rabbit Alexa Fluor 488 secondary antibody (Invitrogen, A11034) was applied for 1 hour at room temperature. Both the primary and secondary antibodies were diluted with 15% NGS to ensure specificity by continuous blocking. Cells were quickly rinsed with distilled water and the cupric sulphate (10mM copper sulphate in 50mM ammonium acetate, pH 5.0) was added for 10 minutes to quench autofluorescence. Cells were quickly rinsed again with distilled water and 2µg/mL DAPI (Thermo Fisher, D1306) was applied for 10 minutes. DAPI is self-quenching so it was applied after the quenching step. Cells were washed 3 times with PBS and quickly rinsed in 70% ethanol. Cells were dehydrated via ethanol dilution series: 5 minutes 70%, 5 minutes 80%, 5 minutes 90%, 15 minutes 100%, and 15 minutes 100%. Coverslips were removed from wells with curved tweezers and air dried overnight in the dark. Coverslips were mounted onto carrier rings with carbon tape and sputter coated with 7nm platinum if necessary. Samples were stored in a dry dark container.

2.5 Amyloid beta and dextran preparation

The HiLyte 555 Aβ 1-40 is a synthetic protein provided by AnaSpec (#AS-60492-01) with a fluorescent tag that allows viewing by fluorescent microscopy. The sequence for this protein was as flows: HiLyte Fluor 555-DAEFRHDSGYEVHHQKLVFFAEDVGSNKGAIIGLMVGGVV; this corresponds to the human amyloid beta that is 40 amino acids in length and commonly found in CAA. The HiLyte 647 Aβ 1-42 is also provided by AnaSpec (#AS-64161) and has the following sequence: HiLyte Fluor 647-DAEFRHDSGYEVHHQKLVFFAEDVGSNKGAIIGLMVGGVVIA corresponding to the human amyloid beta commonly found in senile plaques and is 42 amino acids in length. Both products were supplied as a lyophilized powder and reconstituted with 1% ammonium hydroxide to a final concentration of 200mM before being aliquoted and stored at -80°C. Aliquots were only thawed immediately prior to use and were added directly to pre-warmed media.

Dextran was chosen as a vehicle control for flow experiments as it is biologically inert and has previously been used to demonstrate IPAD via intracerebral injection in a mouse brain (Carare *et al.*, 2008). 10kDa dextran labelled with Texas Red (D186) was purchased from ThermoFisher Scientific. The 25mg powdered dextran was dissolved in 25mL DPBS and mixed thoroughly to produce a stock solution of 100µM concentration. This stock solution was aliquoted and stored at -20^{o}C until needed.

2.6 Millifluidics flow system

Kirkstall Ltd is a biotechnology company based in Rotterham, Sheffield. Established in 2006, the main focus of Kirkstall is 'organ-on-a-chip' technology making research more human relevant and addressing the failures of traditional *in vitro* research and animal research models. Kirkstall designed a patented interconnected cell culture flow system called Quasi Vivo that was designed to introduce flow to the *in vitro* environment, with the aid of a peristaltic pump. This system was used to reproduce the intramural periarterial drainage of Aβ through cell culture models.

2.6.1 Quasi Vivo system

Quasi Vivo has many benefits including: improved cell viability, stable long term culture, close control of multiple variables and flexibility and ease of use. The models generated with Quasi Vivo are more accurate relevant than traditional cell culture making results more physiologically relevant. The system is comprised of a reservoir bottle with air filter for gas exchange, a peristaltic pump to drive the flow system and a chamber where the cells are situated (see supplementary figure 1). Everything is connected with tubing and luer locks, creating a closed and recirculating system and laminar flow is generated at the cell surface (see supplementary figure 2). The Quasi Vivo system is highly adaptable with support for up to 10 interconnected chambers.

2.6.2 Set up

The QV500 starter kit contained three chambers, a reservoir bottle with air filter, ample tubing and connectors to set up the system, as well as holding trays for the reservoir bottle and chambers. QV500 chambers and reservoir bottle were supplied sterile but the tubing and luer locks were not. A male and female connector were added to each end of the tubing and then sent for autoclaving to sterilize it. The kit was assembled by attaching an inlet tube (1/16" internal diameter) to the same size tube on the reservoir bottle and passing this through the peristaltic pump. This was then connected to a QV500 chamber (the number of chambers varied according to experimental set up) which was connected back to the reservoir bottle by an outlet tube (3/32"

internal diameter). A 0.22µm pore air filter was also connected to the reservoir bottle to allow gas exchange. The exact assembly of the system depended on the experimental set up but typically a one, two or four chamber set up was used for the experiments in this project. Before use the system was flushed with sterile PBS at maximum speed for 20 minutes as per the manufacturer's instructions.

2.6.3 Calibration

The Vernier dials on the Parker polyflex dual-head peristaltic pump are arbitrary and the flow rate they can deliver is dependent on the experimental set up, therefore the peristaltic pump required calibration for each different configuration of the quasi vivo system. Calibration for a system using one, two and four QV500 chambers was carried out (see supplementary figures 3 and 4).

To calibrate the pump the Quasi Vivo system was connected to the peristaltic pump and the reservoir bottle was filled with distilled water. The pump was switched on and allowed on fill up with water. The pump was then switched off and the weight of an empty collecting bottle was recorded. The inlet tube was disconnected from the reservoir bottle and placed in a collecting bottle (see **Figure 2-3**) to prevent the recirculation of the water. The pump was set to 100 and then switched on and a timer started. After 5 minutes the pump was switched off and the collecting bottle and water were weighed. The weight of the water dispensed was recorded. This process was repeated for every increment of 100 on the Vernier dial up to a maximum of 1000. Using the results and taking the weight of 1mL distilled water at room temperature as 0.9888g the flow rate (µL/min) can be calculated for each position of the Vernier dial. This process of calibration was carried out every time the configuration of the system was altered.

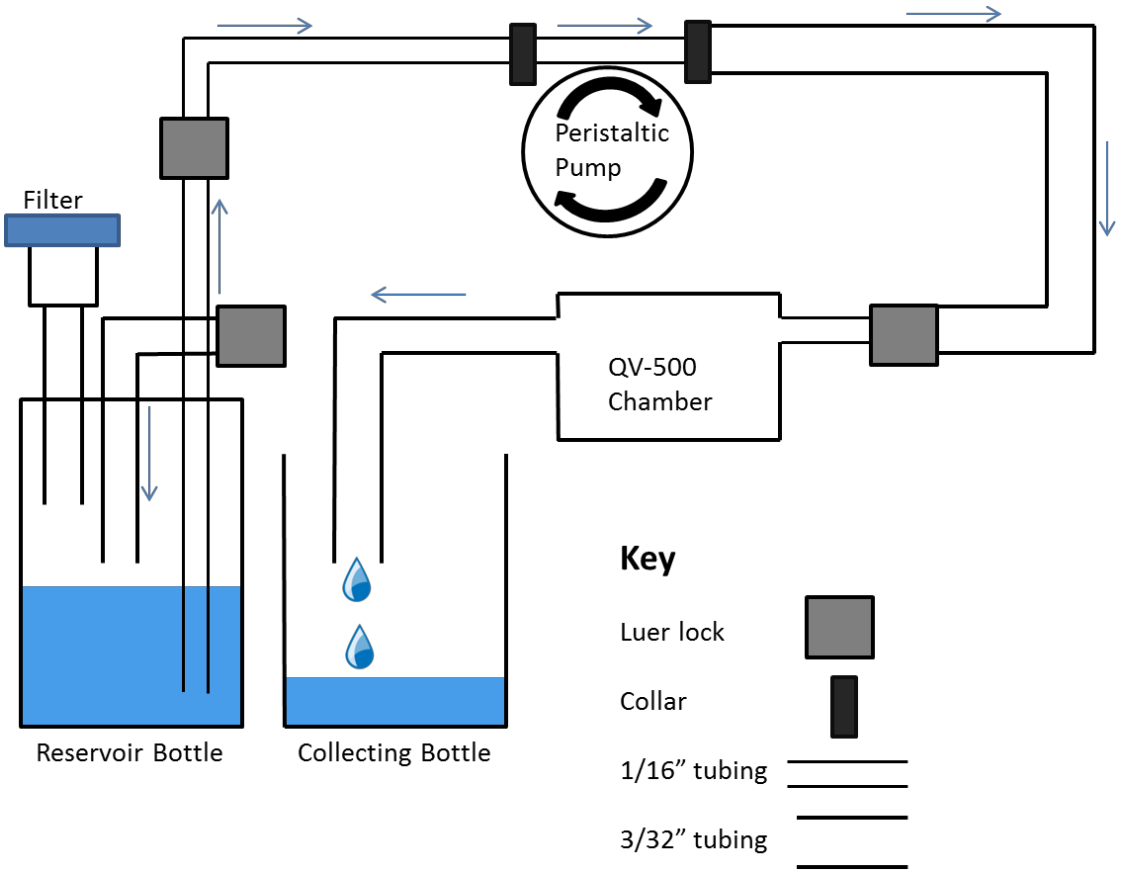

Figure 2-3 - Schematic representation of setup for calibration of Parker peristaltic pump

After initial filling of the system the coupling that allows the water to return to the reservoir bottle is detached and the end of the tubing is placed in a collecting bottle so the amount of water dispensed can be measured. This can be used to calculate the outlet flow rate and can therefore be used to set the pump to the correct speed for experiments.

2.6.4 ApoE astrocyte flow experiments

A two chamber set-up of the Quasi Vivo system was used to test the flow of amyloid beta over astrocytes expressing different isoforms of ApoE. Coverslips were sterilised and placed into a 24 well plate with 1mL astrocyte media. ApoE2, ApoE3 or ApoE4 astrocytes were counted and plated on coverslips in a 24-well plate at a density of $1x10^5$ cells per 12mm coverslip and incubated at 37°C for 24 hours to allow cells to settle and attach. After 24 hours coverslips were transferred into the QV500 chamber for a flow experiment. Astrocyte media containing 100nM HiLyte 555-labelled amyloid beta 1-40 (AnaSpec, #AS-60492-01) was added to the reservoir bottle and the system was connected to the peristaltic pump and left to run at an outlet speed of 10µL/min for 24 hours. Astrocyte media containing no amyloid beta was also tested in these experiments. The coverslips were then removed from the system and the cells were fixed with 4% PFA before immunostaining. Static experiments with cells grown on 12mm coverslips in 24 well plates were

done alongside the flow experiments with and without the addition of HiLyte 555 amyloid beta 1-40.

2.6.5 Smooth muscle cell flow experiments

A four chamber set-up of the Quasi Vivo system was used for these experiments. Coverslips were sterilised and coated with poly-L-lysine as previously mentioned in 2.1.2.3. Coverslips were placed in a 24 well plate and 1mL smooth muscle cell (SMC) medium was added to each well containing a coverslip. HBVSMC were plated onto poly-L-lysine coated coverslips at a seeding density of $5x10^4$ cells per well and incubated for 24 hours in a humidified environment (5% CO_2, 95% air) at 37°C to allow the cells to settle and attach. After 24 hours a coverslip was transferred into each of the four QV500 chambers and the remaining coverslips were left in the 24 well plate for use as static controls. Supplemented media containing either 100nM Aβ 1-40, 100nM Aβ 1-42 or 100nM 10kDa Dextran was made up. 1mL supplemented media was added to each QV500 chamber and 15mL was added to the reservoir bottle for a total of 19mL media circulating the system. Supplemented media was also added to each of the static control wells. This experiment was also run with no additional supplement in the media as a baseline for comparison. The Quasi Vivo system was connected to the peristaltic pump and the speed of the peristaltic pump was set to an outlet of 10µL/min. The Quasi Vivo system and the 24 well plate containing the static controls were returned to the incubator for a further 48 hours. Coverslips were carefully removed from the QV500 chambers and transferred to a 24 well plate. Both static and flow cells were fixed with 4% PFA for 10 minutes at room temperature and immunostained for basement membrane proteins: collagen IV, laminin, fibronectin and perlecan as previously mentioned in section 2.3.

2.7 MTS assay

CellTiter 96 aqueous one solution cell proliferation assay kit (Promega, G3582) was used to assess cell proliferation in the presence of amyloid beta and also under hypoxic conditions. An MTS assay was selected in place of an MTT assay as an MTS assay is more sensitive and is not affected by protein precipitates (Riss *et al.*, 2004). The reduction of the tetrazolium dye by NADH results in the formation of a soluble formazin product which is colormetric and the absorbance can be measured; thereby providing a measurement of metabolic activity which can be used to indicate cell proliferation. Three timepoints were chosen to monitor the proliferation of the cells over a time course: 2 hours (day 0), 24 hours (day 1) and 72 hours (day 3). Six 96-well plates were prepared as shown in **Figure 2-4**. Cells were seeded into poly-L-lysine coated wells at a density of 10^4 cells per well. Three plates were placed in a humidified environment with normoxic conditions (5% CO_2, 95% air) at 37°C and the other three plates were kept in a humidified environment with

hypoxic conditions (8% CO_2, 92% air) at 37°C. At each timepoint 20µL of MTS reagent was added to each well in the corresponding plate. The plate was wrapped in foil and incubated for a further 2 hours for the reagent to develop. Absorbance was measured at 490nm with a Fluorostar optima plate reader and the results were exported to Microsoft Excel.

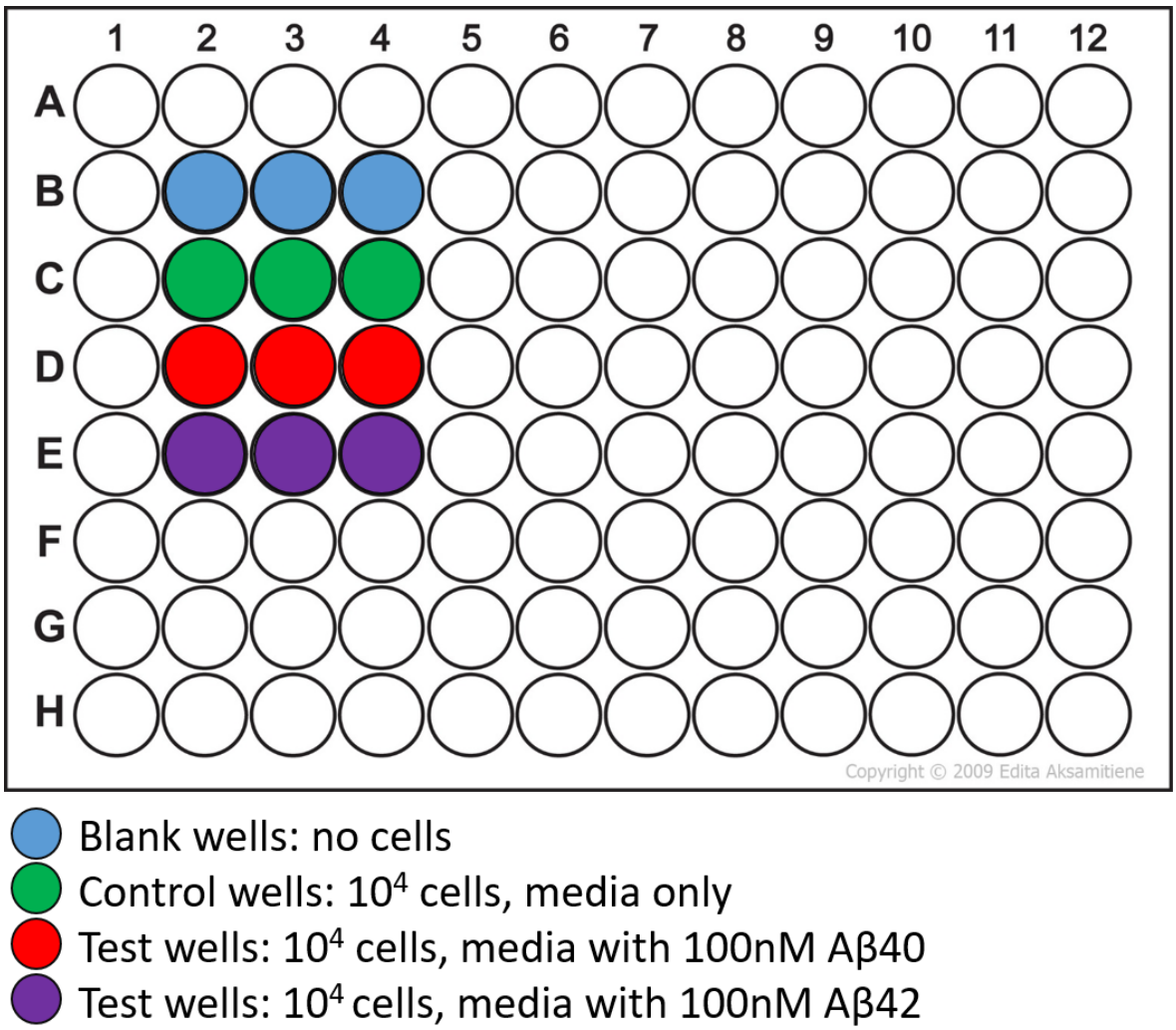

Figure 2-4 Plating for MTS assays

Each MTS plate contained 3 wells with media only as a blank measure, three wells as a control containing cells and smooth muscle cell media and six test wells which contained either Aβ 1-40 or Aβ 1-42 supplemented media.

2.8 Imaging

The purpose of imaging for this study will be to visualise the pattern of extracellular matrix proteins produced by the cells of the neurovascular unit. The different microscopes used for this study have strengths and weaknesses summarised below.

2.8.1 Fluorescence microscopy

Fluorescence microscopy uses fluorescence or phosphorescence to generate an image and that allows the study of an organic or inorganic sample. Tagging a protein of interest with a fluorochrome allows it to be visualised with the aid of a fluorescence microscope. The setup of a basic epifluorescence microscope is shown below (**Figure 2-5**).

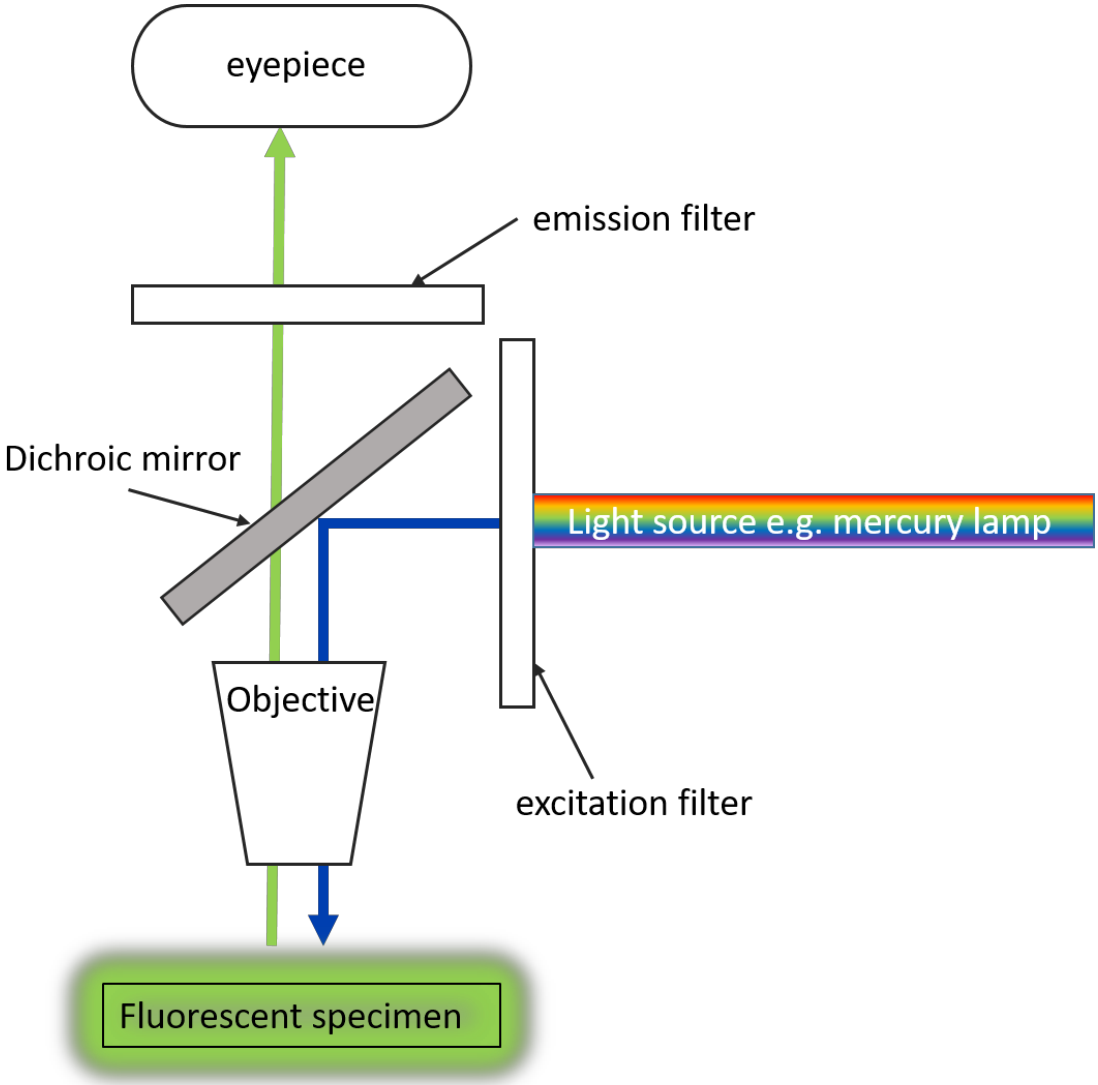

Figure 2-5 – schematic representation of a fluorescence microscope

The specimen is excited with a specific wavelength of light, selected by the excitation filter and reflected onto the sample by the dichroic mirror. This light is absorbed by the fluorophores and they emit a longer wavelength of light that will pass through the dichroic mirror. The emission filter prevents any unabsorbed light from the illumination source from passing through and ensures only the emitted fluorescence is viewed by the user.

Fluorescence microscopy is a useful tool for cell culture as it can be used for live cell imaging and identifying multiple proteins of interest in the same sample, however a more advanced type of fluorescence microscope must be used to capture the multiple channels of fluorescence.

2.8.2 Confocal microscopy

The principle of confocal microscopy was first discussed by Minsky in 1957 (Marvin, 1961). The main advantage of a confocal microscope over traditional epifluorescence is the depth of focus it can achieve. In focus images can be captured in specimens up to 100µm thick and these image stacks can be used to create a three-dimensional picture (Page, 2004). This is particularly useful for biological specimens that cannot be processed into thin slices and have multiple depths of focus such as layers of cells. It can also be a useful tool in ascertaining the arrangement of cells in 3D scaffolds.

The Leica SP8 confocal microscope is equipped with a multi-band spectrophotometer which allows the selection of any part of the light spectrum. By inserting a mechanical slit that can be manipulated and moved over any part of the spectrum, the energy distribution can be measured as a function of position (Borlinghaus, 2013). The SP8 contains a cascading series of highly reflective mirrors (shown in fig 11). The mirrors are infinitely tuneable, put for practical reasons the number of detectors is limited to five. The Leica SP8 confocal used for this study has four fluorescent and one brightfield detector equipped so it is possible to capture four independent fluorescent channels and therefore visualise up to four proteins of interest on one sample.

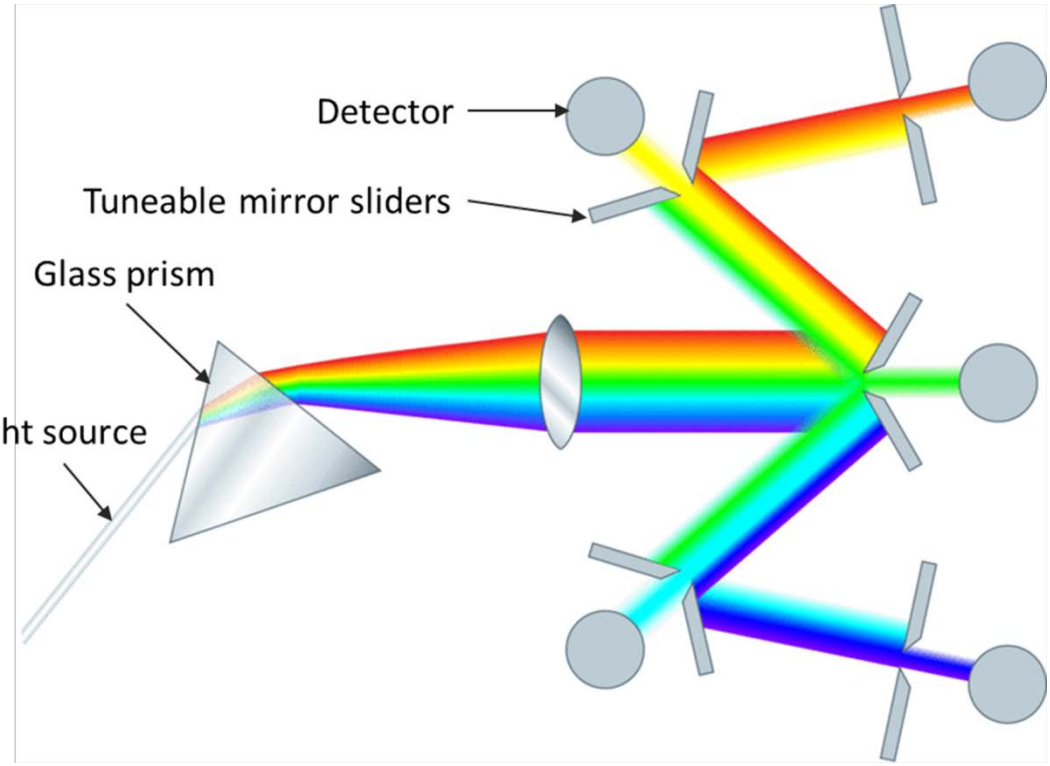

Figure 2-6 - SP detector of a confocal microscope adapted from (Borlinghaus, 2013)

The light spectrum is separated into specific bands by means of highly tunable mirror sliders that can be manipulated by the user. This allows the possibility for the spectrum to be split into any combination of sub-spectra which are then recorded by the detectors.

2.8.3 Correlative light and electron microscopy

Correlative light and electron microscopy (CLEM) refers to a technique that combines an optical microscope, typically fluorescence, with an electron microscope. The combination of these two imaging techniques allows the provision of structural context for a protein of interest labelled fluorescently. It also serves as a useful validation tool to confirm the location of a region of interest. CLEM is a very powerful technique because it is able to combine structural and functional information, which is essential for good understanding of biological systems. A CLEM microscope will be used to assess the morphological changes associated with ApoE genotype in astrocytes and how this influences the extracellular matrix proteins.

2.8.3.1 Independent CLEM

Traditionally CLEM has involved processing two sequential samples independently for both electron and light microscopy. The samples would then be imaged on the relevant microscope and the images overlaid. This makes CLEM very challenging and time consuming. Firstly the differences in sample preparation can lead to artefacts; in particular the dehydration rates can vary dramatically between protocols for electron microscopy and light microscopy. It is therefore

incredibly difficult to obtain an accurate overlay, which is highly dependent on mechanical precision and it is very subjective. Identifying the same region of interest in both samples is also very challenging and can be very time-consuming.

2.8.3.2 Integrated CLEM

Integrated CLEM microscopy eliminates many of the problems of independent CLEM as the hardware is combined into one microscope. This allows for highly accurate overlay that is unbiased with reliable and reproducible results.

The combined efforts of two Dutch companies, Phenom-World (Delft) and Delmic (Eindhoven), have created an all-in-one solution for CLEM called the Delphi. The Delphi is made up of a table top scanning electron microscope combined with an inverted fluorescence microscope (see **Figure 2-7**).

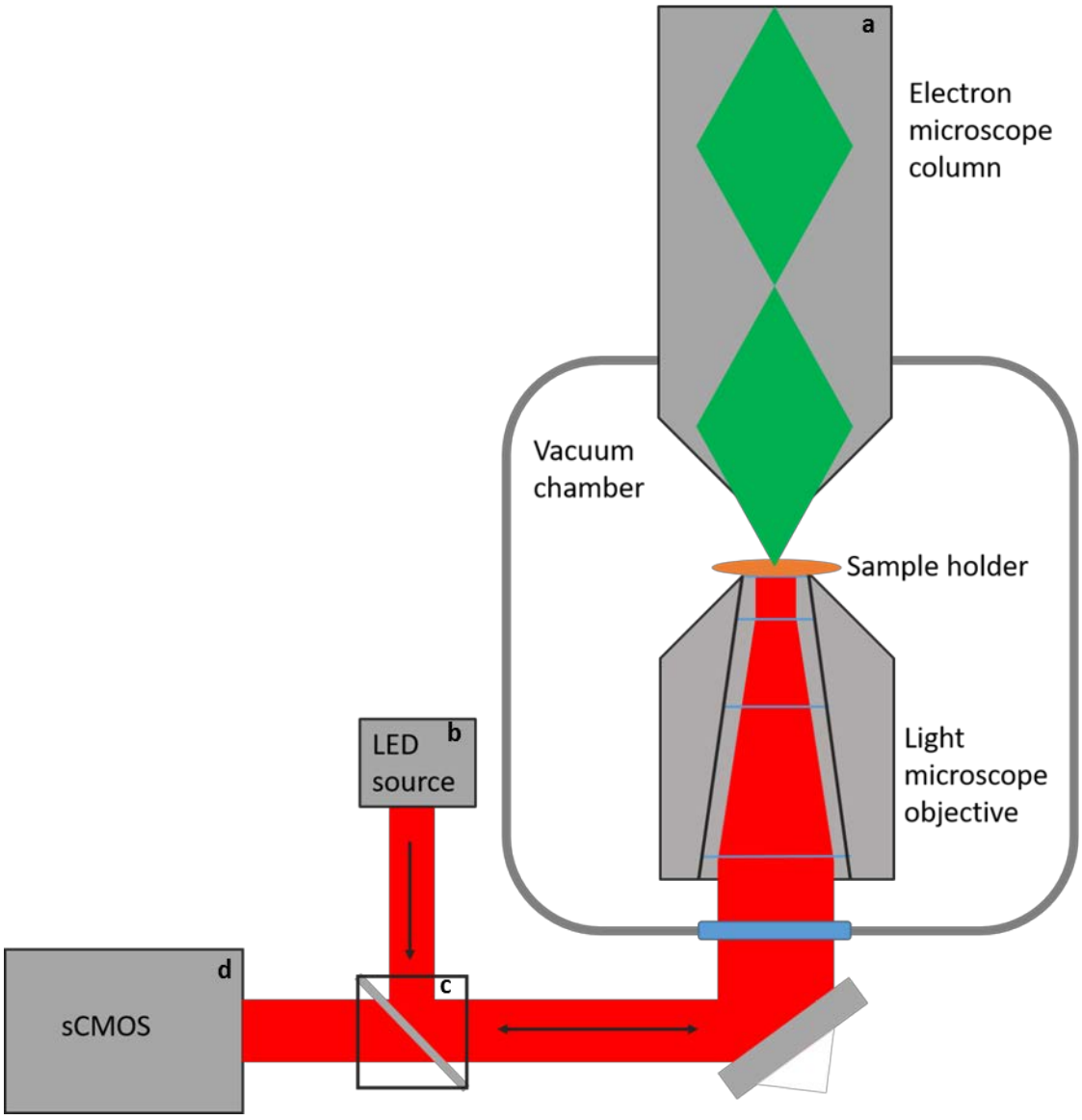

Figure 2-7 – schematic reperesentation of the Delphi

The Delphi has 4 major components as follows: A high sensitivity backscatter electron detector (a) with adjustable acceleration voltage between 4.8 and 10kV, capable of 20-130,000x magnification. A four channel solid-state LED excitation source (b) with excitation at 395, 485, 575 and 650nm, capable of exciting 4 fluorophores simultaneously. A filter cube (c) with multiband Pinkel configuration optimised for DAPI, FITC, TRITC, Cy5 or similar fluorophores and a scientific CMOS camera (d), which has a resolution of 2048x2048 pixels, for capturing the images.

The Delphi also has an integrated software package called ODEMIS that allows the user to control both modalities of the microscope, meaning the sample need only be loaded once and both the fluorescent and electron images may be obtained at the same time.

The alignment procedure used by the Delphi is fully automated and is independent of the user and the sample. The machine uses the physical principal of cathodoluminescence to create a grid

of temporary fiducial markers that can be used to produce perfect alignment and overlay (PhenomWorld, 2017).

The Delphi is very straightforward to use and produces very reliable images, but there are limitations. The protocols for integrated CLEM are complicated and often result in sub-optimal fixation. Some fluorescent proteins are incompatible with electron beams so cannot be used in the Delphi. The resolution of the Delphi is limited to 250nm when using the fluorescence channel, though it is much lower for the EM channel (sub 14nm) (PhenomWorld, 2017). This is too low to resolve any ultrastructural components of the cell that would be possible by traditional EM. The Delphi is currently a prototype and future developments aim to improve the resolution to allow more structural detail. Nevertheless, the Delphi was an appropriate tool for comparison between the isoforms of ApoE astrocytes.

2.8.4 Imaging for ApoE mouse astrocytes

Images for protein quantification were obtained using the tilescan function of the Leica SP8 confocal microscope. A 3x1 grid of images at x40 magnification (20x microscope lens and 2x optical zoom) were obtained via this method. A total of three maximum projections, each with an area of 0.15mm^2, were obtained per coverslip. Overlay images were exported in colour for qualitative comparison. Individual channel images were exported in black and white for maximum sensitivity and quantification. Qualitative images to demonstrate localisation of basement membrane proteins in relation to the cell were obtained using the DELPHI and SEM images were captured for quantification of astrocytes and astrocytic processes using the DELPHI.

2.8.5 Imaging of basement membrane proteins in human cells

Images for quantification were obtained using the tilescan function of the Leica SP8 confocal microscope. A 3x1 grid of images at x40 magnification (20x microscope lens and 2x optical zoom) were obtained via this method for analysis. The grid was set at the centre of the coverslip where the cells were densest and least likely to have been disturbed. A total of three maximum projections with an area of 0.15mm^2 were obtained per coverslip. In the case of indirect co-cultures both sides of the Transwell were imaged using the tilescan. Individual channel and overlay images were exported for qualitative and quantitative comparison.

2.9 Image analysis

For the mouse ApoE astrocytes quantitative analysis was carried out using ImageJ software. The exported maximum projection images were converted to 8-bit black and white images and a

threshold for inclusion of staining was set for each antibody. The threshold was set to include all genuine staining whilst excluding background staining. The percentage area stained was then calculated from this.

The number of cells in an image was determined by converting the DAPI stained image to 8-bit black and white then setting the threshold for analysis at 5. This made all the cells appear as solid black dots. After using the binary watershed tool to separate any overlapping cells the number of particles was automatically determined by the ImageJ measure tool. This method of automatic cell counting was checked with random manual counts using the cell counter in ImageJ. There was high agreement between the two methods and the numbers were always within 5% of each other so the automatic cell count method was determined to be reliable for the purpose of these experiments.

CLEM images were analysed using the ImageJ software. A manual cell counter was used to quantify the number of DAPI positive nuclei within a 350 X 400µm area (0.14mm^2). The cell counter was also used to determine the number of processes found on each astrocyte seen in focus on the SEM channel of the Delphi. For an astrocytic process to be included in this analysis it had to be directly attached to the cell body and at least 100nm at its main branch. The number of processes counted was divided by the number of astrocytes in focus and an average taken.

Quantitative analysis of protein in the human cells was also carried out using ImageJ. Fluorescence intensity was measured using the RGB analyser plugin to generate an arbitrary value to reflect the intensity of the staining and therefore how much protein was present in the image. Fluorescence intensity is an arbitrary scale which assigns a numerical value based upon the brightness values of the pixels in an image correspond to the correct colour channel. The arbitrary fluorescence value for the green channel was obtained for each image.

2.10 Statistics

The immunocytochemical staining of various proteins in the ApoE mouse astrocytes was analysed by one-way analysis of variance (ANOVA) with Bonferroni post-hoc correction for multiple comparisons. The data distribution from the CLEM analysis was determined to be skewed so the equivalent non-parametric Kruskal-Wallis test was used with follow-up Mann-Whitney U to determine which groups were significantly different. Raw MTS assay data was exported to Microsoft Excel and the blank values were subtracted from the test wells and groups were compared using a Kruskal-Wallis test. When comparing the fluorescence intensity of immunostained proteins in human cells the data was not normally distributed so the appropriate

non-parametric test (Mann-Whitney U for two groups and Kruskal-Wallis for more than two groups) was used to determine if differences were statistically significant.

Results were considered to be significant if $p \leq 0.05$. Unless otherwise stated error bars on graphs represent ± one standard error of the mean and n=3.

Chapter 3 Transgenic ApoE mouse astrocytes

3.1 Introduction

Apolipoprotein E is a 299 amino acid protein mapped to chromosome 19 with a molecular mass of 34.2 KDa. It is a major cholesterol transporter in the body and the only known cholesterol transporter in the brain. Apolipoprotein E binds with high affinity to Aβ and has been implicated in the development of sporadic late-onset Alzheimer's disease(Kim, Basak and Holtzman, 2009).

ApoE is part of a multigene family of apolipoproteins including: ApoA-I, ApoA-II, ApoA-IV, ApoB-100, ApoB-48, ApoC-I, ApoC-II, ApoC-III, ApoD, ApoJ and ApoH (Chan, 1989). Apolipoproteins facilitate the movement and uptake of lipoproteins through plasma membranes for catabolism (Erkelens, 1989). Each apolipoprotein multigene family has a specific role within the body and ApoE is the principal cholesterol carrier in the brain (Erkelens, 1989; Puglielli, Tanzi and Kovacs, 2003).

The receptors for ApoE belong to a family of low density lipoprotein receptors (LDLRs) and these are preferentially expressed by neurons, allowing the transport of cholesterol into neurons. Metabolism of cholesterol is crucial for neurotransmission and neurodevelopment in addition to repair after CNS insult.

3.1.1 ApoE in the CNS

The brain is the second highest ApoE synthesising organ, behind the liver, and ApoE is synthesised and secreted primarily by astrocytes (Pitas *et al.*, 1987) but also by oligodendrocytes and microglia (Liao, Yoon and Kim, 2017). Production of ApoE may also be induced in neurons following brain injury (Huang and Mahley, 2014). ApoE is the major lipoprotein in the brain and the principal cholesterol transporter. There are seven known receptors for ApoE which all belong to the highly conserved LDLR family (Rogers and Weeber, 2008). ApoE transports cholesterol to cells via ApoE receptors which are preferentially expressed on neurons (Zhang *et al.*, 2013). The cholesterol is metabolised by neurons and is crucial for many neuronal functions. The bulk of cholesterol in the brain is contained in myelin so ApoE is crucial for the myelination of axons and therefore neurotransmission (Pfrieger and Ungerer, 2011).

3.1.2 ApoE polymorphisms

ApoE is a polymorphic protein and the human APOE gene consists of three alleles (ε2, ε3 and ε4) which encode the three protein isoforms ApoE2, ApoE3 and ApoE4 respectively. These isoforms differ from each other at positions 112 and 158, where a single amino acid substitution of arginine or cysteine determines the isoform. ApoE3 has a Cys112 and Arg158, whereas ApoE2 has cysteine at both positions and ApoE4 has arginine at both positions (see **Figure 1-2**). The amino acid substitutions in ApoE affect binding affinity to lipoproteins. The presence of Cys 112 in ApoE2 and ApoE3 causes preferential binding to high-density lipoproteins whereas the Arg 112 in ApoE4 causes Arg61 to interact with Glu255; this interaction results in preferential binding to very low-density lipoproteins (Phillips, 2014). Cys 158 in ApoE2 causes lower affinity binding to LDLRs, which can result in hyperlipoproteinemia (the inability to break down cholesterol)(Weisgraber, Innerarity and Mahley, 1982). Two copies of the APOE allele are inherited and are co-dominant in expression and individuals may be homozygous or heterozygous with six potential allele combinations. In most populations the majority of the APOE gene pool is occupied by the ε3 allele (70-80%). The ε4 allele accounts for 10-15% of the population and ε2, the rarest allele makes up the remaining 5-10% (Ordovas *et al.*, 1987; Farrer *et al.*, 1997; McKeon-O'Malley and Tanzi, 2001).

3.1.3 ApoE and Alzheimer's disease

The link between ApoE and AD was first demonstrated in 1991 when Pericak-Vance, Roses and colleagues demonstrated that some patients with late-onset AD exhibited an association with genetic markers on chromosome 19 (Pericak-Vance *et al.*, 1991). ApoE4 has since been linked to several AD-relevant pathogenic process including Aβ levels, altered Aβ-signalling and Aβ-independent pathways (Tai *et al.*, 2016). APOE4 is also associated with cerebral hypoperfusion and cerebral blood flow asymmetry (Lehtovirta *et al.*, 1996; Lehtovirta *et al.*, 1998; Hogh *et al.*, 2001). There is little doubt that APOE4 impacts upon the cerebrovasculature and its function in all stages of AD. It is well known that possession of the APOE ε4 allele is a risk factor for developing AD and CAA. APOE has long been identified as the most important susceptibility gene (Genin *et al.*, 2011) and is a major non-modifiable risk factor for AD. The ε4 allele frequency is nearly three times higher in the AD population than the general population, strengthening the strong link between APOE ε4 and AD (Liu *et al.*, 2013). Population studies have demonstrated that 20% of Individuals possessing no ε4 develop AD compared to 90% of individuals that are homozygous for ε4. The age of onset was also decreased from 84 to 68 years with increased number of APOE ε4 alleles (Corder *et al.*, 1993). Possession of an APOE ε4 allele therefore not only increases an individual's risk of developing AD but it also lowers the age of onset.

3.1.4 The relationship between ApoE and amyloid beta

Studies from Strittmater and Salvesen showed that ApoE from the CSF of patients with AD bound with very high affinity to Aβ immobilised on nitrocellulose paper (Strittmatter *et al.*, 1993). ApoE is thought to be involved in the process of Aβ plaque formation and patients with AD that possess an APOE ε4 allele have been shown to have a greater number of Aβ plaques when compared to patients with other APOE alleles. *In-vitro* aggregation studies have demonstrated a clear isoform-specific difference in the accumulation and clearance of Aβ with accumulation highest in the presence of ApoE4 followed by ApoE3 then ApoE2 (Kim, Basak and Holtzman, 2009; Castellano *et al.*, 2011). Targeted replacement mice expressing human APOE4 have a thinner basement membrane with lower levels of laminin and collagen IV (Hawkes *et al.*, 2012), suggesting that the composition of the basement membrane may be dependent on APOE genotype, and this is likely to influence the efficiency of removal of Aβ via IPAD.

3.1.5 Aims and hypothesis

The link between ApoE and AD has been studied and the ApoE isoform dependent effects on Aβ metabolism are reasonably well understood but it has not been reported whether or not ApoE isoform has an effect on the cells that produce it. Using transgenic astrocytes that express only one isoform of ApoE, I aim to test the hypotheses that a) composition of the astrocytic basement membrane and other functionally associated proteins are dependent on the ApoE genotype and b) cells expressing ApoE4 will have a basement membrane profile that favours the fibrillization of Aβ.

3.2 Materials and methods

3.2.1 Cell culture

Three immortalised astrocyte cell lines, generated from mice expressing homozygous human ApoE isoforms (E2, E3 or E4) were produced and donated by Prof David Holtzman (see section 2.1.1.1 for full details). Cells were cultured in advanced Dulbecco's Modified Eagle's Medium (DMEM) supplemented with 10% FBS and 1% geneticin and maintained in a humidified environment with 5% CO_2 at 37°C. Media was replaced every other day until cells were of sufficient density for experiments.

3.2.2 Determining seeding density for experiments

To assess the growth of ApoE astrocytes in culture, a series of experiments involving plating at various densities and culturing at different time points was carried out (see **Figure 3-1**). The aim was to establish when the cells reach confluence after plating at a pre-determined density. A minimum time point of 24 hours was chosen to give cells sufficient time to settle after plating and a maximum of 72 hours as cells typically required passaging after 3 days and became over confluent at later timepoints. After the designated time (either 24, 48 or 72 hours) the cells were examined with a phase contrast microscope. Whilst culturing the ApoE astrocytes it was noted that the different types reached confluence at different times, indicating a discrepancy in growth rate. To determine the difference in the rate of growth between the ApoE alleles the cells were plated at the same density ($0.5x10^5$ cells per 12mm glass coverslip) and left to grow in identical conditions for 72 hours.

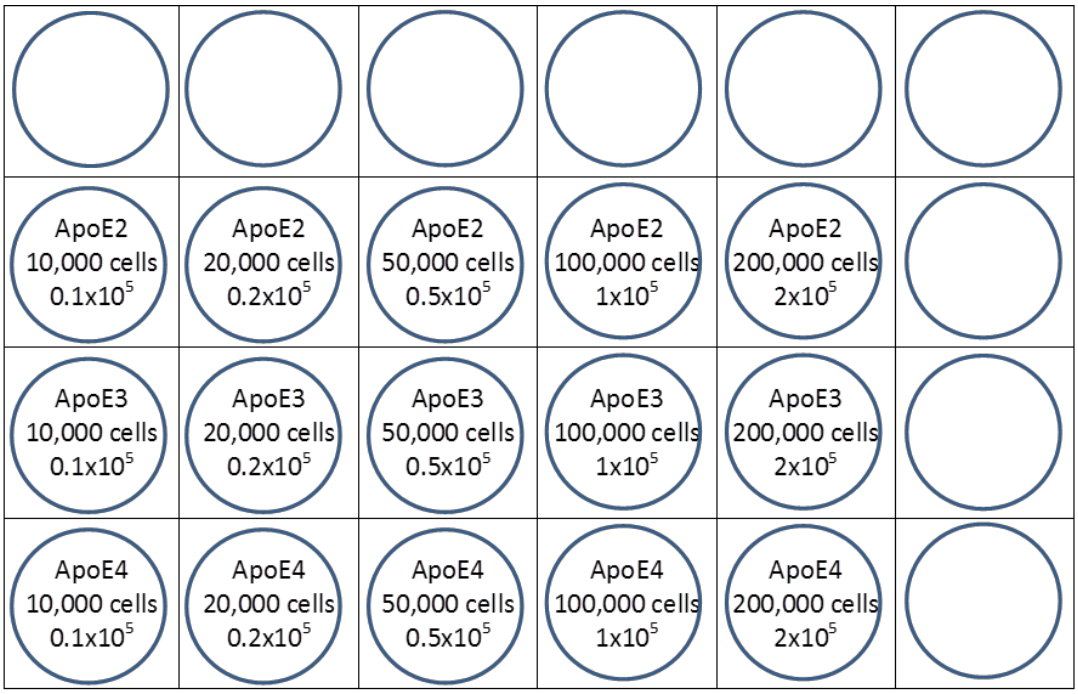

Figure 3-1 determining plating density and time frame for ApoE astrocyte experiments

In order to determine suitable parameters for successive experiments a range of timepoints and seeding densities was tested .Three plates were prepared as shown with a range of cell densities. One plate was fixed after 24 hours, the second after 48 hours and the final plate was fixed after 72 hours. The plates were examined by phase contrast microscopy to determine which wells were close to 100% confluence.

3.2.3 Immunocytochemistry for basement membrane proteins

ApoE astrocytes were plated onto glass coverslips and fixed with 4% paraformaldehyde in 0.01M PBS. For this experiment cells were plated at a density of $0.5x10^5$ cells/coverslip and fixed after 72 hours or allowed to grow to 100% confluence. ApoE2 cells reached confluence after 3 days, ApoE3 cells after 4 days and ApoE4 cells after 5 days. Cells were washed with PBS and blocked with 15% NGS for 1 hour and incubated overnight with collagen IV (Abcam, ab6586), laminin (Sigma, L9393), fibronectin (Sigma, F3648) or perlecan (Santa Cruz, 25848) primary antibody diluted in PBS at 4°C (see **Table 3-1** for full details). After washing three times with PBS, cells were incubated with goat anti-rabbit Alexa Fluor 488 conjugated secondary antibody (Invitrogen, A11034) for 1 hour at room temperature. Cells were washed again with PBS and incubated with 2µg/mL DAPI for 10 minutes. Coverslips were rinsed with PBS and mounted onto slides with Mowiol and Citifluor and examined by confocal microscopy.

3.2.4 Immunocytochemistry for other proteins

ApoE astrocytes were plated at $0.5x10^5$ cells/coverslip and fixed 72 hours after initial plating with 4% paraformaldehyde in 0.01M PBS. Cells were washed with PBS and blocked with 15% NGS for 1 hour and incubated overnight with aquaporin IV (Santa Cruz, 20812), dystoglycan (Leica Biosystems, NCL-b-DG), dystrobrevin (Santa Cruz, 33161), TIMP3 (Abcam, ab93637), GFAP (Dako, Z0334) or ApoJ (Abcam, ab42673) primary antibody at 4°C (see **Table 3-1** for full details). Primary antibodies were diluted in PBS with the addition of 0.1% triton to aid permeabilization. After washing three times with PBS, cells were incubated with the appropriate Alexa Fluor 488 conjugated secondary antibody (see **Table 3-1**) for 1 hour at room temperature. Cells were washed again with PBS and incubated with 2µg/mL DAPI for 10 minutes. Coverslips were rinsed with PBS and mounted onto slides with Mowiol and Citifluor and examined with confocal microscopy.

Table 3-1 – Antibodies used for immunofluorescence staining of ApoE astrocytes

Antibody type	Antigen	Name provided by supplier	Supplier details	Optimal dilution
Primary	Collagen IV	Rabbit anti-collagen IV (ab6586)	Anti-collagen IV antibody polyclonal produced in rabbit, AbCam, Cambridge, UK	1:400

Antibody type	Antigen	Name provided by supplier	Supplier details	Optimal dilution
Primary	Laminin	Anti-laminin antibody produced in rabbit (L9393)	Anti-laminin antibody polyclonal produced in rabbit, Sigma Aldrich, St Louis, USA	1:200
Primary	Fibronectin	Anti-fibronectin antibody produced in rabbit (F3648)	Anti-fibronectin antibody polyclonal produced in rabbit, Sigma Aldrich, St Louis, USA	1:400
Primary	Perlecan	Perlecan antibody (H-300) sc-25848	Perlecan (H-300) rabbit polyclonal antibody 200 µg/ml, Santa Cruz Biotechnology, Heidelberg, Germany	1:400
Primary	Aquaporin IV	AQP4 (H80) sc-20812	AQP4 Antibody (H-80) rabbit polyclonal antibody 200 µg/ml, Santa Cruz Biotechnology, Heidelberg, Germany	1:200
Primary	Dystrobrevin	α-Dystrobrevin (H300) sc-33161	Dystrobrevin (H-300) rabbit polyclonal antibody 200µg/ml, Santa Cruz Biotechnology, Heidelberg, Germany	1:50
Primary	TIMP 3	Anti-TIMP3 antibody (ab93637)	Anti-TIMP3 antibody polyclonal produced in rabbit, AbCam, Cambridge, UK	1:100
Primary	GFAP	Anti-GFAP antibody (Z0334)	Polyclonal rabbit anti-GFAP antibody, Dako, Glostrup, Denmark	1:250
Primary	Dystroglycan	Anti-beta dystroglycan antibody (NCL-b-DG)	Novocastra lyophilized mouse monoclonal antibody beta-dystroglycan, Leica Biosystems, Newcastle, UK	1:50
Primary	ApoJ (clusterin)	Rabbit anti-Apolipoprotein J antibody (ab42673)	Anti-Apolipoprotein J primary antibody polyclonal produced in rabbit, AbCam, Cambridge, UK	1:500

Antibody type	Antigen	Name provided by supplier	Supplier details	Optimal dilution
Secondary	Rabbit IgG	Alexa Fluor 488 goat anti-rabbit (A11034)	Alexa Fluor 488 goat anti-rabbit IgG polyclonal, Invitrogen , Life Technologies, Paisley, UK	1:200
Secondary	Mouse IgG	Alexa Fluor 488 goat anti-mouse (R37120)	Alexa Fluor 488 goat anti-mouse IgG polyclonal, Invitrogen , Life Technologies, Paisley, UK	1:200

3.2.5 Processing for correlative light and electron microscopy

Astrocytes were plated onto Indium tin oxide (ITO) coated coverslips in a 12 well plate at a density of 10^5 cells per coverslip for laminin staining or $2x10^5$ cells per coverslip for GFAP. Cells were fixed with 2.5% paraformaldehyde and 0.25% glutaraldehyde in 0.01M PBS 72 hours after initial plating for laminin staining or 48 hours for GFAP staining. Cells were rinsed with PBS and blocked with 15% NGS for 30 minutes at room temperature before overnight incubation with either laminin (Sigma, L9393) or GFAP (Dako, Z0334) primary antibody at 4°C. After three PBS washes, cells were incubated with a goat anti-rabbit Alexa Fluor 488 conjugated secondary antibody (Invitrogen, A11034) for 1 hour at room temperature. All antibodies were diluted in 15% NGS to facilitate continuous blocking and maximising specificity of binding. Cells were quickly rinsed with distilled water and cupric sulphate (10mM copper sulphate in 50mM ammonium acetate) was added to cells for 10 minutes to quench autofluorescence. Cells were rinsed with distilled water again and then incubated with 2µg/mL DAPI for 10 minutes. Cells were washed 3 times with PBS and quickly rinsed in 70% ethanol. Cells were dehydrated via ethanol dilution series: 5 minutes 70%, 5 minutes 80%, 5 minutes 90%, 15 minutes 100%, and 15 minutes 100%. Coverslips were air-dried overnight in the dark and mounted onto carrier rings with carbon tape.

3.2.6 Amyloid beta preparation

In a healthy brain the Aβ concentration is thought to be in the range of 2-3nM (Verghese *et al.*, 2013), though this is significantly higher in an AD brain (Collins-Praino *et al.*, 2014). To replicate the burden of amyloid in AD brain, 100nM Hilyte 555 Aβ1-40 (Anaspec, AS-60492-01) was added to the culture media at the start of the 24 hour flow experiments. See section 2.5 for full details

on preparation of Hilyte Aβ. A previous study has shown that no fibrils of Hilyte 555 Aβ 1-40 were observed with electron microscopy when using this preparation (Albargothy *et al.*, 2017) It has also been shown by atomic force microscopy that this preparation and use of Hilyte 555 Aβ 1-40 at 37°C resulted in the formation of soluble oligomers only (Morris, 2015). A concentration of 100nM was achieved by adding 1µL of the 200µM stock of amyloid beta per 2mL culture media. Concentrations lower than 100nM did not produce a sufficient fluorescence signal for detection by confocal microscopy, therefore 100nM was as close to a physiological concentration of Aβ in an AD brain as possible whilst still being detectable.

3.2.7 Static amyloid beta experiments

ApoE2, ApoE3 or ApoE4 astrocytes were counted and plated onto glass coverslips in a 24 well plate at a density of $1x10^5$ cells/well. Cells were allowed to grow undisturbed for 24 hours before a media change. Either normal astrocyte medium or astrocyte medium supplemented with 100nM Hilyte 555-labelled Aβ1-40 was added to the cells and incubated at 37°C for another 24 hours. The media was removed and cells were fixed with 4% PFA for 10 mins before immunostaining.

3.2.8 Flow experiments

3.2.8.1 Experimental set up

An interconnected cell culture millifluidics flow system (Quasi Vivo QV500, Kirkstall Ltd, Rotherham) was used to apply flow to the astrocyte cultures. The system was assembled as shown in **Figure 3-2**. A polyflex dual-head peristaltic pump (PARKER, PF22X0103) was calibrated for a 2-chamber set up according to the manufacturer's instructions (See supplementary figures 3 and 4). ApoE2, ApoE3 or ApoE4 astrocytes were counted and plated on 12mm round coverslips in a 24 well plate at a density of $1x10^5$ cells/coverslip and left undisturbed for 24 hours to allow cells to adhere. Coverslips were then transferred into the QV500 chambers for a flow experiment (with or without the addition of HiLyte 555 Aβ1-40) and left to run for 24 hours at a flow rate of 10µL/min. The coverslips were then removed from the system and the cells were fixed with 4% PFA before immunostaining. Experiments were performed with only one isoform of ApoE astrocyte at a time.

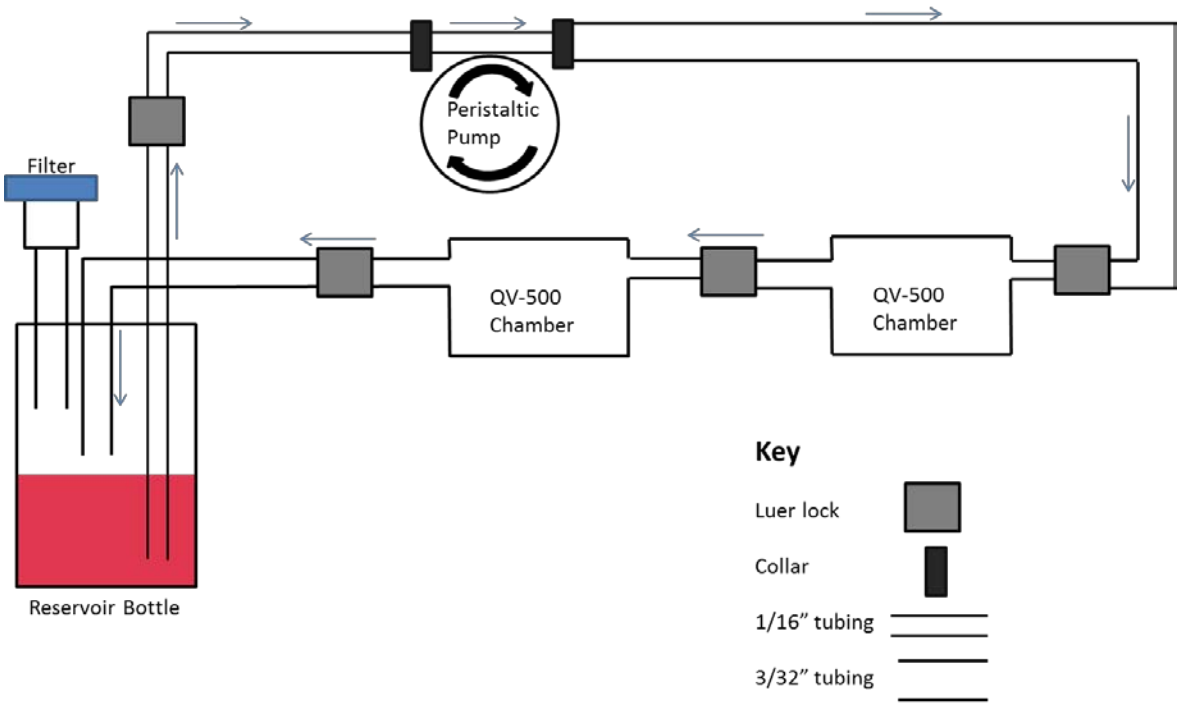

Figure 3-2 Two chamber set-up of Quasi Vivo system

The Quasi Vivo system continuously recycles media in a closed recirculating loop. The outlet tube of the reservoir bottle is run through the peristaltic pump and connected to a QV500 chamber, this is linked to another QV500 chamber which is connected to the reservoir bottle via the inlet tube. The reservoir bottle also has another outlet for an air filter to allow gas exchange. Each QV500 chamber can accommodate a coverslip of cells.

3.2.8.2 Flow rate

The flow rate chosen for these experiments was 10µL/min which corresponds to a speed of $1.56x10^{-7}$m/sec at the cell surface and a shear stress of $1.28x10^{-6}$ Pa or $1.28x10^{-5}$dyn/cm^2 (Mazzei *et al.*, 2010). The exact rate of flow of ISF in the brain is unknown. A study from Abbott proposed an ISF bulk flow rate of 0.1-0.3µl/min/g along perivascular pathways (Abbott, 2004) but the study was carried out in rat brain and is it unknown whether this is translatable to humans. The flow rate for these experiments was selected based on production rate of CSF and what is known about injection rates from experimental surgeries, combined with what is physically possible with the peristaltic pump. The rate of CSF formation in an adult human is 0.3-0.4mL/min (Brinker *et al.*, 2014) but ISF turnover is not as high as CSF. The exact production rate of ISF in humans is unclear as it is not readily accessible like CSF but it has been estimated to be as much as 100 times less than CSF production by the choroid plexus (Brinker *et al.*, 2014). Experimental surgeries in mouse brain require an injection rate of 0.5µL over 2.5 minutes to maintain normal pressure and prevent spillage of ISF into ventricular CSF (Albargothy *et al.*, 2017). Mouse brains are much smaller than

human brains so it is expected that a flow rate closer to that suggested by CSF production rates would not adversely affect the cells of the human brain. A flow rate of 10µL/min means that the entire 10mL volume of media in the Quasi Vivo system makes a complete circuit at least once in the 24 hours.

3.2.9 Imaging and analysis

Images were captured with a Leica SP8 confocal microscope or the Delphi. CLEM images were analysed using the manual cell counter tool in ImageJ (see section 2.9 for full details). A total of twelve images were captured for each ApoE genotype over three experimental runs and the processes of each astrocyte in focus were counted. The average number of processes was calculated by dividing the total number of processes by the number of astrocytes in an image. Quantitative analysis of immunostained proteins was carried out using ImageJ software (see section 2.9) for full details). The cell number was calculated using an automatic cell counting method detailed in section 2.9 and was randomly checked with manual cell counts. The amount of protein produced per cell was calculated by dividing the percentage area stained by the number of cells counted per image. Representative images showing the distribution of amyloid beta in the static and flow amyloid beta experiments were captured at 40x magnification with the Leica SP8 confocal microscope.

Statistical tests were performed using SPSS software (version 24). The cell number and the percentage area stained for proteins at 72 hours was analysed by one-way analysis of variance (ANOVA) with Bonferroni post-hoc correction for multiple comparisons. The CLEM data and percentage area stained for proteins at confluence were not normally distributed so a Kruskal-Wallis non-parametric test was carried out for comparisons between groups. This was followed up with Mann-Whitney U tests to determine which groups were significantly different. Groups were determined to be significantly different if $p \leq 0.05$.

3.3 Results

3.3.1 GFAP expression

GFAP was detected in all 3 of the ApoE astrocyte cell lines with confocal microscopy (see **Figure 3-3**) and CLEM (see **Figure 3-4**). The distribution of GFAP was uniform across the cell layer with all cells expressing GFAP. This indicated that the culture contained glial cells and was not contaminated with pericytes or endothelial cells.

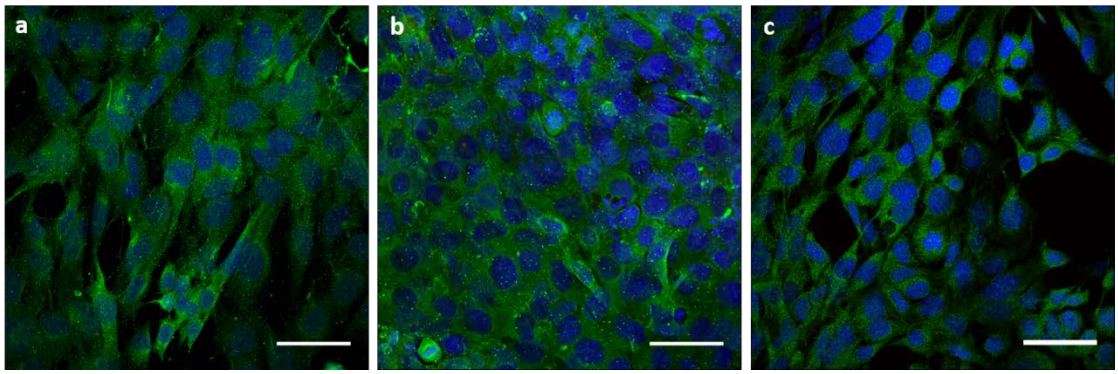

Figure 3-3 – representative GFAP staining of ApoE astrocytes imaged on confocal

Double immunofluorescence staining showing the expression of GFAP in a) ApoE2, b) ApoE3 and c) ApoE4 mouse astrocytes. GFAP staining is shown in green and the cell nuclei are shown in blue stained with the DNA binding nuclear counterstain DAPI. Scale bar 50µm.

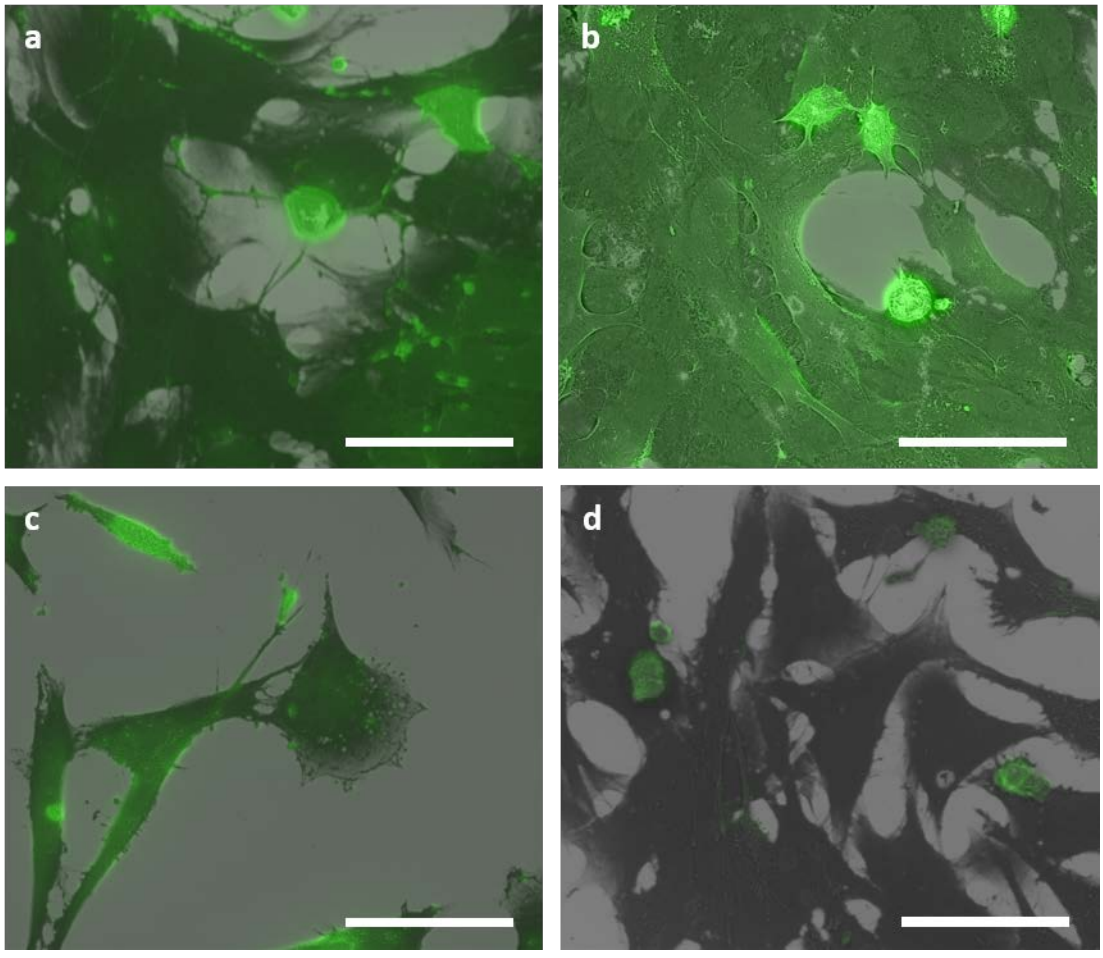

Figure 3-4 – representative GFAP staining of ApoE astrocytes imaged on Delphi

GFAP fluorescence staining combined with SEM for a) ApoE2, b) ApoE3 and c) ApoE4 astrocytes. All three APOE-isoform specific astrocytes express detectable levels of GFAP. d) Negative control to assess autofluorescence caused by the electron beam. Scale bar 40µm.

3.3.2 Growth rate

After examining the seeding density experiment plates, it was concluded that cells typically reached 100% confluence after 72 hours if plated at a density of $0.5x10^5$ cells per 12mm coverslip. Similar levels of confluence were observed after 48 hours if plated at $1x10^5$ cells per 12 mm coverslip. Densities exceeding $1x10^5$ rapidly reach 100% confluence, typically less than 24 hours, and there was evidence of overcrowding and cell atrophy at the 24 hour time point. Densities of less than $0.5x10^5$ cells did not reach confluence within the designated time frames of this experiment and at densities less than $0.2x10^5$ cultures did not proliferate well and the cells were too sparse. During these experiments it was observed there was a discrepancy in the number of cells in the different ApoE astrocyte cultures so this was investigated in more depth. The growth rate of the three ApoE astrocyte cell lines was assessed by comparing the number of cells in each culture after 72 hours grown in identical conditions with the same seeding density of $0.5x10^5$ cells/coverslip.

There is a very significant difference ($p<0.001$) in the number of ApoE2, ApoE3 and ApoE4 astrocytes after 72 hours (see **Figure 3-5**). Using the average number of cells per image (rounded to the nearest whole number) the approximate difference in growth rate can be calculated. For ApoE2 the average cell count was 545, for ApoE3 there were 274 cells and for ApoE4 there were 52 cells on average. This means that over a period of 72 hours the ApoE2 astrocytes grew at almost double the rate of the ApoE3 astrocytes (1.989) and more than 10 times the rate of the ApoE4 cells (10.462). The ApoE3 astrocytes also grew at more than 5 times the rate of the ApoE4 cells (5.269).

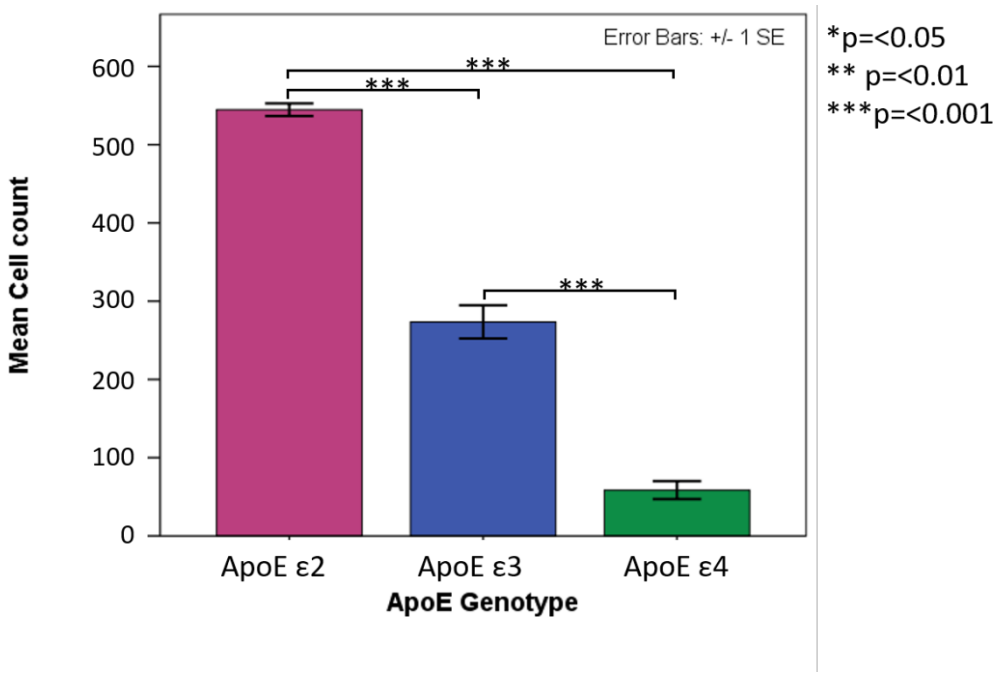

Figure 3-5 – a comparison of the average cell count for each ApoE isoform

There were significantly more ApoE2 astrocytes than the other ApoE isoforms ($p<0.001$) and significantly more ApoE3 cells when compared to ApoE4 ($p<0.001$). Results are based on the average number of DAPI stained nuclei in three non-overlapping images per coverslip. Error bars represent the standard error of the mean and n=18.

3.3.3 Morphology and astrocytic processes

CLEM showed a detailed morphology of the astrocytes and qualitative analysis of the astrocytes revealed that ApoE4 cells appear to have a different shape (see **Figure 3-6**) compared to E2 or E3. ApoE4 astrocytes appeared elongated when compared to E2 or E3 cells, which exhibited fuller bodies with a more classic star shaped appearance. In addition to the observed morphological differences in shape, a quantitative analysis of the number of astrocytic processes showed there were significantly fewer processes extending from the cell body of an ApoE4 astrocyte when compared with ApoE2 or E3 ($p=0.000007$) (see **Figure 3-7**). The ApoE3 astrocytes had the highest number of processes (11 on average) followed by ApoE2 astrocytes (8 on average) and ApoE4 astrocytes had the fewest (3 on average).

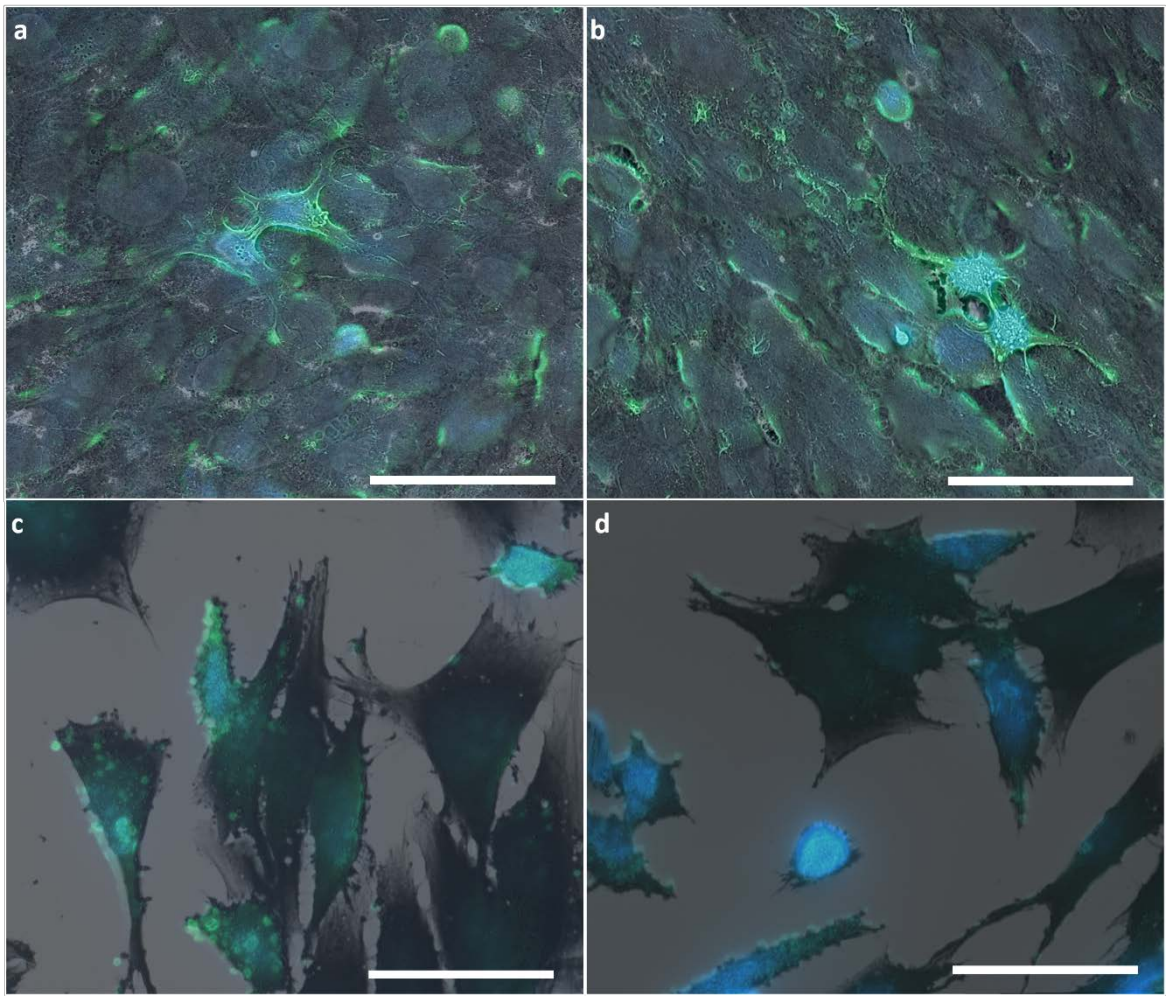

Figure 3-6 ApoE Astrocyte morphology as seen via CLEM

The ApoE astrocytes were immunostained for laminin (shown in green) and counterstained with DAPI (shown in blue) before being imaged by CLEM. a) ApoE2 and b) ApoE3 astrocytes showed confluent monolayers with hexagonal bodies and more visible laminin staining. c) The ApoE4 astrocytes showed a sparser cell layer with more elongated triangular bodies and less visible laminin staining. d) Negative control to assess autofluorescence in green channel. Scale bar 40µm.

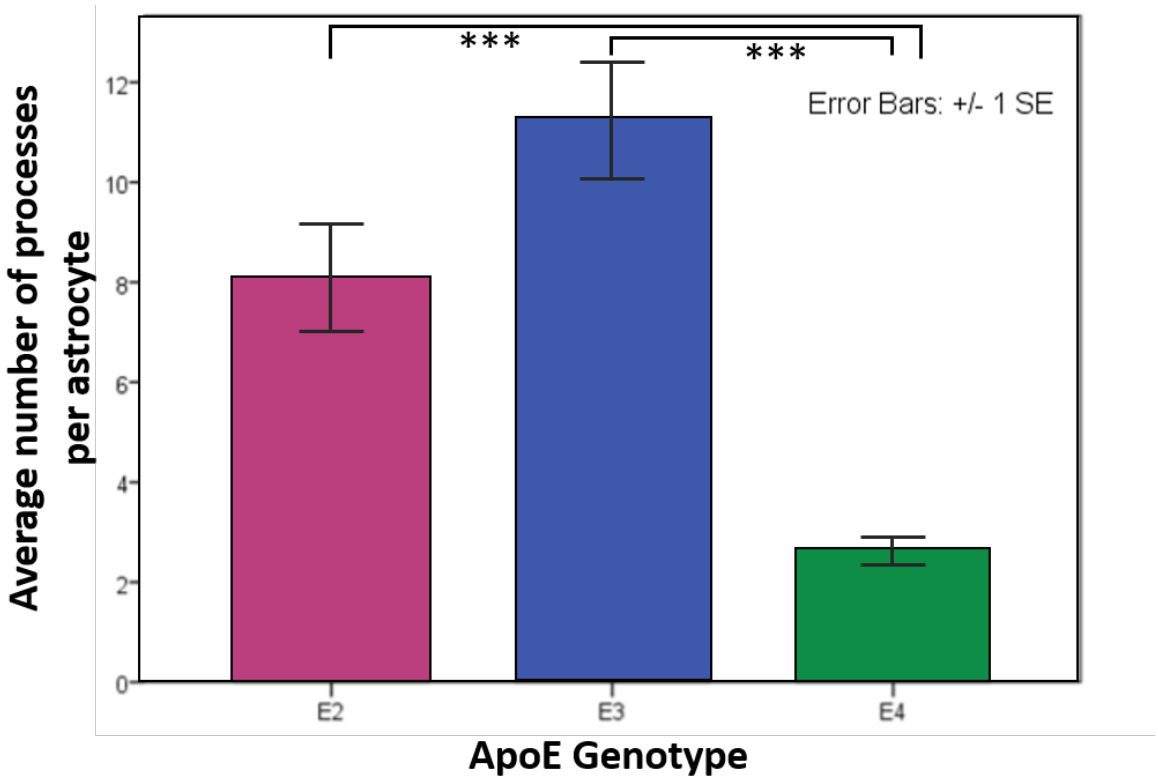

Figure 3-7 Quantification of the number of astrocytic processes in each ApoE astrocyte culture

There were significantly fewer processes extending from ApoE4 astrocytes when compared to astrocytes expressing ApoE2 or ApoE3. There was no significant difference in the number of processes observed between astrocytes expressing ApoE2 and ApoE3. Error bars represent the standard error of the mean and n=3. *** $p<0.001$

3.3.4 Laminin staining on astrocytic processes

When the astrocytes were stained for the basement membrane protein laminin and processed for CLEM, the images showed laminin staining dotted along the processes of ApoE2 and ApoE3 expressing astrocytes (**Figure 3-8**a and b). This was also observed to a lesser extent in the astrocytes expressing ApoE4, however the majority of the laminin was associated with the cell body (**Figure 3-8**c).

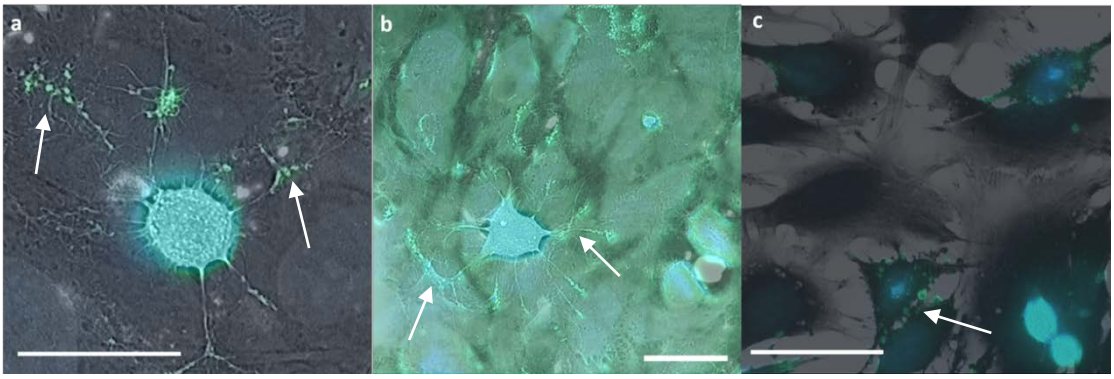

Figure 3-8 – Laminin on astrocyte processes

Laminin (shown in green) and DAPI (shown in blue) on a) ApoE2 and b) ApoE3 astrocytes. The laminin staining extends along the astrocyte processes and is concentrated at the end feet (see arrows in panels a and b). c) ApoE4 astrocytes show laminin positive staining closely associated to the main cell body and very little on the processes (see arrow). Scale bar 20µm.

3.3.5 Basement membrane protein production

The composition of the basement membrane of the ApoE astrocytes was investigated by plating cells at a density of $0.5x10^5$ cells per 12mm coverslip as in section 3.2.3.3 and fixing after 72 hours. Immunostaining for collagen IV, laminin, fibronectin and perlecan was performed as per section 3.2.4. The percentage area stained was quantified and the three ApoE isoforms were compared to assess if ApoE genotype had an effect on the production of these key basement membrane proteins and overall composition of the basement membrane (see **Figure 3-9** and **Figure 3-10**).

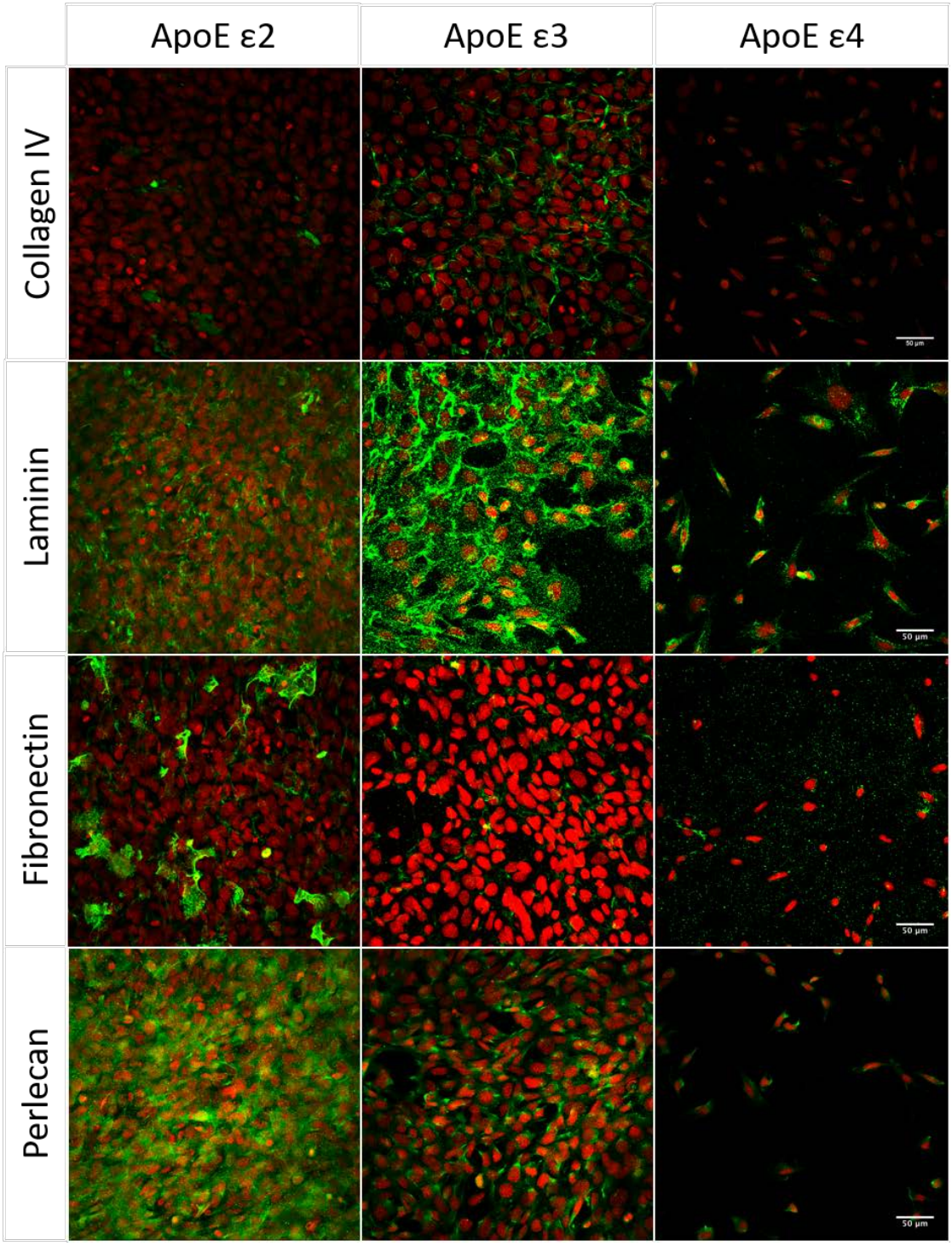

Figure 3-9 – Basement membrane staining in ApoE astrocytes after 72 hours

Representative images to show the staining for key basement membrane components. The glycoproteins collagen IV and laminin and the proteoglycans fibronectin and perlecan are shown in green. To show cell density nuclei are stained with DAPI and shown in red. Scale bar 50µm.

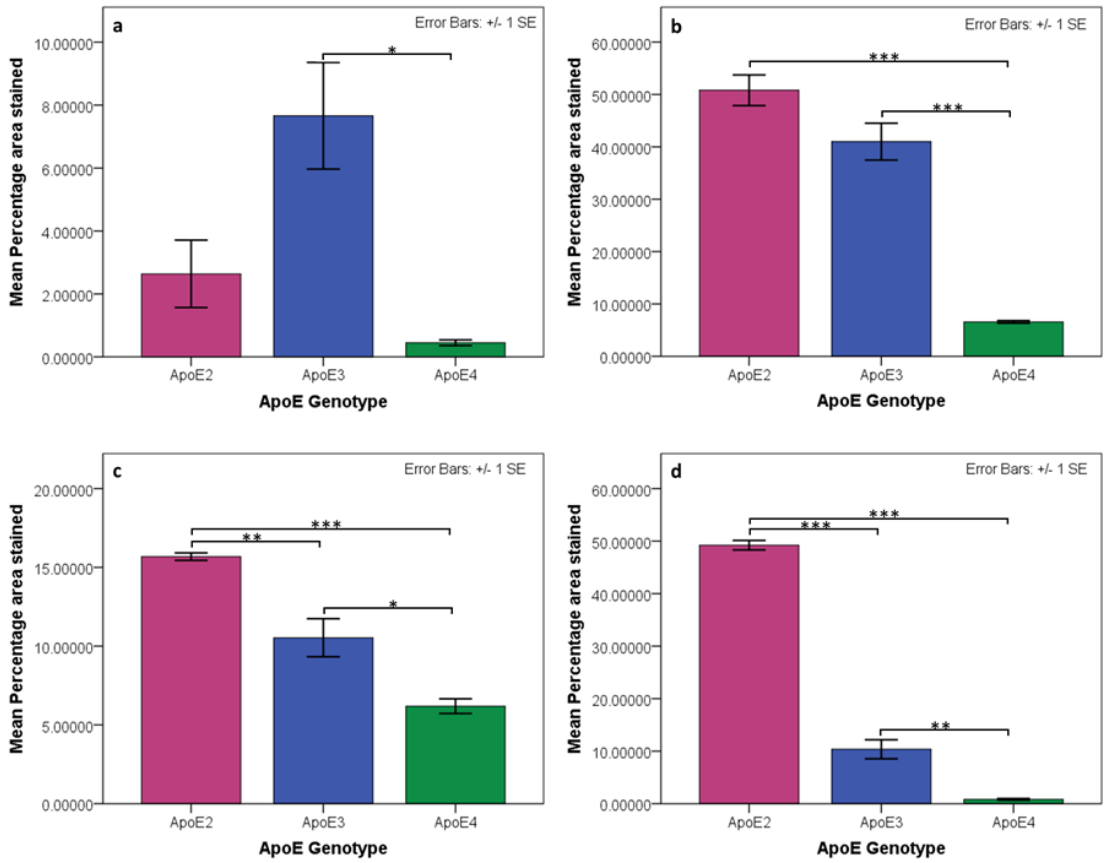

Figure 3-10 – quantification of basement membrane proteins in the ApoE astrocytes after 72 hours

The graphs represent the percentage area stained for: a) collagen IV, b) laminin, c) fibronectin and d) perlecan. The percentage area stained for all these proteins is less in the ApoE4 cells compared to the other ApoE variants. ApoE2 percentage area staining is highest in laminin, fibronectin and perlecan but not collagen IV, which is highest in ApoE3 astrocytes. Average percentage area stained was calculated from three fields of view per coverslip and a total of three coverslips per protein over three independent experiments (n=3) Error bars represent the standard error of the mean and significance is indicated as follows: *p<0.05, **p<0.01, ***p<0.001.

The percentage area stained for collagen IV was significantly higher in ApoE3 astrocytes when compared with ApoE4. The percentage area stained for laminin was significantly higher in ApoE2 and ApoE3 astrocytes than it was in ApoE4 cells. The percentage area stained for fibronectin and perlecan was highest in ApoE2, followed by ApoE3 the ApoE4, with all differences being statistically significant (see **Figure 3-10**).

The amount of protein produced per cell was calculated by dividing the average percentage area stained of a basement membrane protein by the average number of cells and these results are shown in **Figure 3-11**.

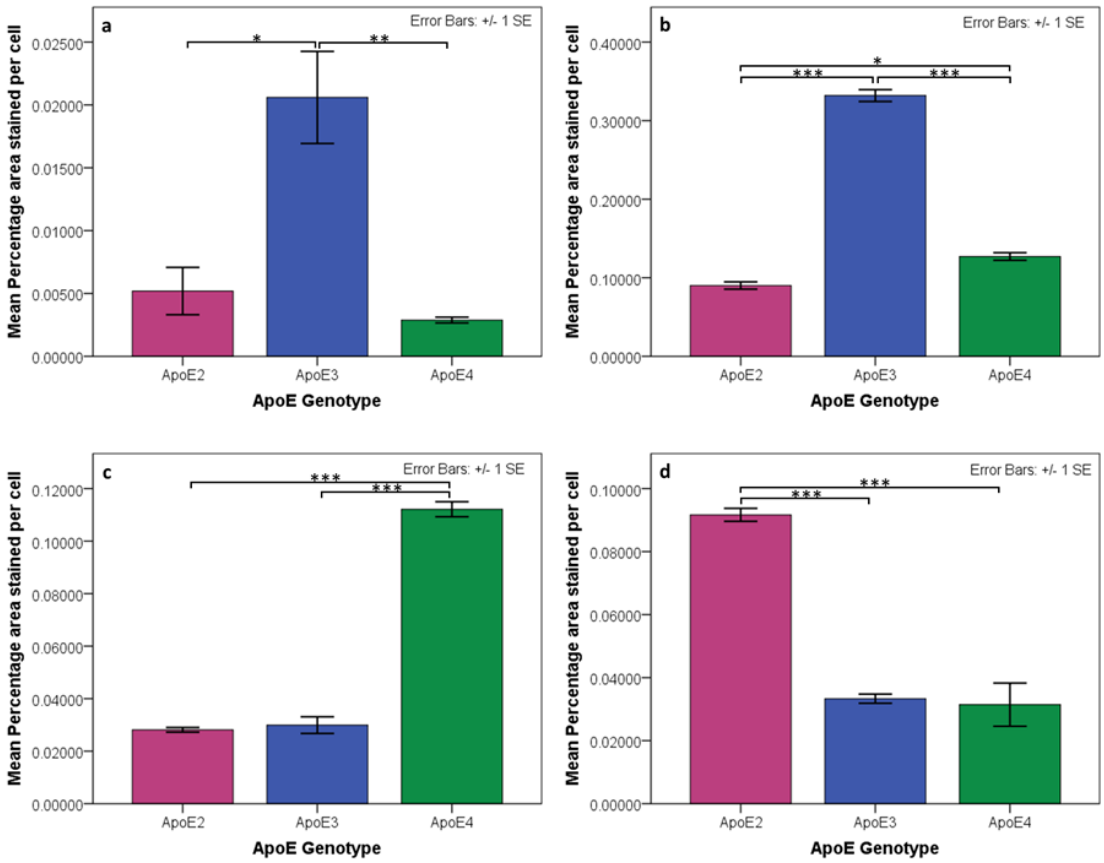

Figure 3-11 – quantification of basement membrane protein produced per cell in ApoE astrocytes after 72 hours

The graphs represent the percentage area stained per cell for: a) collagen IV, b) laminin, c) fibronectin and d) perlecan. The percentage area stained per cell was calculated by dividing the percentage area stained by the cell number. Values were obtained from three fields of view per coverslip and a total of three coverslips per protein over three independent experiments (n=3) Collagen IV and laminin are highest in ApoE3, fibronectin is highest in ApoE4 and perlecan is highest in ApoE2. Error bars represent the standard error of the mean and significance is indicated as follows: *p<0.05, **p<0.01, ***p<0.001.

Once cell density was taken into account, the percentage area stained per cell showed that collagen IV and laminin are most highly expressed in ApoE3 astrocytes, fibronectin is most highly expressed in ApoE4 cells and perlecan is most highly expressed in ApoE2 cells (see **Figure 3-11**).

Given the earlier result that showed the difference in the growth rate of the ApoE astrocytes (**Figure 3-5**), it was not surprising that the percentage area stained for most of the proteins was highest in ApoE2 astrocytes, followed by ApoE3 then ApoE4, following the trend of cell number, suggesting that the more cells that are present the more protein is produced. The exception to this was collagen IV where the highest percentage area stained was in the ApoE3 cells as opposed

to ApoE2. To further investigate this and correct for the difference in cell density between the ApoE isoforms the same experiments were carried out but each cell line was allowed to grow to 100% confluence before being fixed. These results are shown below (**Figure 3-12**).

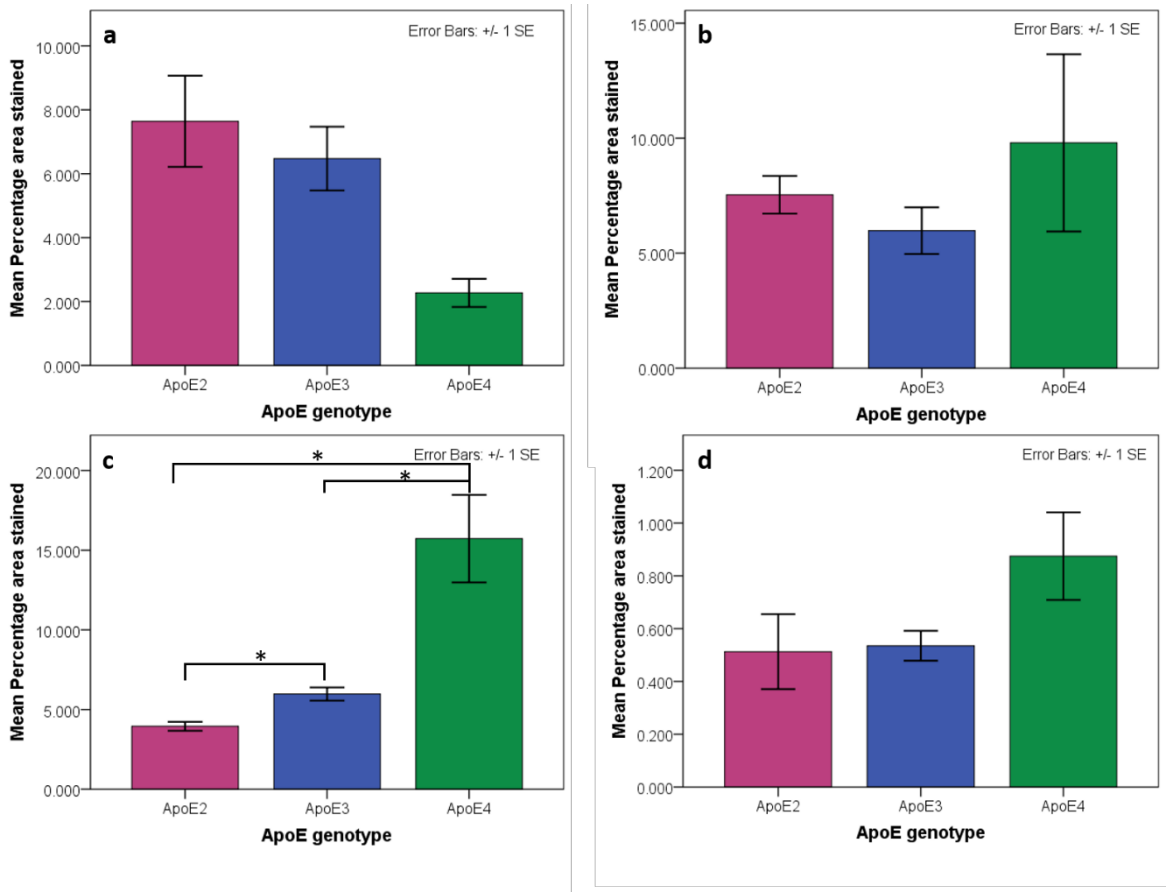

Figure 3-12 quantification of basement membrane proteins in the confluent ApoE astrocytes

The graphs represent the percentage area stained for: a) collagen IV, b) laminin, c) fibronectin and d) perlecan. The mean percentage area stained was calculated from three fields of view per coverslip and a total of three coverslips per protein over three independent experiments (n=3) Astrocytes expressing ApoE4 had the highest expression of laminin, fibronectin and perlecan, with fibronectin staining significantly higher compared to ApoE2 and ApoE3 expressing astrocytes. Collagen IV expression was highest in ApoE2 cells, though was not significantly different from ApoE3 or ApoE4 cells. Error bars represent the standard error of the mean with significance indicated by an asterisk.

When the astrocytes were grown to the same confluence there was largely no significant difference in the expression of basement membrane proteins. The exception was fibronectin where there was a genotype dependent increase in the percentage area stained for fibronectin (E2<E3<E4) with all differences measured as statistically significant ($p=0.027$). Collagen IV expression was lower in ApoE4 expressing astrocytes compared to other genotypes although this was not statistically significant ($p=0.113$).

3.3.6 Other membrane-associated proteins

Immunostaining for other proteins was also carried out (see **Table 3-1** for details). The results below show the percentage area stained for dystrobrevin, aquaporin IV and tissue inhibitor of metalloproteinase 3 (TIMP3) as these were the only antibodies that showed positive staining in the astrocyte cultures.

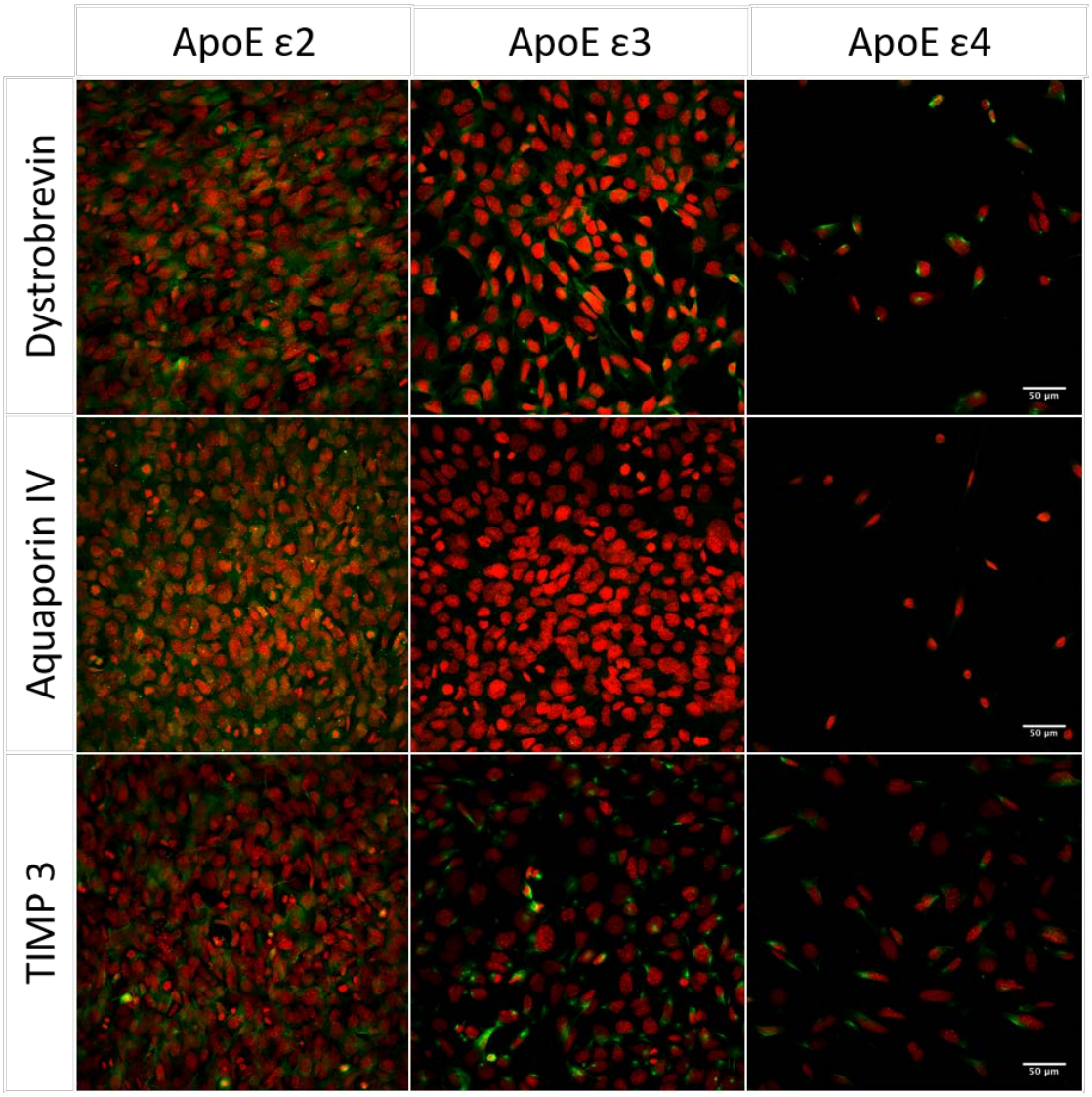

Figure 3-13 – immunofluorescence staining for dystrobrevin, aquaporinIV and TIMP 3 in ApoE astrocytes after 72 hours

Representative images to show the immunostaining for dystrobrevin, aquaporin IV and TIMP 3, shown in green. To show cell density nuclei are stained with DAPI and shown in red. Scale bar 50µm.

Once again, the difference in cell density is very apparent when comparing the DAPI staining between the ApoE isoforms (see **Figure 3-13**) so quantification for the total percentage area stained and the percentage area stained divided by the cell number was performed (shown in **Figure 3-14**).

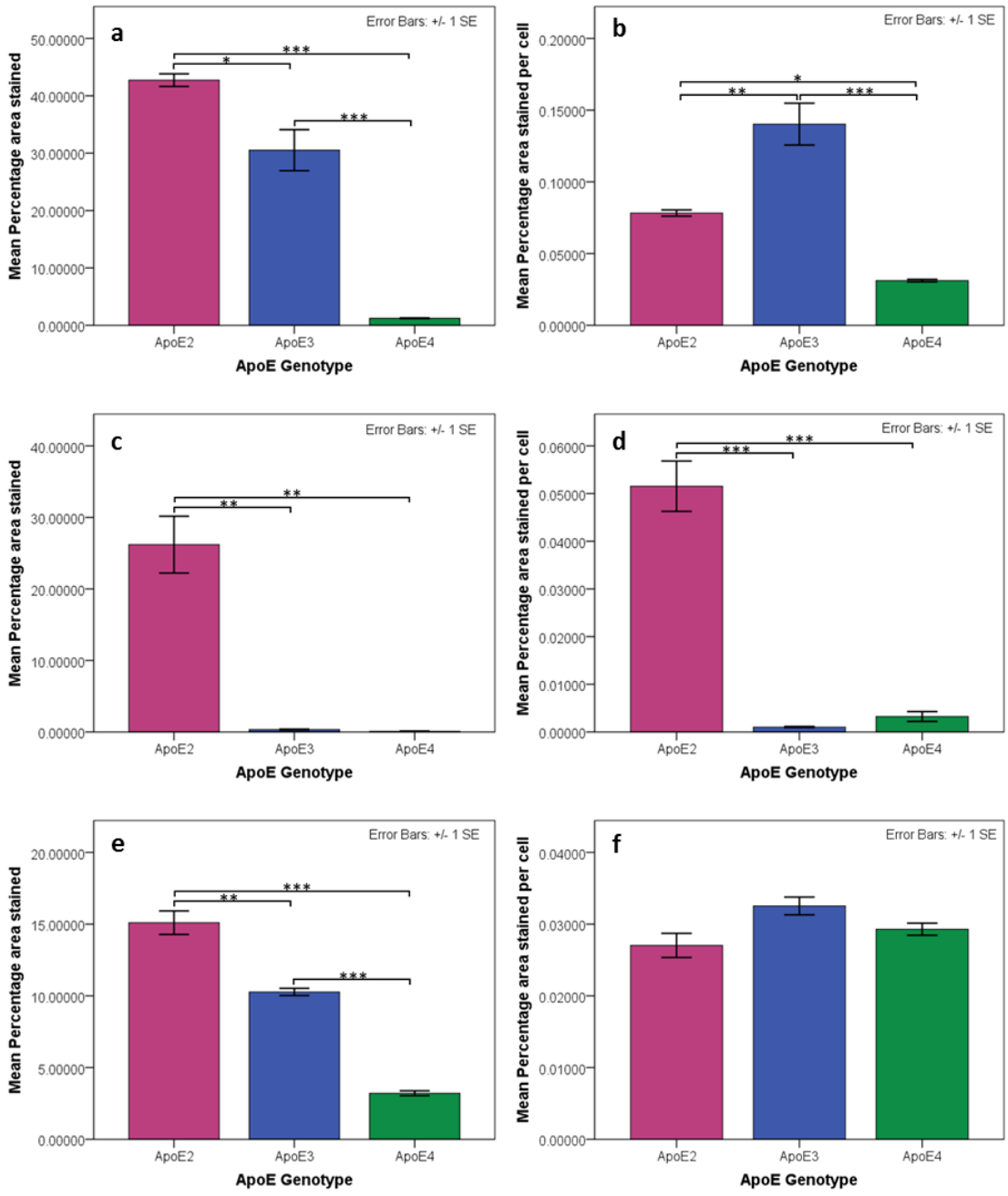

Figure 3-14 – quantification of dystrobrevin, aquaporin IV and TIMP 3 staining in ApoE astrocytes

Graphs a) and b) show dystrobrevin staining, graphs c) and d) show aquaporin IV staining and graphs e) and f) show TIMP 3 staining. Values for percentage area stained and percentage area stained per cell were calculated from three fields of view per coverslip and a total of three coverslips per protein over three independent experiments (n=3) Graphs a), c) and e)

show the total percentage area stained for the protein of interest whilst graphs b), d) and f) show the fraction of the percentage area stained as a function of the number of cells. Error bars represent the standard error of the mean and significance is indicated as follows: *p<0.05, **p<0.01, ***p<0.001

The total percentage area stained for dystrobrevin, aquaporin IV and TIMP 3 was highest in the ApoE2 astrocytes, followed by ApoE3 astrocytes then ApoE4 astrocytes. When the percentage area stained per cell was calculated the results showed that dystrobrevin expression was significantly lower in the ApoE4 astrocytes when compared to astrocytes expressing ApoE2 ($p<0.05$) or ApoE3 ($p<0.001$). Dystrobrevin expression was also significantly higher in ApoE3 astrocytes compared to ApoE2 astrocytes ($p<0.01$). The percentage area stained per cell for aquaporin IV was significantly higher in ApoE2 astrocytes compared to other genotypes ($p<0.001$). There were no significant differences observed in the TIMP3 percentage area staining per cell.

3.3.7 Amyloid beta experiments – static and flow

After calibrating the peristaltic pump the first flow experiment was conducted without the addition of amyloid beta to investigate how well the cells grow within the quasi vivo system and to ascertain if flow alone influences the cells. The results are shown in **Figure 3-15**. The astrocytes grew well inside the Quasi Vivo system, indicating the polymer was biocompatible and did not adversely affect the cells. The astrocytes expressed GFAP regardless of the culture conditions. A qualitative comparison of cell densities between the static and flow cultures showed very little difference, in fact the cells appeared to grow slightly better under flow. The flow rate of 10µL/min also had no adverse effect on the cells. Astrocytes are not exposed to shear stress in an *in vivo* environment and this low flow rate ensured that the shear is negligible in the system.

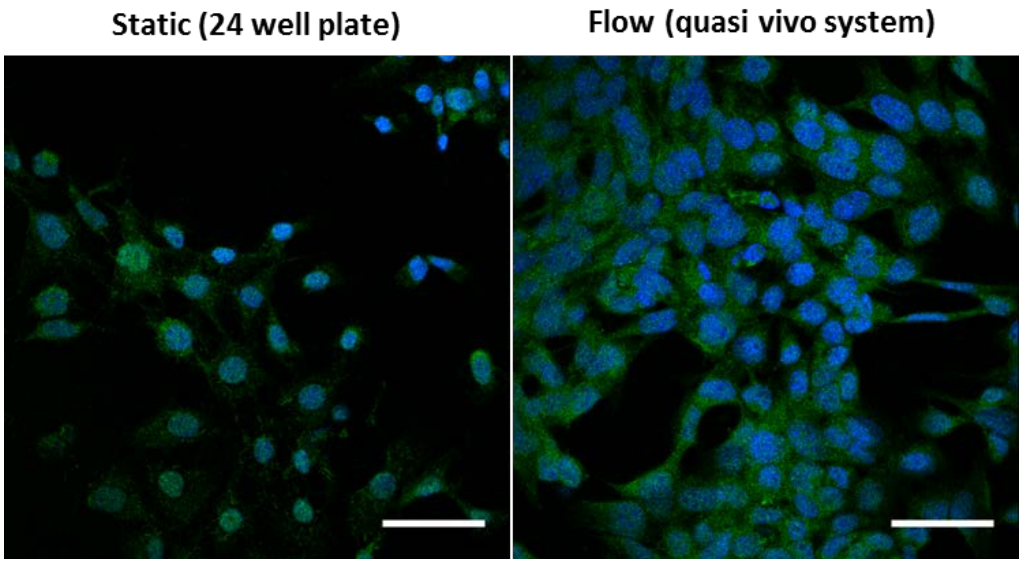

Figure 3-15 Flow is not detrimental to ApoE4 astrocytes grown in culture

ApoE4 astrocytes were grown for 24 hours in either a 24 well plate or the QV500 single chamber set up with 10µl/min flow. There is no obvious or significant difference between the cells grown under static and flow conditions. Densities, shown by DAPI staining in blue, are very similar and pattern of GFAP staining, shown in green, is also comparable. Scale bar 50µm.

Aβ was observed after its application on all three ApoE isoforms. The pattern of distribution of the HiLyte 555-labelled amyloid beta 1-40 was different when the static cultures were compared to the flow cultures (see **Figure 3-16**), with the Quasi Vivo system enhancing the pattern of distribution in all astrocyte cultures.

The ApoE2 astrocytes appeared to be unaffected by the Aβ and the appearance of the cells across the different conditions tested is uniform. The ApoE3 cells also appear largely unaffected by the Aβ, although there is a higher concentration of Aβ present where the ApoE3 cells are densest.

The addition of 100nM Aβ 1-40 had a detrimental effect on the ApoE4 astrocytes (see **Figure 3-16**). This effect appeared to be enhanced when combined with flow. In addition to a reduced number of cells there are morphological alterations to the ApoE4 astrocytes when exposed to Aβ. The cells appear much more isolated than the ApoE2 or ApoE3 astrocytes and contact between the cells is reduced.

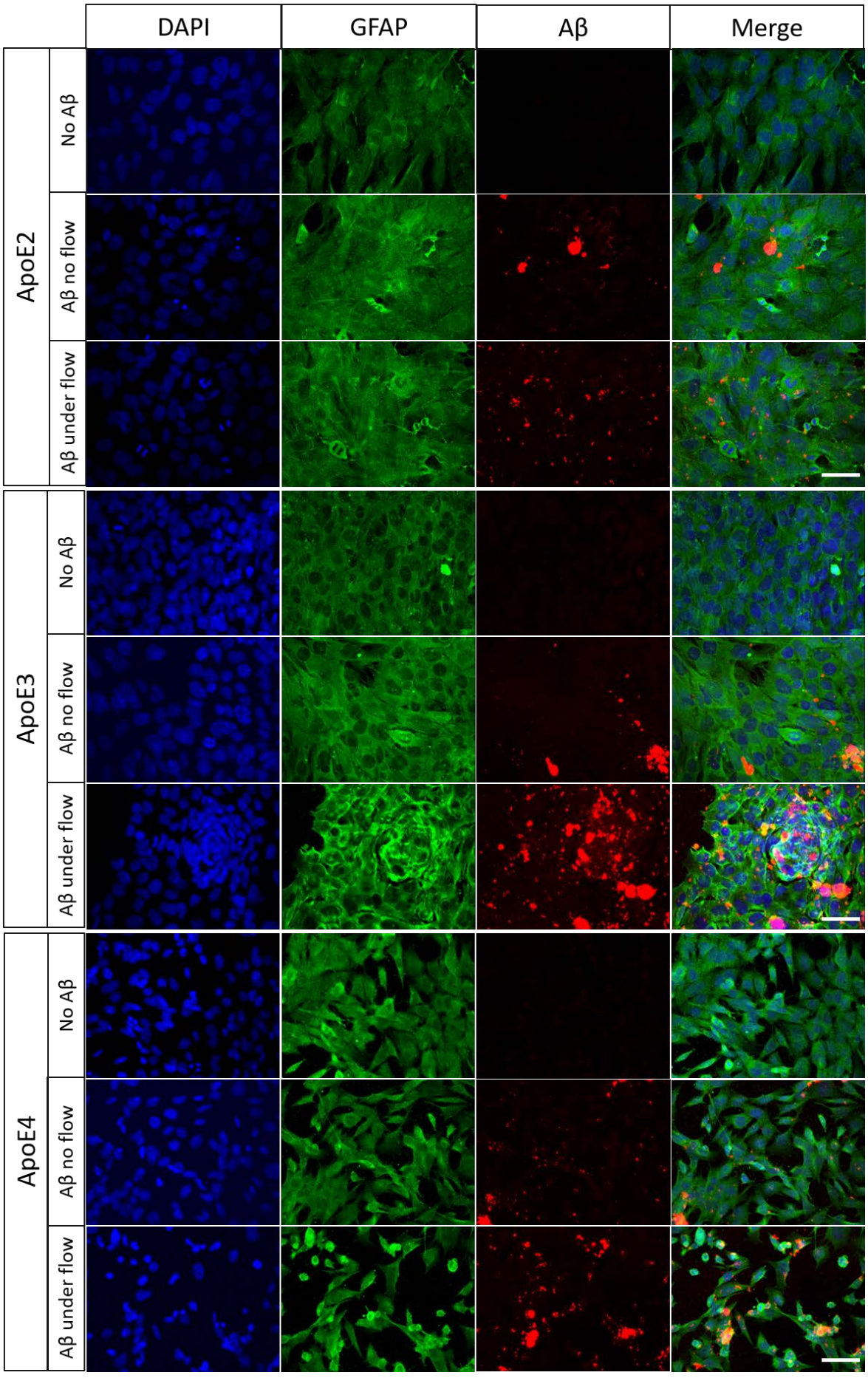
DAPI
GFAP
Aβ
Merge
ApoE2
ApoE3
ApoE4
No Aβ
Aβ no flow
Aβ under flow

Figure 3-16 triple immunofluorescence staining of ApoE astrocytes treated with 100nM Aβ

ApoE astrocytes were grown under static or flow conditions with 100nM Aβ 1-40 supplemented in the growth medium. After 24 hours of exposure the cells were stained for GFAP (green) and DAPI (blue) with the Aβ shown in red. All of the astrocyte cultures appeared to be unaffected by Aβ with no flow and the patterns of GFAP staining appear relatively unchanged. When exposed to flow of Aβ the ApoE4 astrocytes appeared sparser and clusters of ApoE3 astrocytes were observed where there were deposits of Aβ. ApoE2 astrocytes appeared unaffected by a flow of Aβ. Scale bar 50μm.

3.4 Discussion

3.4.1 ApoE genotype influences astrocyte growth rate

All three cell lines were plated at the same density and grown in identical conditions but the number of cells counted after 72 hours was significantly different in cell culture. Astrocytes that express ApoE4 take longer to reach confluence in culture and therefore proliferate at a much slower rate, compared to the other ApoE alleles. This suggests that ApoE genotype influences the growth and proliferation of astrocytes.

Glucose hypometabolism, associated with a decreased uptake of glucose by astrocytes (Nehlig and Coles, 2007), has been observed in non-demented ApoE4 carriers (Small *et al.*, 1995; de Leon *et al.*, 2001; Reiman *et al.*, 2001). This suggests that ApoE4 either affects the metabolic function of astrocytes or there are fewer astrocytes. Studies have demonstrated that modified ApoE can induce an endoplasmic reticulum stress response in astrocytes that may impair their function (Zhong, Ramaswamy and Weisgraber, 2009) but perhaps a reduction in the turnover of astrocytes in ApoE4 carriers, as suggested by this study, may also play a role in the hypometabolism observed in ApoE4 carriers.

3.4.2 ApoE4 genotype affects the morphology of astrocytes in culture

In addition to fewer astrocytes, the morphology of astrocytes expressing ApoE4 also appeared to be altered. Astrocytes are so named for their distinct ‘star shaped’ appearance but the ApoE4 astrocytes looked more triangular when viewed with CLEM. More interestingly they also had significantly fewer processes than astrocytes expressing other ApoE isoforms and less laminin was observed along these processes. The processes of astrocytes terminate in attachments known as end feet. The end feet are applied to the surfaces of blood vessels, dendrites and the pia mater. These connections allow astrocytes to support the function of neurons by regulating ion concentration in the extracellular spaces of the CNS (Walz, 2000) as well as a host of other

potential activities including maintaining the integrity of the BBB and formation of the pial-glial membrane.

The ApoE2 and E3 astrocytes showed laminin staining on the astrocyte processes which was not as apparent on the ApoE4 astrocytes, probably due to the change in shape resulting in fewer processes extending from the cell body. Astrocytic laminin has been shown to have a number of important roles and has a crucial role in maintaining the integrity of the BBB (Yousif, Di Russo and Sorokin, 2013b; Yao *et al.*, 2014). Ablation of astrocytic laminin has also been shown to impair the function of vascular smooth muscle cells and result in haemorrhagic stroke (Chen *et al.*, 2013). Since the main point of contact between astrocytes and the cerebral blood vessels is via the end feet, the localisation of laminin to the end feet observed by CLEM makes sense. The morphological differences in the ApoE4 astrocytes mean there are fewer processes and therefore fewer points of contact with the vessel wall. Further to this, there was less laminin observed on the processes. It is therefore likely that astrocytes expressing ApoE4 are unable to provide the necessary support to maintain a healthy blood brain barrier or vessel wall integrity. It is possible that individuals possessing the ApoE4 allele may also experience problems associated with this; indeed ApoE4 is a risk factor for lobar intracerebral haemorrhage (Woo *et al.*, 2013) providing further evidence to support these findings. It is possible that the combination of a reduced number of processes and a lack of astrocytic laminin in ApoE4 expressing astrocytes may impair the function of vascular smooth muscle cells and fail to provide adequate support to the endothelial cells to maintain the BBB, resulting in a suboptimal vasculature that is more susceptible to microbleeds and haemorrhage. Brain microbleeds are thought to play a key role in the pathophysiology of AD so in addition to increasing the risk of stroke, ApoE4 astrocytes with fewer processes may also contribute to AD pathology. A significant reduction in the number of astrocytic processes may impact the functionality of the astrocyte and reduce its activity.

3.4.3 ApoE genotype may influence Aβ accumulation by changing the basement membrane

When comparing the percentage area stained for basement membrane proteins at the same timepoint, there are more glycoproteins (collagen IV and laminin) produced per cell in ApoE3 astrocytes compared to the other ApoE isoforms. Glycoproteins such as collagen IV and laminin have been shown to induce disassembly of Aβ 1-42 fibrils (Kiuchi *et al.*, 2002) and collagen IV has been shown to inhibit Aβ 1-40 fibril formation by preventing the formation of a beta-structured aggregate of Aβ 1-40, which leads to fibrillization (Kiuchi, Isobe and Fukushima, 2002). Both

ApoE2 and ApoE4 expressing astrocytes produced less glycoprotein per cell indicating they may be more susceptible to accumulation of Aβ by encouraging fibrillization however, ApoE2 expressing astrocytes may be able to compensate for this because of the increased growth rate meaning more cells are available to produce these glycoproteins, making the overall glycoprotein production similar to that of ApoE3 expressing cells. Individuals possessing an APOE ε4 allele are at increased risk of developing AD. The lack of glycoprotein produced by ApoE4 astrocytes may produce conditions that are favourable for the fibrillization of Aβ, allowing it to accumulate more readily and increasing the Aβ burden on the clearance mechanisms of the brain.

The heparan sulphate proteoglycan perlecan has been shown to bind to Aβ, accelerating the formation of Aβ 1-40 and 1-42 fibrils and maintaining their stability (Castillo *et al.*, 1997). Interestingly perlecan expression was quite significantly higher in the ApoE2 cells compared to ApoE3 and ApoE4; this is contrary to what was expected as possession of an ApoE2 allele is thought to offer some protection against AD but higher levels of perlecan favour the formation of Aβ fibrils, one of the pathological hallmarks of AD. It is possible that the increased glycoprotein produced by the ApoE2 astrocytes is enough to cancel out the effect of a high expression of perlecan or perhaps another mechanism is employed to efficiently remove the Aβ. It is also possible that cell density may play a role in the expression of perlecan. When the astrocytes were grown to the same level of confluence perlecan expression was highest in ApoE4 astrocytes though this was not significant. Perlecan expression therefore appears to be correlated with cell density and the high expression observed in the ApoE2 cells at 72 hours may be related to cell density and not just ApoE genotype.

The amount of fibronectin produced per cell is significantly higher in ApoE ε4 cells than other ApoE isoforms. The overall percentage area stained for fibronectin was also significantly higher in ApoE4 expressing astrocytes when the cells were grown to the same confluence, indicating that an astrocyte expressing ApoE4 produces more fibronectin than other ApoE isoforms regardless of cell density. Although the amount of fibronectin has not been shown to be altered in AD, the amount of fibronectin associated with the capillary wall is increased at sites of Aβ deposition (Morris *et al.*, 2014). Fibronectin can also be found in amyloid plaques, indicating there is a relationship between fibronectin and Aβ levels. The higher expression of fibronectin in the basement membrane of ApoE4 expressing astrocytes could further increase the likelihood of Aβ accumulation and the risk of developing AD. The aggregation properties of Aβ were not explored in this study and so it has not been shown conclusively that Aβ fibrilizes and accumulates more easily in the presence of ApoE4 astrocytes. Further work is needed to demonstrate the ApoE genotype dependent composition of the astrocytic basement membrane can influence the aggregation and accumulation of Aβ.

3.4.4 Dystrobrevin and aquaporin IV expression is significantly decreased in ApoE4 expressing astrocytes

Dystrobrevin staining was localised to the cell body in all the ApoE genotypes. There was a significant genotype dependent decrease in the overall percentage area staining for dystrobrevin (E2>E3>E4) but this was different for the percentage area stained per cell with ApoE3 astrocytes producing the most dystrobrevin, followed by ApoE2 cells, then ApoE4 (**Figure 3-14**). Dystrobrevin is part of a complex of proteins known as the dystrophin-associated protein complex (DPC). The DPC forms a transmembrane link between the extracellular matrix and the cytoskeleton, effectively anchoring the basement membrane to the cell. Dystrophin connects the filamentous actin in the cytoskeleton to β-dystroglycan, which in turn is connected to laminin and agrin of the basement membranes (Nagelhus and Ottersen, 2013). Given that the DPC binds to the cytoskeleton of cells, the pattern of dystrobrevin staining was expected. The DPC is required for the localisation of AQP4 on glial end feet so the reduced dystrobrevin in ApoE4 astrocytes may negatively impact the AQP4 channels expressed on the end feet.

Aquaporin IV is a water-channel present on astrocytes. It regulates water transport through plasma membranes and is driven by osmosis. The expression of AQP4 is widely expressed in the astrocyte plasma membrane but is highly concentrated on the astrocytic end feet (Nielsen *et al.*, 1997; Rash *et al.*, 1998) and is in contact with the glia limitans basement membrane. Deletion of AQP4 results in a slowed CSF influx and a reduction in interstitial solute clearance (Iliff *et al.*, 2012), indicating that astrocytic water transport via AQP4 may help to facilitate Aβ clearance. A lack of AQP4 may therefore reduce the astrocytic clearance of Aβ. Although there was no difference observed between ApoE3 and ApoE4 astrocytes in the percentage area stained for aquaporin IV, the reduced levels of dystrobrevin staining in ApoE4 astrocytes may negatively impact the localisation of the aquaporin IV channels to the astrocytic end feet and influence the water transport capabilities of AQP4. The reduced number of processes observed in ApoE4 expressing astrocytes (section 3.3.3) may also influence the water transport driven by AQP4 and reduce interstitial solute clearance. The lower risk of AD in ApoE2 carriers may be due to a more optimal expression of AQP4, compared to the other genotypes, allowing for better control of water movement and fluid homeostasis in the brain. This may in turn lead to better solute clearance and reduced levels of Aβ.

3.4.5 ApoE genotype is a factor in TIMP 3 expression

There is a genotype dependant decrease in total percentage area stained for TIMP 3 (E2>E3>E4) after 72 hours in culture. Tissue inhibitor of metalloproteinases-3 (TIMP 3) belongs to a family of proteins that inhibit matrix metalloproteinases (MMPs). An increased expression of TIMP 3 may serve to protect the basement membrane from degradation by the MMPs and preserve the extracellular environment. It is worth noting there was no significant difference in percentage area staining per cell so the genotype dependent decrease is a result of the difference in cell density observed after 72 hours. TIMP 3 expression is appears to be correlated with cell density and cell density is related to ApoE genotype so although TIMP 3 expression is not altered based solely on ApoE genotype it is a factor.

3.4.6 The relationship between amyloid beta distribution and ApoE genotype

Although the concentration of Aβ was unchanged in the static and flow cultures, the amount of Aβ the cells were exposed to was likely to be different. In static conditions the Aβ settles and remains undisturbed so it can only influence the cells it is in contact with. Aβ has a high affinity for itself (Verdier, Zarandi and Penke, 2004) so can easily form large clumps. Flow allows constant movement of the Aβ which increases its chance of exposure to cells; this leads to a much better and diffuse coverage of Aβ; this is more representative of the brain where Aβ is constantly produced and degraded. This may explain the enhancement that flow has on Aβ induced effects.

The number of ApoE4 expressing astrocytes appeared to be reduced after the addition of Aβ and this was most obvious in the cultures exposed to flow of Aβ. This was in contrast to cultures of ApoE4 cells exposed to flow in the absence of Aβ where there were no obvious differences from the static cultures. The ApoE4 cells also appeared rarefied and more isolated than the ApoE2 or ApoE3 astrocytes and contact between the cells is reduced. Astrocytic ApoE4 has been shown to impair the *in vivo* clearance of Aβ and reduce the lysosomal degradation within cells expressing ApoE4 (Persson *et al.*, 2017). If cell morphology is altered in the presence of Aβ, as suggested by the representative images in **Figure 3-16**, this could impact the cells ability to degrade Aβ and may help to explain the reduced efficiency of Aβ clearance in ApoE4 astrocytes.

The ApoE2 and ApoE3 cultures appeared to be unaffected by the presence of Aβ. Possession of the APOE ε2 allele is thought to offer neuroprotection and reduce the risk of development of AD. Astrocytes expressing ApoE2 appeared to grow normally when exposed to 100nM Aβ 1-40 which may allow the brain to function normally even when Aβ begins to accumulate. There were clusters of cells observed in ApoE3 astrocyte cultures in the presence of Aβ. It is unclear whether the Aβ is attracted to the large clusters of cells or the cells accumulate where there is a high

concentration of Aβ, indicating a potential defence mechanism. The latter is the most logical explanation as these clumps of cells were only observed in the presence of Aβ in ApoE3 expressing astrocytes and were more common under flow.

The ApoE genotype may also influence the Aβ. Almost all of the Aβ was closely associated to the ApoE4 astrocytes whereas Aβ can be found where there are no cells in the other ApoE genotypes. It has been demonstrated that the affinity of Aβ for ApoE4 is highest (Carter, 2005) and these results suggest that the Aβ is attracted to the cells producing ApoE4 but not to the other isoforms. Individuals possessing the APOE ε4 allele are at increased risk of developing AD and the increased sensitivity of ApoE4 astrocytes to Aβ may help to explain this.

3.5 Conclusions

I have demonstrated with the use of immunofluorescence staining and transgenic mouse ApoE astrocytes that the composition of the astrocytic basement membrane is dependent on the ApoE genotype. The basement membrane of ApoE4 astrocytes contains less immunocytochemical expression of collagen IV and laminin, which help to prevent amyloid fibrillization, suggesting that ApoE4 positive cells produce a basement membrane that favours the fibrillization of Aβ and allowing it to accumulate more easily. This may help to explain why ApoE4 increases the risk of development of AD. Astrocytes expressing ApoE2 have increased production of AQP4 which is key in maintaining fluid homeostasis in the brain by the osmotic movement of water through plasma membranes. This may facilitate a more efficient route of Aβ clearance and provides a potential explanation of the neuroprotective role of ApoE2 with respect to AD development. Further to this, the growth rate of the ApoE astrocytes differs in culture (E2>E3>E4).The ApoE4 astrocytes are slower to proliferate and produce protein so they may be slow to react to changing conditions in the brain with age, meaning individuals that express ApoE4 may be less able to deal with the increased amyloid burden as other mechanisms of clearance fail, resulting in the onset of AD.

I have also developed a new technique for processing astrocytes for CLEM and have demonstrated that laminin is secreted along astrocyte processes and the number of processes is reduced in astrocytes expressing ApoE4. The morphological differences between ApoE4 astrocytes and the other isoforms means that laminin is not produced at the astrocyte end feet and this may lead to dysfunction in the vessel wall, which may result in microbleeds and haemorrhage.

This work has provided insight into how APOE genotype may affect astrocytes however it is important to note that these experiments were conducted over a short period (72 hours) and the cells were sub-confluent for most of this time. This prevented overcrowding that would have resulted in cell atrophy, however the differences observed in these experiments may be influenced by this and it is unclear whether a different timeframe would produce different results. This needs to be explored in more detail in the future or validated with *in vivo* experiments.

3.6 Future work

This work has demonstrated a novel insight into the effect of ApoE genotype on both the structure of astrocytes and their extracellular environment. Although the mouse astrocytes used for this study produce the isoforms of human ApoE there are differences in the cell biology of a mouse astrocyte compared to a human astrocyte. Ideally the differences observed in this study would be investigated further using either human astrocytes or human brain samples that have homozygous alleles for ApoE2, ApoE3 and ApoE4 to ascertain whether the genotype dependent effects observed in this study are applicable to humans. Using human brain samples would also remove the time factor limitation and this would more accurately reflect the *in vivo* environment. It would also be interesting to investigate if the number of copies of the E4 allele has an effect. The risk of developing AD increases with the number of ApoE4 alleles so it is possible that the degree to which the basement membrane is altered may also depend on the number of ApoE4 alleles. The relationship between astrocytes expressing ApoE4 and a flow of Aβ needs to be investigated more thoroughly with quantification to assess the decrease in cell number observed qualitatively. Additionally the aggregation characteristics of Aβ and its ability to accumulate in the presence of the different ApoE isoforms was not properly investigated. The Aβ images in **Figure 3-16** suggest that ApoE may influence Aβ accumulation and this should be investigated further, an ELISA would provide a way to measure the Aβ that had been taken up by cells by measuring the Aβ remaining in the media .Analysis of Z-stacks may provide insight into the dimensions of the Aβ clumps observed and could also indicate if Aβ was internalised by the cells or stuck to the surface.

Chapter 4 Cells of the cerebrovasculature have unique basement membrane profiles

4.1 Introduction

Most cells are surrounded by a supporting scaffold of extracellular glycoproteins and proteoglycans that offer anchorage and structural support. These extracellular proteins form a dense sheet known as the basement membrane. The basement membranes of cerebral capillaries and arteries have been shown to be involved in intramural periarterial drainage (IPAD) and the clearance of solutes from the brain parenchyma (Carare *et al.*, 2008; Hawkes *et al.*, 2014; Morris *et al.*, 2014) so it is important to investigate the composition of these drainage channels.

4.1.1 Structure of the basement membrane

The exact composition of basement membranes varies in a temporal and tissue specific manner (Uhlen *et al.*, 2015; 2019), however it is highly conserved and consists of a core set of proteins. Typically each basement membrane will include laminin, collagen IV, nidogen and a heparan sulphate proteoglycan such as perlecan or agrin (Yurchenco, 2011). Fibronectin is also an abundant ubiquitous extracellular matrix component (Wang, Yin and Chen, 2011).The arrangement of these core proteins in the basement membrane is summarised in **Figure 1-9** on page 24.

4.1.2 Function of the basement membrane

The basement membrane was considered to be an inert structure with its primary function to act as a support scaffold that anchors the epithelium to the underlying connective tissue. It is becoming increasingly clear however that the basement membrane is a dynamic and versatile environment that is able to regulate tissue function and repair (Mao *et al.*, 2015). Basement membranes also act as reservoirs, containing multiple growth factors that help to fine tune cellular functions (Mao *et al.*, 2015). The roles of basement membranes in humans are very diverse ranging from angiogenesis (Kubota *et al.*, 1988) to synapse regeneration as well as functioning as a physical barrier and filter controlling the passage of small molecules (Peckham, 2003) and preventing the invasion of malignant cells (Liotta *et al.*, 1980).

4.1.3 Basement membranes and neurodegeneration

Basement membranes are the pathways that are used to clear solutes from the brain. This process is known as intramural periarterial drainage (IPAD). IPAD fails with age and this is thought to allow the accumulation of amyloid beta. In human CAA, the accumulation of Aβ begins between the layers of smooth muscle cells in arterioles and the leptomeningeal arteries (see **Figure 4-1**a), eventually leading to the ablation of the smooth muscle cells (Keable *et al.*, 2016). After the smooth muscle is lost, the amyloid beta has been shown to colocalize with the endothelial basement membrane (see **Figure 4-1**b). This proposed sequence, based on observations in human post-mortem brains and brains of transgenic mice overexpressing Aβ, suggests that amyloid beta preferentially drains along the basement membranes of smooth muscle cells. It is accepted that smooth muscle cells secrete a basement membrane that is morphologically distinguishable from the endothelial basement membrane (Yousif, Di Russo and Sorokin, 2013b) and this is the focus of the study in the present chapter.

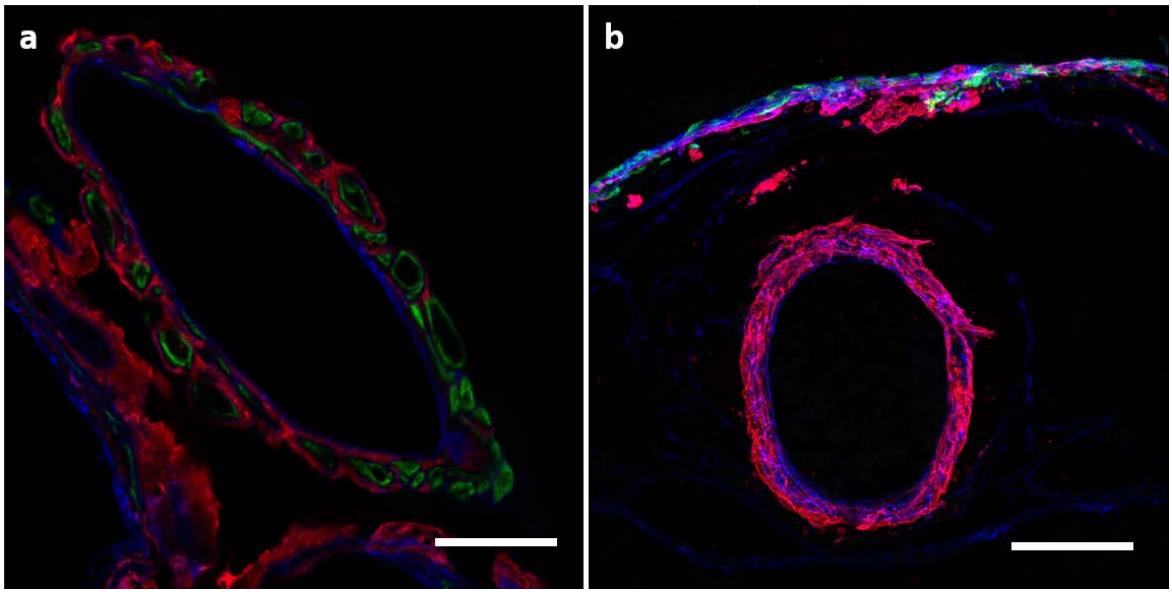

Figure 4-1 the progression of CAA in the walls of cerebral arteries in Alzheimer's disease

(a) Amyloid beta, shown in red, accumulates around the smooth muscle cells (shown in green) in the walls of cerebral vessels. The endothelial basement membrane (shown in blue) is intact and does not colocalize with amyloid beta at this stage. The smooth muscle is eventually completely replaced by amyloid beta (b) and there is colocalization of amyloid beta (red) and collagen IV (blue) in the basement membrane shown in pink. The loss of smooth muscle is likely to impact the integrity of the vessel wall. Scale bar 50µm.

4.1.4 Aims and hypothesis

The basement membrane is a conduit for the elimination of solutes from the brain and its composition may influence its ability to perform this vital task. The aim of this work is to assess the basement membrane produced by cerebrovascular cells in culture to test the hypothesis that smooth muscle cells produce a basement membrane that is attractive to amyloid beta and predisposes it to amyloid accumulation as CAA.

4.2 Materials and methods

4.2.1 Cell culture

Astrocytes (HA), pericytes (HP), smooth muscle cells (HBVSMC) and endothelial cells (hCMEC/D3) of human brain origin were grown according to the manufacturer's instructions in the relevant culture media (see sections 2.1.2.2 and 2.1.3.2 for details on culture media used). Cultures were maintained in a humidified environment (5%CO_2/95% air) at 37^{o}C. Each cell type was plated in 24 well-plates onto 12mm round glass coverslips coated with poly-L-lysine for HA, HP and HBVSMC or collagen I for hCMEC/D3. The initial seeding density of these experiments was 0.5x10^5 cells/coverslip and cells were placed in the incubator and left to grow for 72 hours before fixation and immunostaining.

4.2.2 Immunocytochemistry

Immunocytochemistry was selected as the technique for analysing the expression of basement membrane proteins. The basement membrane proteins are large insoluble fibrils that are resistant to proteases making techniques, such as immunoblotting, difficult to perform with potentially unreliable results. Immunocytochemistry allows qualitative analysis of the pattern of staining of proteins as well as quantitative comparison of protein expression levels within a single cell type. By omitting a permeabilisation step in the protocol only the extracellular protein will be stained, giving a true measure of the basement membrane instead of total protein concentration. The cells were fixed with 4% PFA for 10 minutes at room temperature before immunostaining for basement membrane proteins: collagen IV, laminin, fibronectin and perlecan. Cells were rinsed three times with PBS and then blocked for 1 hour with 15% NGS. Cells were then incubated overnight at 4^{o}C with primary antibodies as shown in **Table 4-1**. Cells were then washed three times with PBS and incubated with goat anti-rabbit Alexa Fluor 488 conjugated secondary antibody (Invitrogen, A11034) for 1 hour at room temperature. After washing three times with

PBS, 2µg/mL DAPI was added to cells for 10 minutes. Cells were rinsed with PBS and coverslips were removed and mounted onto slides with Mowiol and Citifluor.

Table 4-1 details of basement membrane antibodies used for immunofluorescence staining of human cell cultures

Antibody type	Antigen	Name provided by supplier	Supplier details	Optimal dilution
Primary	Collagen IV	Rabbit anti-collagen IV (ab6586)	Anti-collagen IV antibody polyclonal produced in rabbit, AbCam, Cambridge, UK	1:400
Primary	Laminin	Anti-laminin antibody produced in rabbit (L9393)	Anti-laminin antibody polyclonal produced in rabbit, Sigma Aldrich, St Louis, USA	1:200
Primary	Fibronectin	Anti-fibronectin antibody produced in rabbit (F3648)	Anti-fibronectin antibody polyclonal produced in rabbit, Sigma Aldrich, St Louis, USA	1:400
Primary	Perlecan	Perlecan antibody (H-300) sc-25848	Perlecan (H-300) rabbit polyclonal antibody 200 µg/ml, Santa Cruz Biotechnology, Heidelberg, Germany	1:400

4.2.3 Imaging and analysis

Cells were imaged with a Leica SP8 confocal microscope. Representative images were collected for qualitative comparison and 3 non-overlapping maximal projections were obtained per coverslip for quantification. Confocal settings were optimised for each antibody for maximum sensitivity without overexposure. Fluorescence intensity was measured for each image using the RGB measure tool in ImageJ. Fluorescence intensity is an arbitrary scale which assigns a numerical value based upon the brightness values of the pixels in an image correspond to the correct colour channel. The arbitrary fluorescence value for the green channel was obtained for each image and an average value per coverslip was calculated. The ratio of basement membrane proteins was also expressed as a percentage where 100% represents the combined fluorescence intensity of basement membrane proteins in one cell type Graphs were produced using Microsoft Excel and the results are based upon data gathered over three experimental runs (n=3).

4.3 Results

4.3.1 hCMEC/D3 produce endothelial markers and tight junction proteins

To assess the suitability of the hCMEC/D3 cell line and to demonstrate that the cells do retain the BBB properties as claimed by the manufacturer, staining was performed for the endothelial specific marker CD31 and the tight junction protein zonula occludens-1 (ZO1) (see **Figure 4-2**).

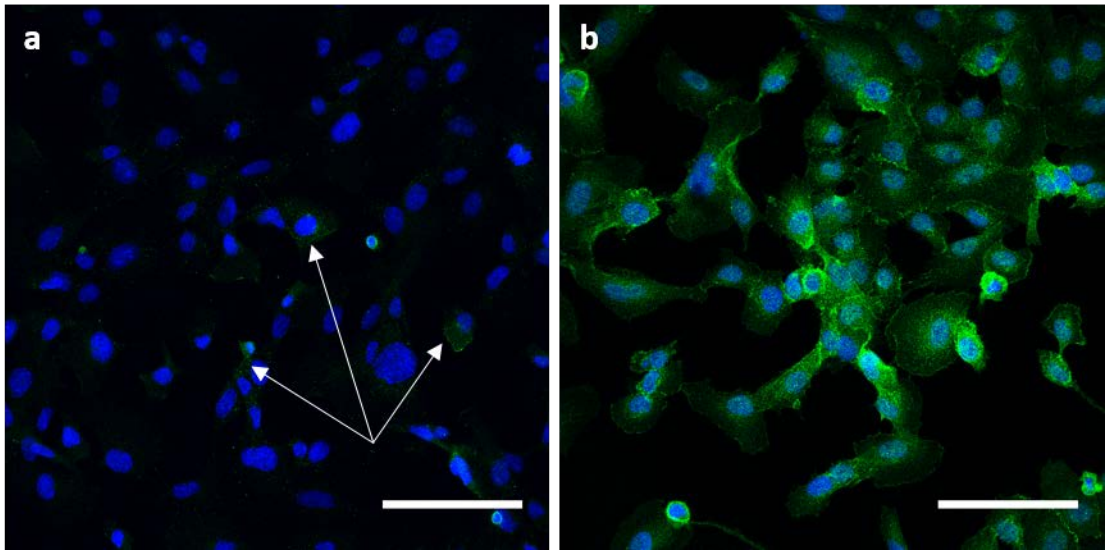

Figure 4-2 – CD31 and ZO-1 immunofluorescence staining of hCMEC/D3

CD31 staining shown in green (a) was very weak and not detectable across the whole slide but it is visible and indicated by the white arrows, showing the cells express at least some PECAM. CD31 expression appeared to be surround DAPI stained nuclei, shown in blue. ZO-1 staining (b) shown in green was clear and expressed by virtually all of the cells, indicating the presence of tight junction proteins in the endothelial cell cultures. Scale bar 100µm.

The CD31 staining was very weak and scarce in the sections but it was detectable and stronger than the signal from negative controls, indicating the cells do produce platelet endothelial cell adhesion molecule (PECAM), albeit in very small amounts. There was a strong expression of ZO-1 throughout the slide. It is important to note that at the time of staining the hCMEC/D3 cultures were only 72 hours old so it is unlikely that tight junctions would be fully formed, however the presence of tight junction proteins is a positive indicator that the cells can form tight junctions. Despite weaker than expected staining for CD31, the staining results support the manufacturers claims of phenotypic retention, indicating they will be suitable for use in this study.

4.3.2 Endothelial cells produce an unstructured basement membrane in culture

In the cultured human endothelial cells, collagen IV, laminin and fibronectin staining was apparent but perlecan was very weak (see **Figure 4-3**). The key components of the basement membrane were observed, but only in small quantities and there was no discernible pattern of staining. The endothelial cells were not capable of assembling a basement membrane when grown in culture for 72 hours.

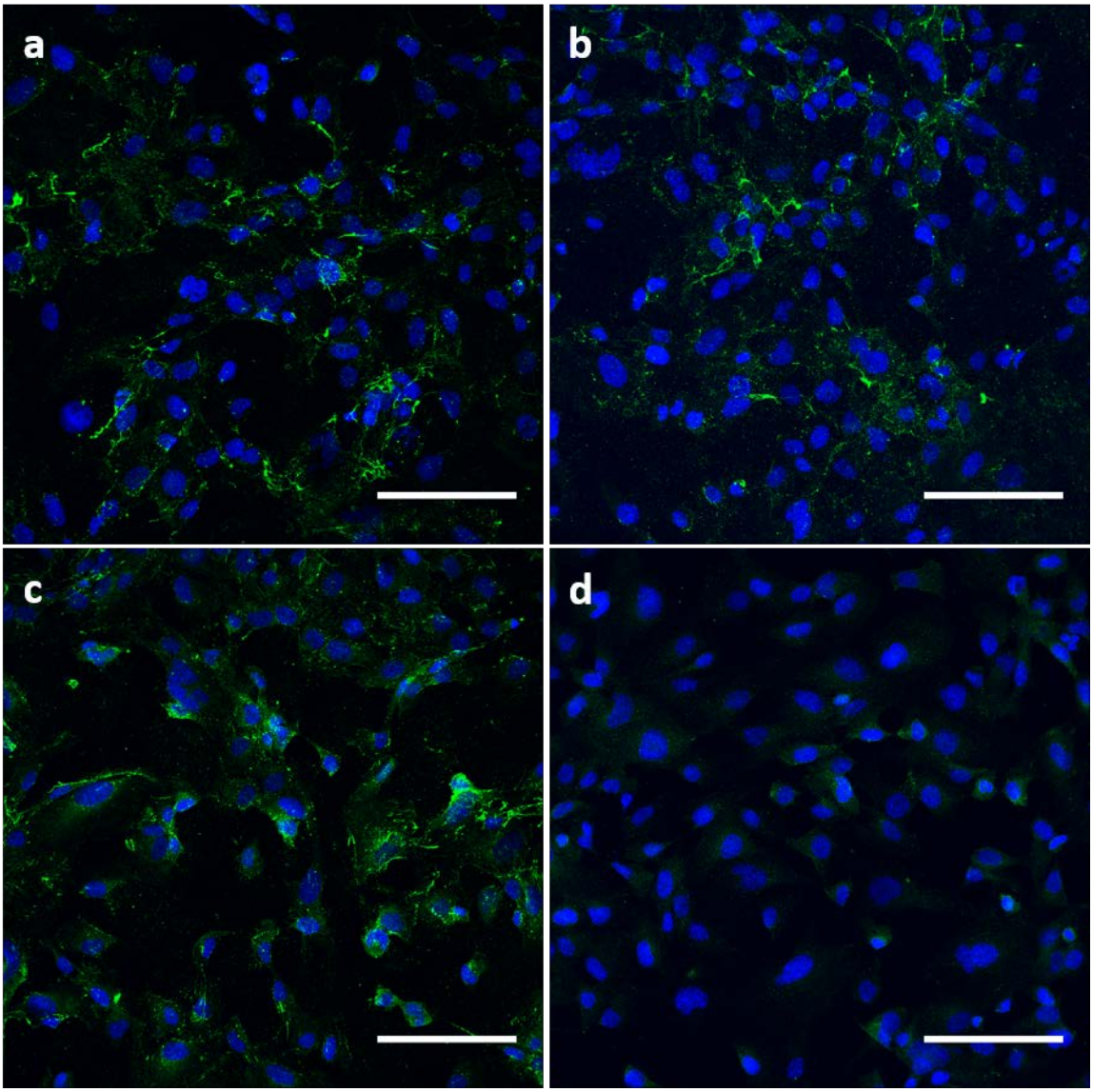

Figure 4-3 Basement membrane immunofluorescence staining in hCMEC/D3 cultures after 72 hours

hCMEC/D3 were immunostained with basement membrane proteins a) collagen IV, b) laminin, c) fibronectin and d) perlecan, shown in green. The DAPI stained nuclei are shown in blue. The pattern of staining for collagen IV, laminin and fibronectin was very similar and perlecan expression was very low. Scale bar 100µm.

4.3.3 Astrocytes and endothelial cell basement membranes have a similar composition

After 72 hours in culture, the staining for collagen IV and fibronectin and to a lesser extent laminin in the HA appeared highly ordered and web-like in their pattern of expression (see **Figure 4-4**). Perlecan staining however appeared to look the same in both endothelial and astrocyte cultures. The staining was very weak and appeared to be mainly focused around the cell nuclei. When comparing the fluorescence intensity of protein expression the quantitative results showed similar levels of protein production in the endothelial and astrocyte cultures. In both cultures the fluorescence intensity for fibronectin was the highest: 13.884 for HA vs 12.888 for hCMEC/D3 which corresponded to 35% and 32% respectively. Perlecan expression was also the lowest (14% for HA and 20% for hCMEC/D3). Despite the difference in structure, collagen IV expression levels were also similar (22% in HA compared to 26% in hCMEC/D3). Laminin expression was higher around astrocytes accounting for 29% compared to 22% in the endothelial cells.

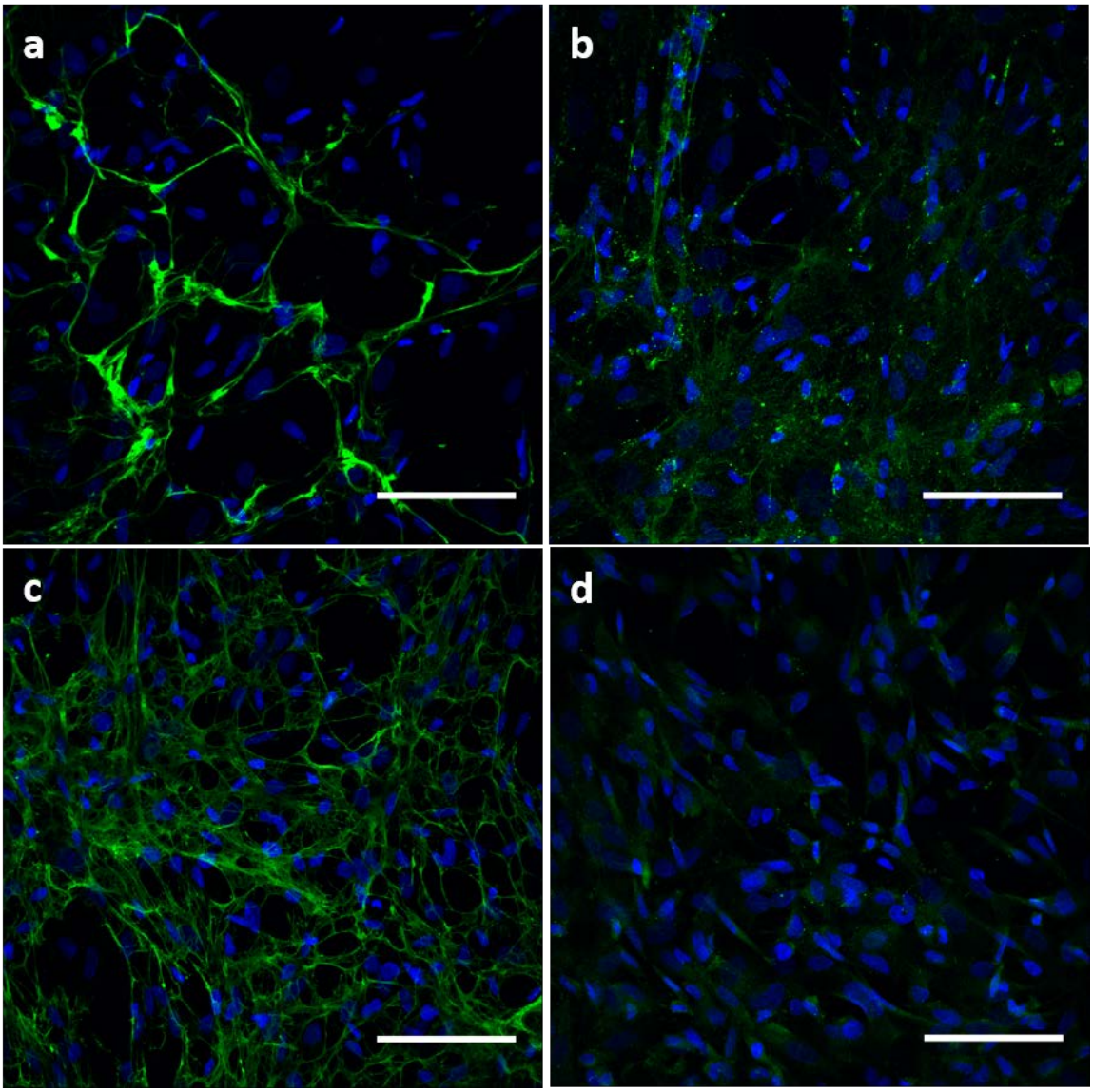

Figure 4-4 basement membrane immunofluorescence staining in HA cultures after 72 hours

HA were immunostained with basement membrane proteins a) collagen IV, b) laminin, c) fibronectin and d) perlecan, shown in green. The DAPI stained nuclei are shown in blue. The staining pattern of fibronectin (c) and to a lesser extent collagen IV (a) was extracellular, like a web. The collagen IV staining was also brighter indicating a higher concentration of staining. Laminin staining (b) appeared more diffuse with some areas of punctate staining. Perlecan staining (d) was very weak and localised closer to the cell nuclei. Scale bar 100µm.

4.3.4 Pericytes and smooth muscle cells have a similar basement membrane profile

There was a striking similarity in the basement membranes produced by HBVSMC and HP. Collagen IV expression was the highest in both cell types and they were composed of a near identical amount of collagen IV (arbitrary fluorescence values of 42.163 and 42.135 respectively), though this equated to a higher percentage in pericytes at 66% compared to 51% in smooth muscle cells. Fibronectin expression was also very similar accounting for 15% and 16% of

basement membrane staining in HBVSMC and HP respectively. When comparing the staining, both collagen IV and fibronectin staining resembled a web-like structure in both cell types (**Figure 4-5** and **Figure 4-6**). The biggest difference observed between HBVSMC and HP was in the expression of laminin. Qualitative comparison of the expression of laminin clearly showed a very different pattern of distribution between pericytes and smooth muscle cells. In cultures of pericytes, laminin staining was concentrated in focal areas and generally found around the nuclei. In contrast in the HBVSMC cultures laminin expression was much higher and formed a very fine mesh that covered the cell layer. This difference is reflected in the quantification, as the fluorescence intensity was more than double for laminin expression in the HBVSMC when compared to HP (18.714 vs 7.403). This difference was also translated to the percentage of laminin expression with 23% in HBVSMC cultures compared to only 11% in HP cultures.

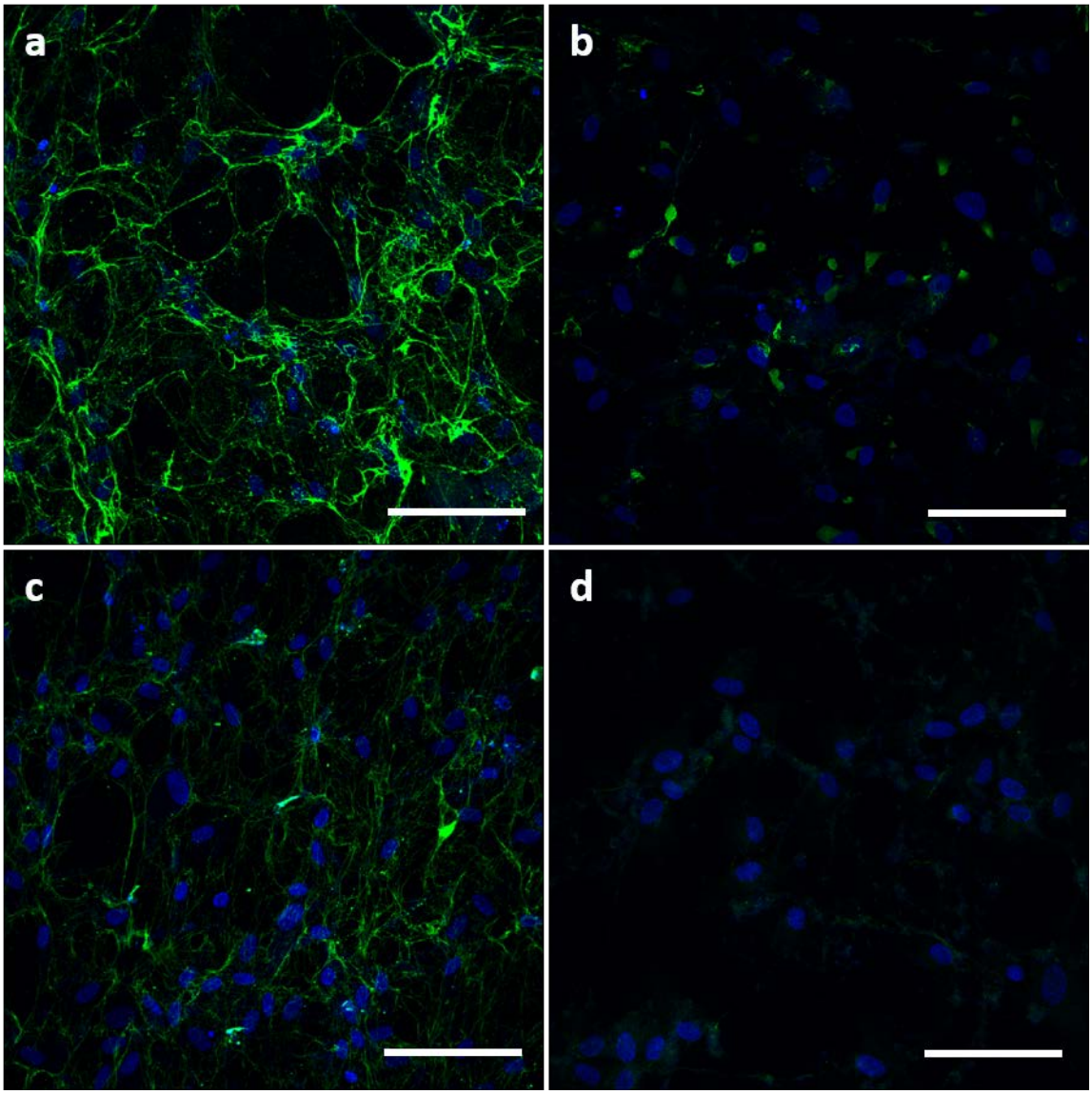

Figure 4-5 basement membrane immunofluorescence staining in HP cultures after 72 hours

72 hours after initial plating HP were immunostained with basement membrane proteins a) collagen IV, b) laminin, c) fibronectin and d) perlecan, shown in green. The DAPI stained nuclei are shown in blue. Collagen IV and fibronectin both demonstrated a reticular pattern of staining and the collagen IV staining was more intense. There were only small areas of focal laminin staining that was generally located around or near the nuclei. The pattern of perlecan staining was similar to laminin but much weaker. Scale bar 100µm.

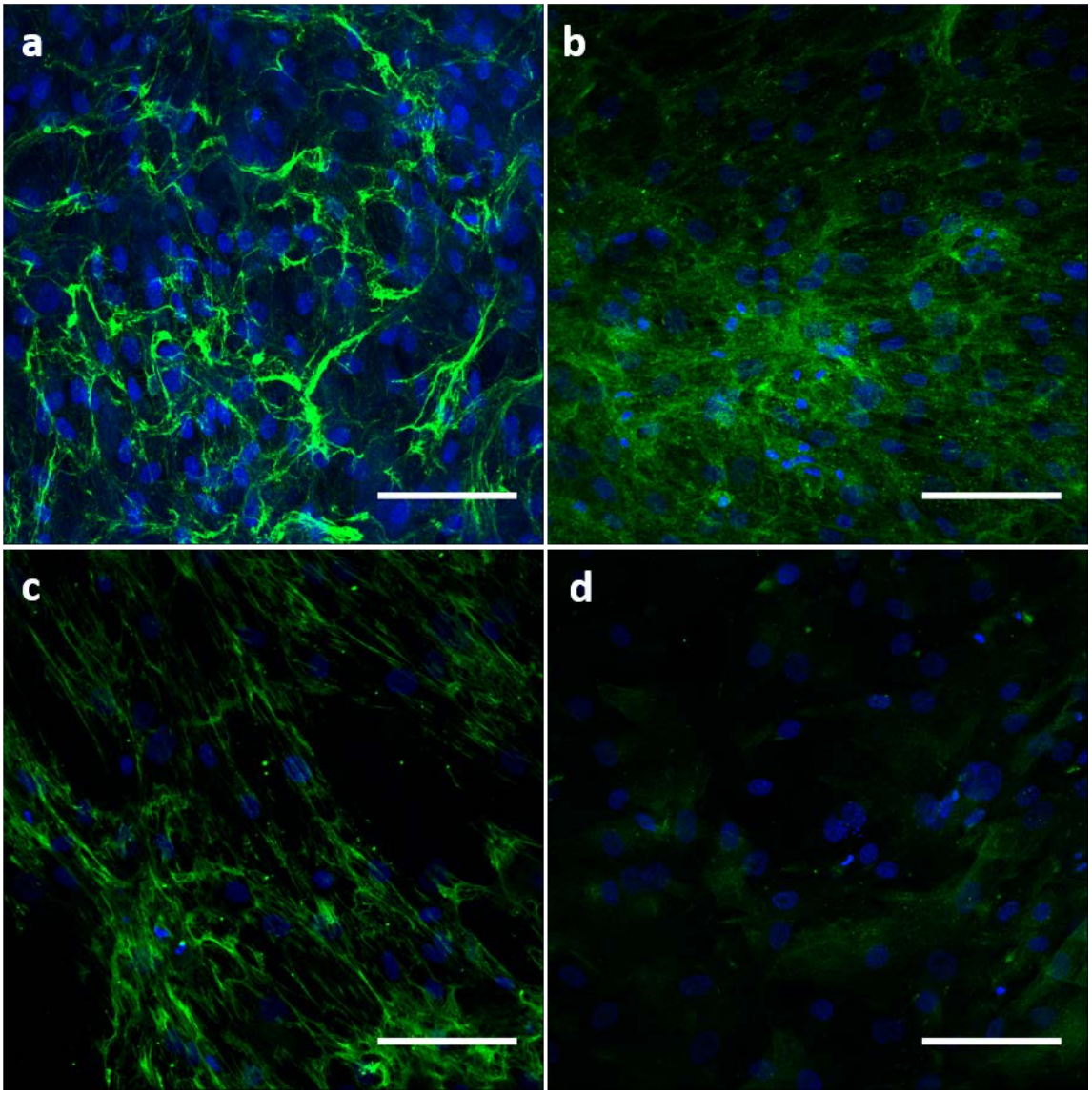

Figure 4-6 basement membrane immunofluorescence staining in HBVSMC cultures after 72 hours

After 72 hours in culture HBVSMCs were immunostained with basement membrane proteins a) collagen IV, b) laminin, c) fibronectin and d) perlecan, shown in green. The DAPI stained nuclei are shown in blue. Collagen IV (a) and fibronectin (c) staining appeared web-like and the collagen IV staining in particular was very intense. Laminin (b) formed a very fine mesh and was evenly distributed and perlecan staining (d) was similar but was much weaker and diffuse than laminin. Scale bar 100µm.

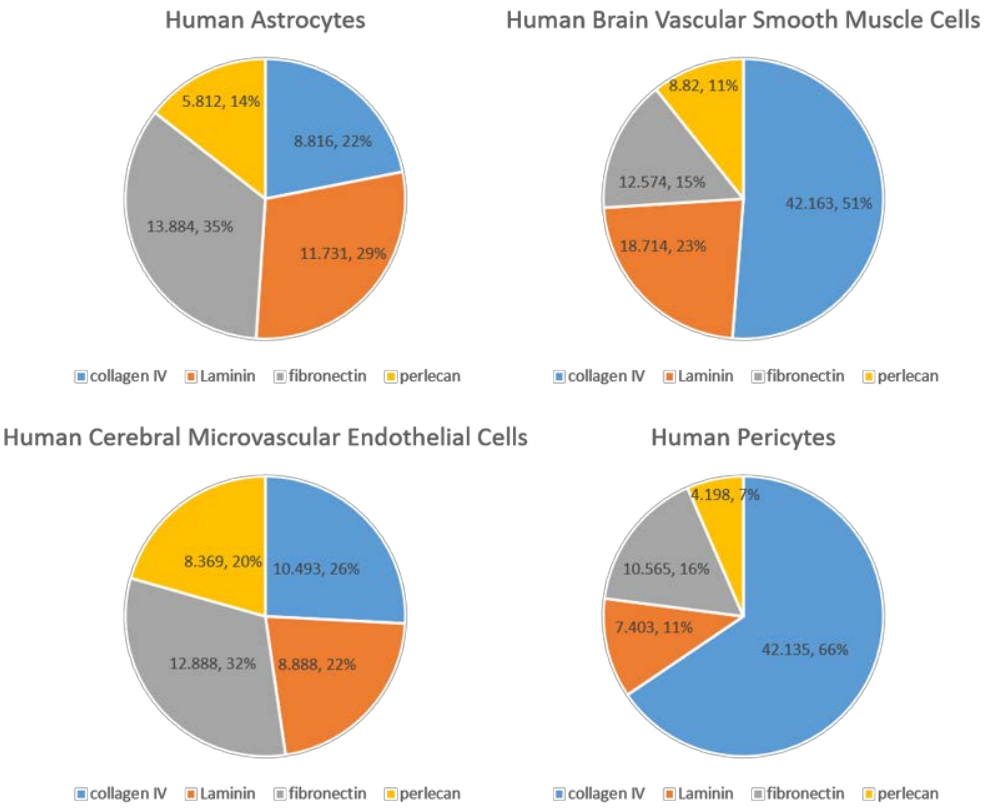

Figure 4-7 the ratio of basement membrane proteins in human cell cultures

The fluorescence intensity of the protein of interest was calculated and expressed as a percentage of total protein expression to demonstrate the ratio of basement membrane proteins in each of the cultures. Collagen IV expression was highest in pericytes and smooth muscle cells (66% and 51%) whereas fibronectin was highest in astrocyte cultures and endothelial cells (35% and 32%). Perlecan expression was lowest in all of the cultures (7-20%). Pericytes and smooth muscle cells appeared to have similar proportions as did the astrocytes and endothelial cells.

4.3.5 Smooth muscle cells produce the most extracellular protein

When comparing raw values for fluorescence intensity, fibronectin staining produced the highest value of arbitrary fluorescence where 82.271 was the combined total of all four proteins. This is more than double the value in the astrocyte cultures (40.243) and endothelial cultures (40.638) and approximately 28% more than the value in the cultures of pericytes (64.301). Since fluorescence intensity is directly proportional to the amount of protein produced, the HBVSMC produced the most extracellular protein in culture, followed by the HP, then the hCMEC/D3 and the HA.

4.4 Discussion

4.4.1 Endothelial cells require input from other cells to form a basement membrane

The hCMEC/D3 cell cultures produced detectable levels of the basement membrane proteins tested but they were unordered and unstructured. It is possible that the genetic modification that these cells have undergone has influenced their capacity to produce and assemble a functional basement membrane; this is a potential limitation of the cell line. BBB-specific transporters and proteins such as occludin and claudin-5 are expressed at much lower levels in hCMEC/D3 compared to primary cerebral endothelial cell cultures (Urich *et al.*, 2012), therefore it is possible that other proteins may also be affected in the same way. Another possible explanation for the low basement membrane production is that endothelial cells may require input from the other cells of the neurovascular unit to function optimally. Astrocytes have been shown to have a strong influence on tight junction formation of endothelial cells and maintenance of the BBB (Yao *et al.*, 2014) so it is not unreasonable to assume that the astrocytes influence the basement membrane of the endothelium. The production of basement membrane proteins in the hCMEC/D3 cultures may also be dependent on time. Since the cultures were only grown for 72 hours before immunostaining and no other timepoints were assessed it is possible that the cells may produce a more structured basement membrane if given more time.

4.4.2 Endothelial cells and astrocytes may combine their secreted proteins to form a basement membrane

The ratio analysis of extracellular proteins highlighted a similarity between endothelial cells and astrocytes. As previously mentioned in 3.4.2 endothelial cells rely on support from astrocytes in their function of forming a blood-brain barrier (Yousif, Di Russo and Sorokin, 2013b). The close association of the two cell types *in vivo* may be the reason why the two cultures produced such similar levels of extracellular proteins It has been shown that endothelial cells and astrocytes produce different isoforms of laminin (Thomsen *et al.*, 2017; Thomsen, Routhe and Moos, 2017a). In cerebral capillaries the endothelial and glial basement membranes appear as a single entity and contain laminin 411 and 511 derived from endothelial cells (Sorokin *et al.*, 1997) and laminin 111 and 211 produced by astrocytes (Sixt *et al.*, 2001), suggesting that both cell types produce extracellular proteins that contribute to the formation of the capillary basement membrane.

4.4.3 Smooth muscle cells produce their own independent basement membrane

When grown in culture the HBVSMC produced higher levels of extracellular proteins than any other cell type tested. The smooth muscle basement membrane has individual characteristics and appears independent of other basement membranes in the brain (Yousif, Di Russo and Sorokin, 2013b). The reason for the discrepancy in the amount of extracellular protein being produced may be because no other cell type contributes to the production and assembly of the smooth muscle basement membrane. Usually multiple cell types contribute to the development of their basement membranes, such as the close relationship between endothelial/glial or pericyte/endothelial basement membranes, suggesting that the phenotype of the basement membrane may be dictated by the adjacent tissue. The sole topographical organisation and relative lack of support from other cells may make the smooth muscle basement membrane more vulnerable to remodelling in response to stress such as in aging and neurodegeneration.

4.4.4 The basement membrane determines phenotype in pericytes and smooth muscle cells

With the exception of laminin, the expression of basement membrane proteins in HBVSMC and HP cultures was very similar. This may be because pericytes and smooth muscle cells have a common lineage. Epicardial mesothelium is a progenitor to both coronary pericytes and vascular smooth muscle cells in the heart (Zhou *et al.*, 2008) and a study in 2002 showed that neuroectodermal precursor cells from the neural crest can differentiate into vascular smooth muscle cells and pericytes (Korn, Christ and Kurz, 2002). In addition to a common ancestry, pericytes and smooth muscle cells are related in other ways. Many of the markers used to identify pericytes such as smooth muscle actin, desmin and vitmentin are also expressed by smooth muscle cells (Yamazaki and Mukouyama, 2018). Pericytes and smooth muscle cells are both contractile mural cells within the walls of blood vessels. Pericytes are present in the walls of microvessels such as arterioles, venules and capillaries, whereas smooth muscle cells cover large-diameter vessels like arteries and veins. Given the similarities between these two cell populations it was not surprising that this study showed many similarities in their basement membrane composition. The amount of collagen IV produced by the HBVSMC and HP is much higher than the other basement membrane proteins. It is also more than four times higher than in the HA or hCMEC/D3 cultures. Collagen IV stimulates binding of serum response factor (SRF) to CArG boxes in the promoters of smooth muscle actin and the heavy chain of smooth muscle myosin (Orr *et al.*, 2009). This is thought to result in elevated expression of contractility proteins and drive the cells to a more contractile phenotype. It is possible that the high ratio of collagen IV secreted by HBVSMC and HP helps to drive the cells into a mature state and contractile phenotype.

Although they share a common lineage, pericytes and smooth muscle cells have been shown to respond very differently to laminin. In smooth muscle cells laminin promotes the expression of contractile proteins and helps to maintain a contractile phenotype however laminin maintains pericytes in an undifferentiated state with low levels of contractile proteins (Yousif, Di Russo and Sorokin, 2013b). This may help to explain the difference in the levels of laminin expression between the two cultures.

The difference in the amount of laminin staining and its pattern of distribution in smooth muscle cells compared to pericytes indicates there may be a difference in the laminin being produced. Smooth muscle cells have been proposed to produce many laminin isoforms including laminins 411, 511, 421, 521 and 221 (Yousif, Di Russo and Sorokin, 2013a) though laminin 211 does not appear to be expressed by mature vascular smooth muscle cells (Jucker *et al.*, 1996). The extent to which pericytes contribute laminin 411 and 511 to the endothelial basement membrane is unknown however studies in pericyte deficient mutant mice have suggested that pericytes produce laminin 211 (Armulik *et al.*, 2010; Menezes *et al.*, 2014). The laminin antibody used for this study was not isoform specific and instead detects total laminin expression and because smooth muscle cells produce more isoforms of laminin this is most likely the reason for the increase in staining observed. Further studies are required to compare the expression of specific laminin isoforms in human cerebral cells.

The ratio between laminin and fibronectin appears to be important in determining the phenotype of smooth muscle cells. It has been demonstrated that laminin maintains arterial smooth muscle cells in a contractile state, whereas fibronectin can induce modulation of arterial smooth muscle cells and cause them to change from a contractile to a synthetic phenotype in culture (Hedin *et al.*, 1988) (Thyberg and Hultgardh-Nilsson, 1994). The relationship between the amount of laminin and fibronectin in the basement membrane of smooth muscle appears to be an important factor in determining phenotype. A higher percentage of laminin compared to fibronectin in the HBVSMC cultures indicates that the culture was likely being maintained in a contractile phenotype which is the normal state in a healthy brain.

4.4.5 The link between the smooth muscle basement membrane and Alzheimer's disease

Following injury, fibronectin is upregulated around vascular smooth muscle cells and induces a phenotypic switch to a synthetic undifferentiated state; this allows the cells to migrate to the affected site. The lack of a contractile phenotype in this instance may negatively impact IPAD which relies on the contraction of vascular smooth muscle as its principal driving force (Aldea *et*

al., 2019). It is also possible that the increased fibronectin may influence amyloid accumulation as increased fibronectin has been associated with sites of Aβ deposition (Morris *et al.*, 2014).

4.5 Conclusions

I have demonstrated that the cells that contribute to the cerebral vessel wall produce components of the basement membrane when grown in culture and they vary from one another. Cells of a common lineage such as pericytes and smooth muscle cells share similarities in the make-up of their basement membrane and the basement membrane of mural cells appears quite different from the endothelial or glial basement membranes in this study. Although there is no evidence to suggest the basement membrane of smooth muscle cells influences Aβ accumulation, the ratio of basement membrane proteins may be an important factor for IPAD as components such as laminin and fibronectin control the contractility of vascular smooth muscle and therefore the driving force for the elimination of amyloid beta and other solutes from the brain. One major limitation of this work is the relatively short time frame for experiments. Cells were not plated at confluence so cells were sub-confluent for part of the experiment time frame and this could affect cell phenotype and protein production.

4.6 Future work

This work has demonstrated the unique extracellular protein profiles in different cells of the brain. The basement membrane is made up of hundreds of core matrix and matrix associated proteins and although the main ones were covered in this study other extracellular proteins, most notably agrin, have been implicated in amyloid beta accumulation (Cotman, Halfter and Cole, 2000). Investigating these proteins may yield important findings. Further investigation into specific laminin isoforms would also be beneficial. The cell cultures were examined after 72 hours but other timepoints may be investigated to track how protein production changes with time. Other techniques such as qPCR can be carried out to quantify the difference in gene expression to support the findings of this study.

Interactions between the basement membrane and the cells may be explored by using an actin stain such as phalloidin in conjunction with immunostaining and imaging 3D stacks at high power. Focal adhesion kinase (FAK) is activated upon localisation to a protein complex which is formed upon cell adhesion to the basement membrane (Tapial Martínez, López Navajas and Lietha, 2020). Detection of the FAK complex, by western blot for example, can therefore indicate the presence of a functional basement membrane in the cultures.

The basement membrane is a conduit for the elimination of solutes from the brain and its composition may influence its ability to perform this vital task. The smooth muscle basement membrane has been shown to be distinct from that of the endothelium *in vivo* and is the initial site of CAA pathology in AD. It has been shown that there is increased fibronectin at sites of amyloid beta accumulation but the sequence of events for this accumulation are still unclear. Monitoring the changes in the basement membranes after the addition of Aβ in cell cultures, preferably in a millifluidics dynamic system, to simulate the development of CAA would be a valuable investigation. The analysis of how the vascular smooth muscle basement membrane responds to different environmental stresses could shed some light on the failure of IPAD and the pathological mechanisms of Alzheimer's disease and other neurodegenerative disorders.

Chapter 5 Pathological mechanisms of Intermural periarterial drainage (IPAD)

5.1 Introduction

A key feature in the pathology of Alzheimer's disease is the build-up of amyloid beta in senile plaques and in the walls of cerebral capillaries and arteries as cerebral amyloid angiopathy (CAA). Many studies have shown amyloid beta accumulation in the vessel walls appears to be linked to the smooth muscle cells (Frackowiak, Zoltowska and Wisniewski, 1994; Wisniewski and Wegiel, 1994) and a study from my own group has provided strong evidence that amyloid beta preferentially accumulates in the smooth muscle basement membrane (Keable *et al.*, 2016). The central focus for this chapter will be the vascular smooth muscle cells.

In sporadic late onset Alzheimer's disease the build-up of Aβ is caused by a reduction in the clearance of the protein due to failure of various clearance mechanisms. It appears that the last clearance mechanism to fail, and the one that is closely associated with basement membranes, is intramural periarterial drainage (IPAD).

IPAD best represents the lymphatic drainage of the brain and works by transporting Aβ and other solutes in the extracellular spaces between cells in the walls of cerebral capillaries and arteries. These extracellular spaces form narrow channels (100-150nm) and are filled with a meshwork of glycoproteins and proteoglycans known as the basement membrane. IPAD is theorised to be driven by the spontaneous contraction of smooth muscle cells and is contrary to blood flow (Aldea *et al.*, 2019). IPAD ceases upon cardiac arrest (Carare *et al.*, 2008) so it cannot be observed easily in animal models and an *in vitro* model of IPAD has yet to be delivered.

5.1.1 Aims and hypothesis

There are currently no *in vitro* models designed specifically to investigate IPAD. The primary aim of this work is to create an *in vitro* model of the flow of interstitial fluid over cerebral vascular smooth muscle cells to test the hypothesis that amyloid beta interacts with the smooth muscle basement membrane and alters its protein composition. Hypoxia will also be tested as a method of inducing stress in smooth muscle cells to test the hypothesis that a stress environment can induce remodelling of the basement membrane, producing an extracellular environment that is vulnerable to amyloid beta accumulation.

5.2 Materials and methods

5.2.1 Cell culture

Human brain vascular smooth muscle cells (HBVSMC) were obtained from Sciencell (sc-1100). Cells were grown in smooth muscle cell medium purchased from Sciencell (sc-1101) supplemented with smooth muscle cell growth supplement (sc-1152), 100U/mL penicillin, 100µg/mL streptomycin (sc-0503) and 2% foetal bovine serum. Cells were maintained in a humidified atmosphere (5% CO_2/95% air) at 37°C and medium was refreshed every 2-3 days according to the manufacturer's instructions. Cells were plated onto poly-L-lysine coated coverslips in a 24-well plate at a density of $0.5x10^5$ cells per coverslip or into a poly-L-lysine coated well in a 96-well plate for assays at a density of $0.1x10^5$ cells per well.

5.2.2 Amyloid beta flow experiments

A novel millifluidics system developed by Kirkstall Ltd was used to apply a flow of media to smooth muscle cell cultures in order to reproduce the flow of interstitial fluid that occurs *in vivo*. A four chamber set-up of the Quasi Vivo system was used for these experiments. The Quasi Vivo system was assembled and calibrated according to the manufacturer's instructions with four QV500 chambers (see supplementary figures 3 and 4). Coverslips were sterilised and coated with poly-L-lysine as previously mentioned in 2.1.2.3. Coverslips were inserted into wells in a 24-well plate and 1mL smooth muscle cell medium was added to each well. HBVSMC were plated onto poly-L-lysine coated coverslips at a seeding density of $0.5x10^5$ cells per well and incubated for 24 hours at 37°C in a humidified environment (5% CO_2, 95% air) to allow for cell attachment. After 24 hours one coverslip was transferred into each of the four QV500 chambers and the remaining coverslips were left in the 24 well plate for use as static controls. Supplemented media containing 100nM amyloid beta 1-40, 100nM amyloid beta 1-42 or 100nM 10kDa Dextran was made up (see Amyloid beta and dextran preparation section 2.5 for full details). This preparation of Aβ has been shown to produce small soluble oligomers (Morris, 2015; Albargothy *et al.*, 2017). Aβ 1-40 and Aβ 1-42 were chosen as they are both implicated in Alzheimer's disease. 10kDa Dextran was selected as a vehicle control as it is a biologically inert polysaccharide that resembles the size of small oligomers of Aβ. 1mL supplemented media was added to each QV500 chamber and 15mL was added to the reservoir bottle to ensure there was an adequate volume of solution to fill the system. Supplemented media was also added to each of the static wells in the 24-well plate. In addition to a flow of Aβ 1-40, Aβ 1-42 and dextran; this experiment was also run with no additional supplement in the media as a baseline for comparison. The Quasi Vivo system was connected to a calibrated Parker polyflex peristaltic pump and the speed was set to an outlet of

10µL/min. The Quasi Vivo system and the 24-well plate containing the static controls were returned to the incubator for a further 48 hours. Coverslips were removed from the QV500 chambers and transferred to a 24-well plate. Both static and flow cells were fixed with 4% PFA for 10 minutes at room temperature and immunostained for basement membrane proteins: collagen IV, laminin, fibronectin and perlecan.

5.2.3 Using hypoxia as a model of aging

Cells were grown in hypoxic conditions (8% CO_2/92% air) to induce oxidative stress as a model of the stress conditions in the aging brain.

5.2.3.1 MTS assay

The-(4,5-dimethylthiazol-2-yl)-5-(3-carboxymethoxyphenyl)-2-(4-sulfophenyl)-2H-tetrazolium (MTS) reagent was used to assess cell viability and proliferation in HBVSMC after exposure to hypoxia and Aβ in static cultures. HBVSMC were plated as described in section 2.7. 100µL of supplemented smooth muscle medium containing 100nM amyloid beta 1-40 or 100nM amyloid beta 1-42 was prepared as previously described (section 2.5) and added to the wells as shown in **Figure 2-4**. Smooth muscle medium containing no additional supplement was also tested to establish a normal control level. Blank wells containing no cells were also included and their absorbance value was subtracted from the test wells. Absorbance was measured at 490nm with a Fluorostar optima plate reader and the results were exported to Microsoft Excel.

5.2.3.2 Basement membrane staining

HBVSMC were plated onto poly-L-lysine coated coverslips at a density of $0.5x10^5$ cells per coverslip with 1mL of smooth muscle medium. Cells were then exposed to either normoxic (5% CO_2/95% air) or hypoxic (8% CO_2/92% air) conditions for 72 hours before being fixed with 4% PFA and immunostained for basement membrane proteins: collagen IV, laminin, fibronectin and perlecan. These experiments were repeated with supplemented media containing 100nM amyloid beta 1-40 and amyloid beta 1-42 as a model of CAA in an aged cerebrovasculature.

5.2.4 Immunocytochemistry

After fixing cells with 4% PFA for 10 minutes, cells were washed three times with PBS and blocked with 15% NGS for 1 hour. Cells were then incubated overnight with collagen IV (Abcam, ab6586), laminin (Sigma, L9393), fibronectin (Sigma, F3648) or perlecan (Santa Cruz, 25848) primary antibody diluted in PBS at 4°C (see **Table 4-1** for full details). After washing three times with PBS, cells were incubated with goat anti-rabbit Alexa Fluor 488 conjugated secondary antibody

(Invitrogen, A11034) for 1 hour at room temperature. Cells were washed again three times with PBS and incubated with 2µg/mL DAPI for 10 minutes. Coverslips were rinsed with PBS and mounted onto slides with Mowiol and Citifluor and examined by confocal microscopy.

5.2.5 Analysis

Three non-overlapping z-stacks were captured per coverslip (each an area of 0.15mm^2) and the fluorescence intensity of the basement membrane proteins for static, flow, normoxic and hypoxic experiments was calculated using the RGB measure tool in ImageJ. The raw MTS data was exported to Microsoft Excel and the average MTS absorbance value was calculated from the triplicate test wells. Pie charts and bar graphs were composed using Microsoft Excel. Statistical analysis was carried out using SPSS statistics version 24. Data was not normally distributed so the appropriate non-parametric test (Mann-Whitney U for two groups and Kruskal-Wallis for more than two groups) was used to determine if differences were statistically significant. Results are based upon data gathered over three experimental runs (n=3) unless otherwise stated.

5.3 Results

5.3.1 Flow does not significantly alter protein production in HBVSMC cultures

The intensity of immunofluorescence staining was measured for key basement membrane proteins in cultures grown in static conditions and under a physiological flow of 10µL/min. The results are summarised below in **Figure 5-1**. Representative images of staining can be seen in **Supplementary figure 5**. Generally there was a trend towards increased protein expression in the cultures exposed to flow with slight increases in fluorescence intensity seen for collagen IV, laminin and fibronectin staining, however these differences were not significant. There was the slightest decrease in the average fluorescence intensity for perlecan staining in flow cultures compared to static cultures but this was also not significant.

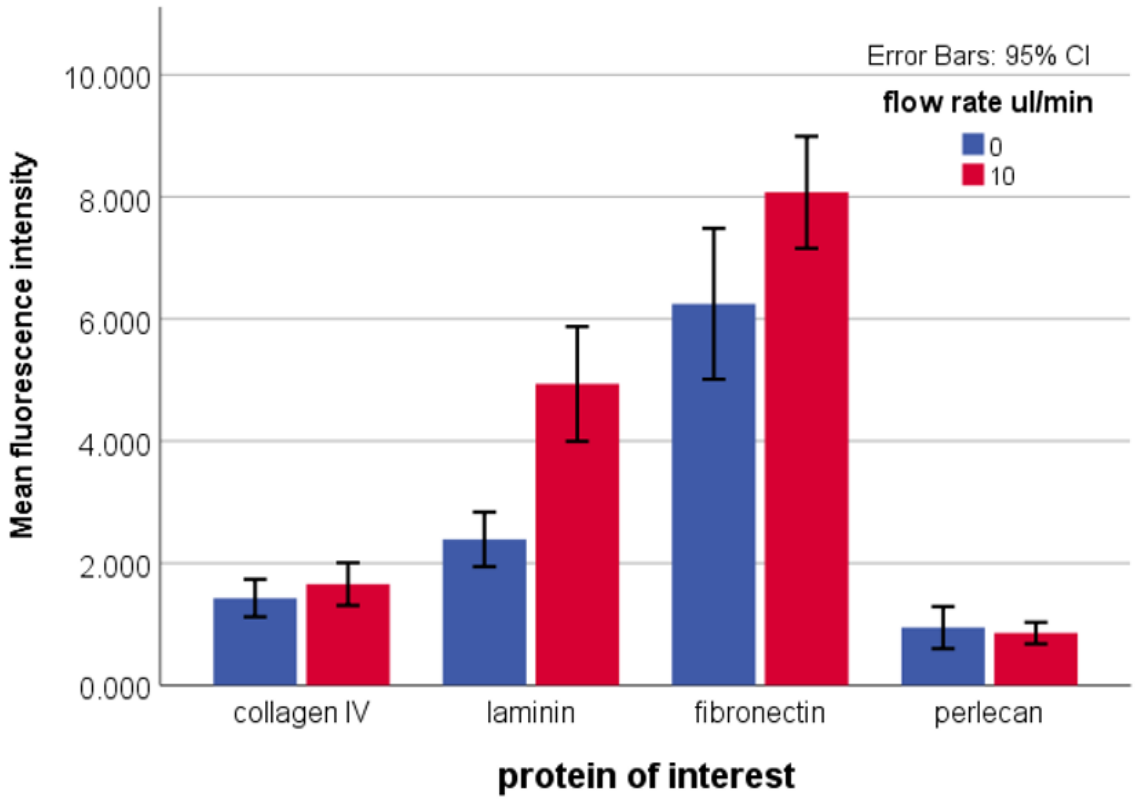

Figure 5-1 basement membrane production in HBVSMC cultures under static and flow conditions

The fluorescence intensity of protein staining in HBVSMC cultures exposed to a flow rate of 10µL/min for 48 hours was not significantly altered compared to standard static cultures. There was an increase in laminin and fibronectin staining under flow conditions but this was not significant. The values for fluorescence intensity of collagen IV and perlecan staining were almost identical in static and flow cultures. The mean fluorescence intensity was calculated from three fields of view per coverslip and a total of twelve coverslips per protein over twelve independent flow experiments (n=12).

5.3.2 Amyloid beta does not significantly alter the basement membrane of smooth muscle cells under normal culture conditions

After establishing a flow based model of interstitial fluid drainage over smooth muscle cells, dextran of 10kDa molecular weight and Aβ 1-40 and Aβ 1-42 were supplemented into the fluid to assess changes in the expression of basement membrane proteins. There was no significant difference in the fluorescence intensity of basement membrane proteins in the flow experiments, regardless of the protein supplemented into the media. **Figure 5-2** shows the ratio of basement membrane proteins in the four flow experiments. Fibronectin expression was the highest in all of the flow experiments ranging from 47% to 56%. Laminin expression ranged from 28% to 35%, collagen IV ranged from 8% to 12% and perlecan expression was between 2% and 10%. The

differences observed were small and not considered to be statistically significant. Aβ 1-40 and Aβ 1-42 did not significantly alter the expression of basement membrane proteins compared to the cultures exposed to media without supplementation or a flow of dextran. This set of experiments demonstrates that Aβ does not alter the profile of basement membrane composition of HBVSMC.

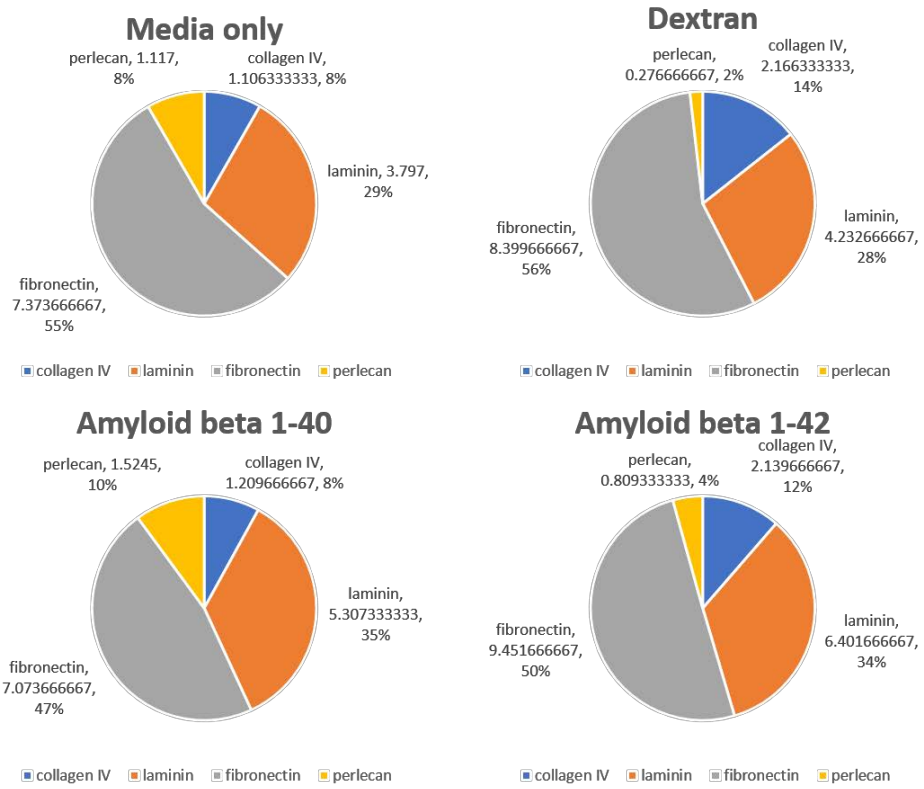

Figure 5-2 the ratio of basement membrane proteins in HBVSMC cultures under flow

The mean fluorescence intensity of each basement membrane protein was calculated by assessing three fields of view of a coverslip of HBVSMC that were exposed to flow of each solute for 48 hours. The values shown are based on data gathered over three independent flow experiments (n=3). The values shown are the average fluorescence intensity of each protein and percentage relative to the total protein expression assessed. The profile of basement membrane expression in HBVSMC was not significantly altered by the presence of the amyloid beta protein. Fibronectin expression was the highest in all flow cultures, followed by laminin. Perlecan had the lowest expression in the cultures with amyloid beta and dextran flow whereas collagen IV expression was slightly lower than perlecan when there was no additional supplement.

5.3.3 Hypoxia decreases the proliferation of smooth muscle cells in culture

Cell viability was assessed by MTS assay at three time points: 2 hours (day 0), 24 hours (day 1) and 72 hours (day 3). All conditions tested showed a positive correlation between MTS absorbance

and time indicating that the cell population is increasing (**Figure 5-3**). Initially (the first 24 hours) it appeared that amyloid beta 1-42 negatively affected cell viability to the same extent as hypoxia combined with either type of amyloid beta and that hypoxia or amyloid beta 1-40 alone did not influence cell viability, however this was not the case at the end. Cell populations grown in hypoxic conditions had a lower MTS absorbance after 72 hours indicating that the number of viable cells was decreased compared to the normoxic cultures. There were on average more viable cells in the normoxic cultures supplemented with Aβ 1-40 or Aβ 1-42 compared to media only. Although the trend was strong none of the differences in MTS absorbance were considered statistically significant.

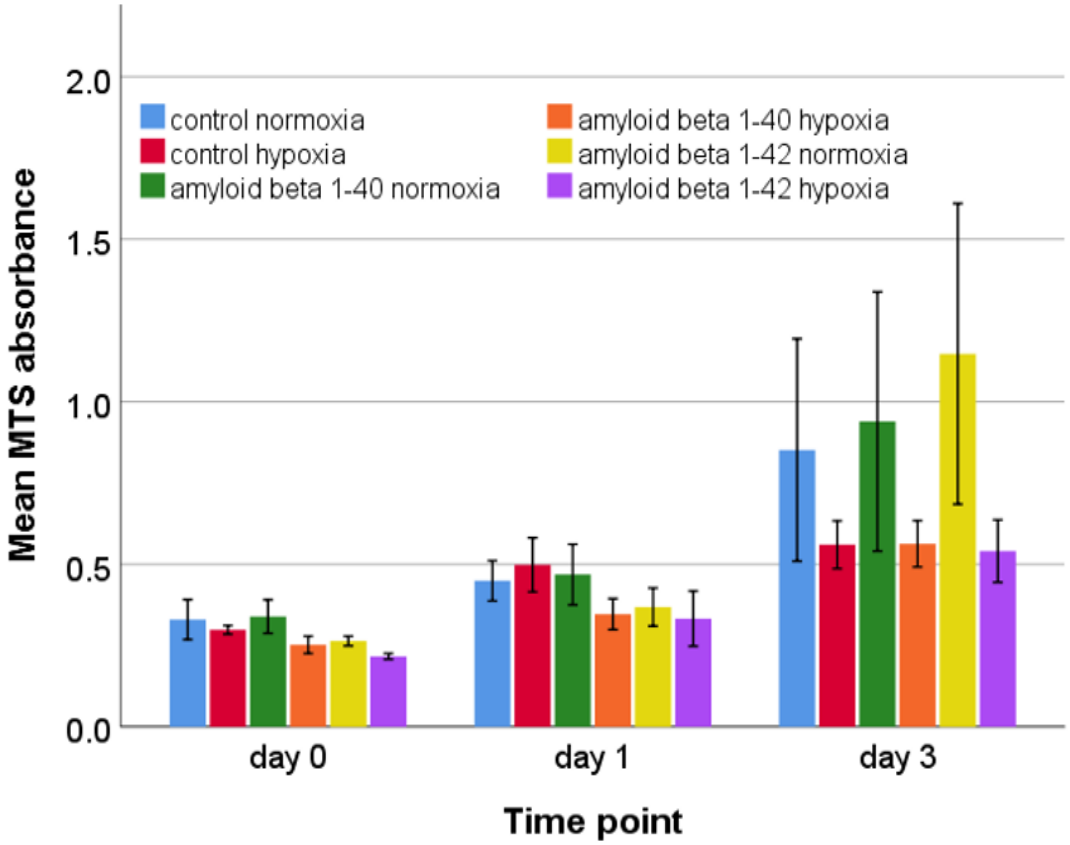

Figure 5-3 Viability of static HBVSMC cultures under various conditions of environmental stress

An MTS assay was used to assess viability of HBVSMC cultures exposed to normoxia and hypoxic conditions in the presence of Aβ 1-40 or Aβ 1-42. Cells exposed to hypoxia for 72 hours (orange, purple and red bars) had on average a lower MTS absorbance than cells exposed to normoxia (blue, green and yellow bars). This indicates that cell metabolism was reduced in hypoxic cultures and suggests cell viability was lower, however these differences were not considered to be statistically significant. The presence of either form of Aβ in the culture media had no obvious impact on MTS absorbance compared to the control, which suggested that Aβ did not affect cell metabolism and cell viability was comparable. The MTS absorbance was calculated from triplicate wells for each condition over two independent experimental runs.

5.3.4 Hypoxia alters basement membrane expression in smooth muscle cells

When the fluorescence intensity of antibody staining in the hypoxia cultures was compared to normoxia there was one significant observation. Following exposure to hypoxic conditions, laminin staining was significantly increased compared to the normoxic culture (p=0.05) (**Figure 5-4**). This upregulation of laminin was also observed in the qualitative images (**Figure 5-5**). There was a decrease in collagen IV and fibronectin staining in the hypoxia cultures though this was not significant. Perlecan appeared unchanged.

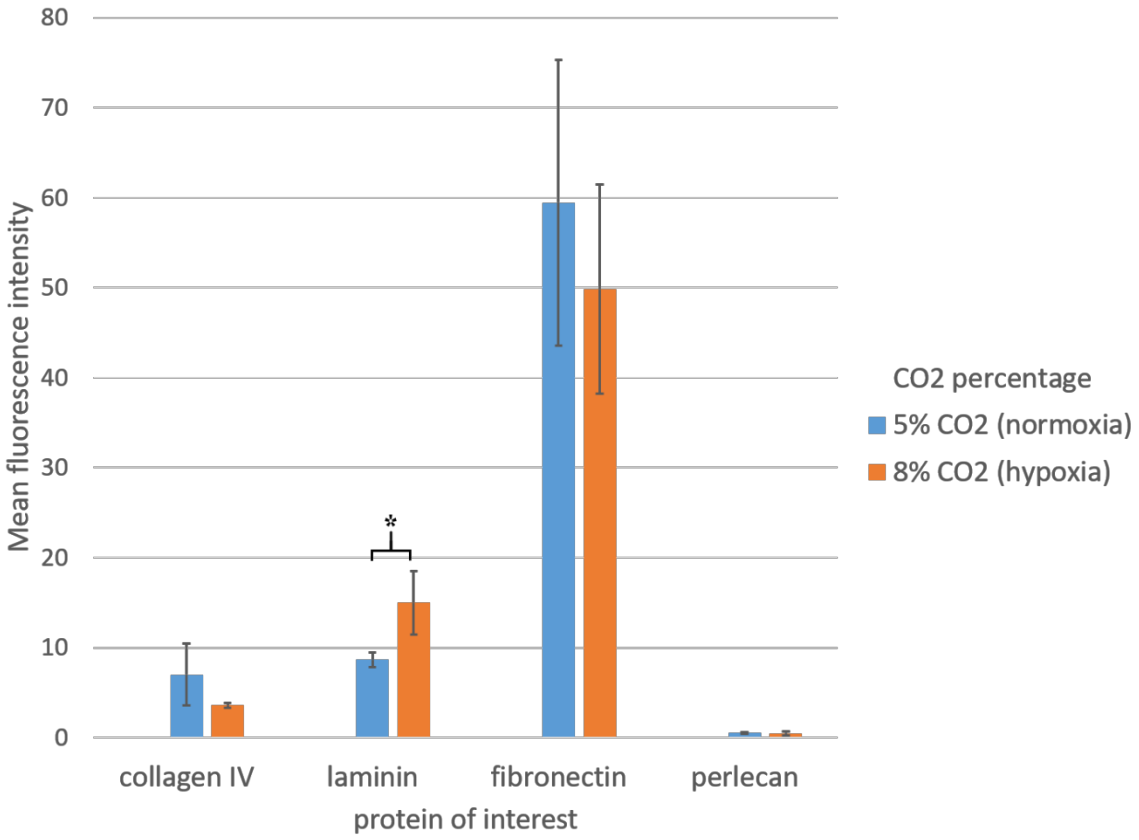

Figure 5-4 fluorescence intensity of basement membrane proteins in static HBVMSC cultures exposed to normoxic and hypoxic conditions

Laminin staining was significantly higher in the HBVMSC cultures that were exposed to hypoxia for 72 hours compared to the normoxic cultures (p=0.05). Hypoxia caused a decrease in collagen IV and fibronectin staining but this was not significant. Hypoxia did not affect perlecan staining.

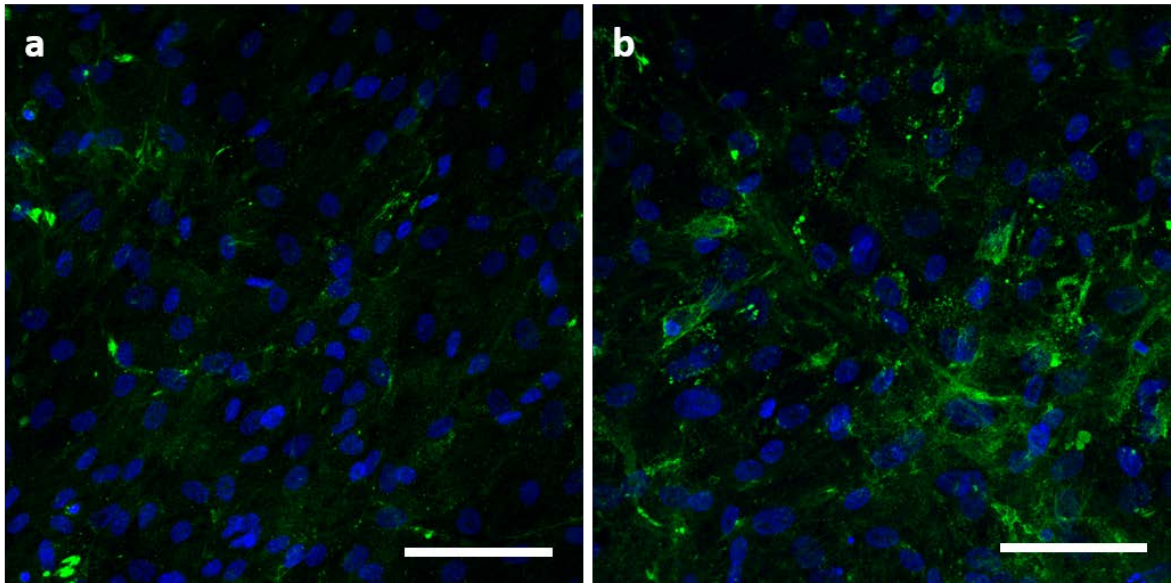

Figure 5-5 immunofluorescence staining showing how laminin expression is altered with hypoxia

The pattern of laminin staining (shown in green) in HBVSMC appeared largely unchanged in response to hypoxia (b) but there was significantly more staining present compared to normoxic cultures (a). DAPI stained nuclei are shown in blue. Scale bar 100µm.

5.3.5 Amyloid beta 1-42 decreases collagen IV in HBVSMC under hypoxic conditions

In the HBVSMC cultures that were exposed to hypoxia, the fluorescence intensity of collagen IV staining was significantly decreased in the cultures that had 100nM Aβ 1-42 supplemented in the culture media compared to those that had 100nM Aβ 1-40 or no Aβ in the culture media ($p=0.027$) (see **Figure 5-6**). Collagen IV staining was also reduced with Aβ 1-42 when compared Aβ 1-40 or no Aβ in the HBVSMC grown in normoxic conditions, however this difference was not statistically significant ($p=0.061$). Under hypoxic conditions there appeared to be an increase in collagen IV expression when Aβ 1-40 was supplemented in the culture medium; when comparing all groups, it was clear that this apparent change was due to a decrease in collagen IV expression in response to hypoxia rather than an increase caused by applying Aβ 1-40.

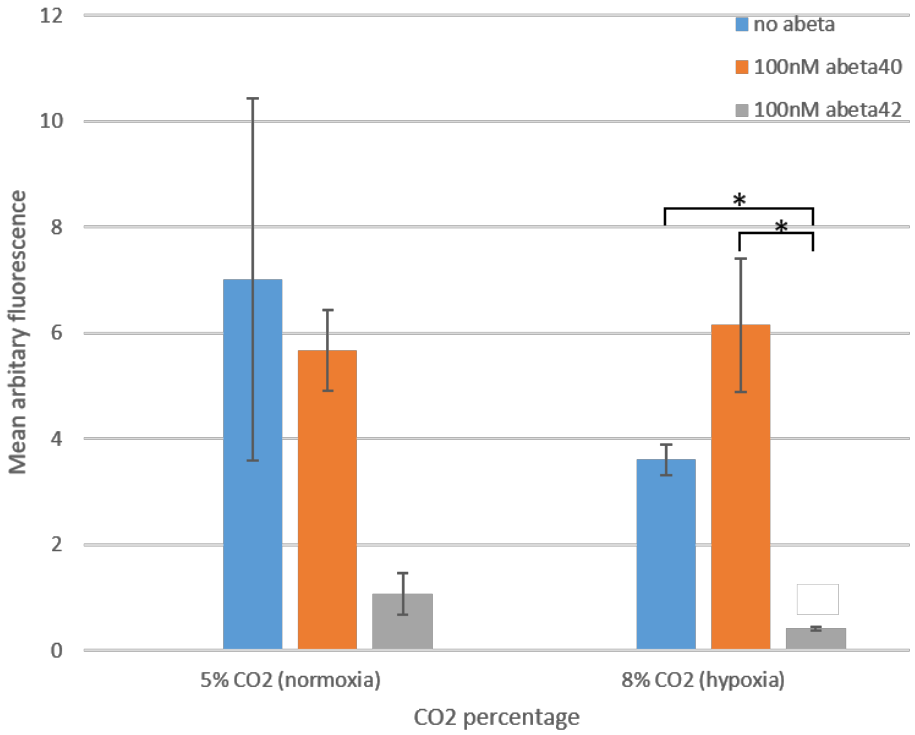

Figure 5-6 Collagen IV expression in HBVSMC cultures exposed to amyloid beta in normoxic and hypoxic conditions

Collagen IV expression was significantly reduced (p=0.027) in hypoxic cultures treated with 100nM amyloid beta 1-42 when compared to other hypoxic cultures. This trend was the same for normoxic cultures though the decrease in collagen IV expression was not statistically significant.

5.3.6 Amyloid beta 1-42 decreases laminin expression in normoxic and hypoxic conditions

In the normoxic HBVSMC cultures there was a significant decrease in laminin expression in cultures exposed to 100nM Aβ 1-42 (p=0.039) compared to other normoxic cultures (see **Figure 5-7**). Hypoxic cultures also experienced a decrease in laminin expression when exposed to 100nM Aβ 1-42 compared to the other hypoxic cultures though this was just outside of statistical significance (p=0.051). However this finding was relevant given that under hypoxic conditions only laminin was upregulated (see 5.3.4), yet when Aβ 1-42 was supplemented into the culture medium the opposite occurred and laminin staining decreased. Although Aβ 1-40 appeared to increase the intensity of laminin staining in normoxic cultures, a pattern not seen in the hypoxic cultures, this increase was not significant (p=0.127). The fluorescence intensity of perlecan and fibronectin staining was not significantly altered in any of the experimental conditions (see **supplementary figures 6 and 7**).

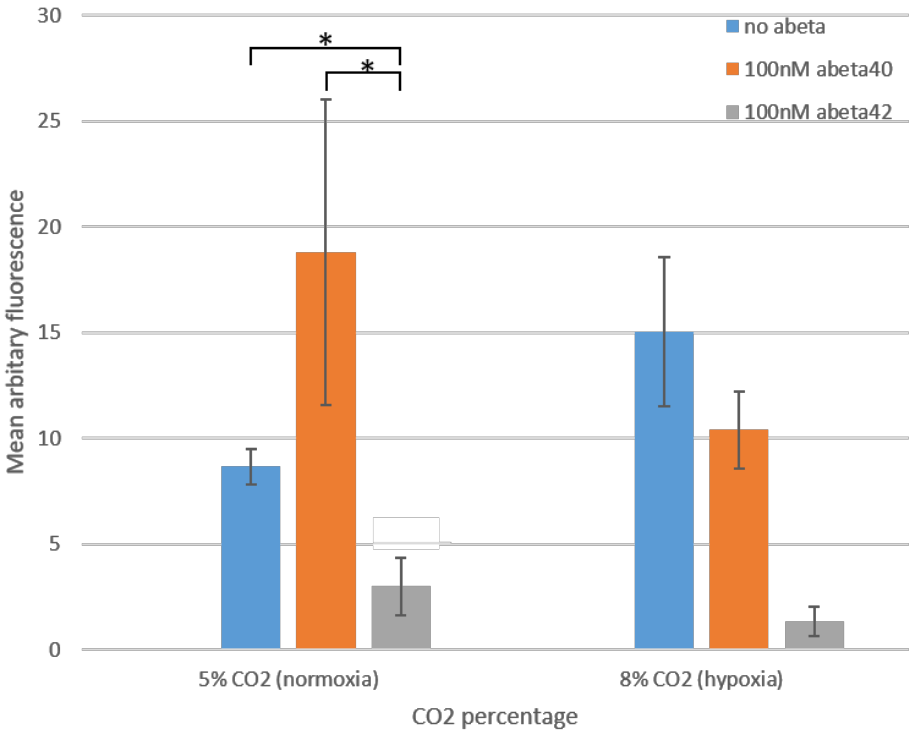

Figure 5-7 Laminin expression in HBVSMC cultures exposed to amyloid beta in normoxic and hypoxic conditions

Laminin expression was significantly reduced (p=0.039) in normoxic cultures treated with 100nM amyloid beta 1-42 when compared to normoxic cultures with no amyloid beta. This trend was the same for hypoxic cultures, though the decrease was not statistically significant (p=0.051).

5.4 Discussion

In this chapter the experiments demonstrated that under normal culture conditions, the addition of a flow of Aβ 1-40 and Aβ 1-42 peptides did not alter the production of basement membrane proteins in smooth muscle cells. Both Aβ 1-40 and Aβ 1-42 peptides are produced throughout life and their presence in the CSF of non-demented patients and neuronal cell cultures indicates that they have a physiological function in the brain (Pearson and Peers, 2006). There is evidence that Aβ depresses synaptic activity which prevents excitotoxicity (Kamenetz *et al.*, 2003) and immunodepletion of Aβ in neuronal cultures results in cell death (Plant *et al.*, 2003), suggesting the production of Aβ is essential for normal neuronal function. In a healthy brain, cells of the cerebrovasculature, including smooth muscle cells, are constantly exposed to Aβ proteins of various lengths, including the Aβ 1-40 and Aβ 1-42 peptides, without consequence so it was not a surprise that the HBVSMC were unaffected.

5.4.1 Hypoxic conditions upregulate laminin

Laminin expression was significantly increased when HBVSMC were exposed to hypoxia. Hawkes et al showed a similar upregulation in laminin following cerebral ischemia in mice (Hawkes *et al.*, 2013). Hypoxia is a common occurrence following stroke (Ferdinand and Roffe, 2016) and laminin has been shown to be important in the maintenance of vascular tone and the integrity of the blood-brain barrier. It is possible that the increase in laminin expression observed is part of a compensatory mechanism to establish regrowth and repair of the cerebral vessels. There is also a plausible link between laminin upregulation in response to hypoxia and cyclooxygenase 2 (COX-2), suggesting that the change in laminin expression may be part of the inflammatory response (Ji and Tsirka, 2012). There were no other significant changes to the basement membrane when cells were challenged with hypoxia so it appears that hypoxia alone does not create an extracellular environment conducive for the accumulation of Aβ.

5.4.2 Hypoxia may be used as a model of aging *in vitro*

Hypoxia contributes to functional decline with increasing age (Cataldi and Di Giulio, 2009; Yeo, 2019) and a hypoxic microenvironment increases reactive oxygen species, leading to oxidative stress (McGarry *et al.*, 2018). It is thought that many age-related functional losses are caused by oxidative stress (Lin and Flint Beal, 2003) which has also been shown to upregulate the amyloidgenic pathway in vascular smooth muscle cells (Coma *et al.*, 2008) and is a factor in cerebrovascular dysfunction in mouse models (Hamel *et al.*, 2008). The present results show that cell proliferation was reduced in HBVSMC cultures subject to hypoxia, but was not significantly toxic as the cell viability still increased with time. As suggested by Auerbach et al, the reduction in HBVSMC cultures exposed to hypoxia was likely due to a reduction in cell proliferation and not cell death as the MTS absorbance was not decreased compared to the initial measurements but simply lower when compared to normoxic cultures (Auerbach *et al.*, 2003). Hypoxia also had very little effect on the expression of basement membrane proteins and only laminin was significantly altered. Hypoxia could therefore be used in future to induce age-related oxidative stress in cell cultures.

5.4.3 Amyloid beta 1-42 is capable of remodelling the basement membrane of smooth muscle cells under stress

Aβ 1-42 caused a significant decrease in the expression of collagen IV and laminin in the hypoxic HBVMSC cultures. Collagen IV and laminin have demonstrated the ability to induce disassembly of Aβ 1-42 fibrils (Kiuchi *et al.*, 2002). This suggests that when cells are exposed to hypoxia Aβ 1-42

can disrupt the basement membrane, reducing collagen IV and laminin, leading to increased fibrilllization of Aβ 1-42. Interestingly high levels of Aβ 1-42 were found to be deposited in cerebral vessels of patients who received Aβ42 immunisation (Boche *et al.*, 2010). Using the results in this study a proposed sequence of events to explain the neuropathology after immunisation can be formulated. It is plausible that following immunisation the increased soluble Aβ 1-42 in the cerebral vessels caused a remodelling of the basement membrane, reducing collagen IV and laminin which would normally prevent amyloid fibrillization and resulting in worsening of CAA.

5.5 Conclusions

The Quasi Vivo system is a useful tool in applying flow to cell cultures and has allowed a partial *in vitro* model of IPAD to be developed. The production basement membrane proteins in healthy smooth muscle cells is not adversely affected by a flow of amyloid beta. In contrast hypoxia induces a stress state that causes a downregulation of glycoproteins in the presence of amyloid beta 1-42. This suggests that hypoxia and other age related stresses make the smooth muscle basement membrane more susceptible to remodelling and more vulnerable to amyloid beta accumulation.

5.6 Future work

Hypoxia has proved to be a useful tool in inducing stress in HBVSMC cultures and could be used in future to artificially age cells in culture to study age-related changes. The Quasi Vivo system allowed application of flow to the HBVSMC cultures creating an *in vitro* model of IPAD however exposing HBVSMC to amyloid beta flow did not have any significant effect on the production of basement membrane. Combining the *in vitro* model of IPAD with hypoxia could produce an advanced *in vitro* model of aging/disease with the physiological flow of IPAD.

Chapter 6 The expression pattern of alpha adrenergic receptors in contractile cells of the cerebrovasculature

6.1 Introduction

The driving force for intramural periarterial drainage, one of the key pathways in the elimination of solutes from the brain, is thought to be the spontaneous contraction of vascular smooth muscle cells (Aldea *et al.*, 2019). Vascular smooth muscle cells receive innervation from both the cholinergic and adrenergic system, with the source of adrenergic supply degenerating early in the pathogenesis of Alzheimer's disease (Mann, Yates and Hawkes, 1982; Mann, Yates and Marcyniuk, 1984). Altering this signalling may alter the driving force for IPAD. This could potentially be used to treat patients with Alzheimer's disease where the elimination of solutes such as amyloid beta has failed, leading to its accumulation as senile plaques and cerebral amyloid angiopathy.

6.1.1 Adrenergic receptors

Adrenergic receptors, also known as adrenoceptors, are G protein-coupled receptors that bind catecholamines such as noradrenaline and adrenaline. There are two major classes of adrenergic receptor known as alpha and beta and nine currently known subtypes (summarised in **Figure 6-1**).

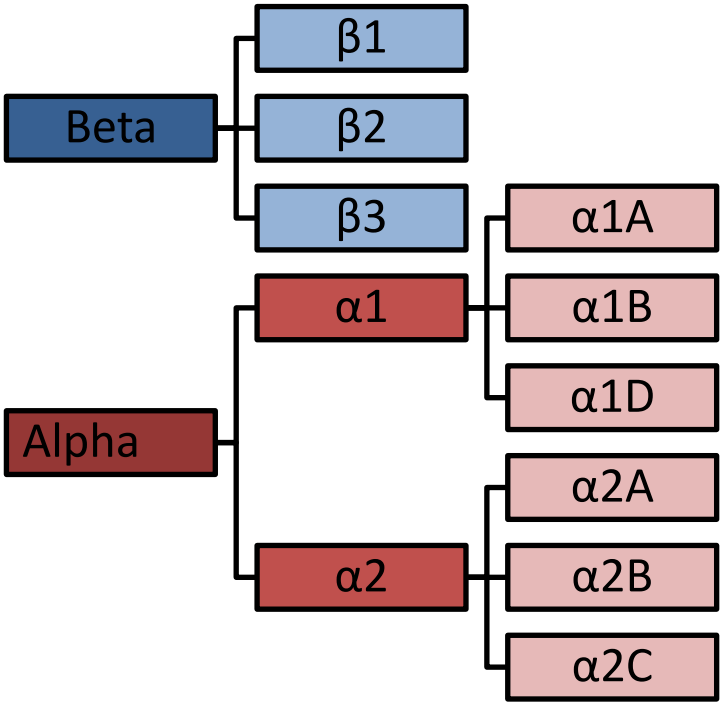

Figure 6-1 the subtypes of adrenergic receptors

There are two classes of adrenergic receptors known as alpha and beta which have opposite actions. There are three main types of beta receptor known as type 1, type 2 and type 3 and two main types of alpha receptor: type 1 and type 2. Both the type 1 and type 2 alpha receptors are further split into three subtypes. For type 1 alpha receptors these are A, B and D and for type 2 alpha receptor they are A, B and C. There is no α1C receptor as the subtype previously labelled C was found to be the same as another previously named subtype and the nomenclature was therefore removed (Hieble *et al.*, 1995).

6.1.1.1 Beta adrenergic receptors

All three types of β receptor are coupled to G-protein$_s$ and when activated they stimulate adenylate cyclase which catalyses the conversion of ATP to cyclic AMP causing relaxation and vasodilation (Wallukat, 2002). β1 receptors are predominantly located in the heart and are responsible for the inotrophic and chronotrophic effects of catecholamines (Ritter *et al.*, 2019). β2 receptors cause smooth muscle relaxation in many organs, most notably the lungs (Bai, 1992). β3 receptors are typically found in adipose tissue and are thought to be involved with lipolysis (Ferrer-Lorente *et al.*, 2005).

6.1.1.2 Alpha adrenergic receptors

There are two types of alpha adrenergic receptors that have been identified: type 1 (α1) and type 2 (α2). α1 receptors are important in the lower urinary tract and cardiovascular system whereas α2 receptors are more commonly associated with neurons (Philipp and Hein, 2004) Excitation of these receptors leads to contraction of vascular smooth muscle resulting in vasoconstriction. On the other hand, α2 adrenergic receptors also cause a negative feedback loop as their activation leads to an inhibition of neurotransmitter release, reducing both adrenergic and cholinergic innervation, which may indirectly lead to vasodilation as less noradrenaline is available for adrenergic receptor activation. See **Figure 6-2** for details of the mechanism of action of alpha adrenergic receptors. Pharmacological studies have suggested that the α2A adrenergic receptor is the principal presynaptic feedback regulator of neurotransmitter release (Trendelenburg *et al.*, 1997).

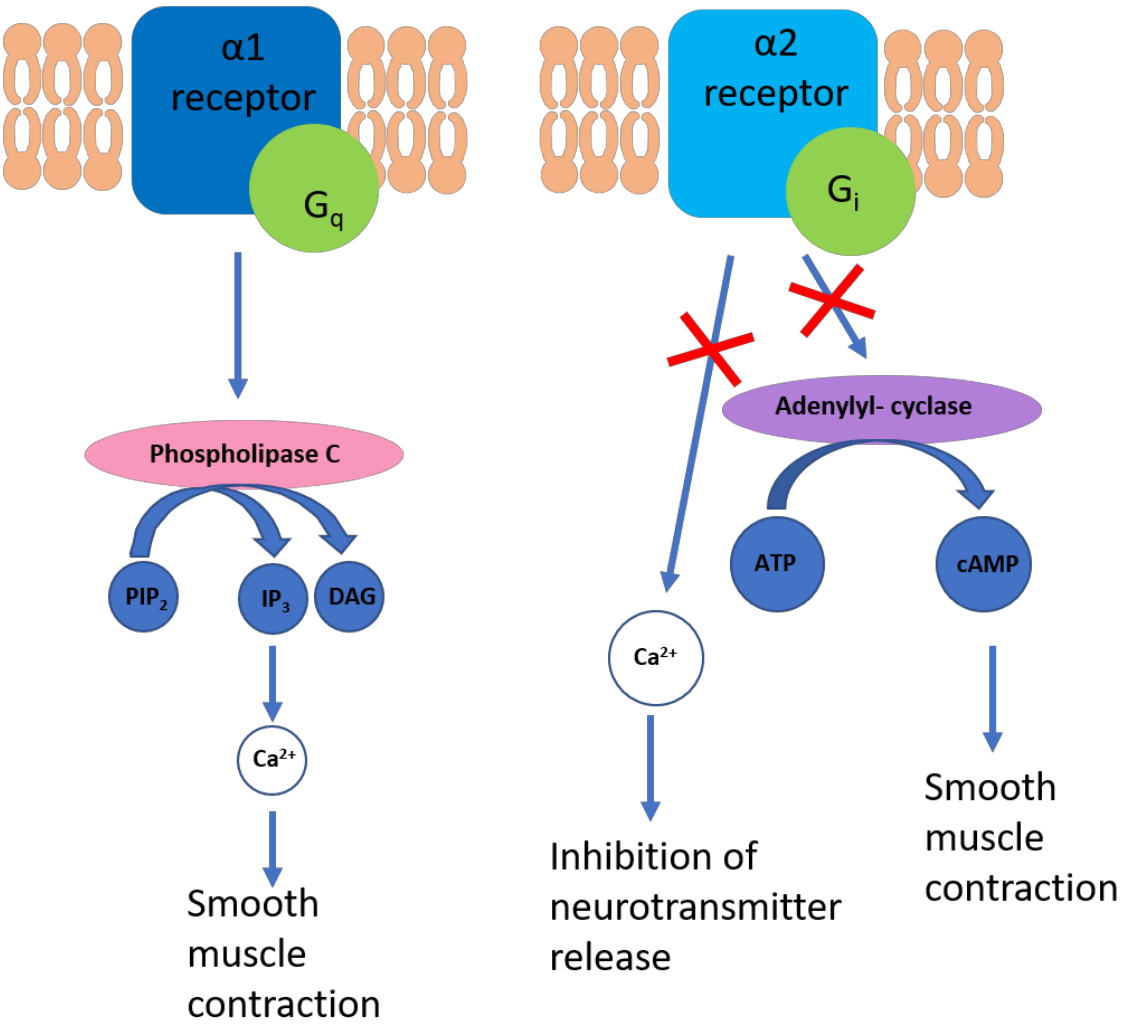

Figure 6-2 mechanism of action of type 1 and type 2 alpha adrenergic receptors

When noradrenaline binds to α1 adrenergic receptors the G protein, G_q, activates phospholipase C which acts on phosphatidylinositol bisphosphorate (PIP_2) leading to an increase in diaglycerol (DAG) and inositol triphosphate (IP_3). The interaction of IP_3 with calcium channels on the endoplasmic and sarcoplasmic reticulum leads to smooth muscle contraction. Binding of noradrenaline to α2 adrenergic receptors can also cause smooth muscle contraction. The Gi protein leads to an inactivation of adenylate cyclase and a decrease in cyclic AMP leading to vasoconstriction. α2 adrenergic receptor agonists also reduce noradrenaline release from the presynaptic neuron via its action on the α2 receptor by inhibiting Ca^{2+} channels and opening K^+ channels, creating a negative feedback loop by decreasing the effects of noradrenaline.

6.1.2 Adrenergic innervation in the brain

The main site of noradrenaline production in the brain is a nucleus in the pons of the brainstem known as the locus coeruleus (Samuels and Szabadi, 2008). Studies in the rat brain have shown that all of the noradrenaline in the cerebral cortex and hippocampus is produced and transported

by neurons in the locus coeruleus (Oleskevich, Descarries and Lacaille, 1989). The adrenergic receptors of the brain, including those that innervate the smooth muscle cells of the cerebral vessels receive stimulation from the locus coeruleus noradrenergic system. An early feature in AD pathogenesis is degeneration of the locus coeruleus (Weinshenker, 2008).

Both α and β adrenergic receptor subtypes are expressed in smooth muscle cells, nerve terminals and endothelial cells (Guimaraes and Moura, 2001) and there is an age-related decrease in β adrenergic receptors in almost all areas of the brain that is thought to be caused by reduced receptor synthesis (Scarpace and Abrass, 1988). There is also some evidence of a reduction in α adrenergic receptors, although recent unpublished work from our lab (Frost *et al.*, 2019) has shown that α adrenergic receptors are fairly well preserved with age and in CAA.

6.1.3 Drugs to target adrenergic receptors

The most well-known examples of drugs that target adrenergic receptors are beta blockers. β antagonists such as propranolol have been used to treat conditions such as angina, heart arrhythmias and can be given after a heart attack to protect against recurrent heart attacks and lower the blood pressure (A, 2019). Selective β2 agonists such as salbutamol can also be used to cause bronchodilation to treat asthma.

Prazosin was the first licensed α blocker. It is an inverse agonist that is selective for the α1 adrenergic receptor and is used in the treatment of hypertension (Ritter *et al.*, 2019). Although prazosin is rarely used in clinical medicine, (there are other α blockers for hypertension that are better tolerated with fewer side effects) it has shown some promise in improving memory deficits in APP23 mice (Katsouri *et al.*, 2013) and has been shown to improve the behavioural symptoms of agitation and aggression in patients with AD (Wang *et al.*, 2009). Prazosin also appears to act via α2 adrenergic receptors though not to the same degree as α1 (Katsouri *et al.*, 2013). A specific experimental drug antagonist for α2 adrenergic receptors, mesedin, has also been shown to have neuroprotective and anti-amyloidgenic properties (Melkonyan *et al.*, 2017). These findings suggest that adrenergic receptors may be suitable therapeutic targets for the treatment of Alzheimer's disease.

6.1.4 Aims and hypothesis

It has been shown that there is a conservation of α1 adrenergic receptors in cerebral cortical microvessels in autopsy cases of multi-infarct dementia and Alzheimer's disease (O'Neill, Fowler and Winblad, 1989). Furthermore, our own yet unpublished data from the Carare group shows preservation of adrenergic receptors with both normal aging and in disease in both human post

mortem tissue and animal models. The study also showed the localisation of certain adrenergic receptor subtypes to the vasculature. In this chapter I aim to demonstrate that this receptor expression can also be visualised in cell cultures and identify the subtypes of α adrenergic receptors expressed by pericytes and smooth muscle cells.

Alpha adrenergic receptor antagonists have demonstrated the ability to improve cognitive function in mouse models of AD. Both α1 and α2 antagonists have been shown to inhibit noradrenaline-induced contraction in smooth muscle cells (Costa *et al.*, 1993) and I hypothesise that this is due to a high expression of α adrenergic receptors present on the contractile cells of the cerebrovasculature (primarily smooth muscle cells but also pericytes).

6.2 Materials and methods

6.2.1 Cell culture

Human brain vascular smooth muscle cells (HBVSMC) and human pericytes (HP) were obtained from Sciencell (sc-1100 and sc-1200) and cultured in smooth muscle cell medium (sc-1101) or pericyte medium (sc-1201). Cells were maintained in a humidified atmosphere (5% CO_2/95% air) at 37°C and medium was refreshed every 2-3 days according to the manufacturer's instructions. The basal medium was supplemented with smooth muscle cell growth supplement (sc-1152) or pericyte growth supplement (sc-1252), 100U/mL penicillin, 100µg/mL streptomycin (sc-0503) and 2% foetal bovine serum. Cells were plated onto poly-L-lysine coated coverslips in a 24 well plate at a seeding density of $0.5x10^5$ per coverslip and returned to the incubator for 72 hours. 72 hours was chosen as the HBVSMC and HP do not contact inhibit and become over confluent if left to grow beyond 3 days.

6.2.2 Immunocytochemistry

After 72 hours cells were fixed with 4% paraformaldehyde for 10 minutes at room temperature then rinsed thoroughly with PBS. Cells were blocked with 15% normal goat serum for 1 hour before overnight incubation with primary antibodies (see **Table 6-1**). Cells were rinsed with PBS before incubation with goat anti-rabbit Alexa Fluor 488 conjugated secondary antibody (Invitrogen, A11034) for 1 hour. After cells were rinsed with PBS, 2µg/mL DAPI (Thermo Fisher, D1306) was applied for 10 minutes. Cells were rinsed with PBS then coverslips were carefully removed from the wells and mounted onto slides with Mowiol and Citifluor. Images were captured using a Leica SP8 laser scanning confocal microscope.

Table 6-1 Adrenergic receptor primary antibodies

Antigen	Name provided by supplier	Supplier details	Optimum concentration
Adrenergic receptor alpha 1A	ADRA1A rabbit polyclonal antibody	Proteintech #19777-1-AP	1:200
Adrenergic receptor alpha 1B	ADRA1B rabbit polyclonal antibody	Proteintech #19776-1-AP	1:200
Adrenergic receptor alpha 2A	ADRA2A rabbit polyclonal antibody	Proteintech #14266-1-AP	1:200
Adrenergic receptor alpha 2B	ADRA2B rabbit polyclonal antibody	Proteintech #19778-1-AP	1:100

6.2.3 Analysis

Three non-overlapping z-stacks were captured per coverslip (each an area of 0.15mm^2) and the fluorescence intensity of the adrenergic receptor staining was measured using ImageJ and an average value per coverslip was calculated. Data was recorded in Microsoft Excel and the ratio of type 1 to type 2 adrenergic receptors was calculated and expressed as a percentage of total adrenergic receptor staining. The ratio of all four subtypes of adrenergic receptor was also expressed as a percentage where 100% represents the total adrenergic receptor expression in a cell type. Pie charts were produced using Microsoft Excel and bar charts were produced using SPSS version 24. Statistical analysis was carried out using SPSS version 24 and Mann-Whitney U and Kruskal-Wallis non-parametric tests were used to determine if any differences were statistically significant. Results are based upon data gathered over three experimental runs (n=3) and were deemed significant if $p \leq 0.05$.

6.3 Results

6.3.1 Pericytes and smooth muscle cells express adrenergic receptors in culture

The immunostaining revealed that all the adrenergic receptor subtypes tested are expressed by pericytes (see **Figure 6-3**). Smooth muscle cells also exhibit a similar profile of adrenergic receptor staining (see **Figure 6-4**).

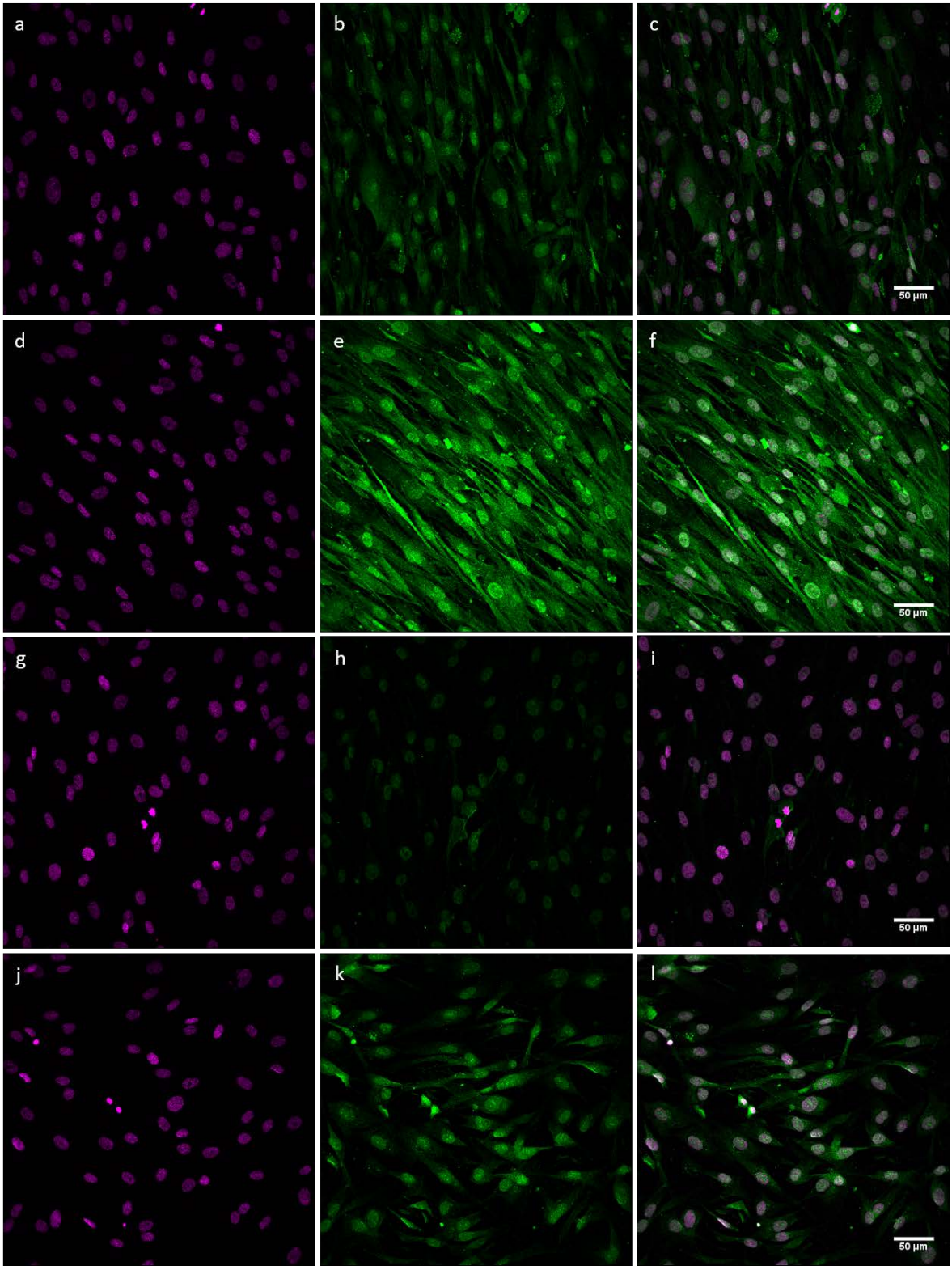

Figure 6-3 representative immunofluorescence images of adrenergic receptor staining on pericytes

HP were cultured for 72 hours and immunostained using sub-type specific adrenergic receptor antibodies. The stained cells were imaged at 40x magnification with a confocal microscope. The pattern of α1A (a-c) and α1B receptors (d-f) was similar with staining throughout the cell body and concentrated in the nucleus however the staining for α1B was

much more intense. α2A (g-i) receptor expression was very low in cultures of HP. α2B receptors (j-l) were also expressed in the nucleus with some weaker staining in the cytoplasm. a, d, g and j show the DAPI stained nuclei in magenta; b, e, h and k depict the adrenergic receptor staining, shown in green and c, f, i and l show an overlay of the two images. Scale bar 50µm.

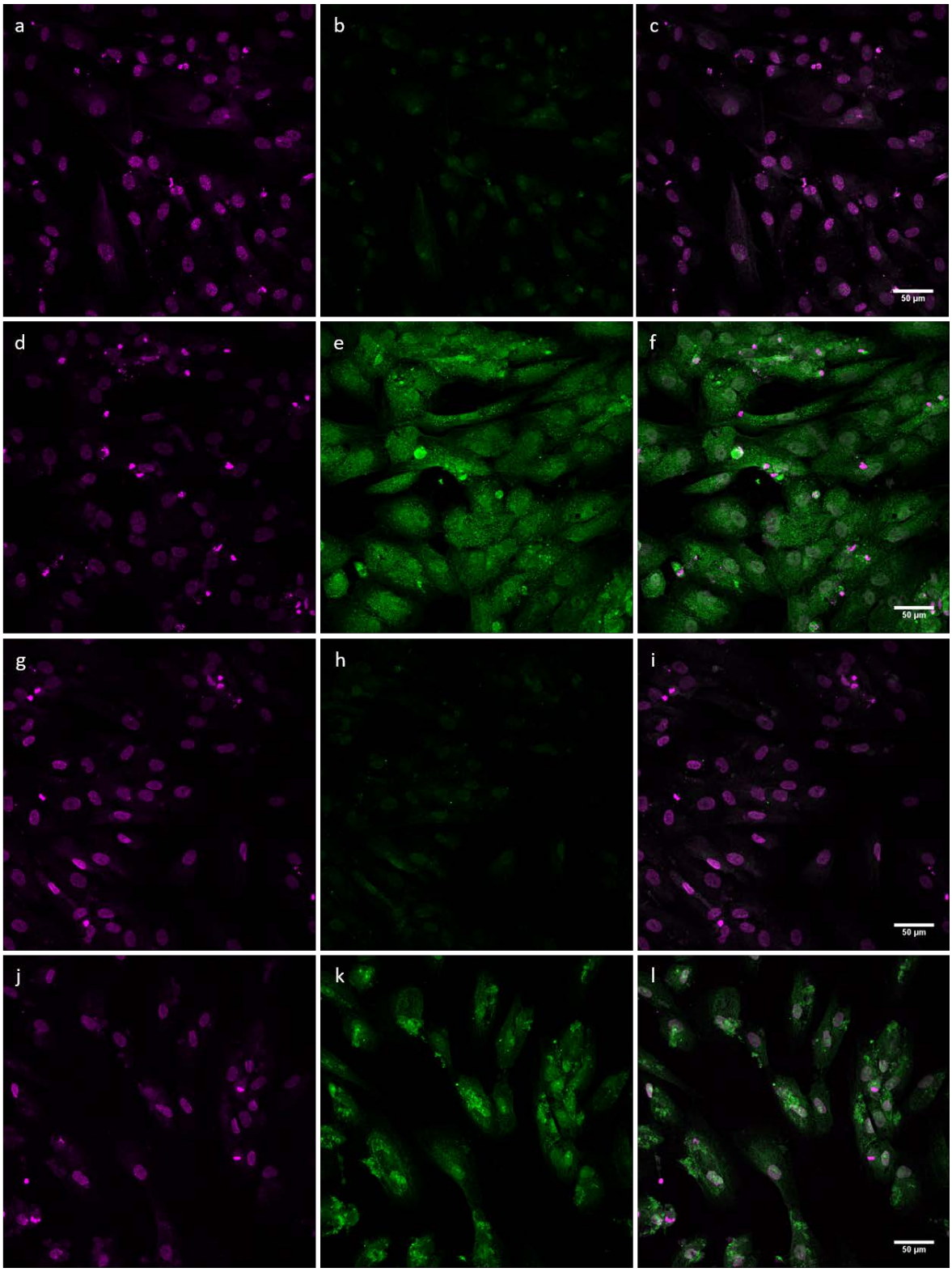

Figure 6-4 representative immunofluorescence images of adrenergic receptor staining on smooth muscle cells

HBVSMC were grown in culture for 72 hours and immunostained using sub-type specific adrenergic receptor antibodies. The stained cells were imaged at 40x magnification with a confocal microscope. α1A (a-c) and α2A (g-i) receptor expression was very low in cultures of HBVSMC. α1B receptors (d-f) were strongly expressed throughout the whole cell body of the

smooth muscle cells. The α2B receptor expression (j-l) was also quite strong in the smooth muscle cell cultures but appeared more punctate and localised to the nucleus. a, d, g and j show the DAPI stained nuclei in magenta; b, e, h and k depict the adrenergic receptor staining, shown in green and c, f, i and l show an overlay of the two images. Scale bar 50µm.

6.3.2 There is no significant difference between α1 and α2 receptor expression in pericytes or smooth muscle cells

The fluorescence intensity of alpha 1 and alpha 2 adrenergic receptors was compared in both pericytes and smooth muscle cells and the results summarised in **Figure 6-5**. There was a slightly higher expression of alpha 1 receptors in pericytes compared to alpha 2 (59% vs 41%) however the Mann-Whitney U test showed this difference was not significant (p=0.423). There was also a higher expression of alpha 1 receptors in the smooth muscle cells compared to alpha 2 (62% compared to 38%) however this was also found to be not significant (p=0.749). These results support the null hypothesis and suggest there is no difference between alpha 1 and alpha 2 adrenergic receptor expression in these cell types.

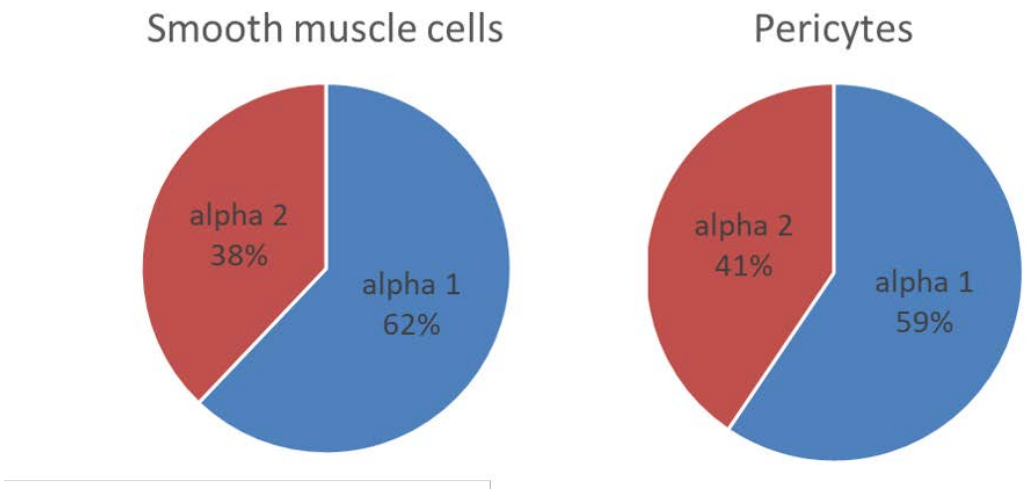

Figure 6-5 a comparison of alpha 1 and alpha 2 adrenergic receptors in smooth muscle cells and pericytes after 72 hours in culture

The fluorescence intensity of alpha 1 receptors was calculated by adding the fluorescence intensity of cells stained with ADRA1A to the fluorescence intensity of cells stained with ADRA1B.The fluorescence intensity of alpha-2 receptors was calculated in the same way but with cells stained for ADRA2A and ADRA2B. These values were then expressed as a percentage of the total adrenergic receptor expression which was calculated by adding the fluorescence intensity of all the adrenergic receptor stains. In both smooth muscle cells and pericytes there is a higher expression of alpha 1 receptors when compared to alpha 2 receptors though this was found to be not significant (p=0.749 and 0.423 respectively).

6.3.3 α1B is the most expressed adrenergic receptor subtype in smooth muscle cells and pericytes

A comparison of the fluorescence intensity of each subtype of adrenergic receptor (α1A, α1B, α2A and α2B) revealed that α1B was the most highly expressed adrenergic receptor subtype in the smooth muscle cell cultures after 72 hours, with 76% of adrenergic receptor expression identified as α1B (**Figure 6-6**). The same was also true of the pericyte cultures with α1B receptor expression making up 56% of the total adrenergic receptor expression (**Figure 6-6**). In fact α1B receptor expression was significantly higher than all of the other adrenergic receptor subtypes in pericytes (**Figure 6-7**).

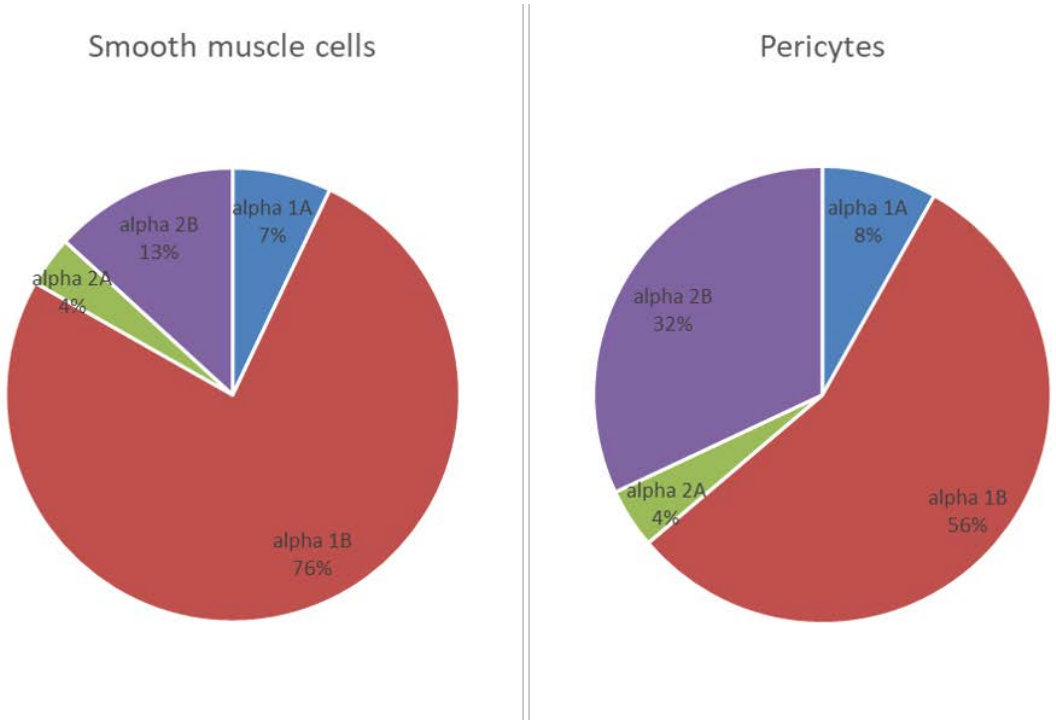

Figure 6-6 the ratio of adrenergic receptor subtypes in smooth muscle cells and pericytes after 72 hours in culture

There was a very high expression of α1B receptors in both smooth muscle cells and pericytes when compared to other adrenergic receptor subtypes (76% and 56% respectively). The α2B receptors were the second most highly expressed receptor subtype with 13% in smooth muscle cells and 32% in pericytes. α1A and α2A receptors had a relatively low expression compared to other receptor subtypes with only 7% and 4% of adrenergic receptors identified as α1A or α2A in smooth muscle cells and 8% and 4% in pericytes. Results are based on an average fluorescence intensity of each receptor subtype measured per coverslip over three independent experiments (n=3) and expressed as a percentage of the total adrenergic receptor expression.

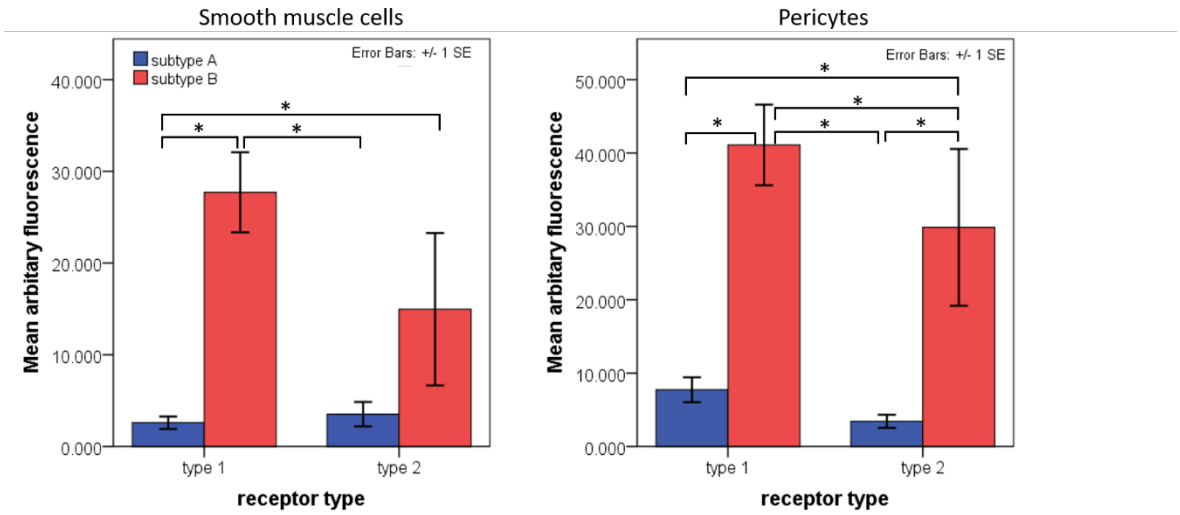

Figure 6-7 fluorescence intensity of adrenergic receptors in smooth muscle cells and pericytes

α1B receptors had the highest expression in smooth muscle cells and was significantly higher than α1A and α2A (p=0.048). α2B receptor expression was also significantly higher than α1A in smooth muscle cells (p=0.048). Similar to smooth muscle cells α1B receptor expression was the highest in pericytes followed by α2B then α1A with α2A showing the lowest receptor expression. All of the differences in receptor expression in pericytes were statistically significant (p=0.029) except when comparing α1A and α2A. Error bars represent the standard error of the mean. Results are based on an average fluorescence intensity measured per coverslip over three independent experiments (n=3). *p<0.05

6.4 Discussion

There are a very wide range of adrenergic receptors expressed in the brain and this must be taken into account when considering a therapeutic approach involving the use of drugs that target adrenergic receptors.

6.4.1 Adrenergic receptor antagonists are likely to influence the contractility of cells

The expression of α adrenergic receptors on pericytes and vascular smooth muscle cells indicates that the cells are likely to contract in response to noradrenaline/epinephrine binding. This suggests contractility of the wall of a cerebral artery can be controlled by targeting adrenergic receptors. Antagonists that block α adrenergic receptor signalling therefore could modulate the smooth muscle contractions that drive IPAD.

6.4.2 Pericytes contain more types of adrenergic receptor than previously thought

Adrenergic receptors on pericytes were identified as early as 1989. Competitive binding studies in bovine microvessels identified the presence of α2 receptors in pericytes (Elfont, Sundaresan and Sladek, 1989). Both α2A and α2B adrenergic receptors were detected by immunostaining (**Figure 6-3**) so this is in agreement with previous studies. α1 receptors were not detected in the 1989 study, but the present study based on immunofluorescence staining of human pericyte cultures has clearly shown the presence of both α1A and α1B adrenergic receptors and when quantifying the intensity of staining the expression of type 2 and type 1 adrenergic receptors was not significantly different. When activated, α adrenergic receptors cause vasoconstriction but the mechanism of action of type 1 and type 2 receptors is different so the identification of both types of receptor in pericytes is significant as there is more capacity for receptor activation and pericyte contraction.

6.4.3 Subtype-specific adrenergic receptor antagonists will not block all adrenergic receptor signalling in cerebral vessels

Adrenergic receptor staining of HBVSMC and HP, after 72 hours in culture, showed there was not a significant difference in the expression of α1 and α2 adrenergic receptors, suggesting that there is an even distribution of these receptor types in the cerebral vessel wall. This means that when applying type specific drugs, such as the α2 antagonist mesedin, only half of the adrenergic receptors on the smooth muscle cells and pericytes will be blocked. There would likely be severe consequences for blocking all adrenergic receptor signalling in the brain with a generic adrenergic receptor antagonist so understanding the ratio of adrenergic receptors in the cells is important when deciding on the best drug candidates.

6.4.4 Increasing antagonist specificity may reduce side effects and improve tolerance

Targeting cerebral vessel innervation with adrenergic receptor antagonists appears to be a valid method in treating the symptoms of Alzheimer's disease however adrenergic receptors are widely expressed throughout the body so there may be some unwanted side effects associated with this. For example prazosin has been shown to improve agitation in Alzheimer's patients (Wang *et al.*, 2009) but it is also known to cause orthostatic hypotension and loss of consciousness, especially following the first dose (Pfizer, 2015). α1B was the most expressed subtype of adrenergic receptor in both cultures by a significant margin and accounted for 76% of the adrenergic receptor staining in HBVSMC and 56% in HP. If the blockage of α1 receptors with antagonists results in cognitive improvement via its action on the cerebrovasculature as suggested by various experimental

studies, then blockage of α1B receptors with a subtype specific antagonist should have the same desired effect in the brain, due to the high expression of α1B adrenergic receptors, but less of an effect in the rest of the body. For example coronary smooth muscle cells express α1D as the predominant adrenergic receptor (Jensen *et al.*, 2009) so are unlikely to be affected by an α1B antagonist which may reduce some of the side effects associated with the cardiovascular system.

6.5 Conclusions

The contractile cells of the cerebrovasculature express detectable levels of both type 1 and type 2 adrenergic receptors when grown in culture. The high expression of α1B adrenergic receptors in HBVSMC and HP suggests that this may be the most important receptor subtype in controlling vascular contraction and is the best target for potential future therapies to modulate IPAD. It is important to note that the receptor expression may change with time and these *in vitro* findings, although insightful, largely represent the adrenergic receptor expression in a sub-confluent culture and may not reflect the true adrenergic receptor expression in the brain; this is a major limitation of this simple model.

6.6 Future work

Drugs to target adrenergic receptors have gained momentum in dementia research. The exact mechanism of action of these drugs is still to be determined and there are many theories as to how these drugs work to improve cognition. One possible theory is that adrenergic receptor drugs can modulate the innervation of the vessel wall which can improve the clearance of amyloid beta via IPAD. Although the presence of adrenergic receptors on the contractile cells of the cerebral vessels is a strong indicator of the link between adrenergic innervation and IPAD, it is still unclear if adrenergic receptor drugs are able to influence IPAD and whether this is beneficial or detrimental to the drainage of solutes from the brain. This needs to be investigated further with both *in vivo* and *in vitro* experiments. Alpha adrenergic receptors are responsible for the contraction of smooth muscle cells and this can be monitored *in vitro* by using a calcium indicator such as Fluo-4-AM and monitoring its uptake into cells in the presence of different subtype-specific adrenergic receptors. It is important to understand how the expression and organisation of receptors changes with time *in vitro* so the expression of adrenergic receptors will need to be examined over a time course and these results compared to receptor expression *in vivo* to identify the most accurate model of adrenergic receptor expression.

Chapter 7 Creating a more physiological model of IPAD

7.1 Introduction

In Chapter 5 I presented an *in vitro* model of IPAD to show the flow of amyloid beta over smooth muscle cells. This provided valuable insight into the patterns of amyloid beta drainage and its effect on smooth muscle cells however the situation is far more complex in the human brain. There are multiple cells that make up the cerebrovasculature and they all have a unique profile of extracellular proteins as demonstrated in Chapter 4, however it is unclear what happens where two different cells meet and to what extent different cells of the cerebral vessel wall contribute to the endothelial basement membrane. Basement membranes are the conduit for clearance of Aβ via intramural periarterial drainage which occurs in the walls of cerebral capillaries, arterioles and arteries (Carare *et al.*, 2008). Here I present a pilot study demonstrating the changes that occur in the basement membrane when cell layers are combined in culture, similar to the *in vivo* arrangement, and present the combination of cells for a triple cell culture that is likely to be the best representation of a cerebral capillary wall. I will also present an adapted version of the QV600 air-liquid interface system capable of supporting two independent flow rates that could be combined with *in vitro* models of the vessel wall to create a model of IPAD.

7.1.1 Arrangement of cells in cerebral blood vessels

IPAD occurs along the vessel walls of cerebral capillaries, arterioles and arteries. Aβ and other solutes enter the IPAD pathway at capillary level so the focus will be on the structure in a cerebral capillary wall. Cerebral blood vessels are composed of a single layer of endothelial cells that are joined together by tight junctions. In capillaries astrocytic end feet surround the abluminal surface. Basement membrane separates the endothelium from the astrocytes. Pericytes surround the endothelium and are embedded in the endothelial basement membrane. The arrangement of cells in a cerebral capillary is summarised in **Figure 7-1**.

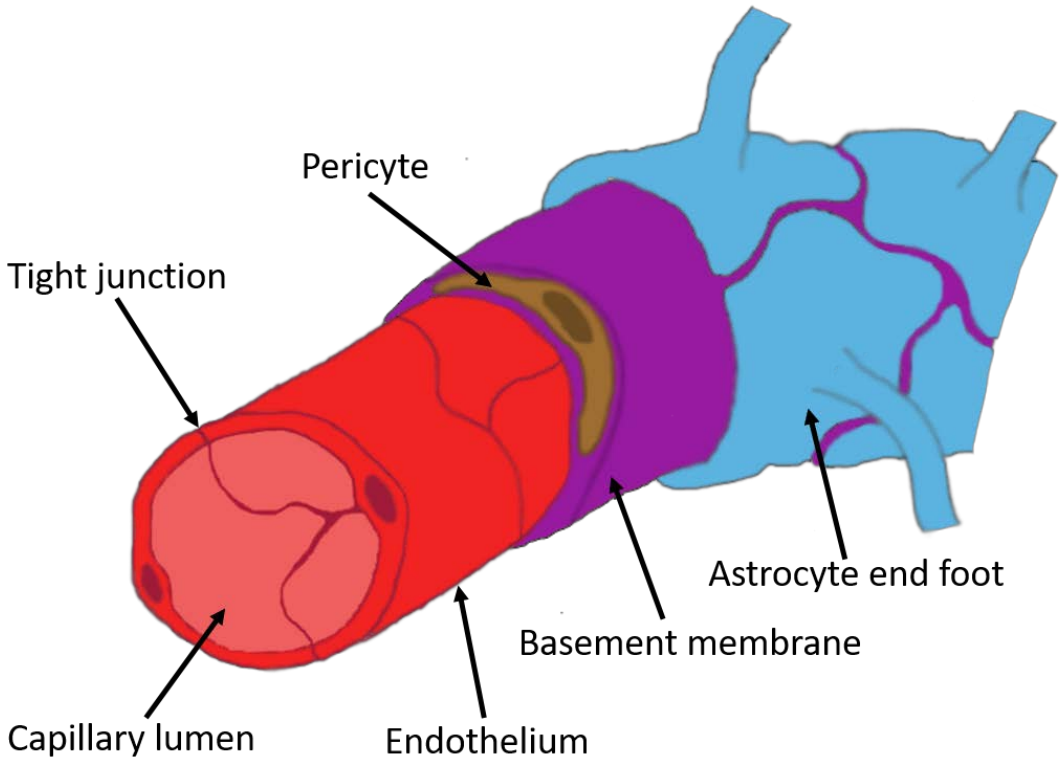

Figure 7-1 schematic diagram of a cerebral capillary

The smallest of the cerebral blood vessels, the lumen of a capillary is formed by a layer of endothelial cells joined by tight junctions. These endothelial cells produce a basement membrane that communicates with the basement membrane of the astrocytes whose end feet are in contact with the vessel wall. Encased within the basement membrane are the perivascular cells known as pericytes.

7.1.2 *In vitro* models

Although *in vitro* models of IPAD are lacking, there are many *in vitro* models that incorporate the cells of the cerbrovasulature to study the blood brain barrier (BBB). Early basic models simply involved a single culture of endothelial cells (see **Figure 7-2**a), however endothelial cells removed from the CNS environment have been shown to lose functional barrier capacity (Rubin *et al.*, 1991). There is increasing evidence that the BBB properties of cells are dictated by the microenvironment so simple monoculture models are not ideal (He *et al.*, 2014). Barrier functionality can be reinstated when endothelial cells are grown in astrocyte conditioned medium (Neuhaus, Risau and Wolburg, 1991) or if astrocytes are incorporated into the culture (Tao-Cheng, Nagy and Brightman, 1987), indicating that astrocytes secrete factors that are important in the formation of the BBB.

7.1.2.1 Co-cultures

Many co-culture models of endothelial cells and astrocytes have been developed to study the BBB (see **Figure 7-2**b) (Kido *et al.*, 2002; Jeliazkova-Mecheva and Bobilya, 2003; Niego and Medcalf, 2013; Kulczar *et al.*, 2017; Zhang *et al.*, 2017). It is unclear what impact astrocytes have on the extracellular environment around the endothelium or to what extent they contribute to the basement membrane.

The location of pericytes also makes them an important contender in models of the cerebrovasculature and the BBB. Pericytes are embedded in the endothelial basement membrane (Winkler, Bell and Zlokovic, 2011) and it is this same basement membrane that separates the cells. Co-culture models of endothelial cells combined with pericytes have also been developed for BBB studies (see **Figure 7-2**c) (Dente *et al.*, 2001; Dohgu *et al.*, 2005; Kuntz *et al.*, 2015). There is evidence that both endothelial cells and pericytes contribute to this basement membrane (Cohen, Frank and Khalifa, 1980; Mandarino *et al.*, 1993) and pericytes further regulate the basement membrane by producing protease inhibitors, most notably TIMP3, when interacting with the endothelium (Davis and Senger, 2005).

It has been shown that incorporation of astrocytes increases trans-endothelial electrical resistance (TEER) measurements and reduce the permeability of the tight junctions (He *et al.*, 2014). Adding pericytes has also been shown to increase TEER measurements compared to endothelial culture alone (Hayashi *et al.*, 2004). Both astrocytes and pericytes are important in regulating the microenvironment for endothelial cells and triple culture models have been developed to reflect this

7.1.2.2 Triple co-cultures

Triple culture models were developed to replicate the anatomical structure of the *in vivo* BBB (**Figure 7-2**d) (Hatherell *et al.*, 2011; Urich *et al.*, 2013; Thomsen, Burkhart and Moos, 2015; Thomsen *et al.*, 2017). The triple co-culture model also has significantly higher TEER and lower permeability than endothelial monocultures (Nakagawa *et al.*, 2009) indicating it is a more relevant and reliable *in vitro* model of the BBB. It is important to note however that some studies have reported a drop in TEER in the triple culture models compared to double cultures (Hatherell *et al.*, 2011; Maherally *et al.*, 2018).

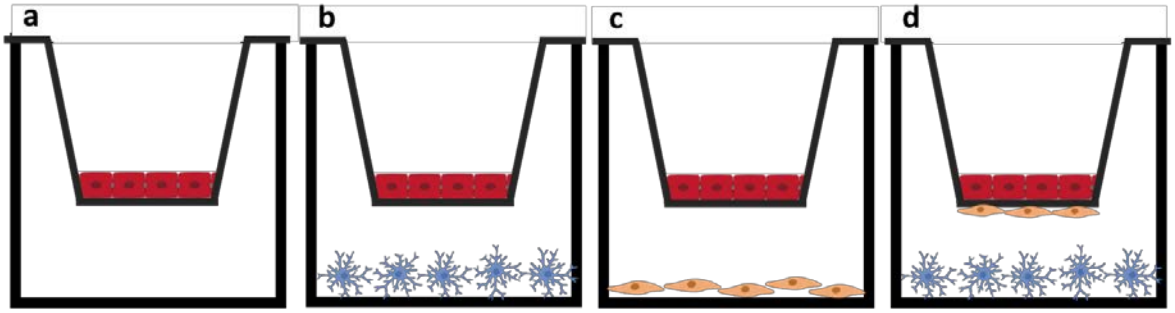

Figure 7-2 arrangement of cells in various BBB models

The most basic of BBB models uses only endothelial cells (a) often supplemented with astrocyte conditioned medium to maintain barrier integrity. Co-culture models involving endothelial cells combined with astrocytes (b) or pericytes (c) are more physiologically relevant and yield barriers with higher TEER and lower permeability compared to single culture models. The most physiologically relevant BBB models involve triple culture of endothelial cells and pericytes grown on opposite sides of a transwell with astrocytes grown in the base of the plate (d).

7.1.2.3 Dynamic models

Shear stress has been shown to affect transporter and tight junction protein expression in endothelial cells (Tarbell, 2010) and incorporating flow has been shown to increase ZO-1 expression and decrease permeability in endothelial cell monolayers (Siddharthan *et al.*, 2007). Several dynamic *in vitro* BBB models now use microfluidics to incorporate fluid flow (Takeshita *et al.*, 2014; Adriani *et al.*, 2015; Wang *et al.*, 2016). These models recreate the physiological shear stress the blood flow exerts on the endothelium, however it is important to note that shear stress may not be beneficial for all cells. Astrocytes in particular are not supposed to suffer shear stress in the brain and astrocytes have been shown to die when exposed to flow rates where the shear stress is in excess of $2x10^{-6}$Pa or $2x10^{-5}$dyn/cm^2 (Miranda-Azpiazu *et al.*, 2018)

Both the anatomical arrangement of cells in the cerebral wall and the physiological flow and shear conditions that the cells are exposed on both sides of the vessel wall should be taken into account when attempting to create an *in vitro* model of IPAD

7.2 Materials and methods

7.2.1 Nanocrystal labelling

To identify different cell types when grown in co-cultures, quantum dot nanocrystals (QDs) were utilised. These QDs were selected as they produced an intense stable fluorescence that can be

transferred to daughter cells but not adjacent cells so were able to track a cell population whilst it was still proliferating. The Qtracker 585 labelling kit (Q25011MP) and the Qtracker 705 labelling kit (Q25061MP) were prepared according to the manufacturer's instructions immediately prior to loading. Initially concentrations of 5, 10 and 20nM were tested and 20nM was selected for the purposes of cell labelling in co-cultures. The 20nM QD solution was added to the cells and incubated at 37^{o}C for a minimum of 2 hours. The QD solution was then removed and cells were rinsed with medium twice before being replaced with fresh culture media. Depending on the experimental set-up, QDs were loaded into cells before trypsinization in the T75 flask, or immediately after plating in a transwell or 24-well plate.

7.2.2 Direct co-cultures

In the cerebral vessel cells are able to communicate with each other as they are in contact. For example astrocytes are in contact with the pericytes embedded in the endothelial basement membrane via their end feet. Initial co-culture experiments were carried out on poly-L-lysine coated glass coverslips in 24-well plates. Different combinations of astrocytes and pericytes were tested to ascertain the best seeding densities and media combination for a successful co-culture. The combinations tested are detailed below in **Figure 7-3**.

7.2.3 Utilising tranwsells

Transwell cell culture inserts are specially designed to produce an environment that is more physiologically relevant than traditional cell culture plastics. They are ideal for use with co-cultures as they provide individual access to the apical and basolateral side of the membrane which means different coating solutions and different media can be used for each side of the membrane. Transwell membranes are composed of polyethylene terephthalate and pore sizes typically vary from 0.4μm to 8μm though other pore sizes are available. The smallest pore size was selected for these studies to prevent cell migration through the membrane whilst retaining communication between cell layers.

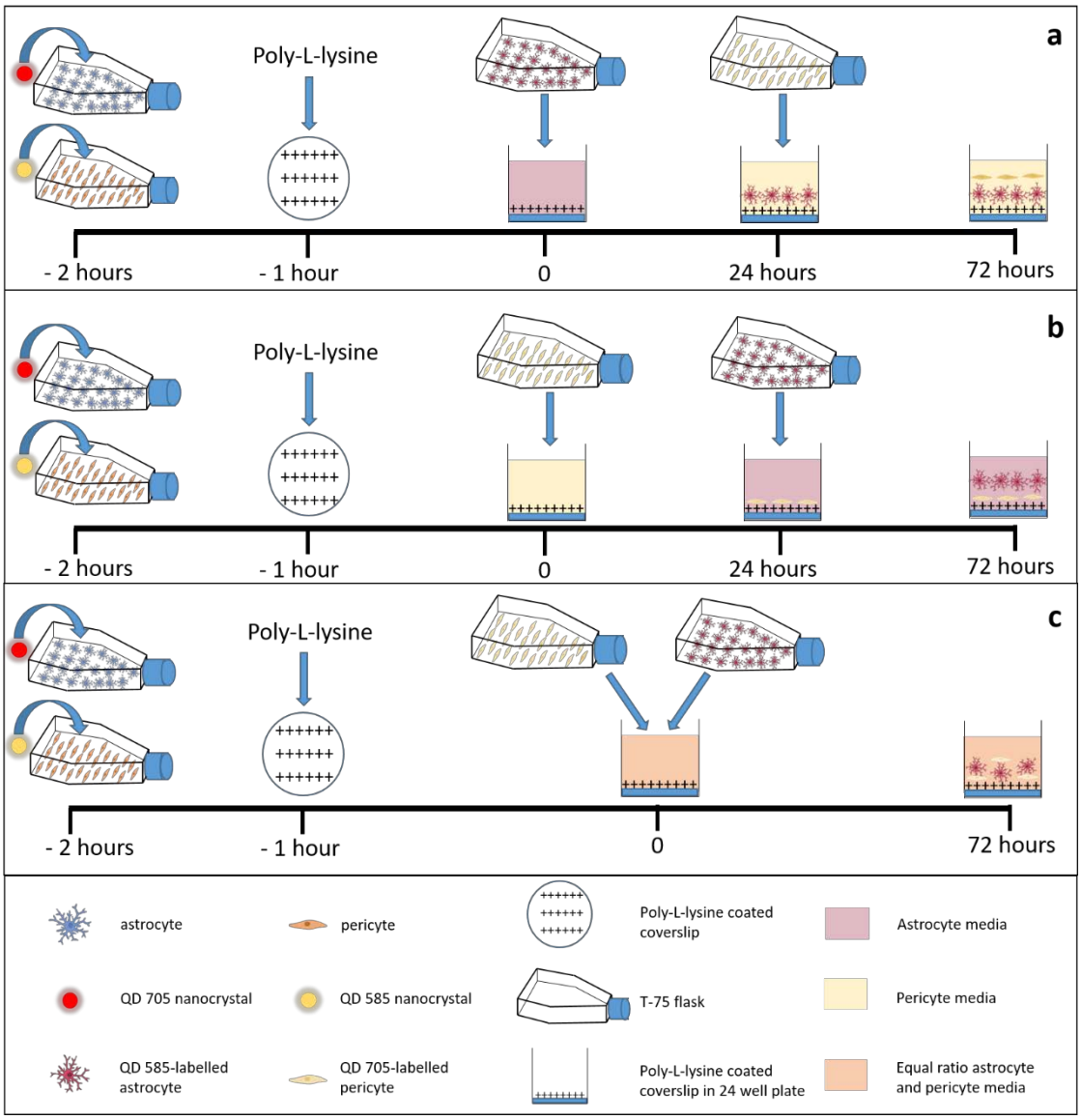

Figure 7-3 experiment timeline for direct co-cultures

a) 705-labelled QDs were loaded into HA and the cells were plated onto glass coverslips in a 24-well plate at a density of $0.5x10^5$ cells/coverslip and incubated at 37°C for 24 hours with astrocyte media. 585-labelled QDs were loaded into HP and the labelled HP were then seeded at a density of $0.5x10^5$ cells/coverslip on top of the HA. The co-culture was incubated for a further 48 hours in pericyte media.

b) 585-labelled QDs were loaded into HP and the cells were seeded at a density of $0.5x10^5$ cells/coverslip. The cells were incubated at 37°C for 24 hours with pericyte media. HA were loaded with the 705-labelled QDs and then seeded at a density of $0.5x10^5$ cells/coverslip on top of the HP. The co-culture was incubated for a further 48 hours in astrocyte media.

c) HP were loaded with the 585-labelled QDs and HA were loaded with the 705-labelled QDs. Both the HA and HP were plated onto glass coverslips in a 24-well plate at a density of $0.5x10^5$ cells/culture/coverslip. The culture was maintained with an equal ratio of astrocyte and pericyte media for 72 hours.

7.2.3.1 Direct co-cultures using Transwell inserts

Transwell inserts were coated with poly-L-lysine. 585-labelled QDs were loaded into HA or HP before plating the cells at a density of $1.2x10^4$ cells/Transwell. 200µL and 600µL of the appropriate media was added to the apical and basolateral compartments respectively. The culture was incubated at 37°C for 48 hours. 705-labelled QDs were loaded into D3 cells prior to plating on top of the HA or HP cell layer at a density of $3x10^4$ cells/Transwell. Media was replaced with EndoGRO media and the co-culture was incubated for a further 72 hours before being fixed with 4% PFA for 10 minutes at room temperature and immunostained. The experimental timeline for this direct co-culture is shown in **Figure 7-4**.

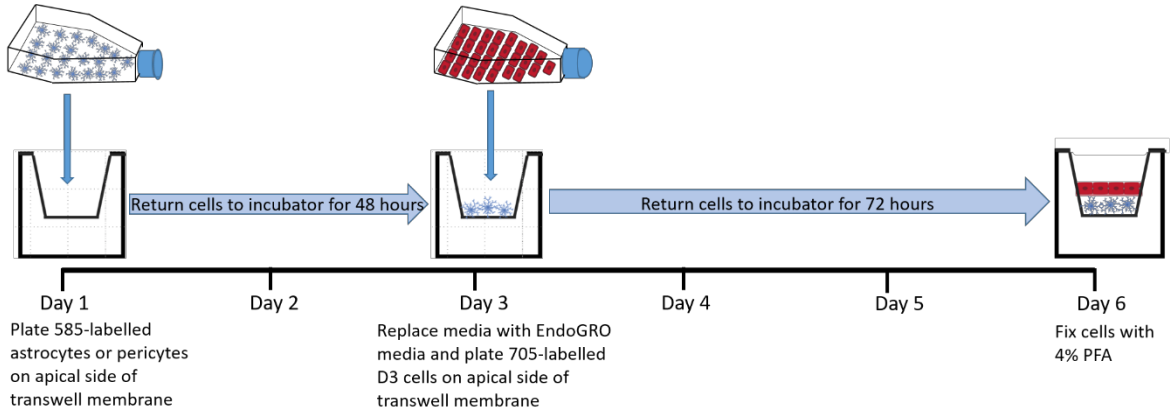

Figure 7-4 timeline for plating cells in direct co-culture models

Prior to day 1 cells must be grown near confluence in culture flasks and loaded with an appropriate QD. Transwell inserts must also be coated with poly-L-lysine. In this case 585-QDs were loaded into pericytes or astrocytes prior to plating on the apical side of a Transwell membrane. The cells were grown for 48 hours in cell specific media before D3 cells loaded with 705-QDs were added to the apical side of the Transwell. Media was changed to EndoGRO media to support the growth of the endothelial cells and the culture was incubated for a further 72 hours before being fixed for immunostaining.

7.2.3.2 Indirect co-cultures using transwells

7.2.3.2.1 Astrocytes and pericytes

Both sides of the Transwell membranes were coated with poly-L-lysine as previously described (section 2.1.2.3). Transwell inserts were inverted in a 12-well plate and HP were plated at a density of $0.5x10^5$ cells/Transwell onto the basolateral side with 100µL pericyte media containing 20nM QDs. The culture was incubated for 2 hours at 37°C. Transwell inserts were then reverted to the correct orientation in a 24-well plate and astrocytes were plated into the apical compartment at a density of $0.5x10^5$ cells/Transwell (see **Figure 7-5**a). The basolateral compartment was filled

with pericyte media and astrocyte media was added to the apical compartment. The culture was incubated for a further 72 hours at 37°C before being fixed and immunostained.

7.2.3.2.2 Endothelial cells and astrocytes or endothelial cell and pericytes

The apical side of the transwell membrane was coated with collagen I solution (as detailed in section 2.1.3.3) for one hour at room temperature. After rinsing with sterile water, the Transwell inserts were inverted in a 12-well plate and the basolateral side of the transwell membrane was coated with poly-L-lysine solution. HA (**Figure 7-5**b) or HP (**Figure 7-5**c) were plated onto the basolateral side at a density of $1.2x10^4$ cells/transwell with 100µL culture media containing 585-labelled QDs and left to adhere for 4 hours at 37°C. The transwell was then returned to its correct orientation in a 24-well plate and culture media added to both compartments before incubating for a further 48 hours. 705-labelled QDs were loaded into D3 cells which were then plated into the apical compartment at a density of $3x10^4$ cells/transwell and the apical media was replaced with EndoGRO media. The co-culture was incubated for a further 72 hours before being fixed and immunostained.

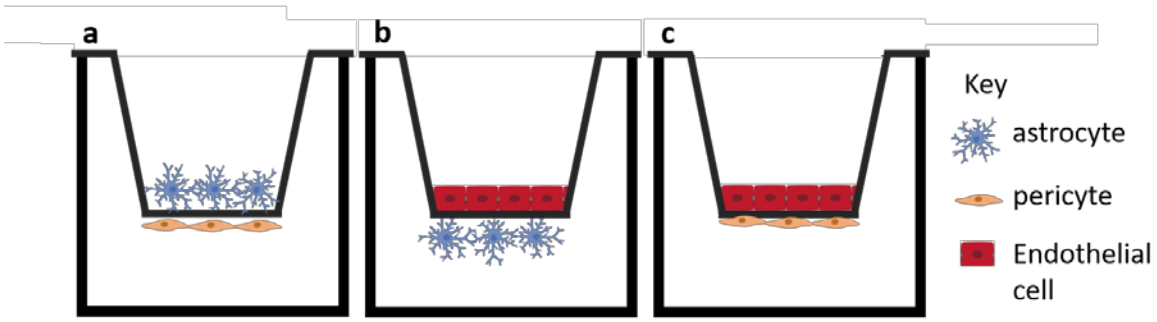

Figure 7-5 combinations of cells used for indirect co-cultures of cells on Transwell inserts

Several combinations of cerebrovascular cells were tested by indirect co-culture. Cells were seeded on the basolateral side of an inverted Transwell and left to adhere before Transwells were flipped and inserted into 24-well plates. Cells were then plated on the apical side of the membrane. Each cell type was maintained in its own medium. Cell combinations were: astrocytes and pericytes (a), astrocytes and endothelial cells (b) and pericytes and endothelial cells (c). These combinations were chosen to reflect the interactions of cells in a cerebral capillary.

7.2.4 Immunocytochemistry

After fixing cells with 4% PFA for 10 minutes, cells were washed three times with PBS and blocked with 15% NGS for 1 hour. Cells were then incubated overnight with collagen IV (Abcam, ab6586) primary antibody diluted 1:400 in PBS at 4°C .After washing three times with PBS, cells were incubated with goat anti-rabbit Alexa Fluor 488 conjugated secondary antibody (Invitrogen,

A11034) for 1 hour at room temperature. Cells were washed again three times with PBS and incubated with 2µg/mL DAPI for 10 minutes. Transwells were removed from the plates and inverted and the membrane was carefully cut from the insert. The membrane was mounted between two glass coverslips with Mowiol and Citifluor. Coverslips were mounted onto slides with Mowiol and Citifluor. Cultures were examined by confocal microscopy.

7.2.5 A dual flow millifluidics system

The Kirkstall QV600 cell culture system has modified chambers that are able to accommodate commercial inserts. The 33mm deep chamber can accommodate Transwells designed for 24-well plates. The chamber also has dual inlet and outlet tubes (see **Figure 7-6**). It was originally designed to create a continuous and stable air-liquid interface for studying surface cultures such as the cornea, skin and respiratory system, however the system can also be modified to create a liquid-liquid interface that is ideal for studying barrier models such as those found in the gut or the blood-brain barrier. The double cavity chamber for liquid-liquid interface is created by using an alternative insert fitted with a silicone O ring to create the seal. Each set of inlet and outlet tubes must be connected to its own reservoir bottle and the tubing passed through a peristaltic pump to create two closed recirculating loops of fluid flow (see **Figure 7-7**). Each compartment of the dual cavity chamber is separated by the porous Transwell membrane, allowing the cells of the apical and basolateral compartments to communicate.

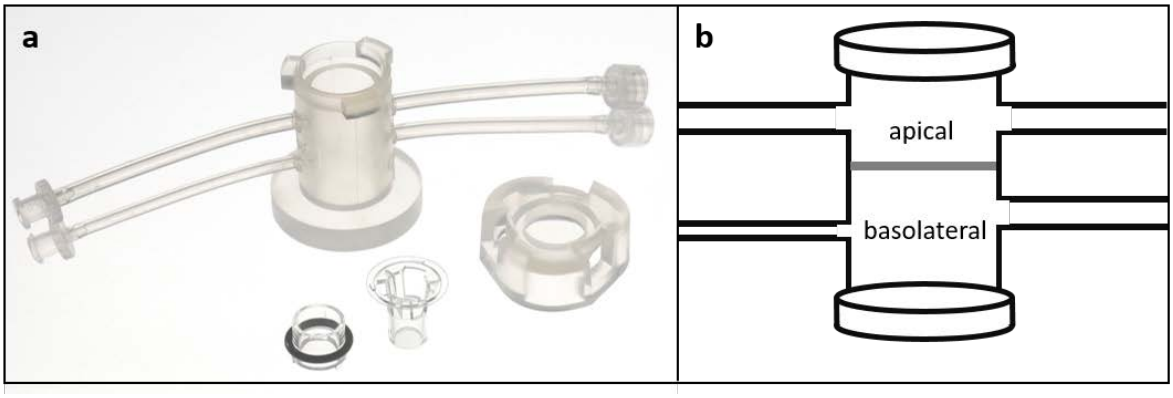

Figure 7-6 The QV600 chamber

The QV600 chamber can accommodate traditional hanging culture inserts for air-liquid interface or can be modified with an adapted insert for liquid-liquid interface. a) Photo of the QV600 chamber and the two different inserts for air-liquid or liquid-liquid interface. b) Schematic representation of the QV600 chamber showing the two compartments of the dual cavity chamber.

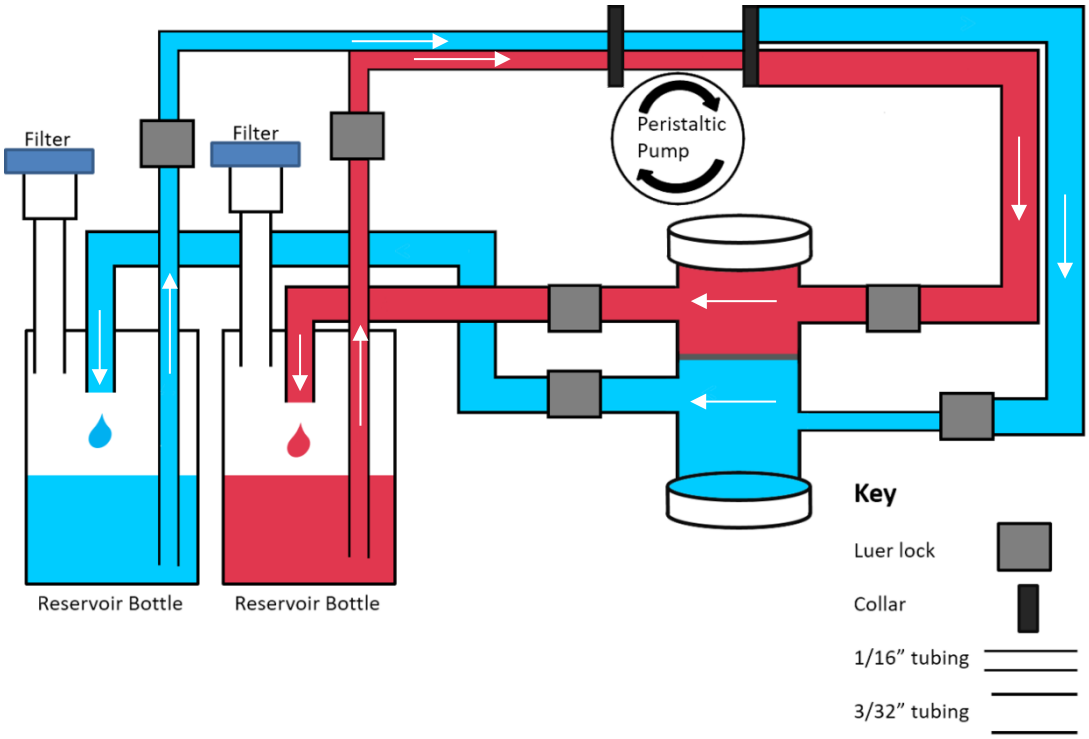

Figure 7-7 Schematic representation of liquid-liquid interface dual cavity QV600 system

The apical and the basolateral compartments of the dual cavity chamber are separated by a porous membrane which is the only point of contact between the two chambers. Each compartment is part of a closed loop of circulating media, which can be selected based upon the requirements of the cells, and is controlled by the peristaltic pump. Arrows indicate the direction of flow.

The Kirkstall QV600 system was assembled with one QV600 chamber. The chamber was divided into apical and basolateral compartments using a 0.4µm Transwell membrane and secured in place with a silicone O ring. Both the apical and basolateral compartment were connected to separate reservoir bottles and connected to the peristaltic pump. In the apical loop the direction of the tubing passing through the peristaltic pump was reversed to create an opposing flow in the apical and basolateral compartments. Reservoir bottles were filled with water containing food colouring and the system was run at maximum speed to test for leaks and any visible turbulence.

7.3 Results

7.3.1 Determining the optimum concentration of nanocrystals for cell tracking

The manufacturer recommended concentrations for QDs is 2-15nM however other users have recommended using up to 20nM (Danner *et al.*, 2013). With this in mind three concentrations of QDs were tested to evaluate the signal strength when imaging. The highest concentration tested was 20nM and it was the best concentration for uptake and detection in the cell cultures (**Figure**

7-8). Lower concentrations were detectable but there was not sufficient uptake into the cells and many cells remained unlabelled so they were unsuitable. The 20nM QD concentration also worked well with co-cultures with good uptake into each culture (see **Figure 7-9**). The QDs were dotted and appeared to congregate around the cell nuclei.

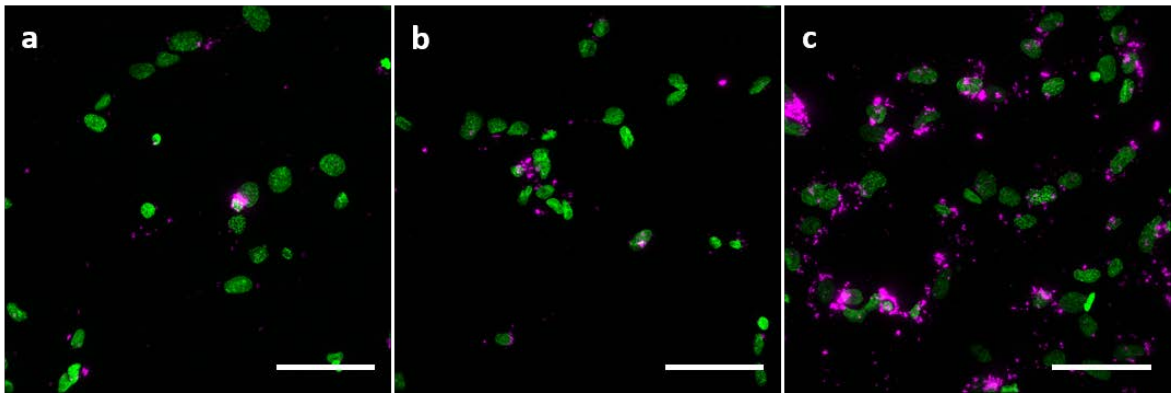

Figure 7-8 uptake of QD nanocrystals in hCMEC/D3 cultures

QD nanocrystals were loaded at various concentrations into hCMEC cultures as follows: a) 5nM, b) 10nM and c) 20nM. Nanocrystal loading (shown in magenta) increased in a dose dependent manner and only the 20nM concentration showed a high degree of loading with the majority of cells taking up the QDs. DAPI stained nuclei are shown in green. Scale bar 100µm.

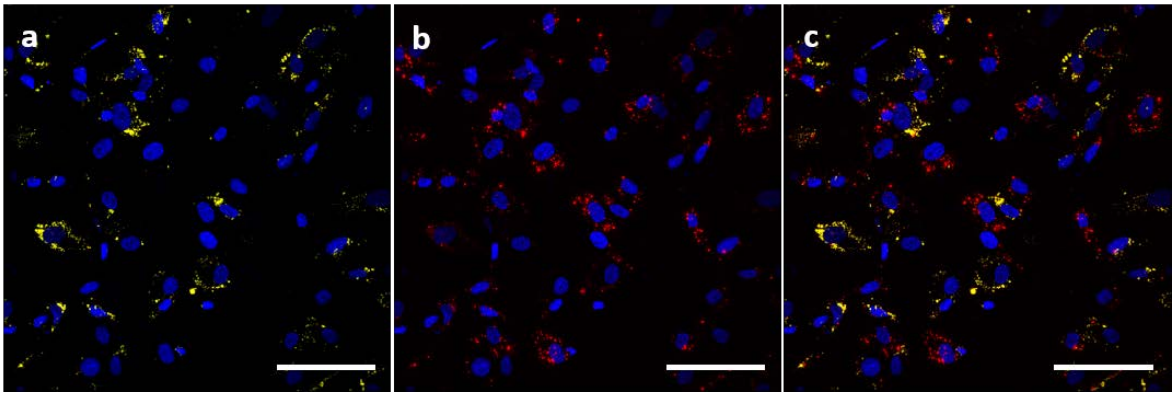

Figure 7-9 Uptake of QD nanocrystals in HA and HP co-culture

20 nM 585 labelled QDs (shown in yellow) were loaded into astrocytes (a) and 20nM 705 labelled QDs (shown in red) were loaded into pericytes (b). When the cells were grown in co-culture the QDs allowed visualisation of the two cell types (c).The QDs appeared to congregate around the nuclei (DAPI stained and shown in blue). Scale bar 100µm.

7.3.2 Different co-culture combinations affect basement membrane production

When HA and HP were plated in direct co-culture both cell types were detected by the QD nanocrystal labelling in all combinations tested. Simultaneously plating HA and HP and

maintaining the culture in a combined media made up of a 1:1 ratio of astrocyte and pericyte media increased the production of collagen IV (**Figure 7-10**g) compared to plating the HA and pericytes in series and maintaining in only one type of medium. A web-like pattern of collagen IV staining was seen in all HA and HP co-cultures (**Figure 7-10**g,h,i) but it was much more detailed and intricate in the simultaneous co-culture maintained in combined medium. The pattern of collagen IV staining was very similar in HA and HP co-cultures regardless of which cell type was plated first (**Figure 7-10**h,i) or which media the culture was maintained in.

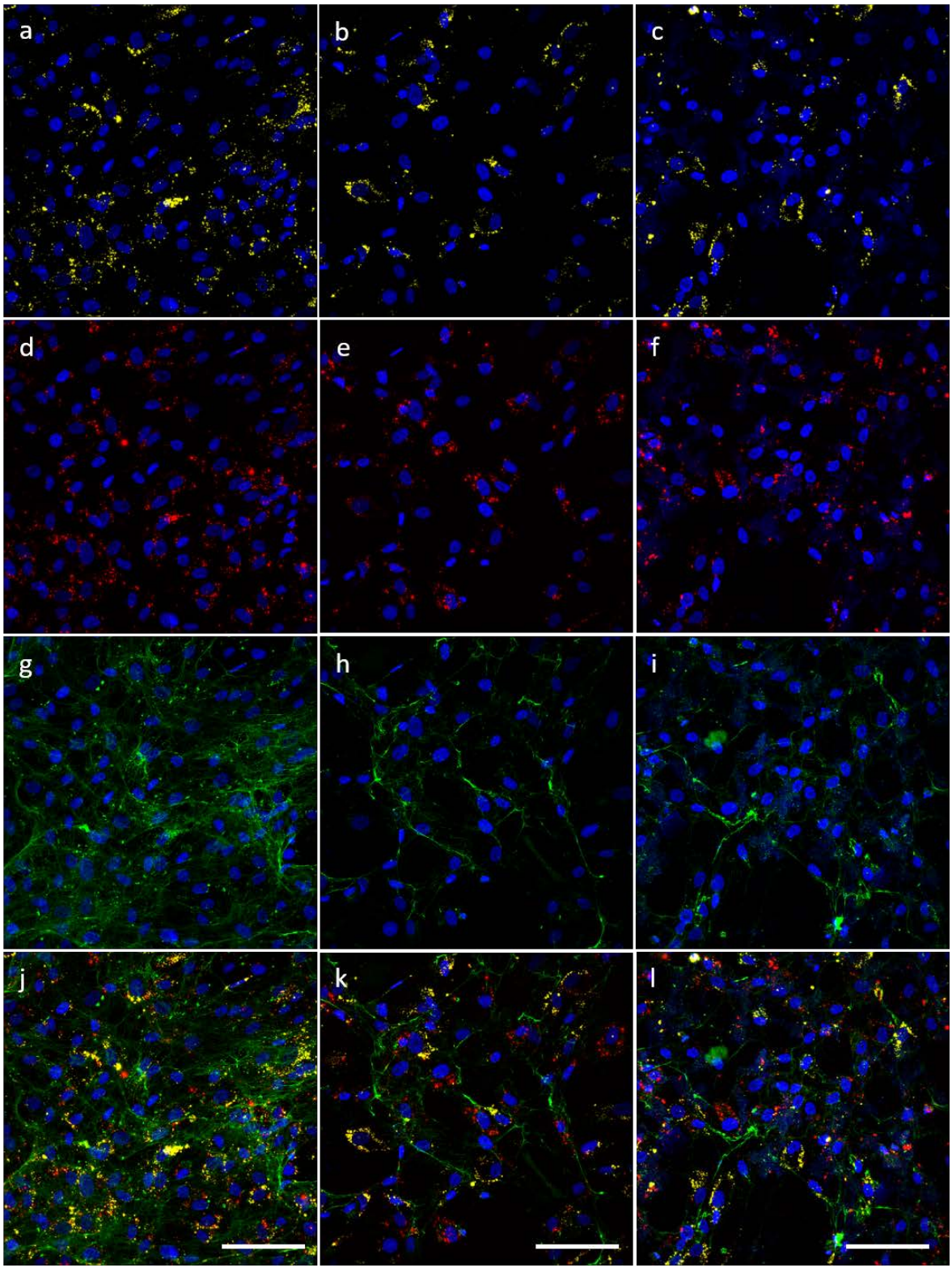

Figure 7-10 Collagen IV expression in astrocyte and pericyte direct co-cultures

Three co-culture set-ups were immunostained for collagen IV (shown in green). Simultaneous HA and HP co-cultures maintained in combined media (a,d,g,j), HA plated followed by HP 24 hours later and maintained in pericyte media (b,e,h,k) and HP plated followed by HA maintained in astrocyte media (c,f,i,l). HA were labelled with 585 QDs (shown in yellow), HP

were labelled with 705 QDs (shown in red) and cells were stained with collagen IV (green) and DAPI (blue). Scale bar 100µm.

7.3.3 Astrocytes and pericytes have the same effect on endothelial cells in co-culture

When hCMEC/D3 were directly co-cultured with HA or HP the pattern of collagen IV staining was indistinguishable (see **Figure 7-11**). There was a uniform coverage across both co-cultures and they both produced an intricate reticulated mesh of collagen IV.

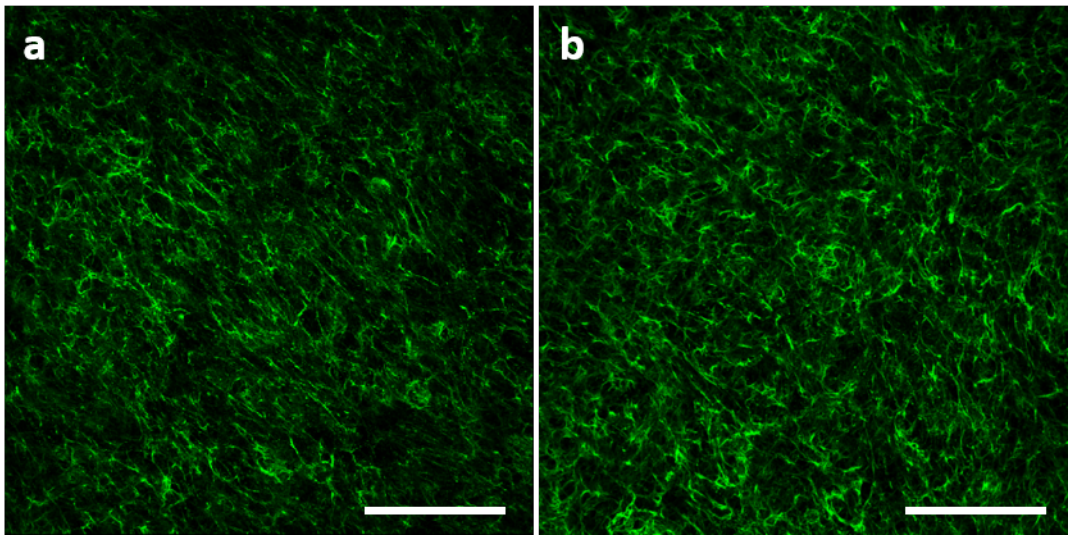

Figure 7-11 collagen IV immunofluorescence staining in endothelial direct co-cultures

When comparing the collagen IV immunostaining (shown in green) in direct co-cultures of hCMEC/D3 and HA (a) and hCMEC and HP (b) there were no distinguishable differences in the pattern of immunostaining. The amount of staining present also appeared to be the same. Scale bar 100µm.

When hCMEC were indirectly co-cultured with either HA or HP on the opposite side of a Transwell membrane a similar pattern of collagen IV staining was observed (**Figure 7-12**).

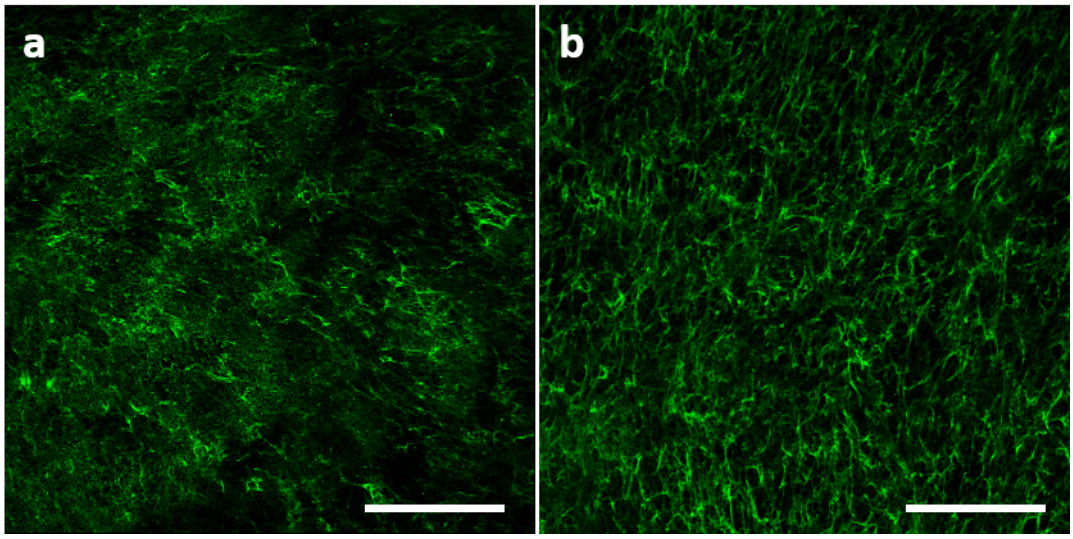

Figure 7-12 collagen IV immunofluorescence staining in endothelial indirect co-cultures

Endothelial cells were cultured with either astrocytes (a) or pericytes (b) grown on the opposite side of a Transwell membrane. Collagen IV immunostaining (shown in green) produced by endothelial cells on the apical membrane appeared to be unaffected by the cell type grown on the basolateral side. Both co-cultures showed a high expression of collagen IV with a web-like mesh of protein expressed across the whole culture. Scale bar 100µm.

The pattern of collagen IV staining across the four co-cultures that use endothelial cells all showed a very similar pattern of staining and appeared to produce similar amounts of collagen IV, though this needs to be confirmed with quantitative analysis before any conclusions can be drawn.

7.4 Discussion

The most successful HA and HP co-culture with regards to collagen IV expression was a direct co-culture where the cells were simultaneously plated and maintained in a combined media. The arrangement of cells in the cerebral capillary means that astrocytes and pericytes are able to directly communicate with each other so this is likely to be the best arrangement for the cells *in vitro* as well. Of the three co-cultures of HA and HP the one maintained in combined media had the highest collagen IV staining, suggesting that supporting a co-culture with growth factors for each cell type is beneficial and leads to increased protein production. Since there is a 24 hour delay when plating cells in series it is also possible that the difference in protein expression observed may be due to this time delay.

There appears to be no difference in the pattern or amount of collagen IV staining in endothelial cells when they are co-cultured with astrocytes or pericytes. In addition is also appears that the type of co-culture has very little effect on the collagen IV production on the apical membrane. This indicates that astrocytes and pericytes do not require direct contact to influence the

endothelium. Astrocytes and pericytes may also not directly contribute to the endothelial basement membrane but instead act on the endothelium promoting the production of basement membrane proteins. Astrocytes secrete vascular endothelial growth factor (VEGF) (Alvarez, Katayama and Prat, 2013) and the interaction of pericytes and endothelial cells causes upregulation of transforming growth factor β1 (TGF-β1) (Jo *et al.*, 2013). Both VEGF and TGF-β1 promote endothelial cell activation and proliferation so this may explain the similarities observed between the co-cultures of endothelial cells with astrocytes and endothelial cells with pericytes. The protein expression needs to be quantified to confirm that there is no change in the amount of protein expressed.

7.4.1 QD nanocrystals are useful for tracking different cell populations

The QDs are not toxic and were not observed to have any detrimental effect on the cells. Using QD nanocrystals I was able to demonstrate the presence of two cell types in a co-culture. Since the QDs were loaded into separate cultures and their properties do not allow transfer to adjacent cells, the presence of both 585 and 705-labelled QDs indicated that both HA and HP were successfully incorporated into the co-culture. QDs could easily be used to track cells in a triple culture. Due to the narrow emission spectrum of QDs, compared to traditional dyes, it is simple to select non-overlapping wavelengths so there is no cross-reactivity when detecting them. This makes QDs a very useful tool when tracing multiple cell populations in mixed cultures. QDs are passed to daughter cells and can be traced through several generations so they could be used in future to monitor the proliferation of different populations of cells as well as migration and motility of cells.

7.4.2 Proposed *in vitro* model of IPAD

The cells that make up the cerebral capillary wall have a very specific anatomical arrangement (shown in **Figure 7-1**). The results of the co-culture experiments suggest that astrocytes and pericytes grow best in direct contact and while astrocytes and pericytes are essential to provide the correct microenvironment for endothelial cells, direct co-culture with endothelial cells does not appear to be necessary.

The Kirkstall QV600 system could be used to induce a dual opposing flow of media to multi-cell cultures and the independent apical and basolateral flows can be optimally set according to the cells in each compartment. This means that different flow rates and therefore different shear stresses may be applied to each compartment.

Using these results combined with the anatomical arrangement of cells in the cerebral capillary I propose a triple co-culture model of endothelial cells on the apical side of a Transwell membrane and a mix of astrocytes and pericytes on the basolateral side as the most suitable *in vitro* model of the cerebral capillary wall. This arrangement of cells in QV600 chamber is shown in **Figure 7-13**.

This triple culture could be loaded into the QV600 chamber to introduce flow to the model (see **Figure 7-14**). Since the endothelial cells would be separated from the other cells by a membrane, a higher flow rate can be used to induce physiological shear stress without being detrimental to the astrocytes or pericytes. The flow in the apical compartment can be set slower to prevent shear-induced astrocyte cell death and mimic the ISF drainage of the brain.

All models have both strengths and weaknesses and the key features of this proposed *in vitro* model of IPAD are discussed in **Table 7-1**.

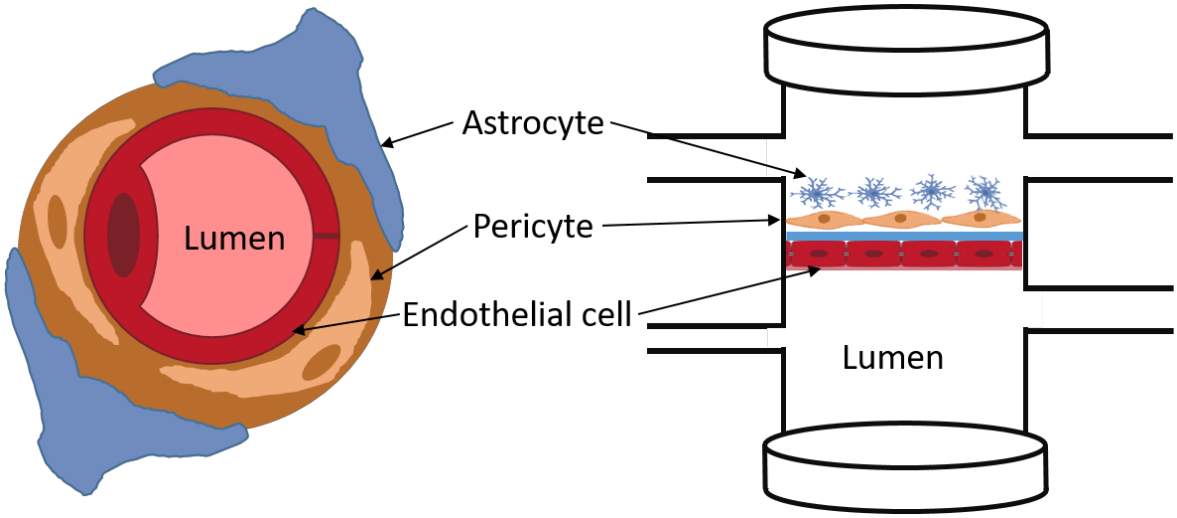

Figure 7-13 *in vivo* arrangement of cells in cerebral capillary and proposed arrangement of cells for *in vitro* IPAD model

Endothelial cells, pericytes and astrocytes make up a cerebral capillary and are all important when modelling the cerebrovasculature. A combination of astrocytes and pericytes plated on the apical side of a Transwell and endothelial cells plated on the basolateral side accurately reflects the arrangement of cells *in vivo*. Inserting the Transwell into a QV600 will allow the application of fluid dynamics further increasing the physiological relevance of the model.

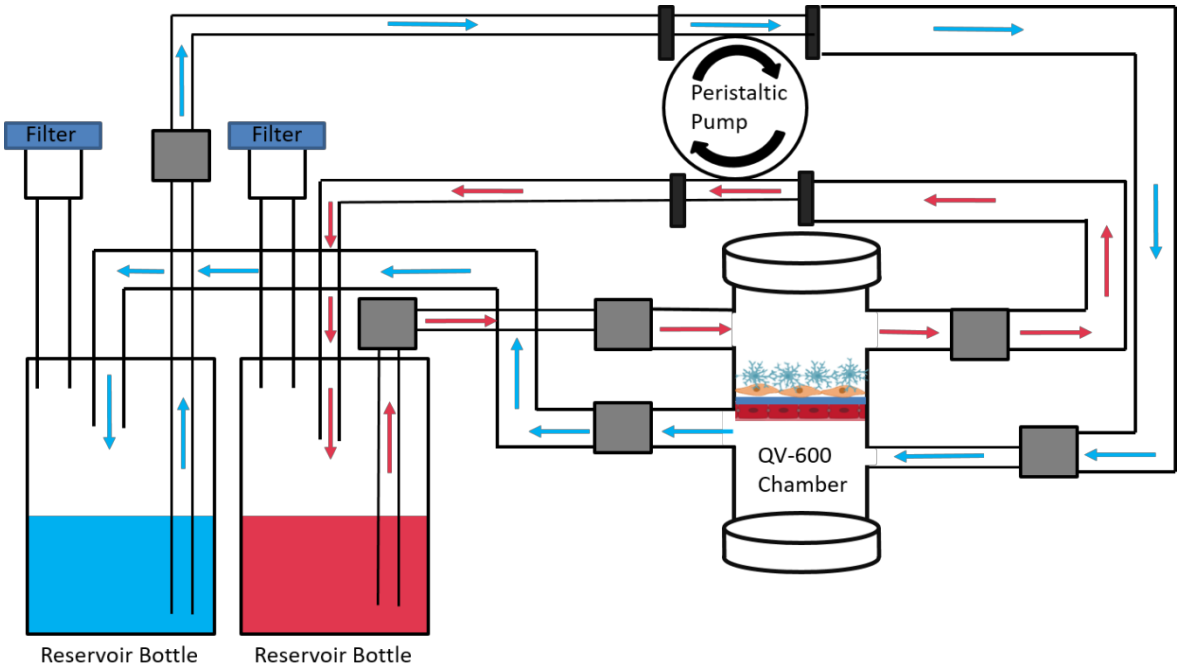

Figure 7-14 Schematic drawing of a dual flow millifluidics system of IPAD

Astrocytes and pericytes in the apical chamber are subjected to a slow flow in one direction (red arrows) whereas endothelial cells in the basolateral compartment can be exposed to a higher flow rate in the opposite direction (blue arrows). This mimics the *in vivo* fluid movements of blood and ISF drainage.

Table 7-1 the advantages and disadvantages of a novel *in vitro* model of IPAD

Advantages of the *in vitro* model of IPAD	**Disadvantages of the *in vitro* model of IPAD**
Anatomically correct arrangement of cells leads to better physiological representation and more relevant results	Presence of the Transwell membrane is not physiological
Including a triple culture allows the cells to support and interact with each other as they do *in vivo*	Difficult to maintain multiple cell types as they compete for space and nutrients in culture
Fluid dynamics allow the study of physiological flow of fluids such as blood and ISF	Every cell type has individual requirements in culture that cannot be properly fulfilled in a multi-cell model
Flow creates physiological shear stress	Multi-cell models are complicated to assemble
A dual cavity chamber allows two independent flow rates to be set that have different speed and directionality	Far more equipment is needed (QV600, pump etc) so set up is more complicated and expensive compared to simpler models

7.5 Conclusions

After assessing the different combinations of double co-cultures and taking into account the physiological arrangement of cells in the cerebral vessel, the combination of cells most likely to reflect the *in vivo* arrangement was determined (**Figure 7-13**). This proposed model has many novel aspects, most notably the potential to incorporate two independent flow rates. Combining this triple co-culture with the dual flow Quasi Vivo system (shown in **Figure 7-14**) may lead to the first *in vitro* model of a cerebral vessel that incorporates both blood flow and the flow of interstitial fluid. Further testing of the multi-cell cultures and mathematical modelling of the flow rates and shear stresses in the dual flow millifluidics system needs to be carried out before this model can be constructed and validated as a physiological model of IPAD.

7.6 Future work

Although the results suggest the arrangement of cells with the best chance of success in a model of IPAD, it is important to note that this conclusion is heavily based on the qualitative assessment of the production of collagen IV and the presence of Qdots to identify the different species of cells present in the culture. Much more testing will be required in future. Only one basement membrane was tested in this study and only qualitative observations were made. Quantitative analysis is required across a range of basement membrane proteins to confirm that the proposed multi-culture model is conducive to basement membrane production similar to *in vivo*. Measuring permeability using fluorescein will also be important in defining the usefulness and relevance of this culture. The longevity of this culture has yet to be determined so tracking the viability of the triple culture and the trans-endothelial resistance across the membrane over time will show the optimum time for conducting future experiments. Computational fluid dynamics and pressure measurements must be carried out on the QV600 system in the proposed configuration to test the streamlines and pressure gradient force exerted by the opposing flow rates. Calculations for shear stress values will also be important before the system can be used in the proposed manner.

Once the system has been properly tested and validated it could be used as an alternative to animal models when investigating the drainage of Aβ in the walls of cerebral vessels. The flow of Aβ may be monitored in real time with time-lapse microscopy providing valuable insight into the exact compartment of the vessel wall that Aβ travels along as it is cleared from the brain. Transcytosis of Aβ could also be measured by adding amyloid beta to the apical loop of the system and then detecting it in the basolateral loop with and ELISA. When considering therapeutic

strategies that improve drainage of Aβ, potential drugs could be tested using this system in future, replacing early animal experiments and reducing the number of animals needed in the drug development process overall.

Chapter 8 Overall conclusions

Throughout this project I have sought to improve the understanding of intramural periarteiral drainage (IPAD) and how it is affected by basement membrane remodelling induced by changes in the environment. I have achieved this by investigating cellular components of the cerebrovasculature and assessing changes in the expression of key extracellular matrix proteins in response to various conditions. Each results chapter investigates a different aspect of the cerebrovasculature and a summary of this is shown in **Figure 8-1**.

In chapter 3 I investigated the relationship between ApoE and AD. The polymorphic APOE gene encodes a protein called apolipoprotein E of which there are 3 isoforms: ApoE2, ApoE3 and ApoE4 and possession of the APOE ε4 allele significantly increases the risk of developing AD. In the CNS ApoE is produced primarily by astrocytes and I used astrocytes expressing different human apolipoprotein E isoforms to investigate if there are isoform dependent effects on the composition of the astrocytic basement membrane (**Figure 8-1**b). I have developed new protocols and used novel techniques such as CLEM to investigate this. I also used a novel millifluidics system to apply a flow of amyloid beta to ApoE astrocytes in culture. I have shown that ApoE4 expressing astrocytes grow at a slower rate than ApoE2 or ApoE3 expressing astrocytes and they also have a distinct morphology with significantly fewer processes. There was also less laminin associated with these processes. The composition of the astrocytic basement membrane was shown to be dependent on ApoE genotype and it was suggested that these differences may contribute to the increased risk of Aβ accumulation and Alzheimer's disease that is observed in people that possess one or more copies of the APOE4 allele.

In chapter 4 I sought to explore the basement membrane produced by cells of the cerebrovasculature. I deconstructed cerebral capillaries and arteries into their individual cellular components (astrocytes, pericytes, smooth muscle cells and endothelial cells) and examined the production of basement membrane proteins of each cell type individually (**Figure 8-1**c). I have demonstrated that the cellular components of a cerebral blood vessel produce basement membrane proteins *in vitro* and each cell type had a different profile of extracellular proteins resulting in a unique extracellular environment that is likely to control cell programming and differentiation. It is clear that every cell type actively contributes to the extracellular environment and loss of cells will likely disrupt the homeostasis and cause a remodelling of the basement membrane which could impact the efficiency of IPAD. For example, the loss of astrocytes associated with a traumatic brain injury (Ng and Lee, 2019) may reduce the astrocytic contribution to the cerebrovascular basement membrane changing its composition. Since

basement membranes are the pathways used to clear solutes from the brain, the efficiency of removal of solutes such as Aβ will likely be affected by a change in the basement membrane composition. This may explain why traumatic brain injury increases the risk of developing AD.

In chapter 5 I developed an *in vitro* model of flow of Aβ over smooth muscle cells that represents a partial model of IPAD (**Figure 8-1**d). In AD and CAA the accumulation of Aβ occurs between the layers of smooth muscle cells in cerebral vessels (Keable *et al.*, 2016) and I used my *in vitro* model to investigate the effect Aβ has on the smooth muscle basement membrane. I also used hypoxia to induce oxidative stress similar to the environment in the aged brain to investigate age related changes to the smooth muscle basement membrane. I showed that under normal conditions the smooth muscle basement membrane does not respond to Aβ, however when hypoxia was applied to induce age-related oxidative stress the extracellular environment was more vulnerable and underwent remodelling when Aβ 1-42 was applied. This remodelling then in turn created an extracellular environment that was lacking in glycoproteins and ideal to promote the fibrillization and accumulation of Aβ. Age is the biggest risk factor for AD and these results suggest a vicious cycle where the basement membrane of smooth muscle cells in the walls of cerebral vessels of the aged brain are susceptible to remodelling when stressed. This remodelling may promote fibrillization and accumulation of Aβ as CAA, which in turn causes further stress and so on. The smooth muscle is eventually completely replaced by Aβ and this loss of smooth muscle not only affects the contractility and integrity of the vessel wall but may impact the efficiency of IPAD as suggested in chapter 4.

In chapter 6 I demonstrated the presence of alpha adrenergic receptors, in particular α1B, on vascular smooth muscle cells and pericytes (**Figure 8-1** e). The presence of alpha adrenergic receptors on these cells suggests that adrenergic innervation controls vascular contractility and therefore the driving force for IPAD. A major feature of AD is the loss of the noradrenergic projection neurons of the locus coeruleus which results in a decrease in adrenergic innervation (Kelly *et al.*, 2017). These receptors may prove useful targets for improving IPAD and preventing Aβ accumulation as seen in AD and CAA.

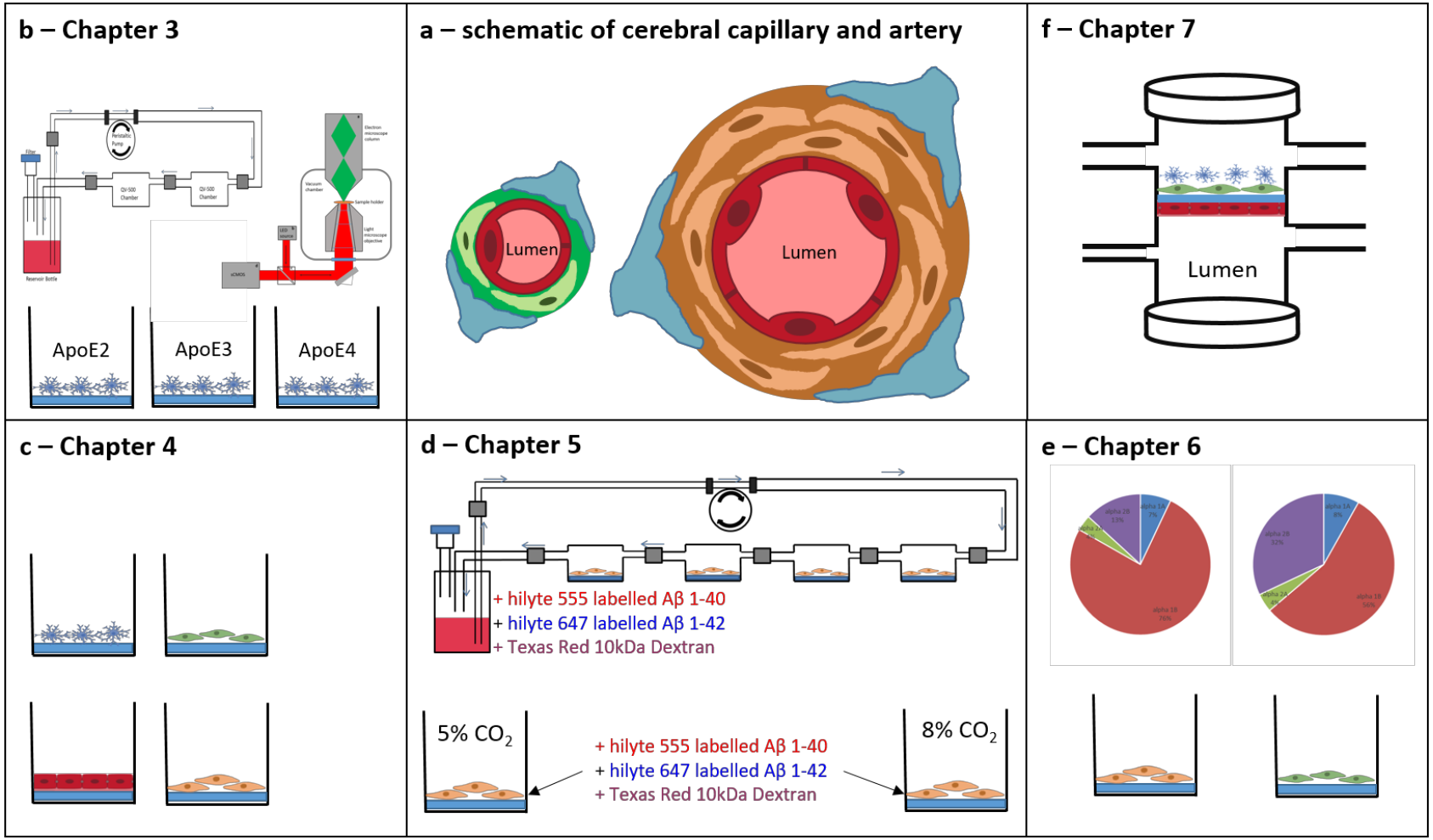

Figure 8-1 Summary of experimental approaches

a) The *in vivo* arrangement of cells in cerebral vessels. b) in chapter 3 astrocytes expressing different isoforms of ApoE were cultured. Cells were exposed to a flow of Aβ and cell morphology was investigated with CLEM. c) in chapter 4 the basement membrane of individual cells of the cerebrovaculature was investigated by immunocytochemistry. d) in chapter 5 the characteristics of smooth muscle basement membranes were tested under various stress conditions including hypoxia, Aβ and flow. e) the expression of adrenergic receptors in the contractile cells of cerebral vessels was explored in chapter 6. f) a pilot study investigated several combinations of co-cultures, and suggested the best combination of cells in a triple culture which accurately reflects the *in vivo* arrangement of cells in a cerebral capillary.

In chapter 7 I explored methods to develop a more comprehensive *in vitro* model of IPAD incorporating not only the cellular components of the cerebral vessel wall but also cerebral blood flow and ISF flow (**Figure 8-1**f). I explored several combinations of co-cultures and tracked cell populations with QD nanocrystals. I introduced a double cavity as a way to potentially model blood flow and ISF flow. Although there is a lot of further work needed to develop this model, including computational modelling of fluid dynamics, pilot data from the co-cultures has suggested the most suitable combination of cells to be used in a triple co-culture; This combination of cells accurately reflects the arrangement of cells in the cerebral capillary (**Figure 8-1**a,f).

I conducted no animal experiments as part of this research and the use of animal derived products was kept to a minimum. This was in line with the aims of the NC3Rs to replace, refine and reduce animals used in research. I have used cell culture combined with a novel millifluidics flow system to model flow of amyloid beta *in vitro*, creating a basic model of IPAD. I have also explored ways to develop this system into a more advanced *in vitro* model of IPAD. Although more work is required to fully optimise this system, it has many potential applications. As hypoxia proved useful in modelling the stress conditions associated with ageing, it would be possible to reproduce an aged cerebral vessel wall in culture. The peristaltic pump could be used to alter flow rates of both the cerebral blood flow and ISF flow to demonstrate what happens to Aβ when IPAD is decreased in real time. The system may also be used in the future to test a drugs capacity to rescue IPAD and improve the removal of Aβ. Utilising this model during the initial stages of drug discovery could dramatically reduce the number of animals required for drug testing. I am hopeful that this work will continue to be developed and that the techniques used in this thesis will be used in future to further improve our understanding of IPAD and reduce the number of animals needed for experiments in this field of research.

Supplementary figures

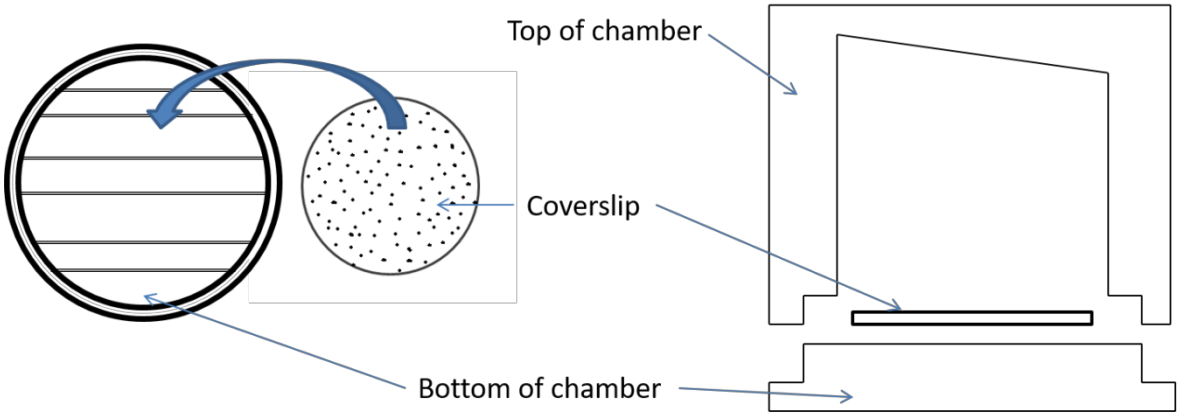

Supplementary figure 1 schematic drawing of QV500 chamber

The geometry of the QV500 chamber is very specifically designed to ensure optimal culture conditions. The height of the chamber ensures a low level of shear stress, even when using high flow rates. The slanted roof of the chamber allows air bubbles to be directed up and away from the cell surface thereby reducing turbulence. The bottom of the chamber is ridged to allow for easy removal of coverslips and the two parts of the chamber are interlocking to provide a leak-proof seal during operation.

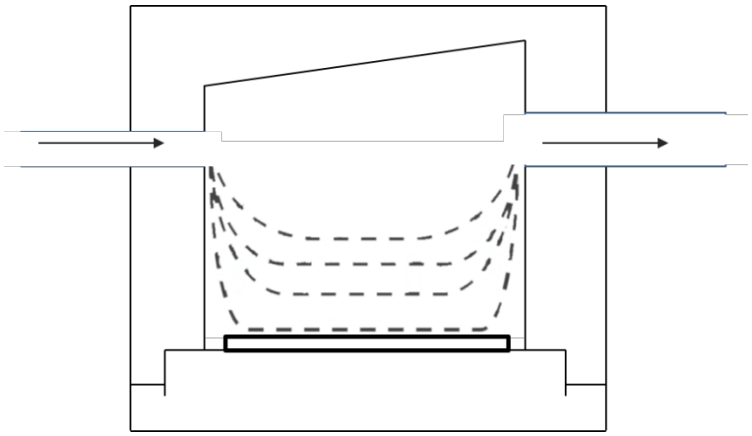

Supplementary figure 2 streamlines of laminar flow in QV500

Fluid dynamic finite-element modelling of the QV500 chambers showed that the streamlines run parallel to the cell surface (Mazzei *et al.*, 2010) creating a uniform laminar flow across the cells. The relative flow rate increases with the height of the chamber.

0

Number of QV500 chambers	Pump speed	Total weight after 5 mins (g)	Weight of water after 5 mins (g)	Weight of water after 1 min (g)	Volume of water after 1 min (mL)	Volume of water after 1 min (µL)
1 QV500 chamber	100	12.043	0.466	0.093	0.092	92.139
	200	12.511	0.934	0.187	0.185	184.733
	300	12.987	1.409	0.282	0.279	278.712
	400	13.433	1.855	0.371	0.367	366.935
	500	13.939	2.362	0.472	0.467	467.104
	600	14.427	2.850	0.570	0.564	563.594
	700	14.903	3.325	0.665	0.658	657.651
	800	15.402	3.824	0.765	0.756	756.336
	900	15.879	4.302	0.860	0.851	850.690
	1000	16.565	4.988	0.965	0.955	954.655
2 QV500 chambers	100	12.072	0.495	0.099	0.098	97.934
	200	12.551	0.974	0.195	0.193	192.565
	300	13.023	1.446	0.289	0.286	285.910
	400	13.515	1.937	0.387	0.383	383.132
	500	14.036	2.459	0.492	0.486	486.326
	600	14.510	2.933	0.587	0.580	580.087
	700	15.026	3.449	0.690	0.682	682.115
	800	15.522	3.945	0.789	0.780	780.088
	900	16.037	4.460	0.892	0.882	881.957
	1000	16.452	4.875	0.975	0.964	964.109
4 QV500 chambers	100	12.106	0.527	0.105	0.104	104.144
	200	12.662	1.083	0.217	0.214	214.200
	300	13.157	1.578	0.316	0.312	312.154
	400	13.722	2.143	0.429	0.424	423.852
	500	14.227	2.648	0.530	0.524	523.665
	600	14.805	3.226	0.645	0.638	637.993
	700	15.358	3.779	0.756	0.747	747.397
	800	15.891	4.312	0.862	0.853	852.708
	900	16.475	4.896	0.979	0.968	968.341
	1000	17.001	5.422	1.084	1.072	1072.366

Supplementary figure 3 table of calibrations for peristaltic pump

Flow rate (µL/min) was calculated by measuring the weight of water expelled from the system over a period of 5 minutes. Taking the weight of water at room temperature to be

0.9888g/mL, the flow rate was calculated by dividing the weight measured by 5 to give weight after 1 minute and multiplying this value by 0.9888. This value was then multiplied by 1000 to give the volume of water expelled from the system after 1 minute.

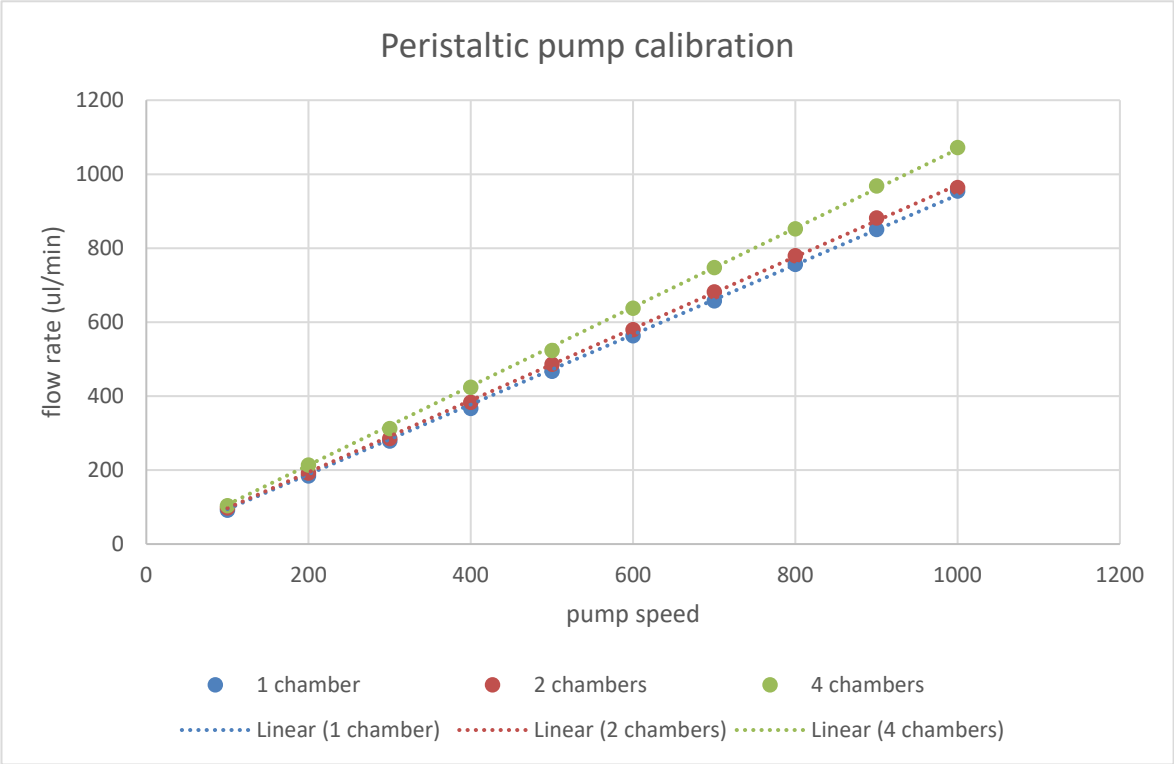

Supplementary figure 4 a graph showing the relationship between pump speed and flow rate

At low speeds the difference in flow rates is very low for the different configurations and below a pump speed of 100 it is negligible. The differences become more apparent at pump speeds exceeding 500. Although these configurations produced very similar flow rates it can vary significantly for different setups so calibration is important before a new setup can be used.

0

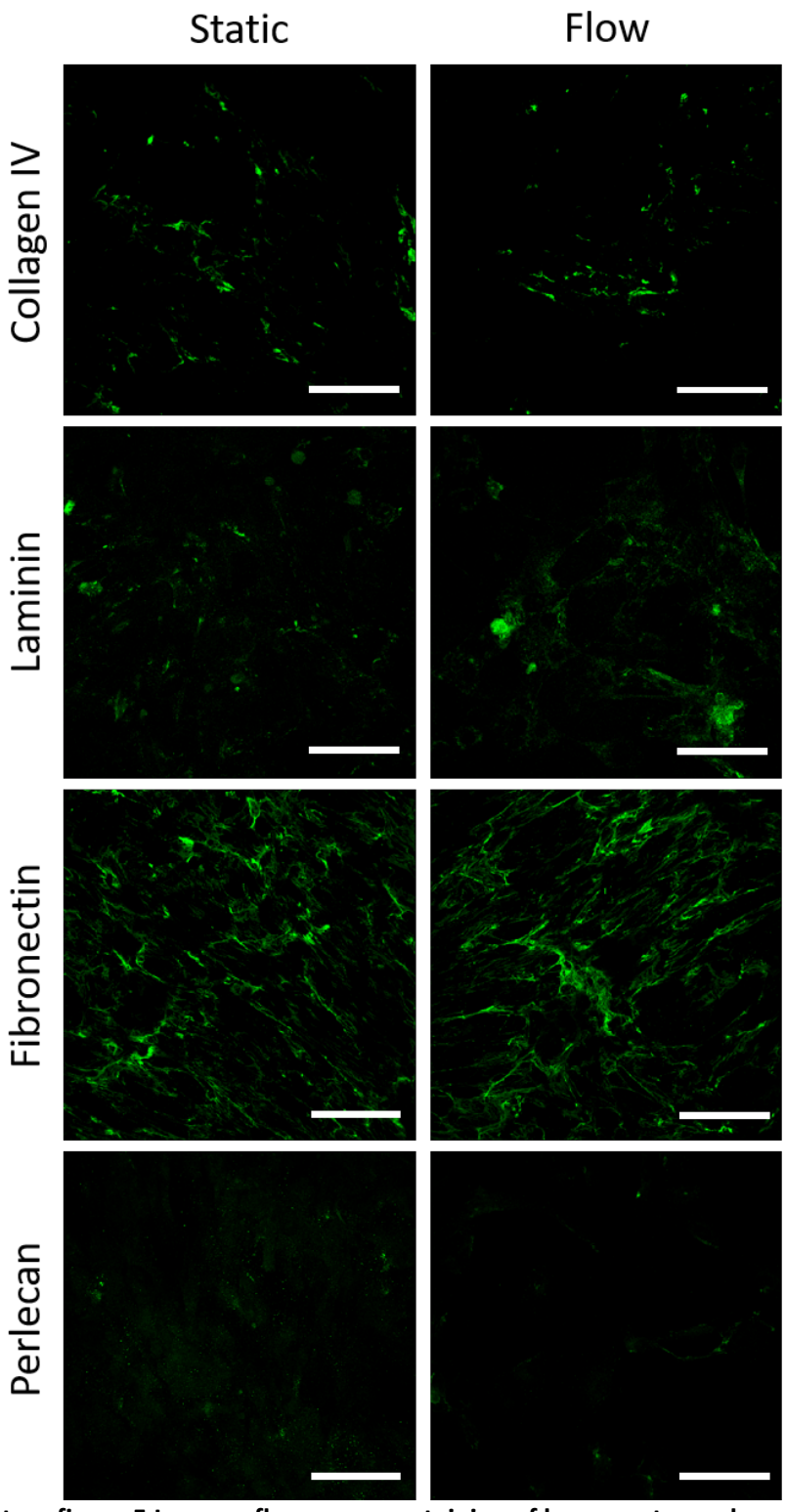

Supplementary figure 5 Immunofluorescence staining of basement membrane proteins in HBVSMC cultures under static and flow conditions

HBVSMC were grown for 24 hours before being exposed to a flow of media at a rate of 10µL/min for 48 hours (right column). Cells were stained with anti-collagen IV, anti-laminin, anti-fibronectin and anti-perlecan antibodies and the results were compared to static HBVSMC cultures grown in a 24 well plate for the same time (left column). The pattern of staining was comparable in the static and flow cultures and there were no obvious differences in the amount of staining present for any of the basement membrane proteins.

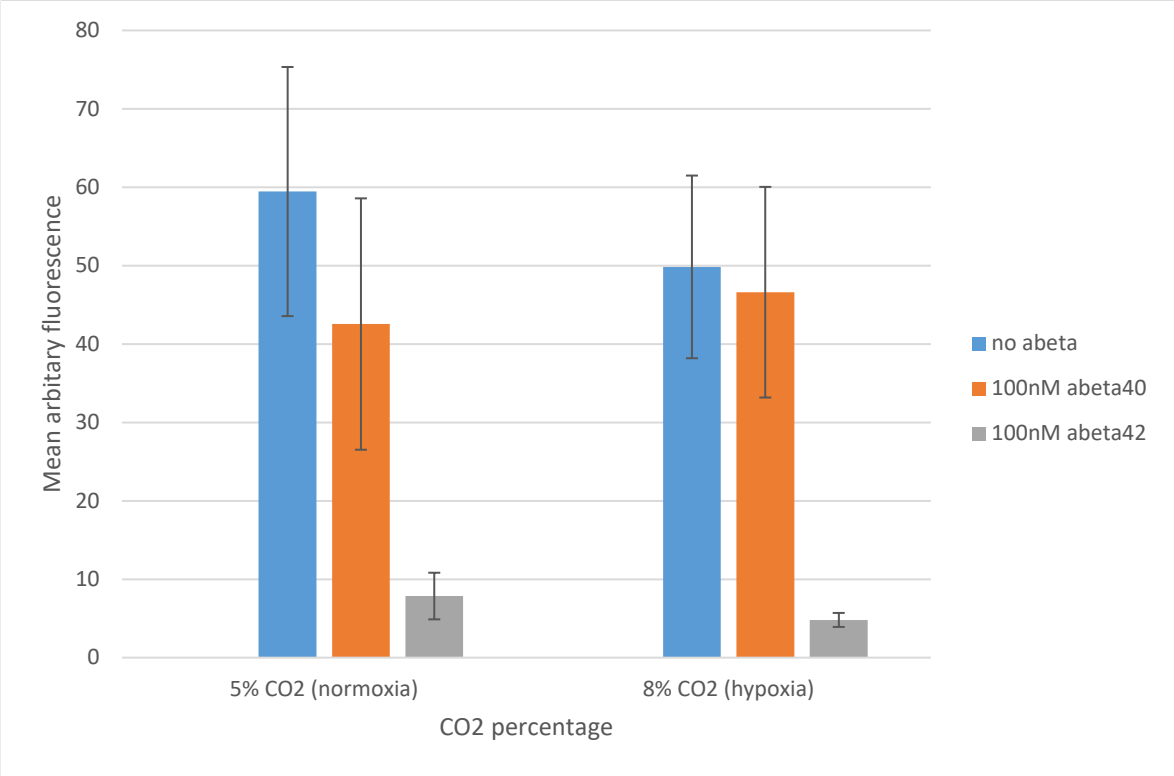

Supplementary figure 6 Fibronectin expression in HBVSMC cultures exposed to amyloid beta in normoxic and hypoxic conditions

Fibronectin expression was decreased when cells were exposed to 100nM amyloid beta 1-40 and even more so when exposed to 100nM amyloid beta 1-42 however these differences were not considered to be statistically significant (p=0.079 in normoxia and p=0.066 in hypoxia).

0

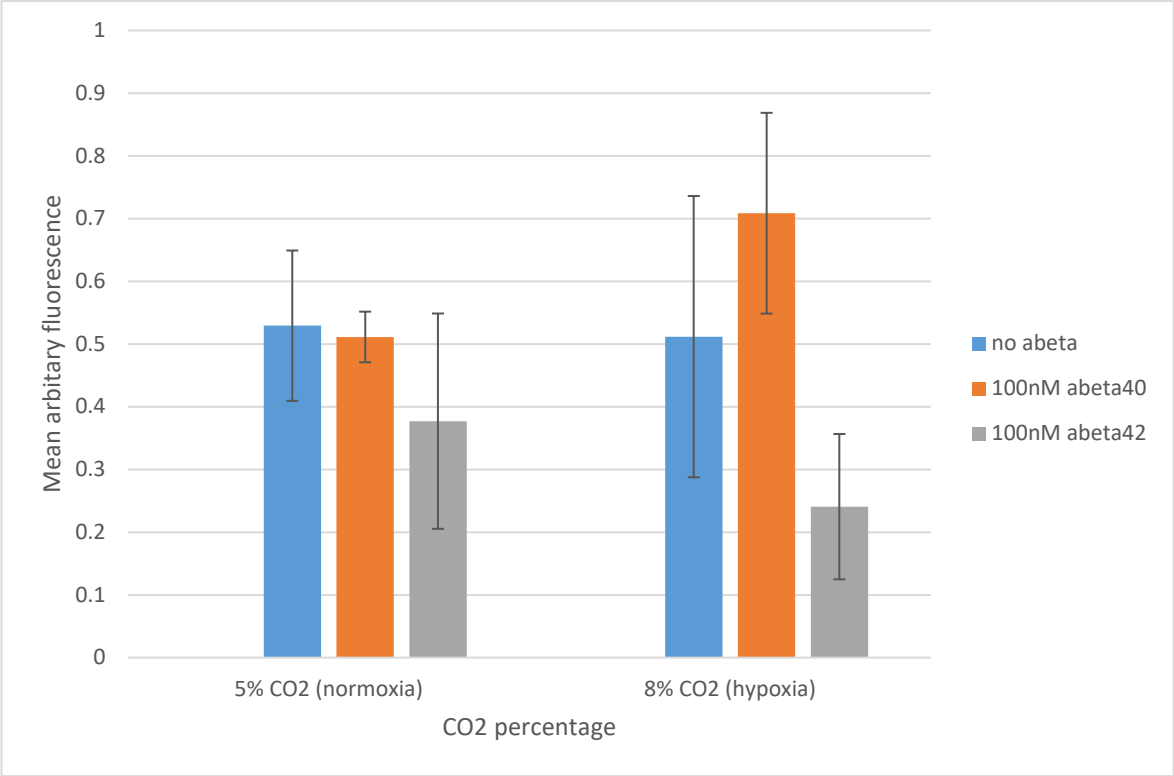

Supplementary figure 7 Perlecan expression in HBVSMC cultures exposed to amyloid beta in normoxic and hypoxic conditions

In normoxic cultures perlecan expression was highest in the HBVSMC exposed to no amyloid beta. It was slightly decreased after exposure to 100nM amyloid beta 1-40 and decreased further when exposed to amyloid beta 1-42. These differences were not considered statistically significant (p=0.957).In hypoxic cultures perlecan expression was increased after exposure to 100nM amyloid beta 1-40 but decreased after exposure to 100nM amyloid beta 1-42 compared to no supplementation. These differences were not statistically significant (p=0.148).

Bibliography

(2008) 'Chapter 6 - Cell Adhesion and the Extracellular Matrix', in Goodman, S.R. (ed.) *Medical Cell Biology (Third Edition)*. San Diego: Academic Press, pp. 191-225.

(2012) 'Prazosin', in *LiverTox: Clinical and Research Information on Drug-Induced Liver Injury*. Bethesda (MD): National Institute of Diabetes and Digestive and Kidney Diseases.

(2019) *The Human Protein Atlas*. Available at: https://www.proteinatlas.org/ (Accessed: 17/11/19).

A, T. (2019) *What are beta blockers and what do they do in the body?* Available at: https://www.bhf.org.uk/informationsupport/heart-matters-magazine/medical/drug-cabinet/beta-blockers (Accessed: 15/11/19).

Abbott, N.J. (2004) 'Evidence for bulk flow of brain interstitial fluid: significance for physiology and pathology', *Neurochem Int*, 45(4), pp. 545-52.

Abbott, N.J. and Friedman, A. (2012) 'Overview and introduction: the blood-brain barrier in health and disease', *Epilepsia*, 53 Suppl 6, pp. 1-6.

Adriani, G. *et al.* (2015) 'Modeling the Blood-Brain Barrier in a 3D triple co-culture microfluidic system', *Conf Proc IEEE Eng Med Biol Soc*, 2015, pp. 338-41.

Albargothy, N.J. *et al.* (2017) 'Investigating the Lymphatic Drainage of the Brain: Essential Skills and Tools', *Methods Mol Biol*, 1559, pp. 343-365.

Aldea, R. *et al.* (2019) 'Cerebrovascular Smooth Muscle Cells as the Drivers of Intramural Periarterial Drainage of the Brain', *Front Aging Neurosci*, 11, p. 1.

Alvarez, J.I., Katayama, T. and Prat, A. (2013) 'Glial influence on the blood brain barrier', *Glia*, 61(12), pp. 1939-1958.

Alzforum (2010) *AlzGene - Meta-Analysis of All Published AD			 Association Studies (Case-Control Only) APOE_e2/3/4*. Available at: http://www.alzgene.org/meta.asp?geneID=83 (Accessed: 07/02/17).

ALZFORUM (2017) *Bapineuzumab*. Available at: http://www.alzforum.org/therapeutics/bapineuzumab (Accessed: 20/03/17).

AlzheimersAssociation (2016) *Alzheimer's Diesease Facts and Figures*.

Anand, R., Gill, K.D. and Mahdi, A.A. (2014) 'Therapeutics of Alzheimer's disease: Past, present and future', *Neuropharmacology*, 76 Pt A, pp. 27-50.

Anderson, J.M. and Van Itallie, C.M. (2009) 'Physiology and Function of the Tight Junction', *Cold Spring Harbor Perspectives in Biology*, 1(2), p. a002584.

Arbel-Ornath, M. *et al.* (2013) 'Interstitial fluid drainage is impaired in ischemic stroke and Alzheimer's disease mouse models', *Acta Neuropathol*, 126(3), pp. 353-64.

Armulik, A. *et al.* (2010) 'Pericytes regulate the blood–brain barrier', *Nature*, 468(7323), pp. 557-561.

AstraZeneca (2018) *Update on Phase III clinical trials of lanabecestat for Alzheimer's disease*. Available at: https://www.astrazeneca.com/media-centre/press-releases/2018/update-on-phase-iii-clinical-trials-of-lanabecestat-for-alzheimers-disease-12062018.html (Accessed: 20/11/2019).

Bibliography

Auerbach, I.D. *et al.* (2003) 'Smooth muscle cells and the pathogenesis of cerebral microvascular disease ("angiomyopathies")', *Exp Mol Pathol*, 74(2), pp. 148-59.

Bai, T.R. (1992) 'Beta2 adrenergic receptors in asthma: A current perspective', *Lung*, 170(3), pp. 125-141.

Ballabh, P., Braun, A. and Nedergaard, M. (2004) 'The blood-brain barrier: an overview: structure, regulation, and clinical implications', *Neurobiol Dis*, 16(1), pp. 1-13.

Bell, R.D. *et al.* (2007) 'Transport pathways for clearance of human Alzheimer's amyloid beta-peptide and apolipoproteins E and J in the mouse central nervous system', *J Cereb Blood Flow Metab*, 27(5), pp. 909-18.

Berger, E. *et al.* (2018) 'Millifluidic culture improves human midbrain organoid vitality and differentiation', *Lab Chip*, 18(20), pp. 3172-3183.

Bernas, M.J. *et al.* (2010) 'Establishment of primary cultures of human brain microvascular endothelial cells to provide an in vitro cellular model of the blood-brain barrier', *Nat Protoc*, 5(7), pp. 1265-72.

Bigica, A. (2019) *Aducanumab Heads to the FDA After Biogen Analysis Proves Positive in Early Alzheimer Disease*. Available at: https://www.neurologylive.com/clinical-focus/aducanumab-heads-to-the-fda-after-biogen-analysis-proves-positive-in-early-alzheimer-disease (Accessed: 20/11/19).

Bird, T. (1999) *Early-Onset Familial Alzheimer Disease*. (Downloaded: 22/02/17).

Black, R.S. *et al.* (2010) 'A single ascending dose study of bapineuzumab in patients with Alzheimer disease', *Alzheimer Dis Assoc Disord*, 24(2), pp. 198-203.

Boche, D. *et al.* (2010) 'Neuropathology after active Abeta42 immunotherapy: implications for Alzheimer's disease pathogenesis', *Acta Neuropathol*, 120(3), pp. 369-84.

Boche, D. *et al.* (2008) 'Consequence of Abeta immunization on the vasculature of human Alzheimer's disease brain', *Brain*, 131(Pt 12), pp. 3299-310.

Borlinghaus, R. (2013) *Spectral Detection - How to Define the Spectral Bands that Collect Probe-specific Emission*. Available at: http://www.leica-microsystems.com/science-lab/spectral-detection-how-to-define-the-spectral-bands-that-collect-probe-specific-emission/ (Accessed: 27/02/17).

Brenowitz, W.D. *et al.* (2015) 'Cerebral amyloid angiopathy and its co-occurrence with Alzheimer's disease and other cerebrovascular neuropathologic changes', *Neurobiology of aging*, 36(10), pp. 2702-2708.

Brinker, T. *et al.* (2014) 'A new look at cerebrospinal fluid circulation', *Fluids and Barriers of the CNS*, 11, pp. 10-10.

Cabeza, R. *et al.* (2002) 'Aging gracefully: compensatory brain activity in high-performing older adults', *Neuroimage*, 17(3), pp. 1394-402.

Caccamo, A. *et al.* (2005) 'Age- and region-dependent alterations in Abeta-degrading enzymes: implications for Abeta-induced disorders', *Neurobiol Aging*, 26(5), pp. 645-54.

Carare, R.O. *et al.* (2008) 'Solutes, but not cells, drain from the brain parenchyma along basement membranes of capillaries and arteries: significance for cerebral amyloid angiopathy and neuroimmunology', *Neuropathol Appl Neurobiol*, 34(2), pp. 131-44.

Carter, D.B. (2005) 'The interaction of amyloid-beta with ApoE', *Subcell Biochem*, 38, pp. 255-72.

Castellano, J.M. *et al.* (2011) 'Human apoE isoforms differentially regulate brain amyloid-beta peptide clearance', *Sci Transl Med*, 3(89), p. 89ra57.

Castillo, G.M. *et al.* (1997) 'Perlecan binds to the beta-amyloid proteins (A beta) of Alzheimer's disease, accelerates A beta fibril formation, and maintains A beta fibril stability', *J Neurochem*, 69(6), pp. 2452-65.

Cataldi, A. and Di Giulio, C. (2009) '"Oxygen supply" as modulator of aging processes: hypoxia and hyperoxia models for aging studies', *Curr Aging Sci*, 2(2), pp. 95-102.

Cebers, G. *et al.* (2017) 'AZD3293: Pharmacokinetic and Pharmacodynamic Effects in Healthy Subjects and Patients with Alzheimer's Disease', *J Alzheimers Dis*, 55(3), pp. 1039-1053.

Chan, L. (1989) 'The apolipoprotein multigene family: structure, expression, evolution, and molecular genetics', *Klin Wochenschr*, 67(4), pp. 225-37.

Chen, G.-f. *et al.* (2017) 'Amyloid beta: structure, biology and structure-based therapeutic development', *Acta Pharmacologica Sinica*, 38(9), pp. 1205-1235.

Chen, Z.L. *et al.* (2013) 'Ablation of astrocytic laminin impairs vascular smooth muscle cell function and leads to hemorrhagic stroke', *J Cell Biol*, 202(2), pp. 381-95.

Cheri, M.S. *et al.* (2014) 'Real-time measurement of flow rate in microfluidic devices using a cantilever-based optofluidic sensor', *Analyst*, 139(2), pp. 431-8.

Cheung, T.L. *et al.* (2016) 'The non-aqueous synthesis of shape controllable Cu(2-x)S plasmonic nanostructures in a continuous-flow millifluidic chip for the generation of photo-induced heating', *Nanoscale*, 8(12), pp. 6609-22.

Chow, V.W. *et al.* (2010) 'An Overview of APP Processing Enzymes and Products', *Neuromolecular medicine*, 12(1), pp. 1-12.

Cipolla, M. (2009) 'Chapter 2 Anatomy and Ultrastrcuture', in *The Cerebral Circulation*. San Rafael: Morgan & Claypool Life Sciences.

ClinicalTrials.gov (2017) *Bapineuzumab*. Available at: https://clinicaltrials.gov/ct2/results?term=bapineuzumab&recr=&rslt=&type=&cond=&intr=&titles=&outc=&spons=&lead=&id=&state1=&cntry1=&state2=&cntry2=&state3=&cntry3=&locn=&gndr=&rcv_s=&rcv_e=&lup_s=&lup_e= (Accessed: 20/03/17).

Cohen, M.P., Frank, R.N. and Khalifa, A.A. (1980) 'Collagen production by cultured retinal capillary pericytes', *Invest Ophthalmol Vis Sci*, 19(1), pp. 90-4.

Cole, S.L. and Vassar, R. (2008) 'BACE1 structure and function in health and Alzheimer's disease', *Curr Alzheimer Res*, 5(2), pp. 100-20.

Collins-Praino, L.E. *et al.* (2014) 'Soluble amyloid beta levels are elevated in the white matter of Alzheimer's patients, independent of cortical plaque severity', *Acta Neuropathol Commun*, 2, p. 83.

Colović, M.B. *et al.* (2013) 'Acetylcholinesterase inhibitors: pharmacology and toxicology', *Current neuropharmacology*, 11(3), pp. 315-335.

Coma, M. *et al.* (2008) 'Oxidative stress triggers the amyloidogenic pathway in human vascular smooth muscle cells', *Neurobiol Aging*, 29(7), pp. 969-80.

Conejero-Goldberg, C. *et al.* (2014) 'APOE2 enhances neuroprotection against Alzheimer's disease through multiple molecular mechanisms', *Mol Psychiatry*, 19(11), pp. 1243-50.

Congdon, E.E. and Sigurdsson, E.M. (2018) 'Tau-targeting therapies for Alzheimer disease', *Nat Rev Neurol*, 14(7), pp. 399-415.

Corder, E.H. *et al.* (1993) 'Gene dose of apolipoprotein E type 4 allele and the risk of Alzheimer's disease in late onset families', *Science*, 261(5123), pp. 921-3.

Coria, F. and Rubio, I. (1996) 'Cerebral amyloid angiopathies', *Neuropathology and Applied Neurobiology*, 22(3), pp. 216-227.

Coric, V. *et al.* (2015) 'Targeting Prodromal Alzheimer Disease With Avagacestat: A Randomized Clinical Trial', *JAMA Neurol*, 72(11), pp. 1324-33.

Costa, P. *et al.* (1993) 'Adrenergic receptors on smooth muscle cells isolated from human penile corpus cavernosum', *J Urol*, 150(3), pp. 859-63.

Cotman, S.L., Halfter, W. and Cole, G.J. (2000) 'Agrin binds to beta-amyloid (Abeta), accelerates abeta fibril formation, and is localized to Abeta deposits in Alzheimer's disease brain', *Mol Cell Neurosci*, 15(2), pp. 183-98.

Cunningham, L.A., Wetzel, M. and Rosenberg, G.A. (2005) 'Multiple roles for MMPs and TIMPs in cerebral ischemia', *Glia*, 50(4), pp. 329-39.

Dale Purves *et al.* (2012) *Neuroscience*. fifth edition edn. Massachusetts USA: Sinauer Associates Inc.

Danner, S. *et al.* (2013) 'Quantum Dots Do Not Alter the Differentiation Potential of Pancreatic Stem Cells and Are Distributed Randomly among Daughter Cells', *Int J Cell Biol*, 2013, p. 918242.

Davis, G.E. and Senger, D.R. (2005) 'Endothelial extracellular matrix: biosynthesis, remodeling, and functions during vascular morphogenesis and neovessel stabilization', *Circ Res*, 97(11), pp. 1093-107.

De Berardis, D. *et al.* (2015) 'Targeting the Noradrenergic System in Posttraumatic Stress Disorder: A Systematic Review and Meta-Analysis of Prazosin Trials', *Curr Drug Targets*, 16(10), pp. 1094-106.

de Leon, M.J. *et al.* (2001) 'Prediction of cognitive decline in normal elderly subjects with 2-[(18)F]fluoro-2-deoxy-D-glucose/poitron-emission tomography (FDG/PET)', *Proc Natl Acad Sci U S A*, 98(19), pp. 10966-71.

Dekaban, A.S. (1978) 'Changes in brain weights during the span of human life: relation of brain weights to body heights and body weights', *Ann Neurol*, 4(4), pp. 345-56.

DeMattos, R.B. *et al.* (2004) 'ApoE and clusterin cooperatively suppress Abeta levels and deposition: evidence that ApoE regulates extracellular Abeta metabolism in vivo', *Neuron*, 41(2), pp. 193-202.

Dente, C.J. *et al.* (2001) 'Pericytes augment the capillary barrier in in vitro cocultures', *J Surg Res*, 97(1), pp. 85-91.

Di Russo, J. *et al.* (2017) 'Endothelial basement membrane laminin 511 is essential for shear stress response', *The EMBO journal*, 36(2), pp. 183-201.

Diem, A.K. *et al.* (2017) 'Arterial Pulsations cannot Drive Intramural Periarterial Drainage: Significance for Abeta Drainage', *Front Neurosci*, 11, p. 475.

Dohgu, S. *et al.* (2005) 'Brain pericytes contribute to the induction and up-regulation of blood-brain barrier functions through transforming growth factor-beta production', *Brain Res*, 1038(2), pp. 208-15.

Doody, R.S. *et al.* (2013) 'A Phase 3 Trial of Semagacestat for Treatment of Alzheimer's Disease', *New England Journal of Medicine*, 369(4), pp. 341-350.

Elfont, R.M., Sundaresan, P.R. and Sladek, C.D. (1989) 'Adrenergic receptors on cerebral microvessels: pericyte contribution', *Am J Physiol*, 256(1 Pt 2), pp. R224-30.

Engelhardt, B. and Sorokin, L. (2009) 'The blood-brain and the blood-cerebrospinal fluid barriers: function and dysfunction', *Semin Immunopathol*, 31(4), pp. 497-511.

Erkelens, D.W. (1989) 'Apolipoproteins in lipid transport, an impressionist view', *Postgrad Med J*, 65(763), pp. 275-81.

Fagan, T. (2019) *Biogen/Eisai Halt Phase 3 Aducanumab Trials*. Available at: https://www.alzforum.org/news/research-news/biogeneisai-halt-phase-3-aducanumab-trials (Accessed: 21/11/19).

Farrer, L.A. *et al.* (1997) 'Effects of age, sex, and ethnicity on the association between apolipoprotein E genotype and Alzheimer disease. A meta-analysis. APOE and Alzheimer Disease Meta Analysis Consortium', *Jama*, 278(16), pp. 1349-56.

Ferdinand, P. and Roffe, C. (2016) 'Hypoxia after stroke: a review of experimental and clinical evidence', *Experimental & Translational Stroke Medicine*, 8(1), p. 9.

Ferrer-Lorente, R. *et al.* (2005) 'Combined effects of oleoyl-estrone and a beta3-adrenergic agonist (CL316,243) on lipid stores of diet-induced overweight male Wistar rats', *Life Sci*, 77(16), pp. 2051-8.

Ferri, C.P. *et al.* (2005) 'Global prevalence of dementia: a Delphi consensus study', *Lancet*, 366(9503), pp. 2112-7.

Frackowiak, J., Zoltowska, A. and Wisniewski, H.M. (1994) 'Non-fibrillar beta-amyloid protein is associated with smooth muscle cells of vessel walls in Alzheimer disease', *J Neuropathol Exp Neurol*, 53(6), pp. 637-45.

Frisoni, G.B. *et al.* (2010) 'The clinical use of structural MRI in Alzheimer disease', *Nature reviews. Neurology*, 6(2), pp. 67-77.

Frost, M. *et al.* (2019) 'Analysis of adrenergic receptors in th ecerebral vasculature: implications for Alzheimer's disease'. University of Southampton.

Garber, K. (2007) 'Notch emerges as new cancer drug target', in *J Natl Cancer Inst*. United States, pp. 1284-5.

Garberg, P. *et al.* (2005) 'In vitro models for the blood-brain barrier', *Toxicol In Vitro*, 19(3), pp. 299-334.

Gauthier, S. *et al.* (2016) 'Efficacy and safety of tau-aggregation inhibitor therapy in patients with mild or moderate Alzheimer's disease: a randomised, controlled, double-blind, parallel-arm, phase 3 trial', *The Lancet*, 388(10062), pp. 2873-2884.

Genin, E. *et al.* (2011) 'APOE and Alzheimer disease: a major gene with semi-dominant inheritance', *Mol Psychiatry*, 16(9), pp. 903-7.

Gottlieb, S. (2000) 'Head injury doubles the risk of Alzheimer's disease', *British Medical Journal*, 321(7269), pp. 1100-1100.

Guimaraes, S. and Moura, D. (2001) 'Vascular adrenoceptors: an update', *Pharmacol Rev*, 53(2), pp. 319-56.

Hamaguchi, T., Ono, K. and Yamada, M. (2010) 'REVIEW: Curcumin and Alzheimer's disease', *CNS Neurosci Ther*, 16(5), pp. 285-97.

Hamel, E. *et al.* (2008) 'Oxidative stress and cerebrovascular dysfunction in mouse models of Alzheimer's disease', *Exp Physiol*, 93(1), pp. 116-20.

Hanisch, U.K. and Kettenmann, H. (2007) 'Microglia: active sensor and versatile effector cells in the normal and pathologic brain', *Nat Neurosci*, 10(11), pp. 1387-94.

Harder, D.R., Zhang, C. and Gebremedhin, D. (2002) 'Astrocytes function in matching blood flow to metabolic activity', *News Physiol Sci*, 17, pp. 27-31.

Hatherell, K. *et al.* (2011) 'Development of a three-dimensional, all-human in vitro model of the blood-brain barrier using mono-, co-, and tri-cultivation Transwell models', *J Neurosci Methods*, 199(2), pp. 223-9.

Hauser, P.S. and Ryan, R.O. (2013) 'Impact of apolipoprotein E on Alzheimer's disease', *Curr Alzheimer Res*, 10(8), pp. 809-17.

Hawkes, C.A. *et al.* (2014) 'Failure of perivascular drainage of beta-amyloid in cerebral amyloid angiopathy', *Brain Pathol*, 24(4), pp. 396-403.

Hawkes, C.A. *et al.* (2013) 'Stroke-induced opposite and age-dependent changes of vessel-associated markers in co-morbid transgenic mice with Alzheimer-like alterations', *Exp Neurol*, 250, pp. 270-81.

Hawkes, C.A. *et al.* (2012) 'Disruption of arterial perivascular drainage of amyloid-beta from the brains of mice expressing the human APOE epsilon4 allele', *PLoS One*, 7(7), p. e41636.

Hayashi, K. *et al.* (2004) 'Effects of hypoxia on endothelial/pericytic co-culture model of the blood-brain barrier', *Regul Pept*, 123(1-3), pp. 77-83.

He, Y. *et al.* (2014) 'Cell-culture models of the blood-brain barrier', *Stroke*, 45(8), pp. 2514-26.

Hedin, U. *et al.* (1988) 'Diverse effects of fibronectin and laminin on phenotypic properties of cultured arterial smooth muscle cells', *J Cell Biol*, 107(1), pp. 307-19.

Henry, M.D. and Campbell, K.P. (1998) 'A role for dystroglycan in basement membrane assembly', *Cell*, 95(6), pp. 859-70.

Henry, N. *et al.* (2018) 'Lipidated apolipoprotein E4 structure and its receptor binding mechanism determined by a combined cross-linking coupled to mass spectrometry and molecular dynamics approach', *PLoS computational biology*, 14(6), pp. e1006165-e1006165.

Hewlings, S.J. and Kalman, D.S. (2017) 'Curcumin: A Review of Its' Effects on Human Health', *Foods (Basel, Switzerland)*, 6(10), p. 92.

Hieble, J.P. *et al.* (1995) 'International Union of Pharmacology. X. Recommendation for nomenclature of alpha 1-adrenoceptors: consensus update', *Pharmacol Rev*, 47(2), pp. 267-70.

Hogh, P. *et al.* (2001) 'Single photon emission computed tomography and apolipoprotein E in Alzheimer's disease: impact of the epsilon4 allele on regional cerebral blood flow', *J Geriatr Psychiatry Neurol*, 14(1), pp. 42-51.

Holmes, C. *et al.* (2008) 'Long-term effects of Abeta42 immunisation in Alzheimer's disease: follow-up of a randomised, placebo-controlled phase I trial', *Lancet*, 372(9634), pp. 216-23.

Hooghiemstra, A.M. *et al.* (2017) 'The Missing Link in the Pathophysiology of Vascular Cognitive Impairment: Design of the Heart-Brain Study', *Cerebrovascular diseases extra*, 7(3), pp. 140-152.

Hu, S. *et al.* (2015) 'Clinical development of curcumin in neurodegenerative disease', *Expert Rev Neurother*, 15(6), pp. 629-37.

Huang, Y. and Mahley, R.W. (2014) 'Apolipoprotein E: structure and function in lipid metabolism, neurobiology, and Alzheimer's diseases', *Neurobiol Dis*, 72 Pt A, pp. 3-12.

Iliff, J.J. *et al.* (2012) 'A paravascular pathway facilitates CSF flow through the brain parenchyma and the clearance of interstitial solutes, including amyloid beta', *Sci Transl Med*, 4(147), p. 147ra111.

Iliff, J.J. *et al.* (2013) 'Cerebral arterial pulsation drives paravascular CSF-interstitial fluid exchange in the murine brain', *J Neurosci*, 33(46), pp. 18190-9.

Iwamoto, T. (2014) '[Prevention of dementia on the basis of modification of lifestyle and management of lifestyle-related diseases: a review]', *Nihon Rinsho*, 72(4), pp. 612-7.

Jayadev, R. and Sherwood, D.R. (2017) 'Basement membranes', *Curr Biol*, 27(6), pp. R207-r211.

Jeliazkova-Mecheva, V.V. and Bobilya, D.J. (2003) 'A porcine astrocyte/endothelial cell co-culture model of the blood-brain barrier', *Brain Res Brain Res Protoc*, 12(2), pp. 91-8.

Jensen, B.C. *et al.* (2009) 'The alpha-1D Is the predominant alpha-1-adrenergic receptor subtype in human epicardial coronary arteries', *J Am Coll Cardiol*, 54(13), pp. 1137-45.

Jensson, O. *et al.* (1989) 'The saga of cystatin C gene mutation causing amyloid angiopathy and brain hemorrhage--clinical genetics in Iceland', *Clin Genet*, 36(5), pp. 368-77.

Ji, K. and Tsirka, S.E. (2012) 'Inflammation modulates expression of laminin in the central nervous system following ischemic injury', *J Neuroinflammation*, 9, p. 159.

Jo, D.H. *et al.* (2013) 'Interaction between pericytes and endothelial cells leads to formation of tight junction in hyaloid vessels', *Molecules and cells*, 36(5), pp. 465-471.

Johnson, J.W. and Kotermanski, S.E. (2006) 'Mechanism of action of memantine', *Curr Opin Pharmacol*, 6(1), pp. 61-7.

Jouanne, M., Rault, S. and Voisin-Chiret, A.-S. (2017) 'Tau protein aggregation in Alzheimer's disease: An attractive target for the development of novel therapeutic agents', *European Journal of Medicinal Chemistry*, 139, pp. 153-167.

Jucker, M. *et al.* (1996) 'Laminin alpha 2 is a component of brain capillary basement membrane: reduced expression in dystrophic dy mice', *Neuroscience*, 71(4), pp. 1153-61.

Jun, G.R. *et al.* (2017) 'Transethnic genome-wide scan identifies novel Alzheimer's disease loci', *Alzheimers Dement*.

Kamenetz, F. *et al.* (2003) 'APP processing and synaptic function', *Neuron*, 37(6), pp. 925-37.

Kanekiyo, T. and Bu, G. (2014) 'The low-density lipoprotein receptor-related protein 1 and amyloid-beta clearance in Alzheimer's disease', *Front Aging Neurosci*, 6, p. 93.

Karran, E., Mercken, M. and De Strooper, B. (2011) 'The amyloid cascade hypothesis for Alzheimer's disease: an appraisal for the development of therapeutics', *Nat Rev Drug Discov*, 10(9), pp. 698-712.

Katsouri, L. *et al.* (2013) 'Prazosin, an alpha(1)-adrenoceptor antagonist, prevents memory deterioration in the APP23 transgenic mouse model of Alzheimer's disease', *Neurobiol Aging*, 34(4), pp. 1105-15.

Keable, A. *et al.* (2016) 'Deposition of amyloid beta in the walls of human leptomeningeal arteries in relation to perivascular drainage pathways in cerebral amyloid angiopathy', *Biochim Biophys Acta*, 1862(5), pp. 1037-46.

Kelleher, R.J., 3rd and Shen, J. (2017) 'Presenilin-1 mutations and Alzheimer's disease', *Proc Natl Acad Sci U S A*, 114(4), pp. 629-631.

Kelly, S.C. *et al.* (2017) 'Locus coeruleus cellular and molecular pathology during the progression of Alzheimer's disease', *Acta neuropathologica communications*, 5(1), pp. 8-8.

Kennedy, M.E. *et al.* (2016) 'The BACE1 inhibitor verubecestat (MK-8931) reduces CNS beta-amyloid in animal models and in Alzheimer's disease patients', *Sci Transl Med*, 8(363), p. 363ra150.

Khoury, R., Rajamanickam, J. and Grossberg, G.T. (2018) 'An update on the safety of current therapies for Alzheimer's disease: focus on rivastigmine', *Ther Adv Drug Saf*, 9(3), pp. 171-178.

Kido, Y. *et al.* (2002) 'Evaluation of blood-brain barrier transporters by co-culture of brain capillary endothelial cells with astrocytes', *Drug Metab Pharmacokinet*, 17(1), pp. 34-41.

Kim, J., Basak, J.M. and Holtzman, D.M. (2009) 'The role of apolipoprotein E in Alzheimer's disease', *Neuron*, 63(3), pp. 287-303.

Kiuchi, Y., Isobe, Y. and Fukushima, K. (2002) 'Type IV collagen prevents amyloid beta-protein fibril formation', *Life Sci*, 70(13), pp. 1555-64.

Kiuchi, Y. *et al.* (2002) 'Disassembly of amyloid beta-protein fibril by basement membrane components', *Life Sci*, 70(20), pp. 2421-31.

Kivipelto, M. *et al.* (2001) 'Midlife vascular risk factors and Alzheimer's disease in later life: longitudinal, population based study', *BMJ*, 322(7300), pp. 1447-51.

Knopman, D.S. *et al.* (2001) 'Practice parameter: diagnosis of dementia (an evidence-based review). Report of the Quality Standards Subcommittee of the American Academy of Neurology', *Neurology*, 56(9), pp. 1143-53.

Korn, J., Christ, B. and Kurz, H. (2002) 'Neuroectodermal origin of brain pericytes and vascular smooth muscle cells', *J Comp Neurol*, 442(1), pp. 78-88.

Krishnaswamy, S. *et al.* (2009) 'The structure and function of Alzheimer's gamma secretase enzyme complex', *Crit Rev Clin Lab Sci*, 46(5-6), pp. 282-301.

Kubota, Y. *et al.* (1988) 'Role of laminin and basement membrane in the morphological differentiation of human endothelial cells into capillary-like structures', *The Journal of cell biology*, 107(4), pp. 1589-1598.

Kulczar, C. *et al.* (2017) 'Development of a direct contact astrocyte-human cerebral microvessel endothelial cells blood-brain barrier coculture model', *J Pharm Pharmacol*, 69(12), pp. 1684-1696.

Kuntz, M. *et al.* (2015) 'Bexarotene Promotes Cholesterol Efflux and Restricts Apical-to-Basolateral Transport of Amyloid-beta Peptides in an In Vitro Model of the Human Blood-Brain Barrier', *J Alzheimers Dis*, 48(3), pp. 849-62.

Lagrange, P. *et al.* (1999) 'Transendothelial permeability changes induced by free radicals in an in vitro model of the blood-brain barrier', *Free Radic Biol Med*, 27(5-6), pp. 667-72.

Lai, A.Y. and McLaurin, J. (2012) 'Clearance of amyloid-β peptides by microglia and macrophages: the issue of what, when and where', *Future neurology*, 7(2), pp. 165-176.

Lehtovirta, M. *et al.* (1998) 'Longitudinal SPECT study in Alzheimer's disease: relation to apolipoprotein E polymorphism', *J Neurol Neurosurg Psychiatry*, 64(6), pp. 742-6.

Lehtovirta, M. *et al.* (1996) 'SPECT and MRI analysis in Alzheimer's disease: relation to apolipoprotein E epsilon 4 allele', *J Neurol Neurosurg Psychiatry*, 60(6), pp. 644-9.

Levy, E. *et al.* (2001) 'Codeposition of cystatin C with amyloid-beta protein in the brain of Alzheimer disease patients', *J Neuropathol Exp Neurol*, 60(1), pp. 94-104.

Li, Y. *et al.* (2017) 'Head Injury as a Risk Factor for Dementia and Alzheimer's Disease: A Systematic Review and Meta-Analysis of 32 Observational Studies', *PLoS One*, 12(1), p. e0169650.

Liao, F., Yoon, H. and Kim, J. (2017) 'Apolipoprotein E metabolism and functions in brain and its role in Alzheimer's disease', *Current opinion in lipidology*, 28(1), pp. 60-67.

Lilly (2016) *Lilly Announces Top-Line Results of Solanezumab Phase 3 Clinical Trial*. Available at: https://investor.lilly.com/releasedetail.cfm?ReleaseID=1000871 (Accessed: 21/01/17).

Lin, M.T. and Flint Beal, M. (2003) 'The oxidative damage theory of aging', *Clinical Neuroscience Research*, 2(5), pp. 305-315.

Ling, H. *et al.* (2017) 'Mixed pathologies including chronic traumatic encephalopathy account for dementia in retired association football (soccer) players', *Acta Neuropathol*, 133(3), pp. 337-352.

Liotta, L.A. *et al.* (1980) 'Metastatic potential correlates with enzymatic degradation of basement membrane collagen', *Nature*, 284(5751), pp. 67-8.

Liu, C.C. *et al.* (2013) 'Apolipoprotein E and Alzheimer disease: risk, mechanisms and therapy', *Nat Rev Neurol*, 9(2), pp. 106-18.

Luhrs, T. *et al.* (2005) '3D structure of Alzheimer's amyloid-beta(1-42) fibrils', *Proc Natl Acad Sci U S A*, 102(48), pp. 17342-7.

MacGregor Sharp, M. *et al.* (2019) 'Solving an Old Dogma: Is it an Arteriole or a Venule?', *Frontiers in aging neuroscience*, 11, pp. 289-289.

Mackay, D.F. *et al.* (2019) 'Neurodegenerative Disease Mortality among Former Professional Soccer Players', *N Engl J Med*, 381(19), pp. 1801-1808.

Maherally, Z. *et al.* (2018) 'Real-time acquisition of transendothelial electrical resistance in an all-human, in vitro, 3-dimensional, blood-brain barrier model exemplifies tight-junction integrity', *FASEB J*, 32(1), pp. 168-182.

Mahley, R.W., Weisgraber, K.H. and Huang, Y. (2009) 'Apolipoprotein E: structure determines function, from atherosclerosis to Alzheimer's disease to AIDS', *J Lipid Res*, 50 Suppl, pp. S183-8.

Mandarino, L.J. *et al.* (1993) 'Regulation of fibronectin and laminin synthesis by retinal capillary endothelial cells and pericytes in vitro', *Exp Eye Res*, 57(5), pp. 609-21.

Mann, D.M., Yates, P.O. and Hawkes, J. (1982) 'The noradrenergic system in Alzheimer and multi-infarct dementias', *J Neurol Neurosurg Psychiatry*, 45(2), pp. 113-9.

Mann, D.M., Yates, P.O. and Marcyniuk, B. (1984) 'A comparison of changes in the nucleus basalis and locus caeruleus in Alzheimer's disease', *J Neurol Neurosurg Psychiatry*, 47(2), pp. 201-3.

Mao, M. *et al.* (2015) 'Chapter Three - Type IV Collagens and Basement Membrane Diseases: Cell Biology and Pathogenic Mechanisms', in Miner, J.H. (ed.) *Current Topics in Membranes*. Academic Press, pp. 61-116.

Markesbery, W.R. (1997) 'Neuropathological criteria for the diagnosis of Alzheimer's disease', *Neurobiol Aging*, 18(4 Suppl), pp. S13-9.

Martin Prince, A.W., Maelenn Guerchet, Gemma-Claire Ali, Yu-Tzu Wu, Matthew Prina (2015) *The Global Impact of Dementia: An analysis of prevalence, incidence, cost and trends*. London: International, A.s.D. Available at: http://www.alz.co.uk/research/WorldAlzheimerReport2015.pdf.

Marvin, M. (1961) *Microscopy apparatus*. Patent no. 3013467. Available at: http://www.freepatentsonline.com/3013467.html.

Mawuenyega, K.G. *et al.* (2010) 'Decreased clearance of CNS beta-amyloid in Alzheimer's disease', *Science*, 330(6012), p. 1774.

May, P.C. *et al.* (2004) 'Multi-compartmental pharmacodynamic assessment of the functional gamma-secretase inhibitor LY450139 in PDAPP transgenic mice and non-transgenic mice', *Neurobiology of Aging*, 25, pp. S65-S65.

Mazzei, D. *et al.* (2010) 'A low shear stress modular bioreactor for connected cell culture under high flow rates', *Biotechnol Bioeng*, 106(1), pp. 127-37.

McCartney, M. (2015) 'Margaret McCartney: The "breakthrough" drug that's not been shown to help in Alzheimer's disease', *BMJ*, 351, p. h4064.

McGarry, T. *et al.* (2018) 'Hypoxia, oxidative stress and inflammation', *Free Radic Biol Med*, 125, pp. 15-24.

McGeer, P.L. and McGeer, E.G. (2007) 'NSAIDs and Alzheimer disease: epidemiological, animal model and clinical studies', *Neurobiol Aging*, 28(5), pp. 639-47.

McKee, A.C. *et al.* (2014) 'The neuropathology of sport', *Acta Neuropathol*, 127(1), pp. 29-51.

McKee, A.C. and Robinson, M.E. (2014) 'Military-related traumatic brain injury and neurodegeneration', *Alzheimers Dement*, 10(3 Suppl), pp. S242-53.

McKeon-O'Malley, C. and Tanzi, R. (2001) '22 - Etiology, Genetics, and Pathogenesis of Alzheimer's Disease', in Hof, P.R. and Mobbs, C.V. (eds.) *Functional Neurobiology of Aging*. San Diego: Academic Press, pp. 333-348.

McKhann, G. *et al.* (1984) 'Clinical diagnosis of Alzheimer's disease: report of the NINCDS-ADRDA Work Group under the auspices of Department of Health and Human Services Task Force on Alzheimer's Disease', *Neurology*, 34(7), pp. 939-44.

Melkonyan, M.M. *et al.* (2017) 'Neuroprotective, Neurogenic, and Amyloid Beta Reducing Effect of a Novel Alpha 2-Adrenoblocker, Mesedin, on Astroglia and Neuronal Progenitors upon Hypoxia and Glutamate Exposure', *Int J Mol Sci*, 19(1).

Menezes, M.J. *et al.* (2014) 'The extracellular matrix protein laminin alpha2 regulates the maturation and function of the blood-brain barrier', *J Neurosci*, 34(46), pp. 15260-80.

Merck (2017) 'Merck Announces EPOCH Study of Verubecestat for the Treatment of People with Mild to Moderate Alzheimer's Disease to Stop for Lack of Efficacy' (Merck. merck.com: Merck Sharp & Dohme Corp. Available at: http://www.mercknewsroom.com/news-release/research-and-development-news/merck-announces-epoch-study-verubecestat-treatment-people.

Miranda-Azpiazu, P. *et al.* (2018) 'A novel dynamic multicellular co-culture system for studying individual blood-brain barrier cell types in brain diseases and cytotoxicity testing', *Sci Rep*, 8(1), p. 8784.

Morikawa, M. *et al.* (2005) 'Production and characterization of astrocyte-derived human apolipoprotein E isoforms from immortalized astrocytes and their interactions with amyloid-beta', *Neurobiol Dis*, 19(1-2), pp. 66-76.

Moroni, F. *et al.* (2018) 'Cardiovascular disease and brain health: Focus on white matter hyperintensities', *International journal of cardiology. Heart & vasculature*, 19, pp. 63-69.

Morris, A. (2015) *The Pathway of Elimination of Amyloid beta from the Brain: Significance for the Pathogenesis of Alzheimer's Disease and Cerebral Amyloid Angiopathy*. Doctor of Philosophy. University of Southampton.

Morris, A.W. *et al.* (2014) 'The Cerebrovascular Basement Membrane: Role in the Clearance of beta-amyloid and Cerebral Amyloid Angiopathy', *Front Aging Neurosci*, 6, p. 251.

Mussap, M. and Plebani, M. (2004) 'Biochemistry and clinical role of human cystatin C', *Crit Rev Clin Lab Sci*, 41(5-6), pp. 467-550.

Nagelhus, E.A. and Ottersen, O.P. (2013) 'Physiological roles of aquaporin-4 in brain', *Physiol Rev*, 93(4), pp. 1543-62.

Nakagawa, S. *et al.* (2009) 'A new blood-brain barrier model using primary rat brain endothelial cells, pericytes and astrocytes', *Neurochem Int*, 54(3-4), pp. 253-63.

Nehlig, A. and Coles, J.A. (2007) 'Cellular pathways of energy metabolism in the brain: is glucose used by neurons or astrocytes?', *Glia*, 55(12), pp. 1238-50.

Neuhaus, J., Risau, W. and Wolburg, H. (1991) 'Induction of blood-brain barrier characteristics in bovine brain endothelial cells by rat astroglial cells in transfilter coculture', *Ann N Y Acad Sci*, 633, pp. 578-80.

Ng, S.Y. and Lee, A.Y.W. (2019) 'Traumatic Brain Injuries: Pathophysiology and Potential Therapeutic Targets', *Frontiers in Cellular Neuroscience*, 13(528).

Nicoll, J.A. *et al.* (2006) 'Abeta species removal after abeta42 immunization', *J Neuropathol Exp Neurol*, 65(11), pp. 1040-8.

Nicoll, J.A. *et al.* (2003) 'Neuropathology of human Alzheimer disease after immunization with amyloid-beta peptide: a case report', *Nat Med*, 9(4), pp. 448-52.

Niego, B. and Medcalf, R.L. (2013) 'Improved method for the preparation of a human cell-based, contact model of the blood-brain barrier', *J Vis Exp*, 12(81), p. e50934.

Nielsen, S. *et al.* (1997) 'Specialized membrane domains for water transport in glial cells: high-resolution immunogold cytochemistry of aquaporin-4 in rat brain', *J Neurosci*, 17(1), pp. 171-80.

NIH (2017) *What Causes Alzheimer's Disease?* Available at: https://www.nia.nih.gov/health/what-causes-alzheimers-disease (Accessed: 24/11/19).

NIH (2019) *24 Months Safety and Efficacy Study of AADvac1 in Patients With Mild Alzheimer's Disease (ADAMANT)*. Available at: https://clinicaltrials.gov/ct2/show/NCT02579252 (Accessed: 17/04/2020).

NIH (2020) *Hereditary cerebral amyloid angiopathy*. Available at: https://ghr.nlm.nih.gov/condition/hereditary-cerebral-amyloid-angiopathy (Accessed: 10/05/2020).

Novak, P. *et al.* (2017) 'Safety and immunogenicity of the tau vaccine AADvac1 in patients with Alzheimer's disease: a randomised, double-blind, placebo-controlled, phase 1 trial', *Lancet Neurol*, 16(2), pp. 123-134.

Novak, P. *et al.* (2019) 'AADvac1, an Active Immunotherapy for Alzheimer's Disease and Non Alzheimer Tauopathies: An Overview of Preclinical and Clinical Development', *J Prev Alzheimers Dis*, 6(1), pp. 63-69.

O'Neill, C., Fowler, C.J. and Winblad, B. (1989) 'Alpha 1-adrenergic receptor binding sites in post-mortal human cerebral microvessel preparations: preservation in multi-infarct dementia and dementia of Alzheimer type', *J Neural Transm Park Dis Dement Sect*, 1(4), pp. 303-10.

Office, H. (2018) *Annual Statistics of Scientific Procedures on Living Animals, Great Britain 2018*. UK.

Oleskevich, S., Descarries, L. and Lacaille, J.C. (1989) 'Quantified distribution of the noradrenaline innervation in the hippocampus of adult rat', *J Neurosci*, 9(11), pp. 3803-15.

Ordovas, J.M. *et al.* (1987) 'Apolipoprotein E isoform phenotyping methodology and population frequency with identification of apoE1 and apoE5 isoforms', *J Lipid Res*, 28(4), pp. 371-80.

Orr, A.W. *et al.* (2009) 'Molecular mechanisms of collagen isotype-specific modulation of smooth muscle cell phenotype', *Arterioscler Thromb Vasc Biol*, 29(2), pp. 225-31.

Orrell, M. *et al.* (2015) 'Dementia prevention: call to action', *Lancet*, 386(10004), p. 1625.

Page, A.M. (2004) 'Probing with light: how the confocal laser scanning microscope is transforming our view of the brain', *Neuropathology and Applied Neurobiology*.

Pan, X.D. *et al.* (2011) 'Microglial phagocytosis induced by fibrillar beta-amyloid is attenuated by oligomeric beta-amyloid: implications for Alzheimer's disease', *Mol Neurodegener*, 6, p. 45.

Paulsson, M. (1992) 'Basement membrane proteins: structure, assembly, and cellular interactions', *Crit Rev Biochem Mol Biol*, 27(1-2), pp. 93-127.

Pearson, H.A. and Peers, C. (2006) 'Physiological roles for amyloid beta peptides', *The Journal of physiology*, 575(Pt 1), pp. 5-10.

Peckham, M. (2003) *The Histology Guide - Basal Lamina*. Available at: https://www.histology.leeds.ac.uk/tissue_types/connective/con_basal_lam.php (Accessed: 17/11/19).

Peddie, C.J. *et al.* (2014) 'Correlative and integrated light and electron microscopy of in-resin GFP fluorescence, used to localise diacylglycerol in mammalian cells', *Ultramicroscopy*, 143, pp. 3-14.

Pericak-Vance, M.A. *et al.* (1991) 'Linkage studies in familial Alzheimer disease: evidence for chromosome 19 linkage', *Am J Hum Genet*, 48(6), pp. 1034-50.

Persson, T. *et al.* (2017) 'Apolipoprotein E4 Elicits Lysosomal Cathepsin D Release, Decreased Thioredoxin-1 Levels, and Apoptosis', *Journal of Alzheimer's disease : JAD*, 56(2), pp. 601-617.

Pfizer (2015) 'Minipress prescribing information' (Administration, U.S.F.a.D. Pfizer.

Pfrieger, F.W. and Ungerer, N. (2011) 'Cholesterol metabolism in neurons and astrocytes', *Prog Lipid Res*, 50(4), pp. 357-71.

PhenomWorld (2017) *Delphi*. Available at: https://www.delphimicroscope.com/ (Accessed: 10/02/17).

Philipp, M. and Hein, L. (2004) 'Adrenergic receptor knockout mice: distinct functions of 9 receptor subtypes', *Pharmacol Ther*, 101(1), pp. 65-74.

Phillips, M.C. (2014) 'Apolipoprotein E isoforms and lipoprotein metabolism', *IUBMB Life*, 66(9), pp. 616-23.

Pitas, R.E. *et al.* (1987) 'Astrocytes synthesize apolipoprotein E and metabolize apolipoprotein E-containing lipoproteins', *Biochim Biophys Acta*, 917(1), pp. 148-61.

Plant, L.D. *et al.* (2003) 'The production of amyloid beta peptide is a critical requirement for the viability of central neurons', *J Neurosci*, 23(13), pp. 5531-5.

Puglielli, L., Tanzi, R.E. and Kovacs, D.M. (2003) 'Alzheimer's disease: the cholesterol connection', *Nat Neurosci*, 6(4), pp. 345-51.

Purkayastha, S. and Raven, P.B. (2011) 'The functional role of the alpha-1 adrenergic receptors in cerebral blood flow regulation', *Indian journal of pharmacology*, 43(5), pp. 502-506.

Qiu, Z. *et al.* (1999) 'Alpha2-macroglobulin enhances the clearance of endogenous soluble beta-amyloid peptide via low-density lipoprotein receptor-related protein in cortical neurons', *J Neurochem*, 73(4), pp. 1393-8.

Ramanathan, A. *et al.* (2015) 'Impaired vascular-mediated clearance of brain amyloid beta in Alzheimer's disease: The role, regulation and restoration of LRP1', *Frontiers in Aging Neuroscience*, 7(136).

Rash, J.E. *et al.* (1998) 'Direct immunogold labeling of aquaporin-4 in square arrays of astrocyte and ependymocyte plasma membranes in rat brain and spinal cord', *Proceedings of the National Academy of Sciences of the United States of America*, 95(20), pp. 11981-11986.

Reiman, E.M. *et al.* (2001) 'Declining brain activity in cognitively normal apolipoprotein E epsilon 4 heterozygotes: A foundation for using positron emission tomography to efficiently test treatments to prevent Alzheimer's disease', *Proc Natl Acad Sci U S A*, 98(6), pp. 3334-9.

Riss, T.L. *et al.* (2004) 'Cell Viability Assays', in Sittampalam, G.S. *et al.* (eds.) *Assay Guidance Manual*. Bethesda (MD): Eli Lilly & Company and the National Center for Advancing Translational Sciences.

Ritter, J. *et al.* (2019) 'Noradrenergic Transmission', in *Rang & Dale's Pharmacology*. ninth edn. Elsevier, pp. 197-216.

Rogers, J.T. and Weeber, E.J. (2008) 'Reelin and apoE actions on signal transduction, synaptic function and memory formation', *Neuron Glia Biol*, 4(3), pp. 259-70.

Rubin, L.L. *et al.* (1991) 'A cell culture model of the blood-brain barrier', *J Cell Biol*, 115(6), pp. 1725-35.

Sabayan, B. *et al.* (2016) 'Cardiac and Carotid Markers Link With Accelerated Brain Atrophy: The AGES-Reykjavik Study (Age, Gene/Environment Susceptibility-Reykjavik)', *Arteriosclerosis, thrombosis, and vascular biology*, 36(11), pp. 2246-2251.

Saido, T. and Leissring, M.A. (2012) 'Proteolytic degradation of amyloid beta-protein', *Cold Spring Harb Perspect Med*, 2(6), p. a006379.

Salloway, S. *et al.* (2009) 'A phase 2 multiple ascending dose trial of bapineuzumab in mild to moderate Alzheimer disease', *Neurology*, 73(24), pp. 2061-70.

Samuels, E.R. and Szabadi, E. (2008) 'Functional neuroanatomy of the noradrenergic locus coeruleus: its roles in the regulation of arousal and autonomic function part I: principles of functional organisation', *Current neuropharmacology*, 6(3), pp. 235-253.

Sastre, M. *et al.* (2004) 'Binding of cystatin C to Alzheimer's amyloid beta inhibits in vitro amyloid fibril formation', *Neurobiol Aging*, 25(8), pp. 1033-43.

Scarpace, P.J. and Abrass, I.B. (1988) 'Alpha- and beta-adrenergic receptor function in the brain during senescence', *Neurobiol Aging*, 9(1), pp. 53-8.

Schenk, D. *et al.* (1999) 'Immunization with amyloid-beta attenuates Alzheimer-disease-like pathology in the PDAPP mouse', *Nature*, 400(6740), pp. 173-7.

Schley, D. *et al.* (2006) 'Mechanisms to explain the reverse perivascular transport of solutes out of the brain', *J Theor Biol*, 238(4), pp. 962-74.

Schneider, J. *et al.* (1999) 'EUROCARE: a cross-national study of co-resident spouse carers for people with Alzheimer's disease: I--Factors associated with carer burden', *Int J Geriatr Psychiatry*, 14(8), pp. 651-61.

Sciencell (2017) *Human astrocytes*. Available at: http://www.sciencellonline.com/products-services/primary-cells/human-astrocytes.html (Accessed: 10/02/17).

Seawright, J.W. *et al.* (2018) 'Vascular Smooth Muscle Contractile Function Declines With Age in Skeletal Muscle Feed Arteries', *Frontiers in physiology*, 9, pp. 856-856.

Sevigny, J. *et al.* (2016) 'The antibody aducanumab reduces Abeta plaques in Alzheimer's disease', *Nature*, 537(7618), pp. 50-6.

Shibata, M. *et al.* (2000) 'Clearance of Alzheimer's amyloid-ss(1-40) peptide from brain by LDL receptor-related protein-1 at the blood-brain barrier', *J Clin Invest*, 106(12), pp. 1489-99.

Siddharthan, V. *et al.* (2007) 'Human astrocytes/astrocyte-conditioned medium and shear stress enhance the barrier properties of human brain microvascular endothelial cells', *Brain research*, 1147, pp. 39-50.

Sigurdsson, E.M. (2018) 'Tau Immunotherapies for Alzheimer's Disease and Related Tauopathies: Progress and Potential Pitfalls', *Journal of Alzheimer's disease : JAD*, 64(s1), pp. S555-S565.

Sixt, M. *et al.* (2001) 'Endothelial cell laminin isoforms, laminins 8 and 10, play decisive roles in T cell recruitment across the blood-brain barrier in experimental autoimmune encephalomyelitis', *The Journal of cell biology*, 153(5), pp. 933-946.

Small, G.W. *et al.* (1995) 'Apolipoprotein E type 4 allele and cerebral glucose metabolism in relatives at risk for familial Alzheimer disease', *Jama*, 273(12), pp. 942-7.

Song, J. *et al.* (2013) 'Extracellular matrix of secondary lymphoid organs impacts on B-cell fate and survival', *Proceedings of the National Academy of Sciences of the United States of America*, 110(31), pp. E2915-E2924.

Sorokin, L.M. *et al.* (1997) 'Developmental regulation of the laminin alpha5 chain suggests a role in epithelial and endothelial cell maturation', *Dev Biol*, 189(2), pp. 285-300.

Strittmatter, W.J. *et al.* (1993) 'Binding of human apolipoprotein E to synthetic amyloid beta peptide: isoform-specific effects and implications for late-onset Alzheimer disease', *Proc Natl Acad Sci U S A*, 90(17), pp. 8098-102.

Suarez, B.K. and Schonfeld, G. (1981) 'Characterization of apolipoprotein E (ApoE) apoprotein levels in the various ApoE phenotypes', *J Clin Endocrinol Metab*, 53(2), pp. 435-8.

Sun, Y. *et al.* (1998) 'Glial fibrillary acidic protein-apolipoprotein E (apoE) transgenic mice: astrocyte-specific expression and differing biological effects of astrocyte-secreted apoE3 and apoE4 lipoproteins', *J Neurosci*, 18(9), pp. 3261-72.

Sundelöf, J. *et al.* (2008) 'Serum cystatin C and the risk of Alzheimer disease in elderly men', *Neurology*, 71(14), pp. 1072-1079.

Sundman, M.H., Hall, E.E. and Chen, N.K. (2014) 'Examining the relationship between head trauma and neurodegenerative disease: A review of epidemiology, pathology and neuroimaging techniques', *J Alzheimers Dis Parkinsonism*, 4, p. 137.

Tai, L.M. *et al.* (2016) 'The role of APOE in cerebrovascular dysfunction', *Acta Neuropathol*, 131(5), pp. 709-23.

Takeshita, Y. *et al.* (2014) 'An in vitro blood-brain barrier model combining shear stress and endothelial cell/astrocyte co-culture', *J Neurosci Methods*, 232, pp. 165-72.

Tao-Cheng, J.H., Nagy, Z. and Brightman, M.W. (1987) 'Tight junctions of brain endothelium in vitro are enhanced by astroglia', *J Neurosci*, 7(10), pp. 3293-9.

Tapial Martínez, P., López Navajas, P. and Lietha, D. (2020) 'FAK Structure and Regulation by Membrane Interactions and Force in Focal Adhesions', *Biomolecules*, 10(2), p. 179.

Tarbell, J.M. (2010) 'Shear stress and the endothelial transport barrier', *Cardiovasc Res*, 87(2), pp. 320-30.

TauRX (2020) *Phase 3*. Available at: https://taurx.com/phase-3.html (Accessed: 17/04/2020).

Thomsen, L.B., Burkhart, A. and Moos, T. (2015) 'A Triple Culture Model of the Blood-Brain Barrier Using Porcine Brain Endothelial cells, Astrocytes and Pericytes', *Plos One*, 10(8).

Thomsen, M.S. *et al.* (2017) 'Synthesis and deposition of basement membrane proteins by primary brain capillary endothelial cells in a murine model of the blood-brain barrier', *J Neurochem*, 140(5), pp. 741-754.

Thomsen, M.S., Routhe, L.J. and Moos, T. (2017a) 'The vascular basement membrane in the healthy and pathological brain', *J Cereb Blood Flow Metab*, 37(10), pp. 3300-3317.

Thomsen, M.S., Routhe, L.J. and Moos, T. (2017b) 'The vascular basement membrane in the healthy and pathological brain', *Journal of cerebral blood flow and metabolism : official journal of the International Society of Cerebral Blood Flow and Metabolism*, 37(10), pp. 3300-3317.

Thyberg, J. and Hultgardh-Nilsson, A. (1994) 'Fibronectin and the basement membrane components laminin and collagen type IV influence the phenotypic properties of subcultured rat aortic smooth muscle cells differently', *Cell Tissue Res*, 276(2), pp. 263-71.

Timpl, R. and Aumailley, M. (1989) 'Biochemistry of basement membranes', *Adv Nephrol Necker Hosp*, 18, pp. 59-76.

Trendelenburg, A.U. *et al.* (1997) 'A re-investigation of questionable subclassifications of presynaptic alpha2-autoreceptors: rat vena cava, rat atria, human kidney and guinea-pig urethra', *Naunyn Schmiedebergs Arch Pharmacol*, 356(6), pp. 721-37.

Trojanowski, J.Q. and Lee, V.M. (1995) 'Phosphorylation of paired helical filament tau in Alzheimer's disease neurofibrillary lesions: focusing on phosphatases', *Faseb j*, 9(15), pp. 1570-6.

Tumer, N. *et al.* (2014) 'The effects of aging on the functional and structural properties of the rat basilar artery', *Physiol Rep*, 2(6).

Uhlen, M. *et al.* (2015) 'Proteomics. Tissue-based map of the human proteome', *Science*, 347(6220), p. 1260419.

Urich, E. *et al.* (2012) 'Transcriptional profiling of human brain endothelial cells reveals key properties crucial for predictive in vitro blood-brain barrier models', *PLoS One*, 7(5), p. e38149.

Urich, E. *et al.* (2013) 'Multicellular self-assembled spheroidal model of the blood brain barrier', *Sci Rep*, 3(1500), p. 1500.

Valenzuela, M.J. *et al.* (2012) 'Multiple biological pathways link cognitive lifestyle to protection from dementia', *Biol Psychiatry*, 71(9), pp. 783-91.

Van Dorpe, J. *et al.* (2000) 'Prominent cerebral amyloid angiopathy in transgenic mice overexpressing the london mutant of human APP in neurons', *Am J Pathol*, 157(4), pp. 1283-98.

Verdier, Y., Zarandi, M. and Penke, B. (2004) 'Amyloid beta-peptide interactions with neuronal and glial cell plasma membrane: binding sites and implications for Alzheimer's disease', *J Pept Sci*, 10(5), pp. 229-48.

Verghese, P.B. *et al.* (2013) 'ApoE influences amyloid-beta (Abeta) clearance despite minimal apoE/Abeta association in physiological conditions', *Proc Natl Acad Sci U S A*, 110(19), pp. E1807-16.

Vinci, B. *et al.* (2011) 'Modular bioreactor for primary human hepatocyte culture: medium flow stimulates expression and activity of detoxification genes', *Biotechnol J*, 6(5), pp. 554-64.

Vinci, B. *et al.* (2012) 'An in vitro model of glucose and lipid metabolism in a multicompartmental bioreactor', *Biotechnol J*, 7(1), pp. 117-26.

Wallukat, G. (2002) 'The β-Adrenergic Receptors', *Herz*, 27(7), pp. 683-690.

Wang, D.S. *et al.* (2003) 'Oxidized neprilysin in aging and Alzheimer's disease brains', *Biochem Biophys Res Commun*, 310(1), pp. 236-41.

Wang, J., Yin, L. and Chen, Z. (2011) 'New insights into the altered fibronectin matrix and extrasynaptic transmission in the aging brain', *Journal of Clinical Gerontology and Geriatrics*, 2(2), pp. 35-41.

Wang, J.D. *et al.* (2016) 'Organization of Endothelial Cells, Pericytes, and Astrocytes into a 3D Microfluidic in vitro Model of the Blood-Brain Barrier', *Mol Pharm*.

Wang, L.Y. *et al.* (2009) 'Prazosin for the treatment of behavioral symptoms in patients with Alzheimer disease with agitation and aggression', *Am J Geriatr Psychiatry*, 17(9), pp. 744-51.

Weinshenker, D. (2008) 'Functional consequences of locus coeruleus degeneration in Alzheimer's disease', *Curr Alzheimer Res*, 5(3), pp. 342-5.

Weisgraber, K.H., Innerarity, T.L. and Mahley, R.W. (1982) 'Abnormal lipoprotein receptor-binding activity of the human E apoprotein due to cysteine-arginine interchange at a single site', *J Biol Chem*, 257(5), pp. 2518-21.

Weller, R.O., Boche, D. and Nicoll, J.A.R. (2009) 'Microvasculature changes and cerebral amyloid angiopathy in Alzheimer's disease and their potential impact on therapy', *Acta Neuropathologica*, 118(1), p. 87.

Weller, R.O. *et al.* (2009) 'Lymphatic drainage of the brain and the pathophysiology of neurological disease', *Acta Neuropathol*, 117(1), pp. 1-14.

Weller, R.O. and Nicoll, J.A. (2003) 'Cerebral amyloid angiopathy: pathogenesis and effects on the ageing and Alzheimer brain', *Neurol Res*, 25(6), pp. 611-6.

Weller, R.O. *et al.* (2008) 'Perivascular drainage of amyloid-beta peptides from the brain and its failure in cerebral amyloid angiopathy and Alzheimer's disease', *Brain Pathol*, 18(2), pp. 253-66.

Whitesides, G.M. (2006) 'The origins and the future of microfluidics', *Nature*, 442(7101), pp. 368-73.

Willem, M. *et al.* (2006) 'Control of peripheral nerve myelination by the beta-secretase BACE1', *Science*, 314(5799), pp. 664-6.

Winkler, E.A., Bell, R.D. and Zlokovic, B.V. (2011) 'Central nervous system pericytes in health and disease', *Nat Neurosci*, 14(11), pp. 1398-1405.

Wischik, C.M., Harrington, C.R. and Storey, J.M. (2014) 'Tau-aggregation inhibitor therapy for Alzheimer's disease', *Biochem Pharmacol*, 88(4), pp. 529-39.

Wisniewski, H.M. and Wegiel, J. (1994) 'Beta-amyloid formation by myocytes of leptomeningeal vessels', *Acta Neuropathol*, 87(3), pp. 233-41.

Wolfe, M.S. (2008) 'Inhibition and modulation of gamma-secretase for Alzheimer's disease', *Neurotherapeutics*, 5(3), pp. 391-8.

Woo, D. *et al.* (2013) 'Apolipoprotein E, Statins and Risk of Intracerebral Hemorrhage', *Stroke; a journal of cerebral circulation*, 44(11), p. 10.1161/STROKEAHA.113.001304.

Wu, L. and Zhao, L. (2016) 'ApoE2 and Alzheimer's disease: time to take a closer look', *Neural regeneration research*, 11(3), pp. 412-413.

Yamazaki, T. and Mukouyama, Y.-S. (2018) 'Tissue Specific Origin, Development, and Pathological Perspectives of Pericytes', *Frontiers in cardiovascular medicine*, 5, pp. 78-78.

Yao, Y. *et al.* (2014) 'Astrocytic laminin regulates pericyte differentiation and maintains blood brain barrier integrity', *Nat Commun*, 5(3413).

Yeo, E.-J. (2019) 'Hypoxia and aging', *Experimental & Molecular Medicine*, 51(6), p. 67.

Yousif, L.F., Di Russo, J. and Sorokin, L. (2013a) 'Laminin isoforms in endothelial and perivascular basement membranes', *Cell adhesion & migration*, 7(1), pp. 101-110.

Yousif, L.F., Di Russo, J. and Sorokin, L. (2013b) 'Laminin isoforms in endothelial and perivascular basement membranes', *Cell Adh Migr*, 7(1), pp. 101-10.

Yurchenco, P.D. (2011) 'Basement membranes: cell scaffoldings and signaling platforms', *Cold Spring Harb Perspect Biol*, 3(2).

Zhang, J.X. *et al.* (2017) 'Luteolin Inhibits Fibrillary beta-Amyloid1-40-Induced Inflammation in a Human Blood-Brain Barrier Model by Suppressing the p38 MAPK-Mediated NF-kappaB Signaling Pathways', *Molecules*, 22(3).

Zhang, Z. *et al.* (2013) 'Aberrant apolipoprotein E expression and cognitive dysfunction in patients with poststroke depression', *Genet Test Mol Biomarkers*, 17(1), pp. 47-51.

Zhong, N., Ramaswamy, G. and Weisgraber, K.H. (2009) 'Apolipoprotein E4 domain interaction induces endoplasmic reticulum stress and impairs astrocyte function', *J Biol Chem*, 284(40), pp. 27273-80.

Zhou, B. *et al.* (2008) 'Epicardial progenitors contribute to the cardiomyocyte lineage in the developing heart', *Nature*, 454(7200), pp. 109-13.

Zhou, X. *et al.* (2019) 'Memantine Improves Cognitive Function and Alters Hippocampal and Cortical Proteome in Triple Transgenic Mouse Model of Alzheimer's Disease', *Exp Neurobiol*, 28(3), pp. 390-403.

Zlokovic, B.V. *et al.* (2010) 'Low-density lipoprotein receptor-related protein-1: a serial clearance homeostatic mechanism controlling Alzheimer's amyloid beta-peptide elimination from the brain', *J Neurochem*, 115(5), pp. 1077-89.